POLITECNICO DI TORINO

Corso di Laurea Magistrale
in Ingegneria Meccanica

Tesi di Laurea Magistrale

A mechanical model of cardiovascular system for blood pressure estimation

Relatori
Prof. Elvio Bonisoli
Ing. Domenico Lisitano
Prof. Marco Amabili

Candidato
Maria Schiavone

Anno accademico 2020/2021

Index

Abstract

The Non-invasive Physiological Activity Monitoring System (NiPAMS) project is being developed by the research group of Prof. Plant at McGill University. The system is based on vibrations detected by a six-degree of freedom MEMS accelerometer, placed at the xiphoid process of the sternum, using Vibrational Cardiography (VCG) technique. The aim is to build a non-invasive, continue and central system for blood pressure estimation using VCG data acquired experimentally.

This thesis describes my contribution to the project, which is based on a lumped parameter model for cardiovascular system (CVS). A simple hydraulic CVS model was selected from literature. An equivalent electric model is obtained correlating blood flow rate to the current “through” electric elements, and blood pressure drop to the voltage drop “across” each element. Hydraulic capacitances are correlated to inertial effects, resistances to damping and inductances to stiffness. This approach implies Firestone analogy to transform the electric CVS model into the equivalent mechanical one. Finally, a linear mass-damper-spring model (MCK) with 12 degrees of freedom (DOF) is obtained, where each DOF represents a significant compartment of the cardiovascular system, including four heart chambers.

Some springs connected to ground are added to ensure static state for the model; then, mass, damping and stiffness matrices are derived. In this CVS model, damping is not classical, i.e. not proportional; therefore, complex modal analysis is implemented in the numerical analyses. Complex eigenvectors and eigenvalues are obtained, hence 24 natural frequencies and damping ratios are calculated. LUPOS FEM code is used to evaluate and to visualise vibrational modes.

Assuming non-classical damping, the system performs two modes of rigid body motion, sixteen underdamped modes and six overdamped modes. The two rigid body modes can be interpreted as two moments when blood flow through vessels looks like rigid body motion. The frequency range for CVS model goes from 1.3 Hz to 21 Hz. That confirms model validity because time-frequency spectrograms of VCG signals show a high frequency contribution in the same range. Furthermore, heart rate measured in NiPAMS tests corresponds to frequencies around 1.3 Hz. Besides, some HR super harmonics correspond to significant frequencies in VCG Continuous Wavelet Transformation graphs.

To confirm the robustness of the simple lumped model, heart excitation is included. Pulsating heart action is assumed to depend only on left and right ventricles contractility. It implies to define two pressure functions over time for the two ventricles, which correspond to velocities, according to analogies used.

Displacement and acceleration come from velocity integration and derivation, hence imposed kinematics is applied on left and right ventricular DOFs. The model is implemented in LUPOS and Simulink to solve the new time-dependent dynamic problem.

Finally, time response is obtained with displacement, velocity and acceleration over time for each DOF. Resulting pressure waveforms can be directly compared with invasive pressure recordings. Heart chambers pressure curves show a straightforward correspondence; more investigation is required to assess waveforms for the other DOFs. Moreover, a CVS model without rigid body modes is proposed adding two springs connecting masses to ground. It generates more reliable time responses. Discussion on reference data concludes this work.

Introduction

The main characteristics and objective of NiPAMS project are discussed in the first chapter of this thesis. Some details about the experiments performed is also provided, as well as an explication of the techniques used, which is Vibrational Cardiography including seismocaridography and gyrocardiography.
Moreover, there is a brief description of the cardiac cycle and the blood pressure waveforms, which is the current object of study for NiPAMS project. In addition, an overview of the most useful hemodynamic parameters is provided, since they are widely encountered when treating this topic.
The aim of my thesis is to propose a mechanical model of cardiovascular system to estimate blood pressure starting from VCG signals detected. In order to find a correlation between the model and the experimental data, time-frequency domain is considered. For this reason, in chapter 3, the spectrograms with Continuous Wavelet Transforms are reported for some acceleration and gyration measurements. Tests and subjects presented have been selected from data set because of their steady frequency over time. It is important to see how heart rate frequency and super harmonics represent experimental data in frequency domain. Consequently, the main frequency range for VCG signals will be found to be the same frequency range of CVS model created.
In the fourth chapter, the alternative analogies to convert hydraulic CVS to electric model are described. There is a discussion about two possible approaches and it is demonstrated which one is the most suitable for CVS. Finally, Firestone electro-mechanical analogy is applied and the mass-damper-spring model is built and some adjustments are applied to ensure model statics.
Mass, damping and stiffness matrices representative of the system are defined in details in the following chapter, to be coherent with the analogies chosen. For the actual CVS model, damping is not proportional, but the proportional case will be analysed too for comparison. Complex eigenvectors and eigenvalues are derived and natural frequencies and damping ratios are calculated.
The sixth chapter shows the vibrational modes visualisation obtained implementing CVS model in LUPOS FEM code. It is useful to starts interpreting mechanical modes as hemodynamic events during cardiac cycle.
Finally, heart excitation is considered in order to make the model more robust. According to the assumptions made, pulsating heart action is described only by ventricular pressure functions over time. Thus, they are defined and applied to the related two DOFs of the model as imposed kinematics because the analogies used implies pressure equivalent to mechanical velocity. Therefore, time responses of the system are obtained for displacement, velocity and acceleration of every DOF. An initial comparison between pressure waveforms predicted by the model and actual pressure recordings is proposed. Then, time-varying heart rate is applied to the model and results are compared to measurements in time-frequency domain.

1. Non-invasive Physiological Activity Monitoring System and blood pressure estimation

Remote and continuous heath monitoring has attracted significant interest among the healthcare community in recent years because of the global increase in cardiovascular disease. It is important to create a wearable and accessible system to monitor the physiological parameters on earth and space, where real-time communication with earth can be more complicated. This is the main motivation for the Non-invasive Physiological Activity Monitoring System or NiPAMS project. The NiPAMS is being developed by the research group of Professor David Plant at McGill University, Montreal (CA), in collaboration with MDA, a space systems and sensors engineering company based in Ontario.
The project consists of a wearable wireless sensor placed at the xiphoid of the sternum to detect vibrations in all six directions using Vibrational Cardiography (VCG). The objective is to analyse the signals detected in order to monitor key physiological parameters. The current goal of the research is to find and demonstrate a correlation to derive blood pressure (BP) from VCG signal. In order to do that, it is necessary to consider the valve motion in the heart, because they are directly connected to the vibrations detected and to the blood pressure itself. Furthermore, it will help identifying the frequency range where ventricular contractions mostly occur. Experiments have been performed on 64 subjects in good health. The electrocardiography (ECG) and the impedance cardiography (ICG) were used as reference. Together with VCG signals, radial blood pressure has been measured with a cuff at the finger for every subject. This detected pressure is called non-invasive blood pressure or NIBP. It is a useful measurements but it is only a radial pressure. The blood pressure measurement that NiPAMS project would like to derive is central blood pressure. It usually corresponds to blood pressure at aortic root and only invasive methods to do that are known so far.

1.1 NiPAMS project overview

The Non-invasive Physiological Activity Monitoring System (NiPAMS) consists of a wearable, wireless sensing platform that monitors, records and analyses key physiological parameters. The main need that it is supposed to satisfy is accessible health monitoring on earth and in space [1].
First, Wearable Sensor Modules (WSMs) are attached to the subject; the raw signal acquired includes acceleration, gyration and optical measurements. The sensors are connected by Bluetooth, so wirelessly, to a Sensor Interface Board (SIB) in order to perform real time Digital Signal Processing (DSP) on the sensor signals. Then it is connected with the Data Analytics Server (DAS) for the post processing study.

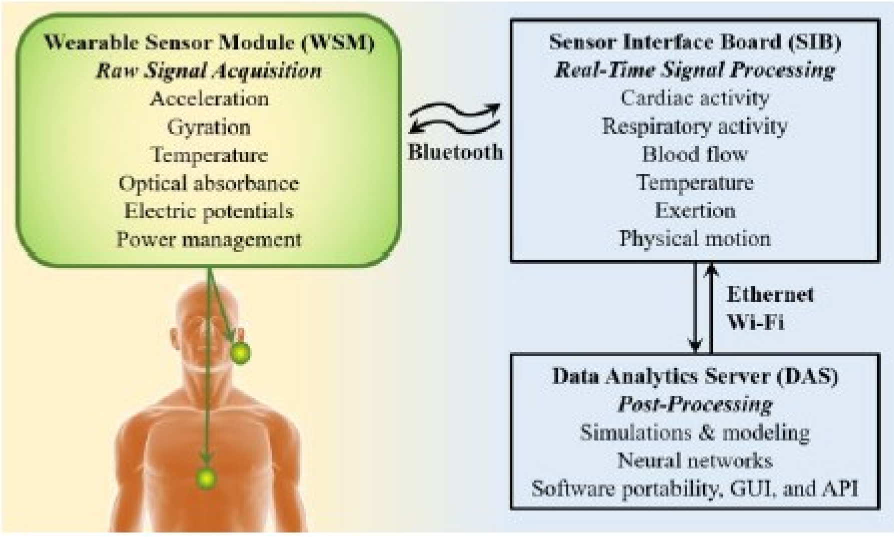

Figure 1.1.1– Schematic of NiPAMS.

The NiPAMS monitors the main physiological parameters of human body. It is possible to classify them in:

- Cardio-respiratory activity (CRA):
  - Respiration activity: respiration rate (RR) , volume (RV), phase, peripheral oxygen saturation (SpO2), lung capacity
  - Cardiac activity: heart rate (HR) , efficiency, HR variability, left ventricular ejection time and fraction (LVET, LVETF), stroke volume, beat-to-beat duration (BTB)
  - Blood flow: blood pressure (BP) , ejection velocity, viscosity
- Body*:*
  - surface body temperature (BT) , physical exertion level (EL)
- Physical motion:
  - Motion capture (MoCap) information for motion artifact (MoArt) cancellation

1.2 Experiments performed

The experiments for the NiPAMS project have been performed in a specific laboratory located in room 814A of McConnell Engineering Building at McGill University. There was a physiological monitoring test bench with a massage bed, a computer and a measurement equipment as showed in Figure 1.2.1.

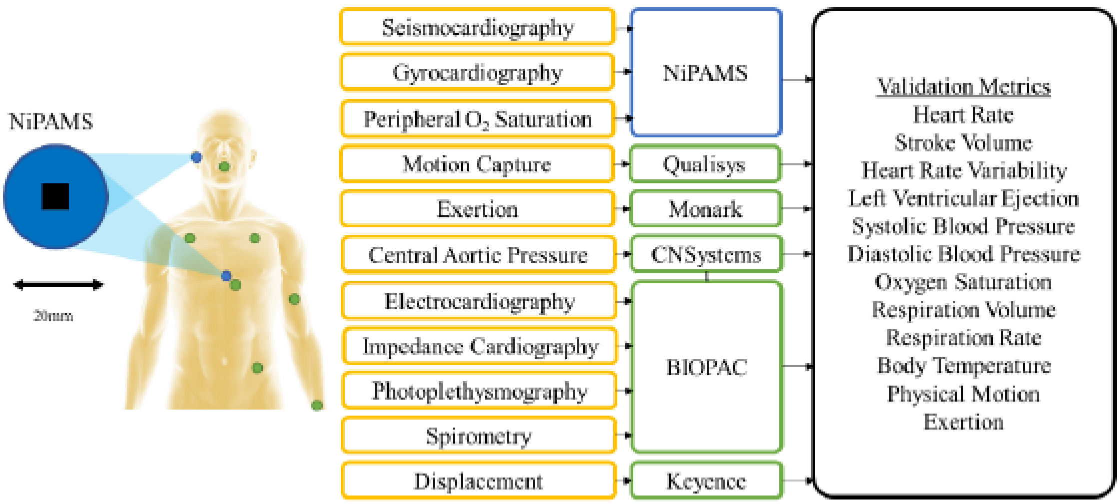

Figure 1.2.1 –Measurement equipment for NiPAMS tests.

In particular, the NiPAMS receives the signals from seismocardiography (SCG) and gyrocardiography (GCG) that together correspond to the vibrational cardiography (VCG) signals. The main objective is to find a correlation between the VCG signals detected and the effective Blood Pressure (BP) and, especially, to prove that.

1.2.1 Acquisition system

The acquisition system for this project has to be small and robust because it has to work wirelessly and on space, where it is more complicated than on earth. In fact, one of the main objective of NiPAMS is to guarantee a wearable system for physiological parameters monitoring.
There is an inertial measurement unit (IMU) sensor placed at the xiphoid process of the sternum. The IMU sensor used is a nine-axis InvenSense Motion Processing Unit ICM-20602, used as accelerometer and gyroscope (Figure 1.2.1.1). It consists of a MEMS 3-axis accelerometer, 3-axis gyroscope and a 3-axis digital compass that was not used in the NiPAMS experimental work. The sensitivity of the accelerometer was set at $\pm 2g$, where g is the gravitational acceleration, and the sensitivity of the gyroscope was set at $\pm 250°/s$.

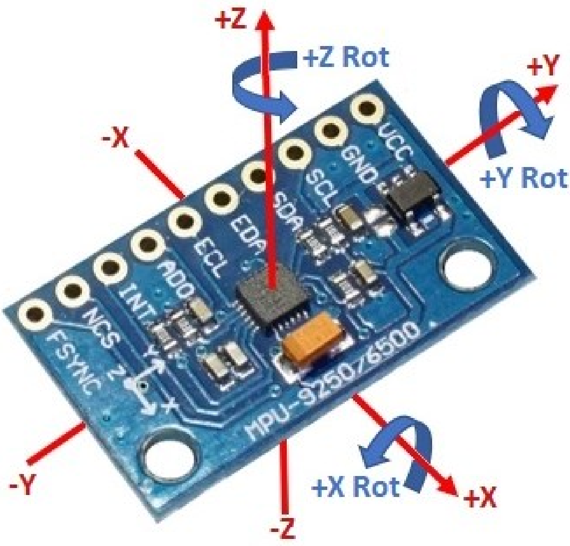

Figure 1.2.1.1 – MPU-9250 MEMS device with 3-axis for acceleration and 3-axis for gyration.

The IMU is connected to a Raspberry PI Zero W micro-controller that employs a PIZ Uptime battery shield to provide wireless mobility, as shown in Figure 1.2.1.2. In addition, the BIOPAC clock is connected to the RPI for a post-acquisition synchronization between IMU detection and BIOPAC data.

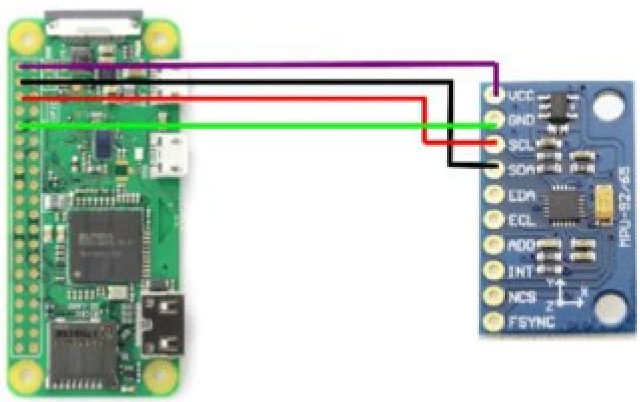

Figure 1.2.1.2 – Raspberry PI Zero W micro-controller connected to the IMU sensor.

A Micro SD Card is used to storage data from RPI in a text file.
Using only one sensor, attached at the xiphoid process, the sampling rate is about 560 Hz.
Another sensor could be attached on the back perpendicularly to the first one, in order to detect motion artifact. In this case, the sampling rate for the system decreases to 270 Hz. However, the back sensor was not used on the 64 subjects during the BP study.
Another important device of the acquisition system is the BIOPAC to record signals from: electrocardiography (ECG), impedance cardiography (ICG), spirometry, non-invasive blood pressure (finger cuff) and photoplysmography (PPG).

Figure 1.2.1.3 – Example of BIOPAC.

There is also a Keyence laser displacement sensor to track the orthogonal displacement of the IMU sensor.

Figure 1.2.1.4 – Example of Keyence displacement sensor.

The signals detected have to be filtered before using them for correlation with vital parameters. Signal filtration is being still investigated in order to detect any source of noise during tests and cleaning the signal.

1.2.2 Testing Protocol

The study population was composed by 64 participants, 57% of them were males. They were between 20 and 30 years old. The testing procedure was applied for each subject. It was composed of:

- 15 minutes for set-up and attachment,
- 3 minutes rest when displacement sensor and spirometer were used,
- 6 minutes breathing when the subject had to breathe through the spirometer, in this test the displacement sensor was not utilized,
- 10 minutes static respiration volume (RV) tests that included holding breath at high lung volume (HLV) and at low lung volume (LLV), recorded by the displacement sensor, no spirometer was used,
- 2 minutes rest,

- 2 minutes exertion when data were not recorded,
- 5 minutes recovery, when the subject had to breathe normally through the spirometer and displacement sensor was not required,
- 3 minute to recalibrate blood pressure,
- 2 minutes exertion,
- 5 minutes recovery,
- 2 minutes rest,
- 5 minutes for detachment.

In the following table, the tests performed are shown with their subtests and some comments. It is reported when the displacement sensor was used (Disp).

Table 1.2.2.1 – Testing Protocol

Time	Test	Subtest	Comments
15	*Attach sensors*	Calibration, connections	Equipment setup and connections should be done prior to subject arrival, strapping prior to electrode connections.
3	*Rest*		Disp
6	*Breathing*	1 Lung capacity (HLV, LLV)	Repeat two times, start from HLV. Add timestamp when first test is done.
		2 slow, deep breathing	
		2 fast, shallow breathing	1 min normally, 30 sec at HLV, 30 sec at LLV
		30sec diaphragm breathing	At normal rate
		30sec rib cage breathing	At normal rate
10	*Static RV*	Hold breath at HLV	Disp. No spirometer, repeat 3 times each, let the subject rest for 10 secs between tests
		Hold breath at LLV	
2	*Rest*		Disp
2	*Exertion*		Legs suspended in the air, bicycle, dumbbell, ankle weights
5	*Recovery*		
1	*Recalibrate BP*		
2	*Exertion*		Same exertion workout
5	*Recovery*		
2	*Rest*		Disp
5	Detach		

1.3 VCG measurements

The method of Vibrational Crdiography (VCG) incorporates a combination of linear Seismocardiography (SCG) and angular Gyrocardiography (GCG) in a single sensor [2]. Both SCG and GCG signals show some fiducial points that are directly correlated to relevant cardiac activities, like muscle contraction, valve movement or blood flow turbulence. In particular, the vibrations associated with the two main heart sounds detected by phonocardiography (PCG) are prominent in VCG signals.

1.3.1 Seismocardiography

Seismocardiography measures cardiac-induced mechanical vibrations at the chest surface. These vibrations are usually measured in the form of acceleration in m/s^2. A classical SCG can be identified [3], then, the signals change slightly their morphology for various subjects. The general trend of SCG signal shows that aortic valve opening peak (AO) has some neighbouring peaks, and mitral valve closure peak (MC) is smoother. In order to identify the points characteristic of valve operations, also the recording of electrocardiogram ECG and phonocardiogram PCG are required. The classical SCG signal is reported in the following figure.

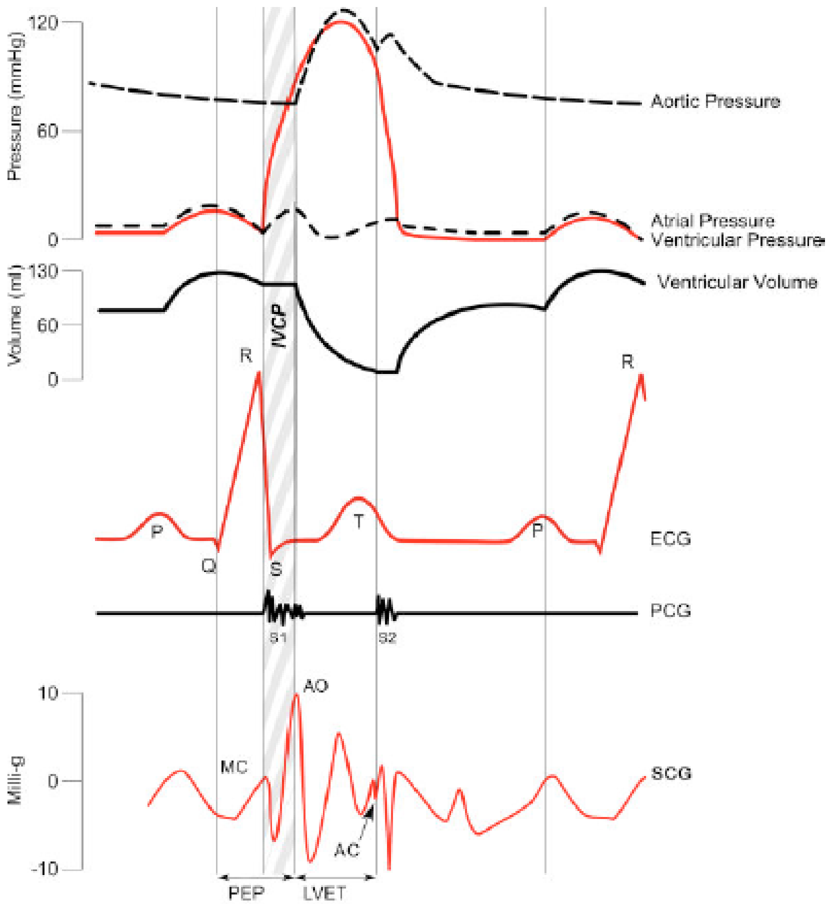

Figure 1.3.1.1 – General Wiggers diagram with ECG, PCG and typical SCG signal.

In NiPAMS experiments, linear acceleration is recorded in three-axis directions. The IMU sensor used has a coordinate system defined for acceleration as in Figure 1.2.1.1, from datasheet. However, the accelerations detected experimentally result to have a different coordinate system. It is illustrate in Figure 1.3.1.2 on the right and it involves a left-hand system. Therefore, for acceleration readings, the X-axis points from the foot to the head, the Y- axis points laterally from human right to left and Z- axis points from back to front. It means that there is a left hand coordinate system for accelerations detected.

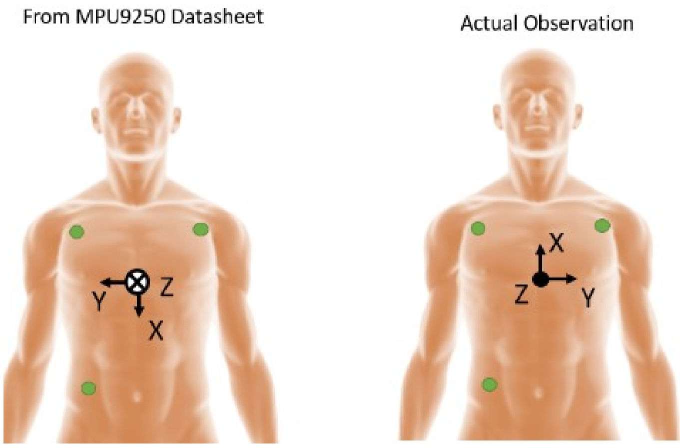

Figure 1.3.1.2 – Schematic of MPU sensor orientation from datasheet (left) and for acceleration detection (right) in NiPAMS experiments.

Figure 1.3.1.3 and Figure 1.3.1.4 show the SCG signals detected for a generic subject during NiPAMS experiments (subject identified with number 225), for rest test and for holding breath at high lung volume test (HLV). Accelerations in Y and Z directions (detected according to Figure 1.3.1.2) are reported for a heart period because they result to be clearer and more comparable to the classical SCG waveform seen in Figure 1.3.1.1.

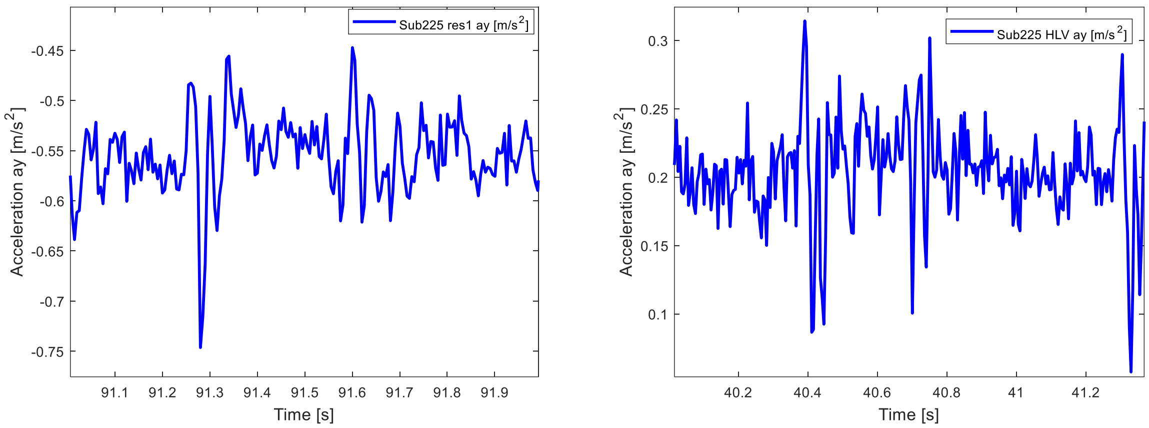

Figure 1.3.1.3 – Acceleration in Y-direction detected for subject 225, rest test (left) and holding breath at high lung volume HLV (right).

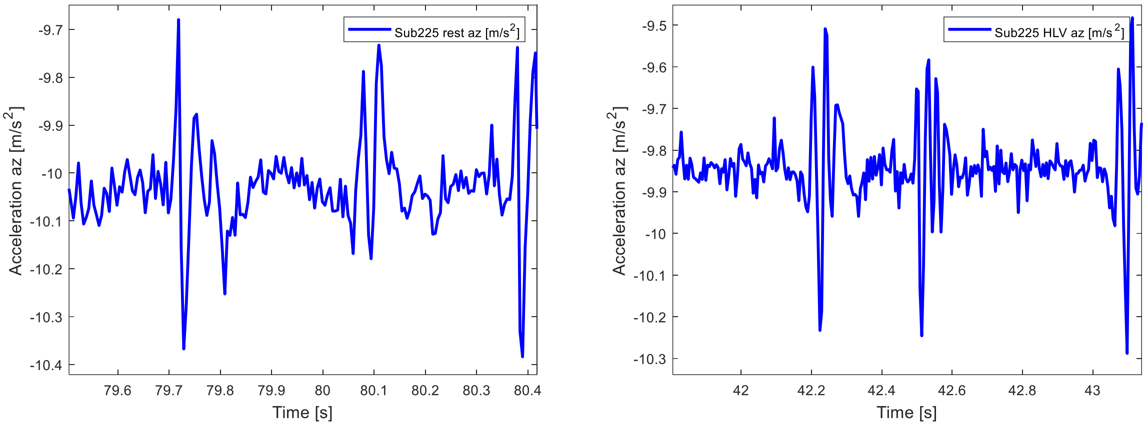

Figure 1.3.1.4 – Acceleration in Z-direction detected for subject 225, rest test (left) and holding breath at high lung volume HLV (right).

Acceleration in Y and Z directions show two peaks during a heart period, which correspond to AO and AC peaks usually seen in SCG waveforms. However, some waveform variations exist when subject or test change.

1.3.2 Gyrocardiography

Gyrocardiography (GCG) measures angular velocity or gyration with a gyroscope sensor attached to the skin anterior to sternum. A previous study [4] demonstrated that GCG signals were similar in amplitudes and in waveform shapes, even if they came from different subjects and measurement devices. It was noted that the fiducial points were the same in the GCG signals measured with different conditions. The experimental set up and the axis coordinates used for that study are shown in the following figure.

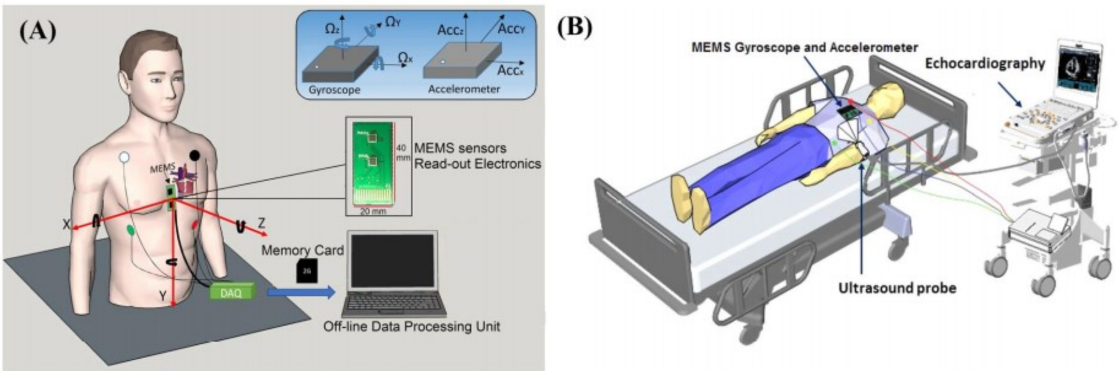

Figure 1.3.2.1 – Schematic of the experimental set up in 2017 [1] of MEMS placement and processing (A) and echocardiography set up (B).

Figure 1.3.2.2 shows the general GCG waveform obtained from gyration detection. There is also the correspondence with the ECG signal and the main time intervals that are connected to valve motion.

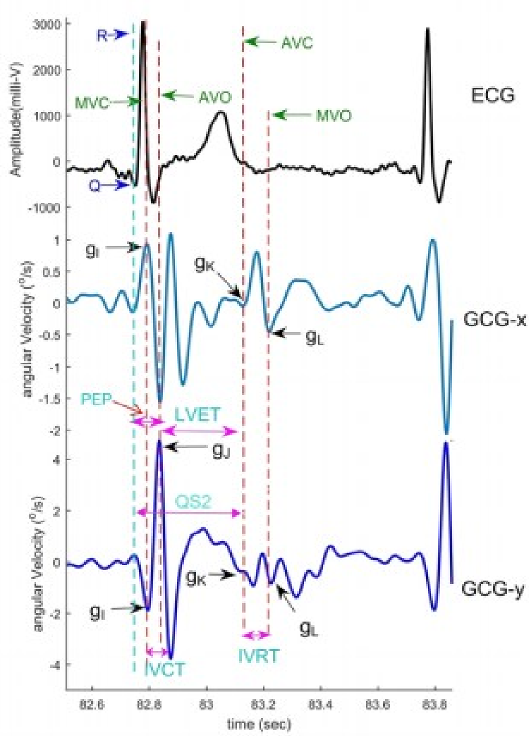

Figure 1.3.2.2 – GCG waveform shape around X- axis and Y-axis, with ECG signals and corresponding fiducial points.

The fiducial points that must be found in the GCG-y waveform are called g_I, g_K and g_L in Figure 1.3.2.2. The g_I point corresponds to the R peak in the echocardiography (ECG) signal, which is the first peak in the GCG waveform considered. A second important peak occurs after the T peak of the ECG signal. This peak has a lower amplitude, two notches can be identified just before and after it, which are denoted as g_K and g_L respectively. These points in the GCG-x have a corresponding definition in the GCG-y. In the GCG-y waveform showed in figure 1.3.2.2, another fiducial point is identified with g_J and it corresponds to the aorta opening event. By using both the gyration signals, some characteristic time intervals can be defined visually, like the isovolumetric contraction time (IVCT), the isovolumetric relaxation time (IVRT), the left ventricular ejection time (LVET), the pre-ejection period (PEP) and the total electromechanical systole (QS2).

For the NiPAMS experiments, the MPU sensor was placed with an orientation different from the experiments discussed above. Gyration readings respect the axis coordinates described in the MPU datasheet (Figure 1.2.1.1). Therefore, the X-axis points from the head to the foot, the Y-axis points laterally from left to right and Z- axis points from front to back, perpendicular to the xiphoid process of the sternum, as showed in the following figure. It confirms a right hand coordinate system for gyrations.

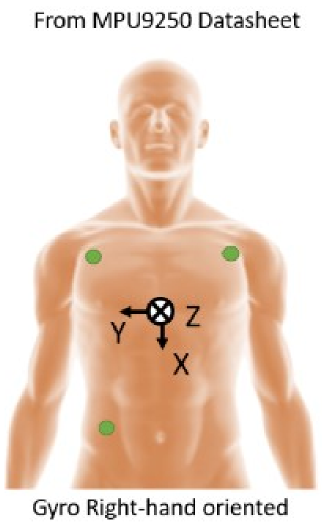

Figure 1.3.2.3 – Schematic of MPU sensor orientation for gyration detection in NiPAMS experiments.

It can be deduced that X and Y axis orientation used in NiPAMS experiments are inverted with respect to the study described before (Figure 1.3.2.1 and Figure 1.3.2.2). The gyration around Y-axis (g_y) obtained from NiPAMS recordings is expected to be the same waveform as GCG-x signal in Figure 1.3.2.2, and the gyration around X-axis (g_x) is expected to look like the GCG-y signal in that figure.

Figure 1.3.2.4 and Figure 1.3.2.5 show the GCG signals detected for a generic subject during NiPAMS experiments (subject identified with number 225), for rest test and for holding breath at high lung volume test (HLV). Gyrations around X-axis and Y-axis (detected according to Figure 1.3.2.3) are reported for a heart period. They should be compared with the classical GCG waveforms seen in Figure 1.3.2.2.

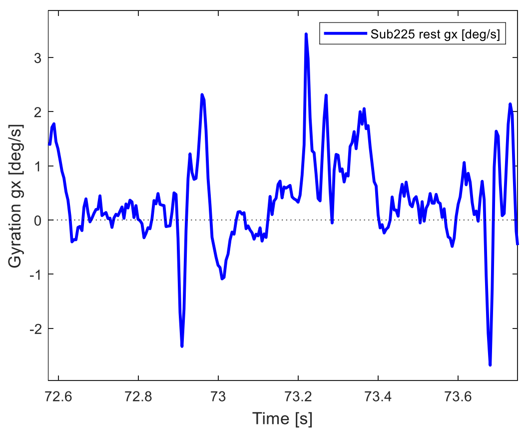

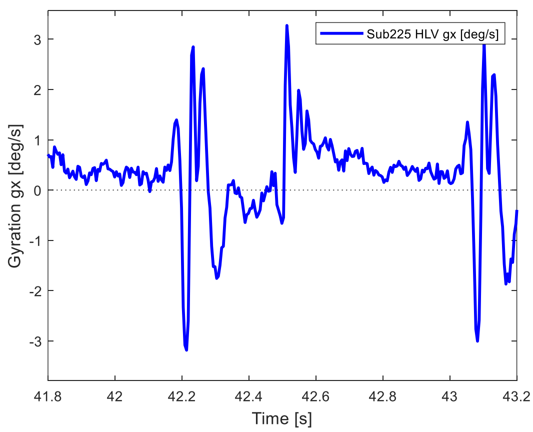

Figure 1.3.2.4 –Gyration around X-axis detected for subject 225, rest test (left) and holding breath at high lung volume HLV (right).

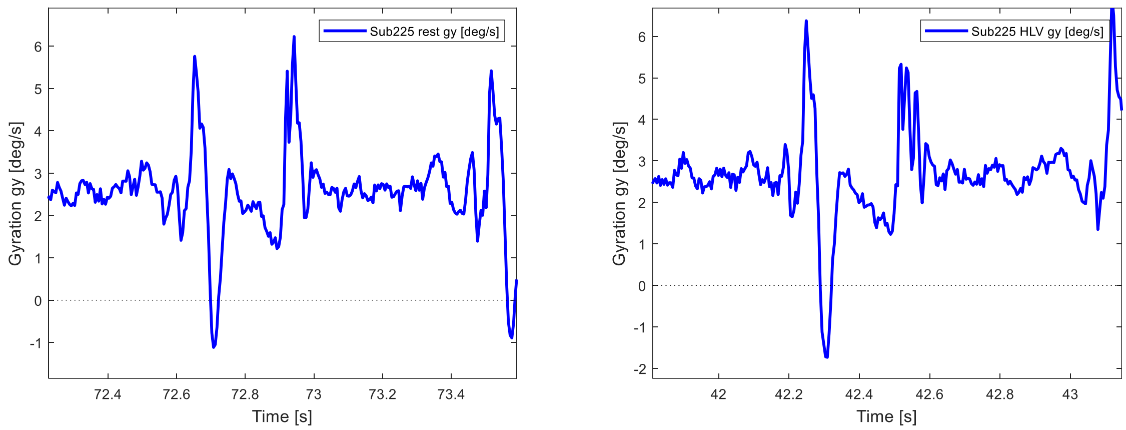

Figure 1.3.2.5 – Gyration around Y-axis detected for subject 225, rest test (left) and holding breath at high lung volume HLV (right).

It can be noted that some relevant peaks can be identified in the GCG signals detected and a more detailed correlation between gyration and cardiac activity can be investigated. However, some waveform variations exist when subject or test change.

2. Relevant hemodynamic concepts and parameters

The term "hemodynamics" refers to the dynamics of blood flow. There are some hemodynamic concepts and parameters that are widely used in NiPAMS project in order to achieve the objective. Therefore, it is useful to give a brief description of the most relevant ones. It will give a better insight of the procedure applied in this thesis.
First, it is important to have an overview of the pumping action of the heart, which determines blood flow and pressure.

2.1 Cardiac cycle and valve motion

The human heart pumps blood to every part of the body. The heart is made up of four chambers, the two top chambers are called the left and the right atrium and the bottom two chambers are called the left and right ventricles (Figure 2.1.1).
There are two valves in the left side of the heart. The mitral valve (MV) connects the left atrium and left ventricle. The aortic valve (AV) connects the left ventricle with the aorta. In the right side of the heart, there are other two valves: the tricuspid valve that connects right atrium and right ventricle, and the pulmonary valve that connects the right ventricle with the pulmonary artery [5].

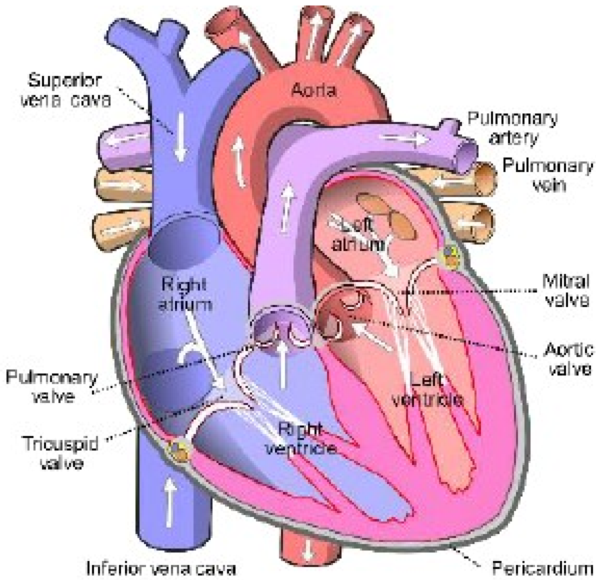

Figure 2.1.1 –Schematic of the heart.

The cardiac cycle is composed of two main phases: systole and diastole. The succession of a systolic and a diastolic phase represents a heart period.
This study focuses on the activity of the left ventricle because it is responsible for the circulation of blood through the body. Therefore, the cardiac cycle can be described looking at the left side of the heart.
During systole:

- The left ventricle contracts and mitral valve is closed (MC),
- The aortic valve opens (AO) and blood is ejected into the aorta,
- The left atrium is refilled passively,

- Ventricular pressure is higher than the aortic pressure: $p_{LV} > p_{aor}$.

During diastole:

- The left ventricle relaxes,
- The aortic valve closes (AC),
- The left ventricle is refilled by the atrium so the mitral valve opens (MO),
- Ventricular pressure is lower than the aortic pressure: $p_{LV} < p_{aor}$.

The cardiac cycle for right side of the heart is composed by the same phases as the left side. The operations of the mitral valve correspond to the tricuspid valve, while the operations of the aortic valve correspond to the pulmonary artery ones. Similarly, aortic pressure of the left side corresponds to pressure in the pulmonary artery on the right side.

The valve motion is directly correlated to blood pressure in heart. It is possible to visualise blood pressure waveforms with respect to valve operations in the so-called Wiggers diagram, in Figure 2.1.2. In addition, the ventricular volume change curve is reported over heart period. The relationship between pressure and volume will be discussed in details in the last chapter about pulsating heart modelling. That final chapter will also explain how ventricular and aortic pressure waveforms determine blood flow rate from left ventricle to the body. In the diagram below, there is also an electrocardiogram or ECG, which performs its R-peak at the beginning of each systolic phase. Another important information for the diagram below is the phonocardiogram or PCG. It shows the sounds made by the heart during a cardiac cycle, which are interpreted as two main impulses at the beginning of systole and diastole.

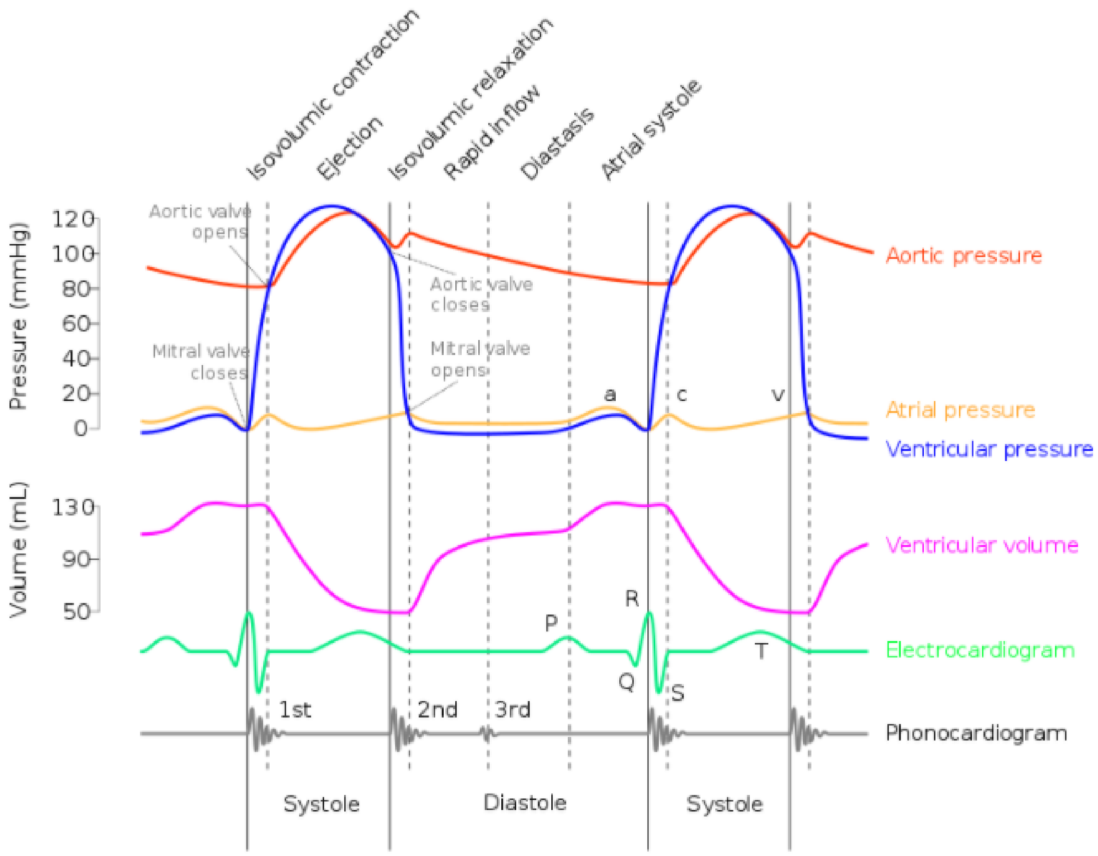

Figure 2.1.2 – Wiggers diagram with synchronized changes in aortic pressure (red line), left ventricular pressure (blue), left atrial pressure (yellow line), ventricular volume (magenta), ECG and PCG.

The Wiggers diagram usually refers to left side of the heart for the reason discussed above. However, for the right side of the heart, blood pressure and volume waveforms have the same trend and the same correspondence, over the entire heart period.

2.2 Central and Peripheral blood pressure

The methods used to measure blood pressure affect the type of pressure waveforms obtained. Mainly, it can be central or peripheral and the medical information that each one can provide is quite different. Recent studies demonstrate that central blood pressure is more strongly related to cardiovascular events than peripheral pressure, and responds differently to certain drugs [6]. Therefore, central pressure is becoming a fundamental measurement to take into account when evaluating cardiovascular diseases or other relevant events.
In fact, the final objective of NiPAMS project is to predict central blood pressure using accelerations and gyrations detected with Vibrational Cardiography.
Central blood pressure is also called aortic pressure because it is usually measured in the ascending aorta or at the aortic root. The most direct method to assess it involves cardiac catheterization in the ascending aorta, where a pressure-sensing catheter is used for blood pressure recording. This method proved the most reliable central pressure measurement but it is highly invasive. Actually, a number of non-invasive methods have been developed, where peripheral pressure waveform is recorded from carotid, brachial, radial or digital arteries. Then, the central pressure is estimated using a general transfer function from peripheral measurements. In the following figure [7], the sites commonly used for non-invasive measurements are shown: carotid artery in the neck, brachial artery in the upper arm, radial artery in the forearm and digital arteries in the fingers. The devices most used are tonometry for carotid and radial arteries and cuff-based oscillometry devices for brachial and digital arteries.

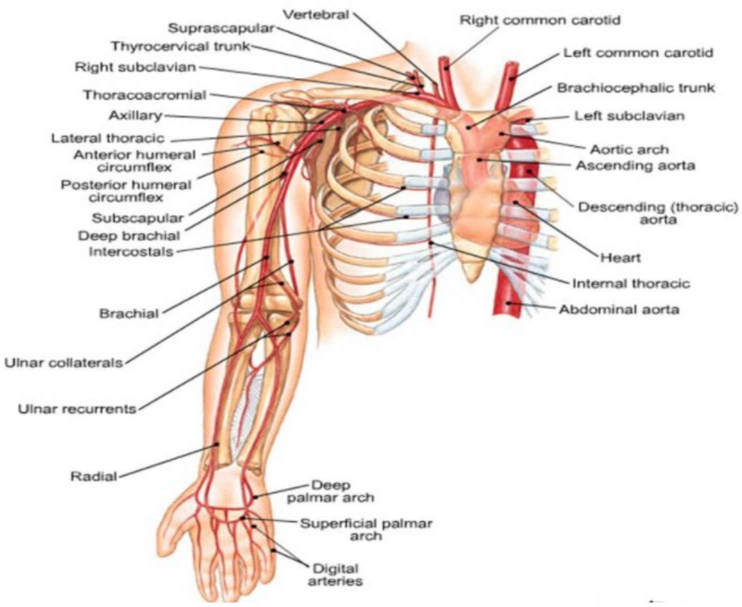

Figure 2.2.1 – Schematic of a part of the arterial tree where ascending aorta and carotid, brachial, radial and digital arteries are shown.

This difference exists because the shape of pressure waveform changes continuously through the arterial tree [6]. In particular, there is an amplification of pressure waveform moving away from aorta. It is maybe due to an increase in arterial stiffness moving from the aorta to the radial or digital arteries. In fact, as arteries become stiffer, the upper portion of the wave becomes narrower and the peak increases as shown in Figure 2.2.2.

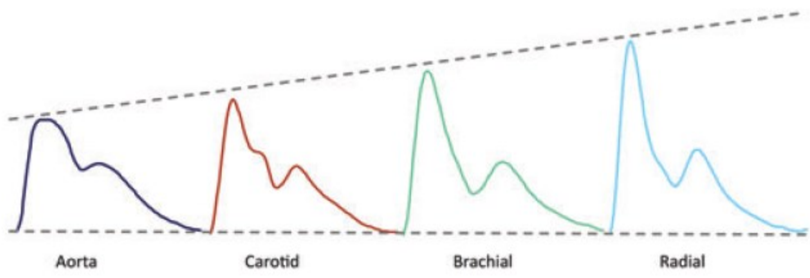

Figure 2.2.2 – Schematic of blood pressure amplification form aorta (central) to radial artery (peripheral).

2.2.1 Central pressure waveform and pulse pressure

During systole, ventricle contraction occurs and the ejection of blood into the arteries causes the pressure within the arteries to rise. The highest blood pressure reached is called Systolic Blood Pressure (SBP). During diastole, ventricular relaxation occurs and there is no active ejection of blood. The lowest pressure reached is called Diastolic Blood Pressure (DBP).
Pulse Pressure (PP) is the difference between SBP and DBP. Central aortic blood pressure waveform can be simplified as in Figure 2.2.1.1. It was obtained applying Windkessel model to arterial system [8].

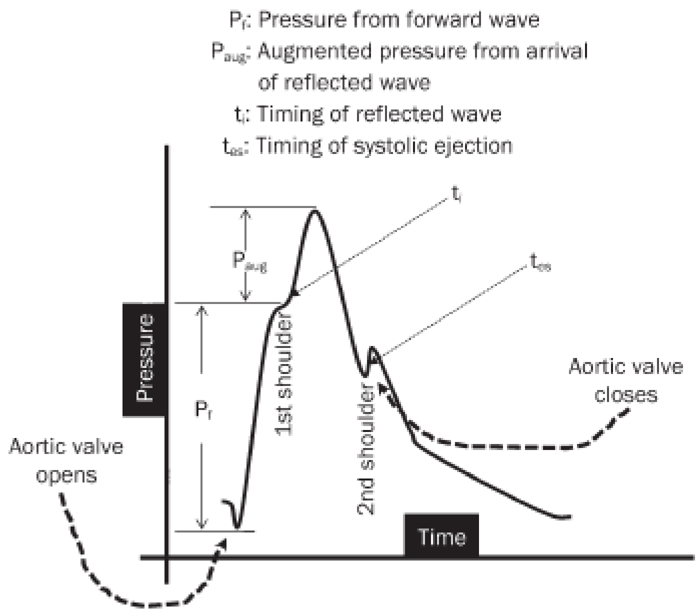

Figure 2.2.1.1 –Schematic of aortic pressure waveform.

When the aortic valve opens and systole starts, a forward propagated pressure wave is created in the aorta, it is called P_f in Figure 2.2.1.1. While it propagates, it encounters difference impedance when the elastic aortic wall gives way to the more muscular vessels. The elastic arteries ‘walls are made of elastic fibres gathered in concentric layers. They allow the vessels to distend when blood volume increases during systole. On the contrary, the more muscular vessels have walls composed of smooth muscle fibres, which maintain tone of the vessels and closely regulate blood flow. During systole, when the forward propagated wave faces with different impedance, two components of the wave arise. The first is a transmitted pressure wave (P_t) which has the same direction as P_f. The second is a backward pressure wave (P_b) that arrives at the aortic root at time t_i, in late systole and creates the first shoulder of the graph. It increases PP, so the corresponding rise in pressure is called pressure augmentation (P_{aug}), as shown in Figure 2.2.1.1. It must be noted that the waveform in the figure above refers to central aortic waveform that is different from the peripheral pressure. In late systole, the blood flow at the aortic root diminishes, so PP decreases rapidly until it reaches the second shoulder, when the aortic valve closes. The closure of the valve generates perturbations of pressure, therefore, after the second shoulder, the pressure rapidly reaches diastolic levels.

2.2.2 Augmentation index

The contribution of the reflected pressure wave to PP, called pressure augmentation (P_{aug}), is very important to study the physical state of the arterial system. For this reason, a mathematical parameter is used in pulse wave analysis: Augmentation Index (AI). The index is calculated as the increment in pressure from the first shoulder to the second systolic peak called ΔP, expressed as a percentage of the PP:

$$AI = \frac{\Delta P}{PP} \cdot 100\,[\%] \tag{2.2.2.1}$$

The following figure shows the pressures used in the equation.

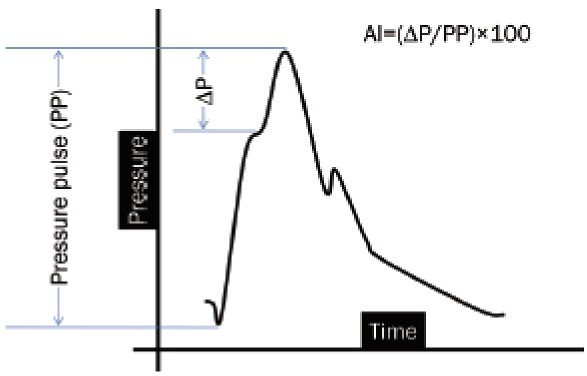

Figure 2.2.2.1 –Augmentation Index.

Augmentation index is directly dependent on these factors:

- Pulse wave velocity (PWV),
- Amplitude of the reflected wave,
- Cardiac cycle (heart rate).

It is used as a marker of aortic stiffness, too. The stiffening of central aortic vessels is strictly connected with aging. The aortic vessels stiffen as well as dilate with age. In fact, vascular aging is strongly associated with the presence of arteriosclerosis. The thickness of the aortic walls increases, stiffness increases and the reflected wave is conducted backwards with more efficiency, so tends to arrive in the ascending aorta during early systole. Therefore, the pressure augmentation contribution increases as well as PP peak. The transmitted and reflected waves are illustrated in Figure 2.2.2.2 with the effect of aging and stiffening of central aortic vessels.

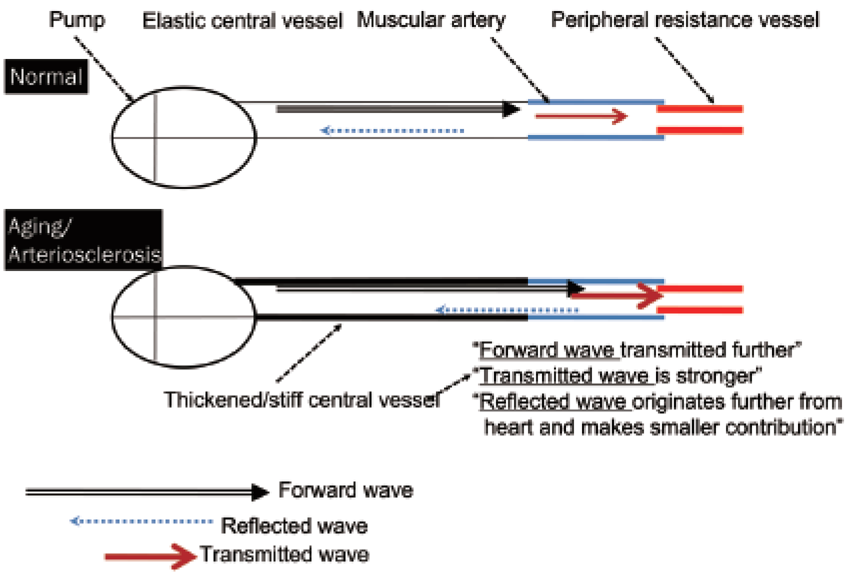

Figure 2.2.2.2 –Schematic of reflected and transmitted wave with stiffening and aging effects.

The same effects can be seen in the corresponding aortic pressure waveform in the following figure.

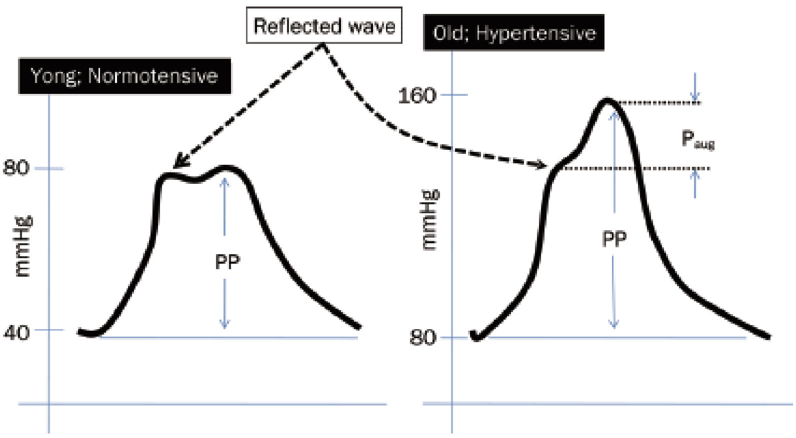

Figure 2.2.2.3 –Schematic of reflected wave for young and old people.

The relationship between AI and heart rate (HR) was found experimentally in 2002 [9] that will be described in detail in the following chapter. The augmentation index was calculated from the central pressure waveform. The results showed that AI declines linearly when HR increases. In fact, a linear regression analysis was performed. The slope of the regression line was -0.56, it means that there is a reduction of 5.6% of AI for each HR increment of 10 beats/min (Figure 2.2.2.4).

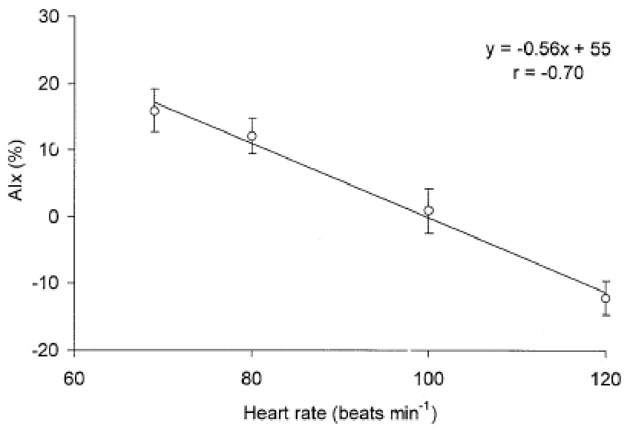

Figure 2.2.2.4 – Relationship between augmentation index (AI) and heart rate (HR), linear regression.

2.3 Heart rate

Heart Rate (HR) is the number of times the heart beats per minute. A heartbeat includes a heart period, that means a systolic and a diastolic phase together, or the distance between two R-peaks of ECG signal. The best places to find it are wrists, side of the neck, top of the foot or inside the elbow [10].

The resting heart rate is the heart pumping the lowest amount of blood because the subject is not doing exercises. Normally it is between 60 and 100 beats/min or bpm. Resting HR is usually lower than 60 bpm for very active people, because their heart muscle works better and it does not need to work hard to maintain a steady beat. Other factors that can affect HR are:

- Air temperature, when temperature increases, the heart tends to pump more blood,
- Body position, resting sitting or standing the pulse remains the same, it slightly changes while standing up,
- Emotions, for example stress or anxiety can increase HR,
- Body size, with high obesity HR increases,
- Medication use, for example medications that slow adrenaline tend to slow pulse.

When HR increase, a greater volume of blood is pumped and healthy blood vessels dilate.

It must be noted that HR and blood pressure (BP) do not change at the same rate. For example, during exercises, HR could become double safely, while BP may respond by only increasing a modest amount. When the exercise ends, HR does not return normal immediately, it depends on how much fit is the subject.

For NiPAMS experimental work, the heart rate was recorded for each subject during all the duration of the tests performed. Figure 2.3.1 shows the HR measurement for a single subject using the proposed monitoring system (NiPAMS) [11]. The HR was obtained with the auto correlated differential algorithm ADA that provides heart rate monitoring starting from SCG and GCG. A beat detection was also performed using ECG as a reference.

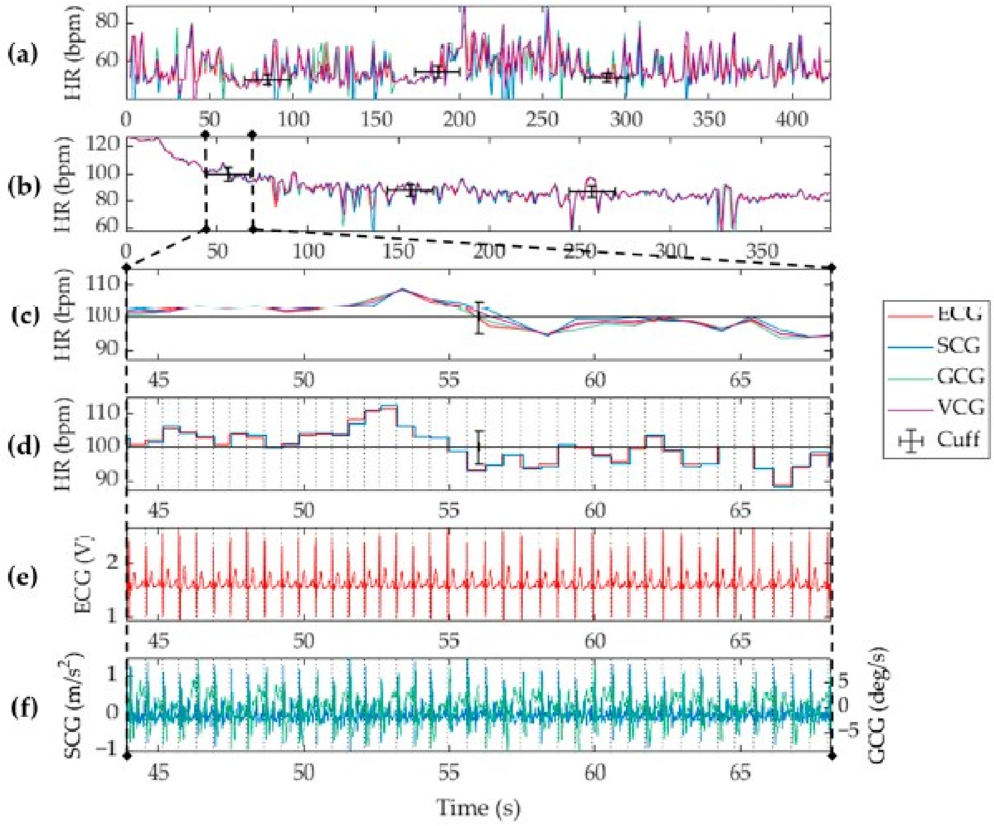

Figure 2.3.1 – Biometric measurements using the proposed cardiac monitoring system from a single subject lying supine at rest (a) and during recovery from physical exertion (b) with a zoom on ADA-based heart rate (c) and beat-to-beat based heart rate (d) are shown.

It can be noted that the NiPAMS autocorrelated approach smooths heart rate measurements, as seen comparing ADA results with instantaneous heart rate. Therefore, heart rate has been properly recorded with the proposed real-time monitoring system and ADA algorithm.

2.4 Left Ventricular Ejection Time

Left Ventricular Ejection Time (LVET) is defined as the time of ejection of blood form the left ventricle. It begins with the aortic valve opening (AO) and ends with the aortic valve closure (AC). Therefore, the LVET can be provided from SCG as the interval between AO and AC. Furthermore, it could be derived from ICG as the interval between B and X points. It is shown in the following figure [12], where also pre-ejection period (PEP), total systolic time (TST) and electromechanical delay (EMD) are represented.

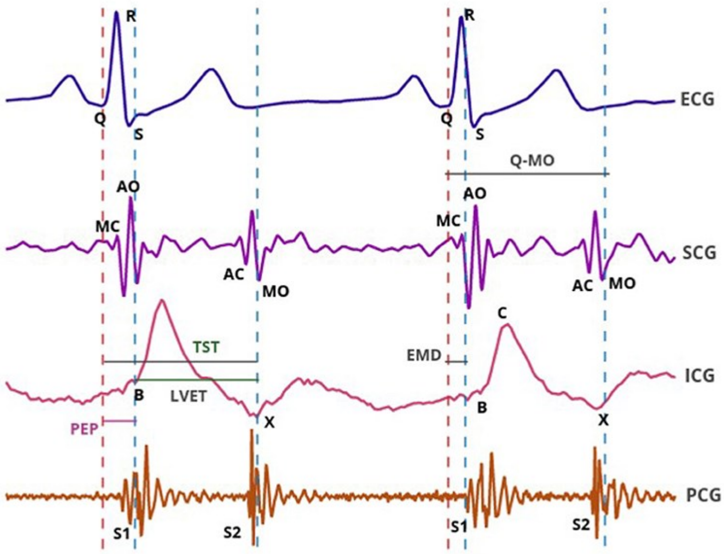

Figure 2.4.1 – Simultaneous sample recordings of ECG, SCG, ICG and PCG
for a 40 years old man in supine position.

So LVET definition can be written as:

$$LVET = t_{AC} - t_{AO} \tag{2.4.1}$$

It can be noted that LVET does not exactly correspond to systolic phase. Generally, systole is assumed to start when mitral valve closes, which is at the R-peak of ECG, as shown in Figure 2.1.2. Besides, it does not include all the pre-ejection period PEP illustrated in Figure 2.4.1. However, systolic phase can be approximated properly by LVET. Therefore, heart period (T) can be defined as the sum of the LVET and diastolic time (DT). It corresponds to the reciprocal of the heart rate, where HR is in bpm and T in seconds:

$$T = \frac{60}{HR} \tag{2.4.2}$$

$$T = LVET + DT \tag{2.4.3}$$

The diastolic time is the interval between the mitral valve opening and mitral valve closure. It is the period when the left ventricle fills with blood from the left atrium, it corresponds to diastolic phase. It is shown in Figure 2.4.2 for the central aortic pressure curve [13].

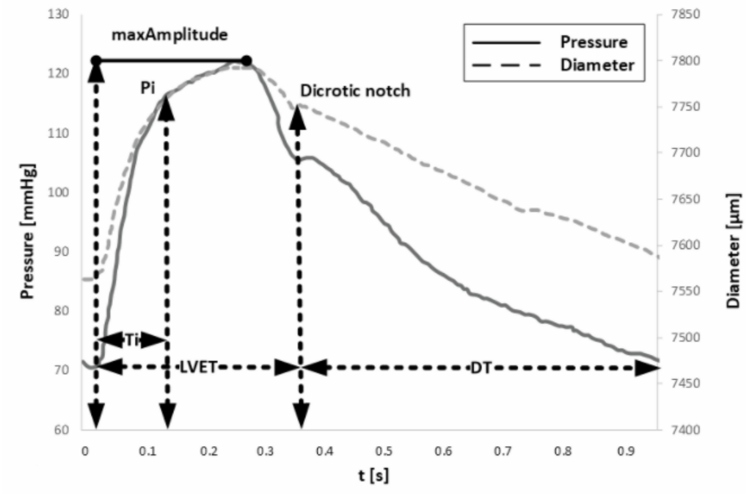

Figure 2.4.2 – Central aortic pressure and aortic diameter waves with LVET, DT and dicrotic notch.

A previous experimental study [14] measured pressure and timing values for seventeen males who were heart transplant recipients around 50 years old. They performed tests at rest and cold pressor tests (CPT). Beat-to-beat changes and the spontaneous fluctuations in heart period, LVET and DT were considered. A strong relationship was found between heart period and DT, with a correlation coefficient r=0.96. Meanwhile, the relationship between heart period and LVET was less relevant, with r=0.45. They are showed in the following figure.

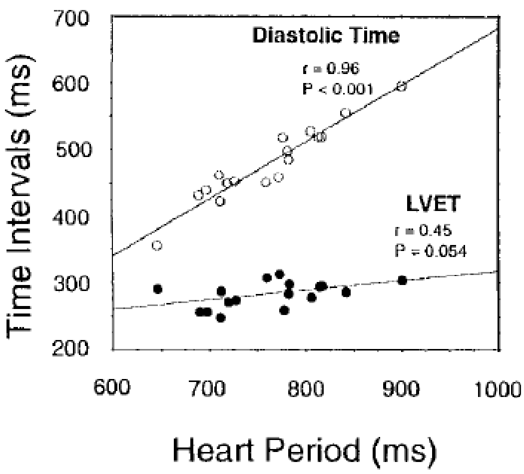

Figure 2.4.3 – Relationship between heart period, DT and LVET in one subject at baseline.

Furthermore, in all patients, there was a strong positive linear relationship between beat-to-beat LVET and beat-to-beat PP. It is shown in Figure 2.4.4 for all patients at baseline, over a continuous 15 s period with 20±2 beats.

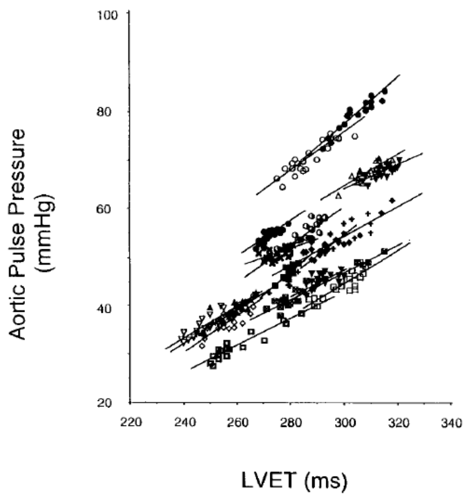

Figure 2.4.4 – Relationship between LVET and pulse pressure for all patients at baseline (each patient is represented by a different symbol).

Figure 2.4.5 shows how aortic pulse pressure varies with LVET for one patient, at baseline and cold pressor test. It was found a strong positive linear relationship in both cases. Compared with baseline, with CPT pulse pressure increased, LVET increased but DT decreased, because the total heart period decreased. In fact, a strong negative linear relationship was found between PP and DT.

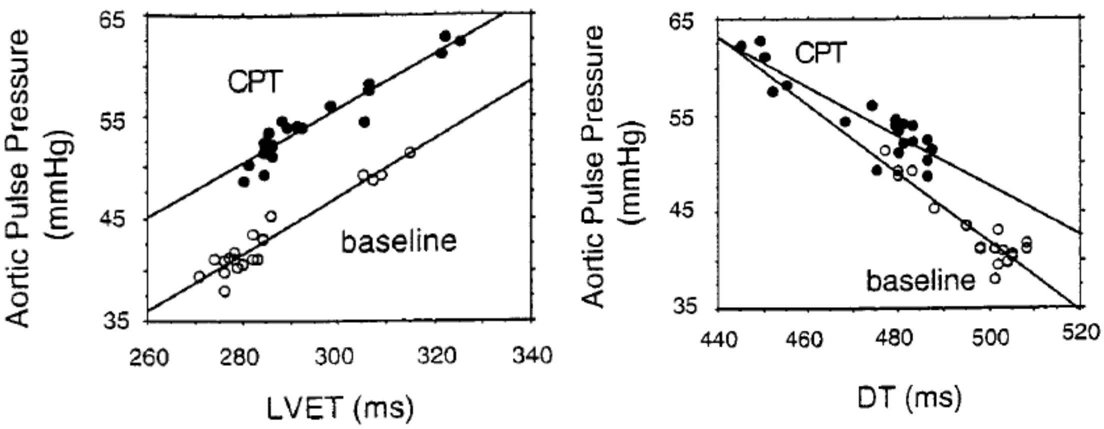

Figure 2.4.5 – Relationship between aortic pulse pressure and LVET (left) and DT (right) at baseline and cold pressor test for one subject.

2.5 Blood flow parameters

2.5.1 Cardiac Output and Stroke Volume

Each time the heart beats, a volume of blood contained within the left and right ventricles is ejected into the aorta and pulmonary artery, respectively. The volume of blood pumped by the left and right ventricles every minute is the cardiac output (CO), usually given in litres per minute. Generally, CO is defined as [15]:

$$CO = HR \cdot SV \tag{2.5.1.1}$$

where HR is the heart rate often given in beats/min and SV is the stroke volume, that in Eq. 2.5.1.1 should be expressed in litres (or dm^3) in order to give a CO in l/min, which are medical units.
The average amount of blood ejected each beat into the aorta is the same as the volume of blood ejected into the pulmonary artery and it is called stroke volume [18]. In fact, stroke volume (SV) is the volume of blood pumped out of the left ventricle during each systolic cardiac contraction. The blood that fills the heart by the end of diastole, which is called end-diastolic volume (EDV) cannot be ejected at all from the heart during systole. Therefore, the volume left in the heart at the end of systole is called end-systolic volume (ESV). The SV volume may be calculated as the difference between these two volumes:

$$SV = EDV - ESV \tag{2.5.1.2}$$

Another way to derive stroke volume is the integration of the blood flow rate Q over heart period T:

$$SV = \int_0^T Q(t)\ dt \tag{2.5.1.3}$$

It means that the area under the graph of blood flow rate waveform represents the volume of the blood ejected per cardiac cycle. The SV is usually in ml/beat in medical units.
The following figure [17] shows the stroke volume defined in the pressure-volume diagram. The point E in Figure 2.5.1.1 represents the maximum systolic pressure.

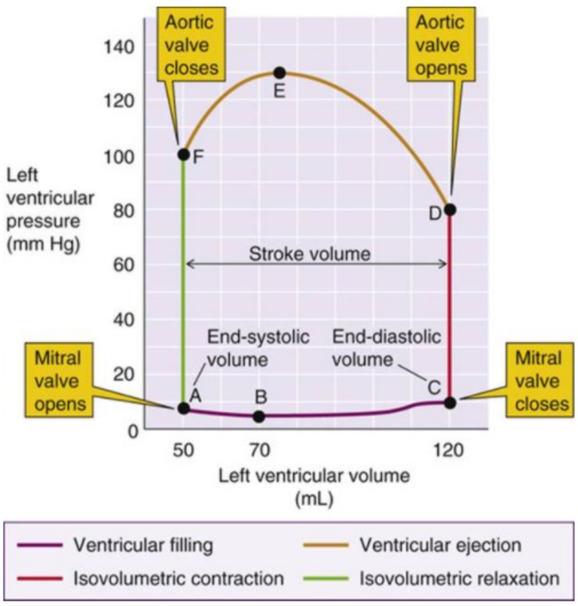

Figure 2.5.1.1 – Left ventricular pressure and stroke volume during cardiac cycle.

An increase in stroke volume increases pressure because an extra volume of blood is pumped into the aorta during each heartbeat. Therefore, a large stroke volume, as it can be seen in trained athletes, increases systolic pressure or maintains it at a steady level. In the same time, heart rate decreases to allow more time between beats, and the diastolic pressure decreases. Figure 2.5.1.2 shows how pressure changes with stroke volume variation [18].

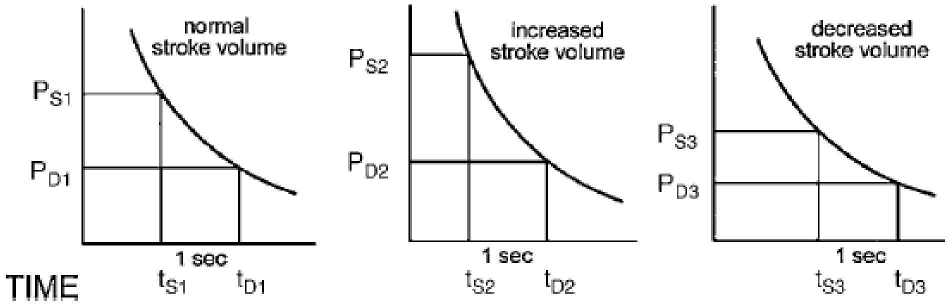

Figure 2.5.1.2 – Effect of stroke volume on pressure.

Another study [19] considered the volume of blood ejected into the aorta up to the time of peak pressure. They used a 2-element Windkessel model to simulate the blood pressure and calculate the pulse pressure. However, the relationship obtained is shown in the following figure.

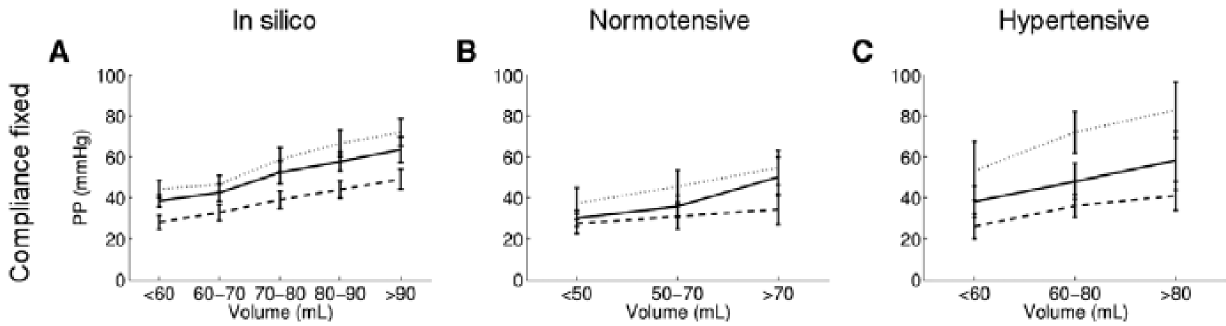

Figure 2.5.1.3 – Effect of volume of blood ejected up to peak pressure on pulse pressure, using 2-element Windkessel model, for in silico, normotensive and hypertensive data. The compliance is fixed at 0.5-1 ml/mmHg (solid line), 0.1-0.5 ml/mmHg (dashed line), 1-1.5 ml/mmHg (dotted line).

The volume considered in Figure 2.5.1.2 is correlated to stroke volume; it was found a correlation coefficient r = 0.86 and a p-value lower than 0.001. Therefore, as stroke volume increases, pulse pressure increases slightly. The volume used in graph in Figure 2.5.1.3 can be approximated with the stroke volume.

2.5.2 Capacitance

The arterial capacitance represents the compliance of the blood vessel that is the aorta in the specific case. It can be shown that the compliance C_V of a cylindrical vessel of radius R_i, length L, wall thickness h and Young's modulus of elasticity E is [13]:

$$C_V = \frac{3\pi R_i^{\,3} L}{2Eh} \tag{2.5.2.1}$$

The arterial compliance is usually expressed in ml/mmHg in medical units.
A previous study [14], demonstrated that the total arterial compliance can be estimated only suing the stroke volume to pulse pressure ratio. They performed some experiments and reported the results in the following graph.

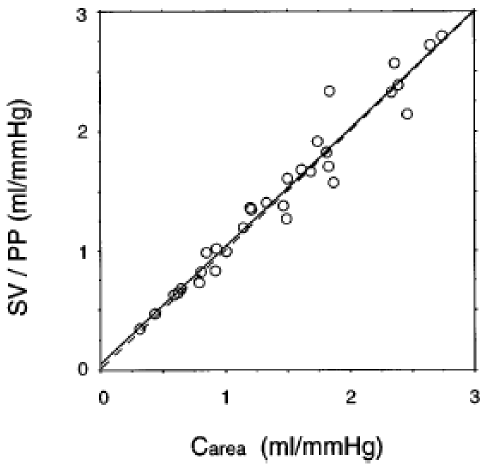

Figure 2.5.2.1 – Relationship between arterial compliance (C_{area}) and SV/PP.

The results show a linear regression:

$$\frac{SV}{PP} = 0.99 C_{area} + 0.05 \qquad (2.5.2.2)$$

with a correlation coefficient: r = 0.98. The conclusion was that the ratio SV/PP gives a reliable estimate of arterial compliance.
When the stroke volume is fixed, if compliance increases, the pulse pressure decreases. This inverse relationship between compliance and volume was also found by the study seen in the previous paragraph [18], as shown in the following figure.

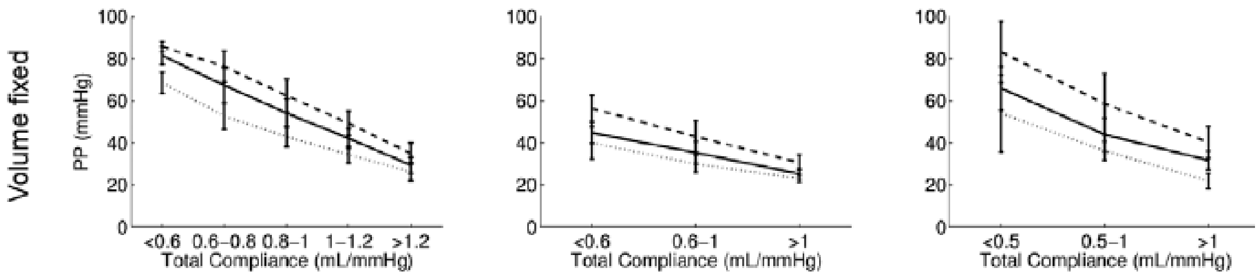

Figure 2.5.2.2 – Effect of total arterial compliance on pulse pressure, using 2-element Windkessel model, for in silico, normotensive and hypertensive data. The volume is fixed at 60-70 ml (solid line), 80-90 ml (dashed line), 40-90 ml (dotted line).

2.5.3 Resistance

The resistance refers to the blood flow resistance that the specific blood vessel encounters. There is an arterial resistance and a peripheral resistance. The medical unit for resistance is mmHg/ (ml/s).
The arterial resistance R_V is the resistance encountered by the artery considered. In this case it is the ascending aorta. It can be calculated as:

$$R_V = L\left(c_v \frac{8\mu}{\pi R_i^{\ 4}}\right) \qquad (2.5.3.1)$$

where c_v is the resistance coefficient, μ is the blood viscosity, L is the length of the vessel considered and R_i is the internal radius of the vessel. All these coefficients can be found considering the kind of vessel.
The peripheral resistance R is the resistance encountered by the systemic arterial system. It can be defined as.

$$R = \left(\frac{60}{1000}\right)\frac{MAP}{CO} \qquad (2.5.3.2)$$

where CO is the cardiac output as defined in Eq. (2.5.1.1) and MAP is the mean arterial pressure of the entire cardiovascular system. MAP can be defined with the following equation, with the systolic blood pressure P_s and the diastolic blood pressure P_d.

$$MAP = P_d + \frac{1}{3}(P_s - P_d) \qquad (2.5.3.3)$$

The peripheral resistance comes from the resistance found in capillaries, and when more capillaries are open, there will be a lower resistance. If the need for oxygenated blood increases in peripheral tissues, more capillaries open to allow more blood to flow into the tissue, so the peripheral resistance decreases. The following figure shows how pressure changes with peripheral resistance. It can be noted that when peripheral resistance decreases, the systolic pressure decreases but the pulse pressure value increases.

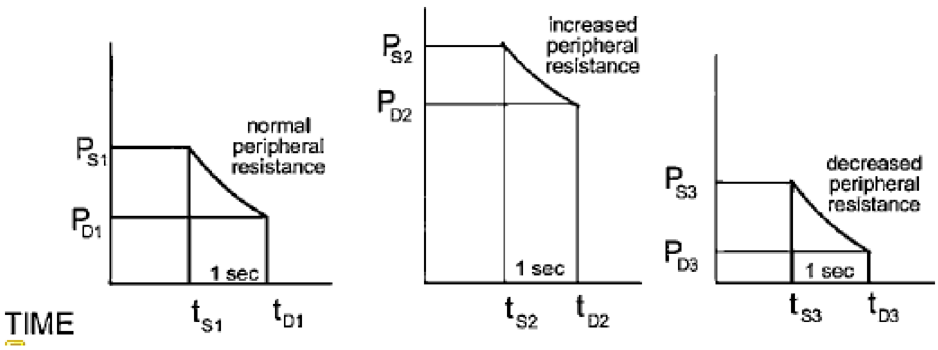

Figure 2.5.3.1 – Effect of peripheral resistance on pressure.

2.5.4 Inductance

The inductance L_V is the inertia of the blood flow in the vessel considered. In the case of ascending aorta it can be defined as:

$$L_V = L\left(c_u \frac{\rho}{\pi R_i^{\ 2}}\right) \qquad (2.5.4.1)$$

where c_u is the so-called "inertance" coefficient, which is a coefficient for inductance defintion, and ρ is blood density. The medical units for inductance is mmHg/(ml/s^2).
The inductance coefficient c_u and the resistance coefficient c_v are called Fry parameters. They are important coefficients to consider the fluid parameters as electrical parameters. They can be obtained from the curve of Womersley number. The Womersley number α is defined as:

$$\alpha = R_i \left(\sqrt{\frac{\omega_{HR} \rho}{\mu}} \right) \tag{2.5.4.2}$$

with:

$$\omega_{HR} = 2\pi f \tag{2.5.4.3}$$

$$f = \frac{HR}{60} \tag{2.5.4.4}$$

where f is the frequency of the heartbeat in Hz and HR is the heart rate in beats/min.
The corresponding figure of the Womersley number and coefficients is shown in the following figure.

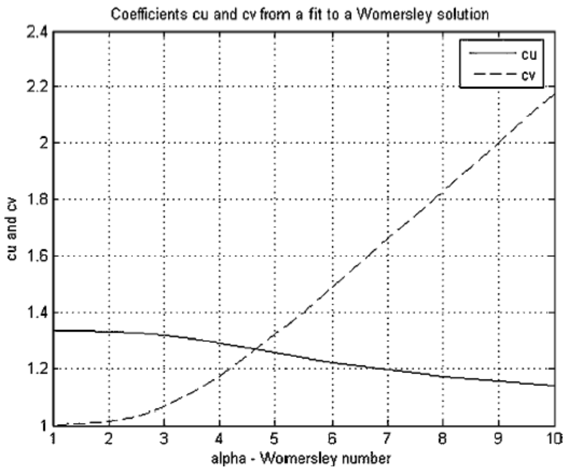

Figure 2.5.4.1 – Graph of inductance coefficient c_u and resistance coefficient c_v to fit a Womersley solution.

3. Time-frequency domain analysis

One of the main objective of the NiPAMS project is to find an analytical correlation between the blood pressure and the vibrational cardiography (VCG) signals measured. In order to do that, low frequencies have to be considered because heart rate occurs around 1 Hz for all subject. In the same time, at higher frequencies, other noisy and events occurring during experiments could have been detected.
Therefore, heart rate frequency for a test of a single subject is considered, together with some super harmonics obtained multiplying it by integer numbers 2, 3, 4 and 5. It is interesting to see which harmonics represent a significant frequency content of the VCG signal detected. This evaluation will be performed thanks to CWT spectrograms of the signal measured. In particular, a single test for a single subject is initially counted, that is rest test for subject 225. Then, some examples of inter-subject and intra-subject variations will be provided, which are HLV test for subject 225 and rest test for subject 19. These subjects have been chosen because they mainly show a steady state in time-frequency domain.

3.1 Heart rate frequency and super harmonics

Experimental measurements of heart rate for NiPAMS tests show that heart rate always varies over time. Since it slightly varies during the duration of a test, it is reasonable to assume a mean value.
Obviously, all the signals detected during the same test have the same heart rate.

3.1.1 Rest test

In this case, experimental data from test at rest for subject 225 are counted. The corresponding mean heart rate frequency for rest test is:

$$\text{mean}(f_{HR}) = 1.34 \text{ Hz} \tag{3.1.1.1}$$

Multiplying heart rate frequency by 2, 3, 4 and 5, the super harmonics of the heart rate can be calculated. Also for super harmonics, the mean values over time are calculated:

$$\text{mean}(f_{HR} \cdot 2) = 2.67 \text{ Hz} \tag{3.1.1.2}$$

$$\text{mean}(f_{HR} \cdot 3) = 4.01 \text{ Hz} \tag{3.1.1.3}$$

$$\text{mean}(f_{HR} \cdot 4) = 5.34 \text{ Hz} \tag{3.1.1.4}$$

$$\text{mean}(f_{HR} \cdot 5) = 6.68 \text{ Hz} \tag{3.1.1.5}$$

It can be noted that the heart rate frequencies determined above are true only for the rest test considered. In particular, the heart rate mean value for another test for the same subject 225 will be slightly different.

3.1.2 Intra-subject variation: HLV test

For the same subject 225, another test is considered, that is holding breath at high lung volume HLV. As expected, heart rate is different from the rest test and it slightly changes over time. In this test, the frequency of the heart rate is:

$$\text{mean}(f_{HR}) = 1.11 \text{ Hz} \tag{3.1.2.1}$$

Multiplying heart rate frequency by 2, 3, 4 and 5, the super harmonics of the heart rate can be calculated. It results that in HLV test, the heart rate frequency is a bit lower than rest test and this behaviour occurs for super harmonics, too.

3.1.3 Inter-subject variation: rest test of another subject

In addition, there is a variation of heart rate between different subjects. It means that, for example, for subject 19, the heart rate measured each instant of the time interval considered, will be different from the values measured for subject 225 during the same timeframe. Therefore, considering the same rest test for subject identified with number 19, the frequency of the heart rate is:

$$\text{mean}(f_{HR}) = 1.14 \text{ Hz} \tag{3.1.3.1}$$

It is a bit lower than the heart rate frequency for rest test of subject 225. It means that also the related super harmonics will be a bit lower. However, the difference is very tight so that it can be assumed negligible.

3.2 Time-frequency analysis: rest test

VCG signals detected during NiPAMS experiments are analysed in time and frequency domain. The objective is to see how much heart rate frequencies are representative of VCG frequencies. Another goal is to figure out which super harmonics are significant to describe the detected signals in time-frequency domain. Finally, the main frequency range of the VCG signals measured will be determined.
In order to do this study, a single test performed for one subject is considered. Rest test of subject denoted with number 225 is used in this study. The signals counted are gyration around X-axis detected by the MEMS accelerometer placed on the sternum, and the non-invasive blood pressure NIBP measured at the finger.

3.2.1 Gyration around X-axis

Gyration around X-axis is an angular velocity detected by the accelerometer placed at sternum. Data has been detected for the entire duration of the test, with a constant delta-time between each sample. The following graph demonstrates that the delta-time of gyration data acquired have a constant delta time.

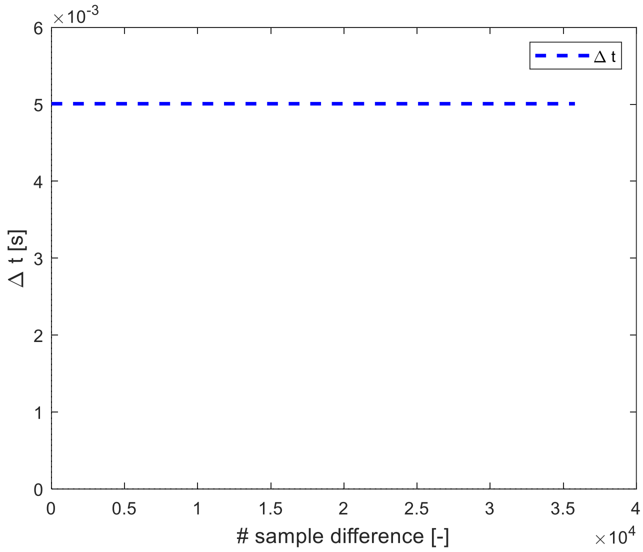

Figure 3.2.1.1 – Delta-time of gyration around X-axis for subject 225, rest test.

It can be noted that the delta-time is equal to 0.005 s because it depends on the sampling frequency assumed. For NiPAMS data acquisition, the sampling frequency has been assumed to be 200 Hz because the most important events for blood pressure occur within 50 Hz, so an integer multiple of it is considered. The following figure shows a generic trend of the gyration g_x signal measured over time.

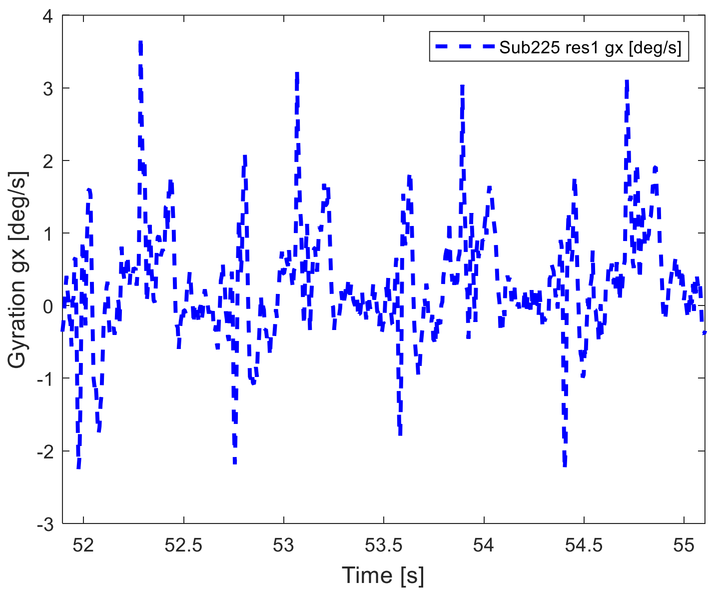

Figure 3.2.1.2 – Gyration around X-axis over a reduced time interval of rest test, for subject 225.

The gyration signal acquired is expressed in frequency domain with its Fast Fourier Transform FFT, in particular its modulus and phase.

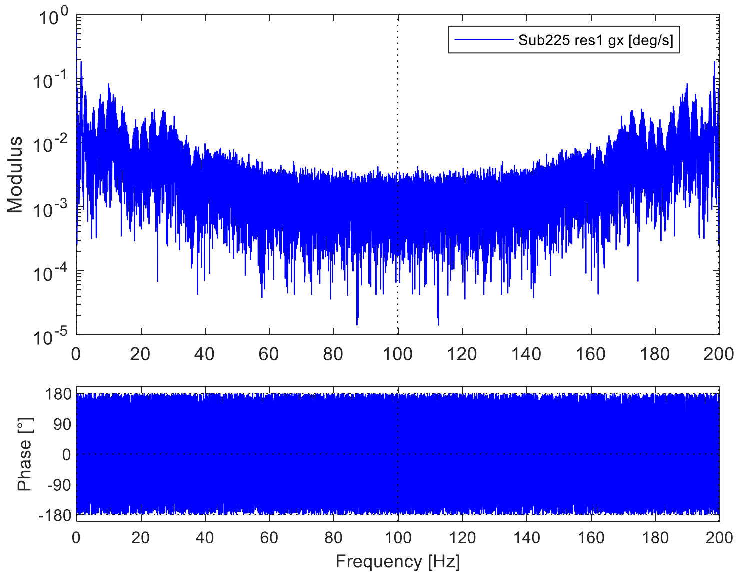

Figure 3.2.1.3 – FFT modulus and phase for g_x signal (blue solid line),
for rest test of subject 225.

It can be noted that the FFT modulus is symmetric with respect to the Nyquist frequency, while the phase is antisymmetric.

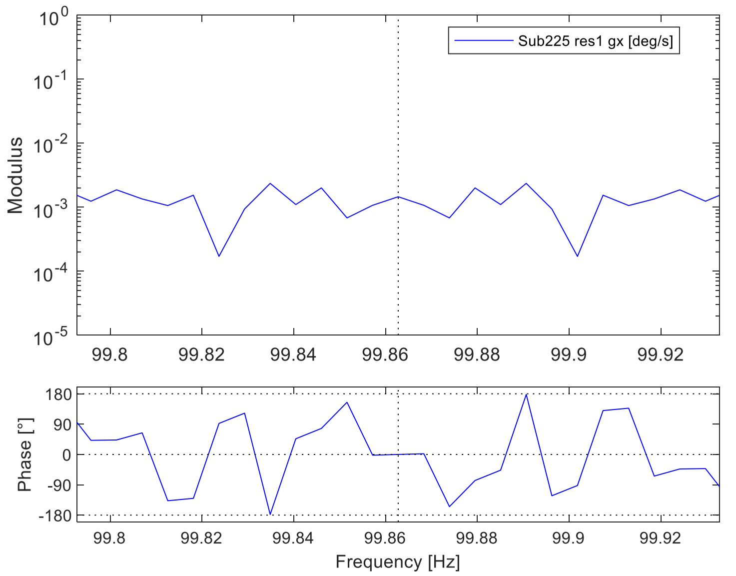

Figure 3.2.1.4 – FFT modulus and phase for g_x signal (blue solid line), detail of symmetric modulus and antisymmetric phase respect to the Nyquist frequency (black dashed line) for rest test, subject 225.

The same signal detected can be analysed in time-frequency domain. For example, Continuous Wavelet Transform CWT is used to obtain its spectrogram.

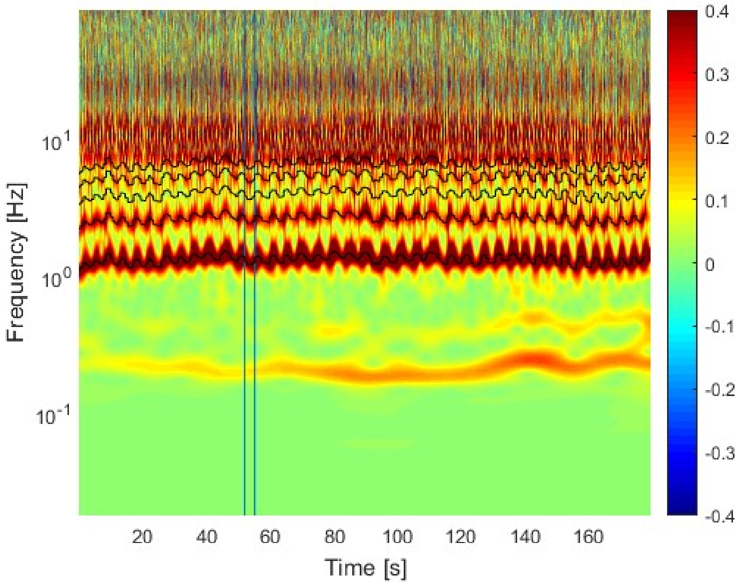

Figure 3.2.1.5 – Gyration g_x in time-frequency domain with CWT, for rest test of subject 225; blue lines indicates the reduced time window considered.

A reduced time window is considered in the following analysis in order to achieve the objective. The time window has been chosen so that the gyration signal remains exactly periodic in the window selected. The main reason is that band pass filters will be applied to it and the windowed signal must be periodic in order to avoid leakage problem. It is delimited by two blue vertical lines in the figure above and it is:

$$51.89\ \mathrm{s} \leq t_w \leq 55.1\ \mathrm{s} \tag{3.2.1.1}$$

Looking at the reduced window, overlapping heart rate frequency and super harmonics in the time-frequency graph, it is possible to figure out which frequencies are the most significant.

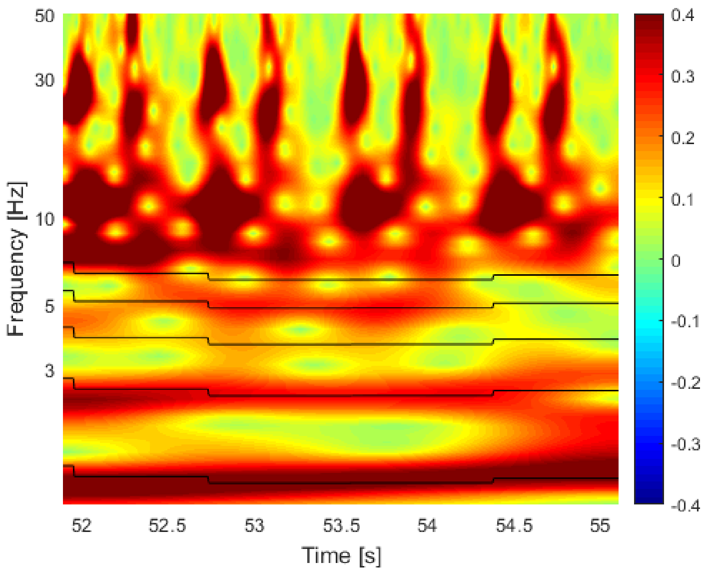

Figure 3.2.1.6 – Gyration g_x in time-frequency domain with CWT, for a reduced time window, with heart rate frequencies and super harmonics (black solid lines), for rest test of subject 225.

It can be noted that the heart rate frequency with a mean of 1.34 Hz represents a very high contribution in frequency. Then, the heart rate multiplied by 2 and 4 show the highest frequency contents. Figure 3.2.1.6 shows another high contribution in frequency from 7 Hz to 20 Hz.
In order to find out the main range of frequency for gyration signal, a band pass filter can be applied. Initially, a filter passing all frequencies form 0 Hz to 23 Hz is applied to the FFT of the gyration.

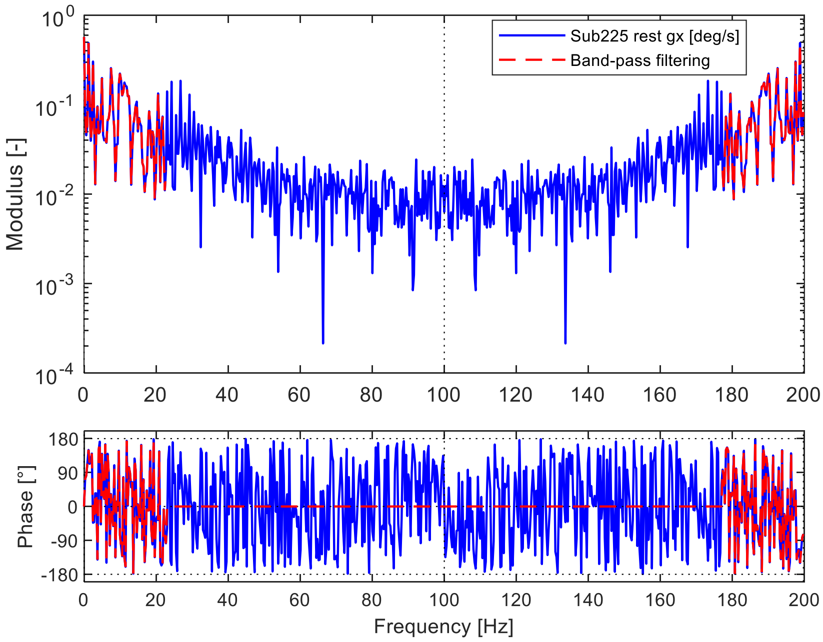

Figure 3.2.1.7 – FFT modulus and phase for g_x signal in the reduced time window considered (blue solid line) with the band filtered from 0 Hz to 23 Hz (red dashed line).

The filtered signal in frequency domain is converted into a signal in time domain applying Inverse Fast Fourier Transform IFFT. It can be noted that the signal obtained using only frequencies up to 23 Hz is quite a good representation of the original signal. There are some peak values that are only approximated, so it may mean that they depend on events occurring after 23 Hz.

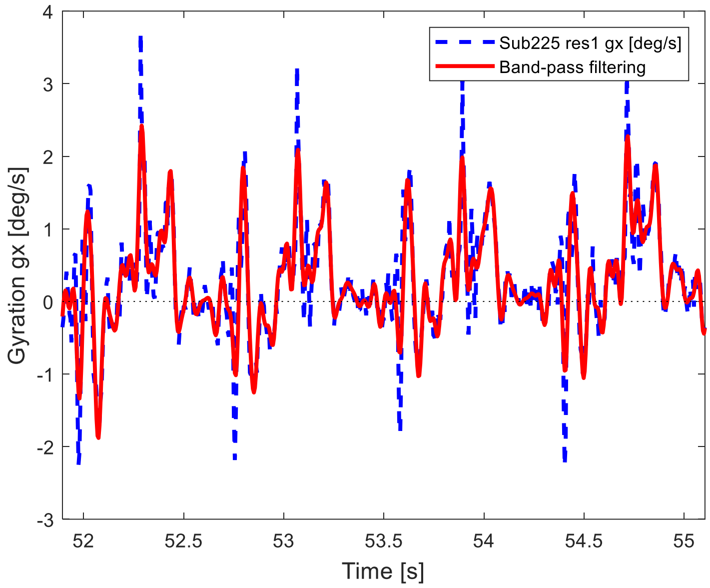

Figure 3.2.1.8 – Gyration g_x for subject 225 at rest test, in time domain, original signal (blue dashed line) and after a band pass filter from 0 to 23 Hz (red solid line), for the reduced time window.

Considering a larger frequency range for band pass filtering, a very good result is obtained. In particular, passing frequencies up to 30 Hz, the original gyration signal in time domain is represented entirely.

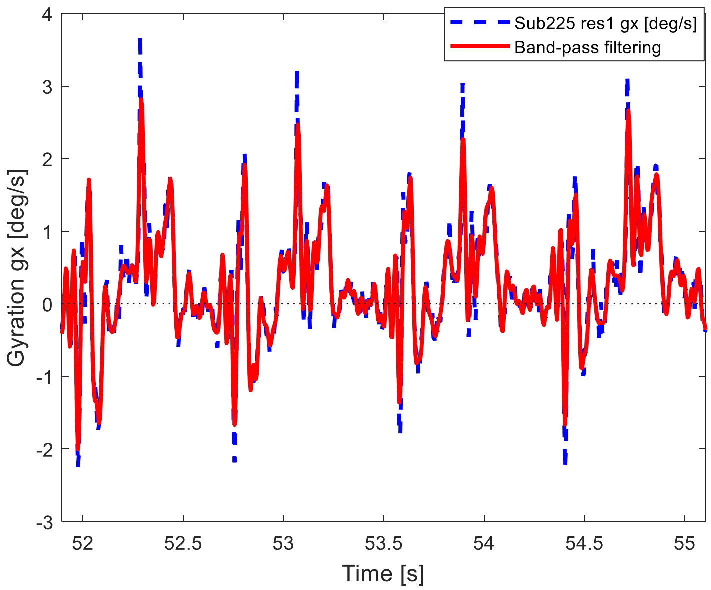

Figure 3.2.1.9 – Gyration g_x for subject 225 at rest test, in time domain, original signal (blue dashed line) and after a band pass filter from 0 to 30 Hz (red solid line), for the reduced time window.

3.2.2 Acceleration around Y-axis

Another kind of signal detected experimentally is acceleration. In this case, acceleration measured along Y-axis for rest test of subject 225 is considered. The duration of the test is the same as the gyration discussed above, so the constant delta-time of timestamps has been already demonstrated.
This is the acceleration signal detected in a generic time interval, in time domain.

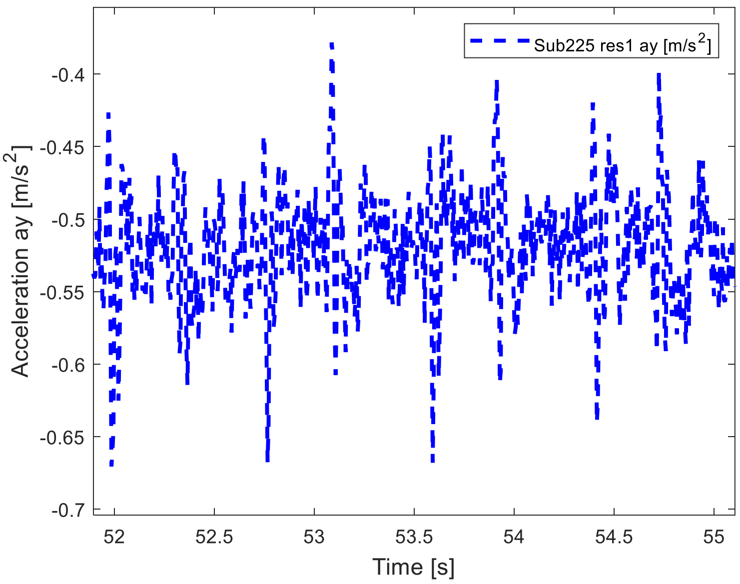

Figure 3.2.2.1 – Acceleration along Y-axis over a reduced time interval of rest test, for subject 225.

The acceleration signal acquired is expressed in frequency domain with its Fast Fourier Transform FFT, in particular its modulus and phase.

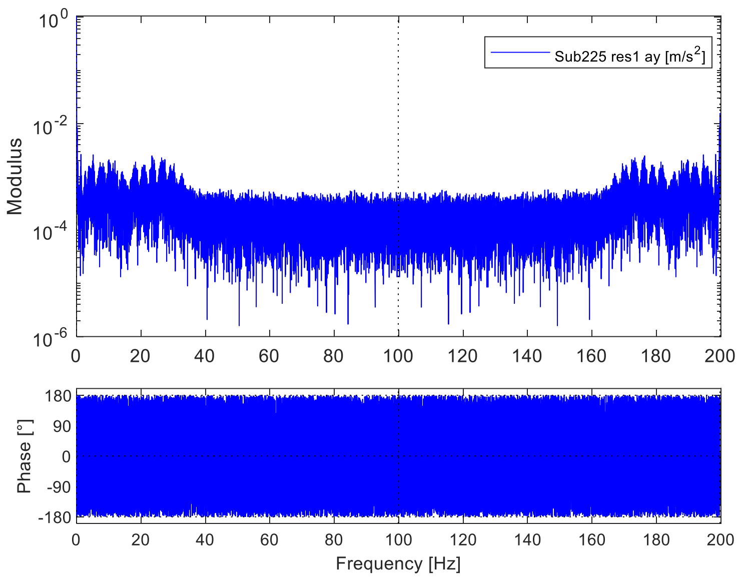

Figure 3.2.2.2 – FFT modulus and phase for a_y signal (blue solid line), for rest test of subject 225.

It has been already seen in details that the FFT modulus is symmetric with respect to the Nyquist frequency, while the phase is antisymmetric.
The same signal detected can be analysed in time-frequency domain. Continuous Wavelet Transform CWT is used to obtain its spectrogram.

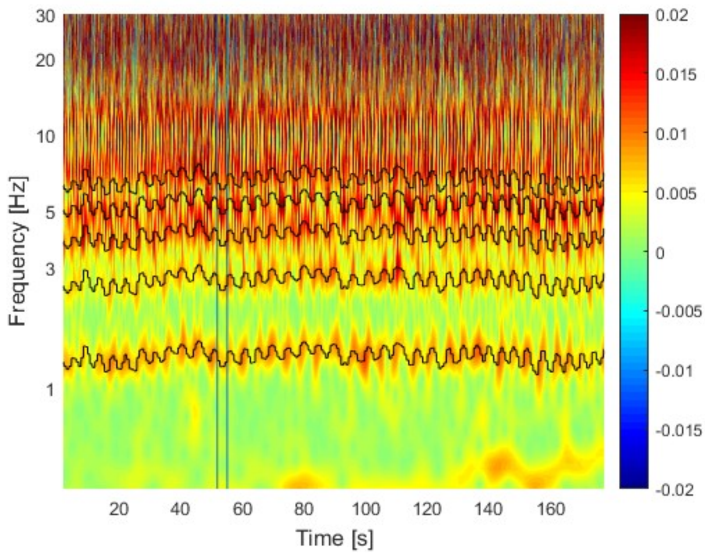

Figure 3.2.2.3 – Acceleration a_y in time-frequency domain with CWT, for rest test of subject 225; blue lines indicates the reduced time window considered.

A reduced time window is considered in the following analysis in order to achieve the objective. The time window has been chosen so that the gyration signal remains exactly periodic in the window selected in order to avoid leakage problem with filtering. It is delimited by two blue vertical lines in the figure above and it is the same as window for gyration:

$$51.89\ \mathrm{s} \leq t_w \leq 55.1\ \mathrm{s} \tag{3.2.2.1}$$

Looking at the reduced window and overlapping heart rate frequency and super harmonics in the time-frequency graph, it is possible to figure out which frequencies are the most significant.

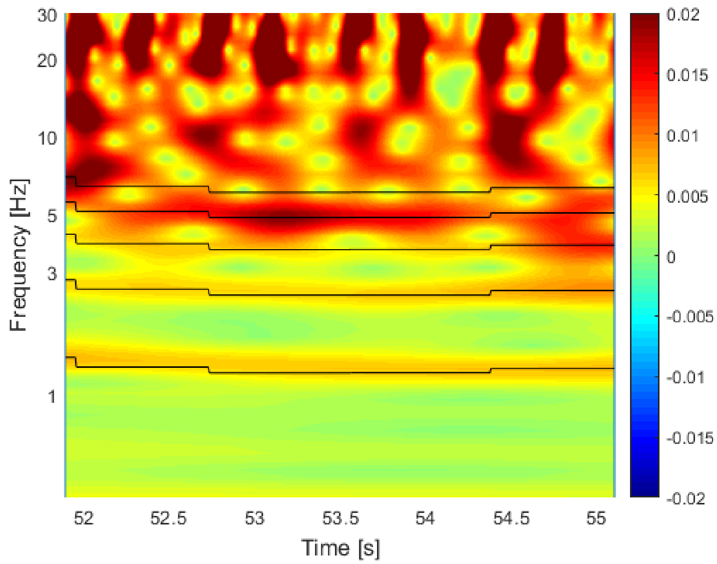

Figure 3.2.2.4 – Acceleration a_y in time-frequency domain with CWT, for a reduced time window, with heart rate frequencies and super harmonics (black solid lines), for rest test of subject 225.

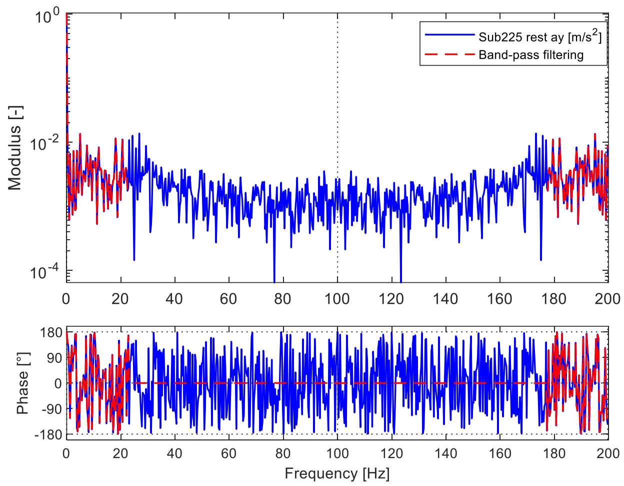

Figure 3.2.2.5 – FFT modulus and phase for a_y signal in the reduced time window considered (blue solid line) with the band filtered from 0 Hz to 23 Hz (red dashed line).

The filtered signal in frequency domain is converted into a signal in time domain applying Inverse Fast Fourier Transform IFFT. It can be noted that the signal obtained using only frequencies up to 23 Hz is quite a good representation of the original signal. There are some peak values that are only approximated, so it may mean that they depend on events occurring after 23 Hz.

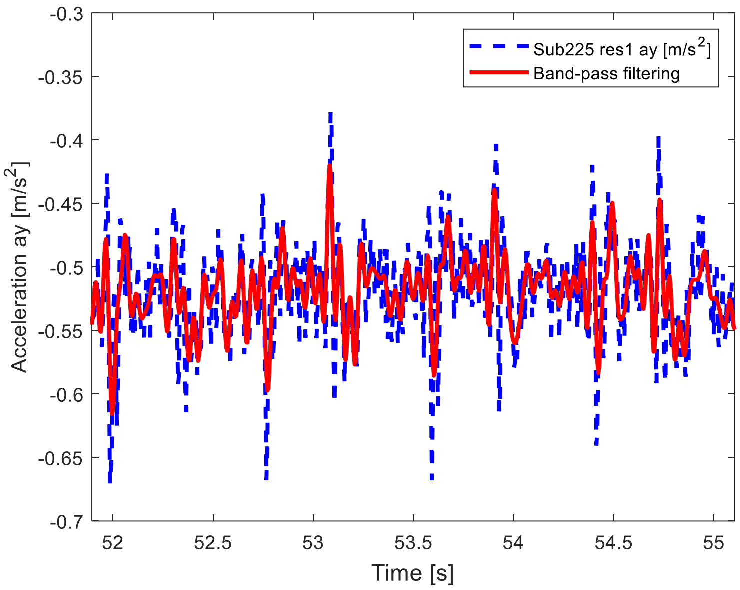

Figure 3.2.2.6 – Acceleration a_y for subject 225 at rest test, in time domain, original signal (blue dashed line) and after a band pass filter from 0 to 23 Hz (red solid line), for the reduced time window.

Considering a larger frequency range for band pass filtering, a very good result is obtained. In particular, passing frequencies up to 30 Hz, the original gyration signal in time domain is represented almost entirely.

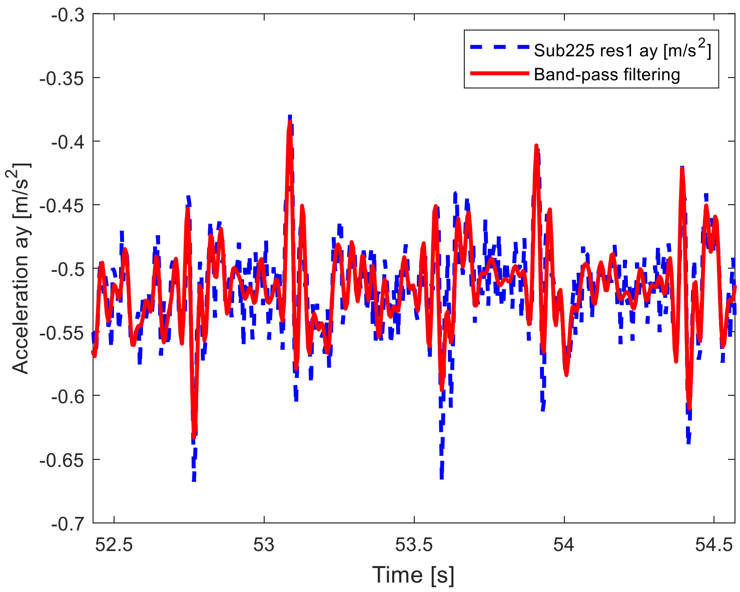

Figure 3.2.2.7 – Acceleration a_y for subject 225 at rest test, in time domain, original signal (blue dashed line) and after a band pass filter from 0 to 30 Hz (red solid line), for the reduced time window.

3.2.3 NIBP: non-invasive blood pressure measured at finger

It is interesting to analyse time-frequency characteristics of blood pressure measured by a finger cuff and to see their correlation with heart rate. In this case, the same subject with the same test is considered, that is rest test for subject 225.
Non-invasive blood pressure NIBP measured by finger cuffs is sampled with constant delta-time, according to the sampling frequency considered. For NIBP, the sampling frequency chosen is 1000 Hz, so delta-time for sampling is equal to 0.001 s. The following graph demonstrates that it is constant.

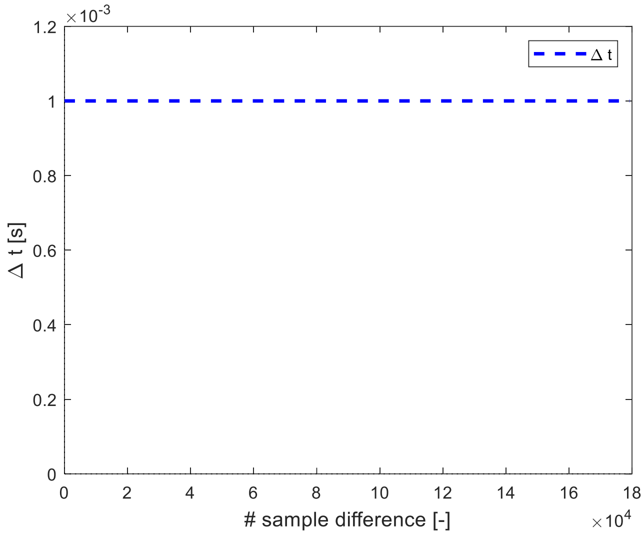

Figure 3.2.3.1 – Delta-time of NIBP measurements, for subject 225, rest test.

Blood pressure measured at the finger has the typical waveform showed in the following figure for a reduced time interval. It must be noted that this pressure signal has the same waveform as the central aortic pressure but it is not central. In fact, blood pressure measured at the finger always overestimate the actual central aortic blood pressure [20, 21].

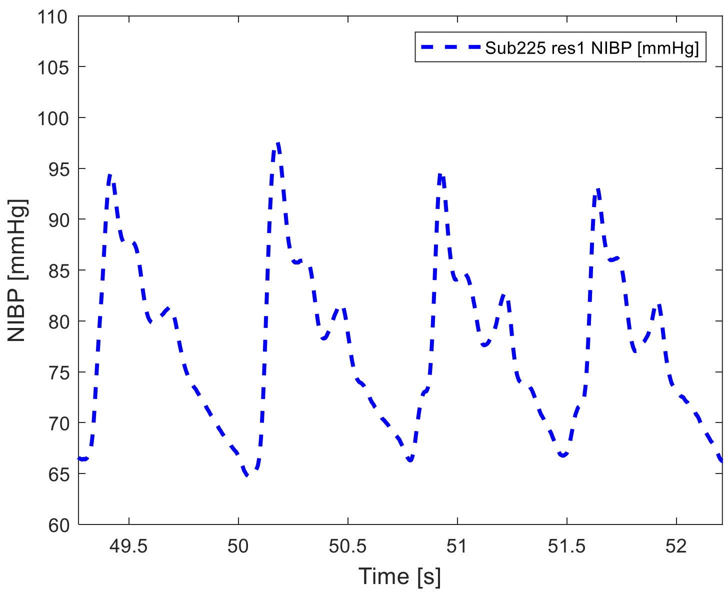

Figure 3.2.3.2 – NIBP measured by finger cuff, for a reduced time interval, for rest test of subject 225.

The NIBP signal for the entire duration of the test is expressed in frequency domain applying FFT.

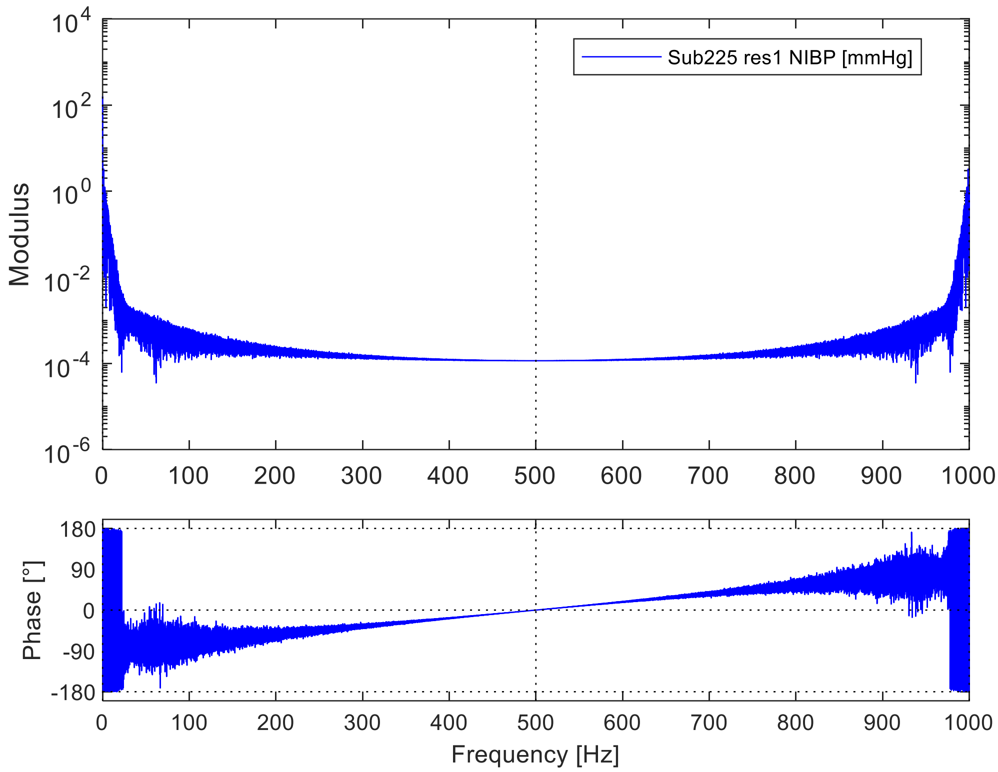

Figure 3.2.3.3 – FFT modulus and phase for NIBP signal (blue solid line), for rest test of subject 225.

It can be easily seen that the modulus is symmetric with respect to the Nyquist frequency, while the phase is antisymmetric.
The spectrogram of the signal in time-frequency domain is obtained applying CWT.

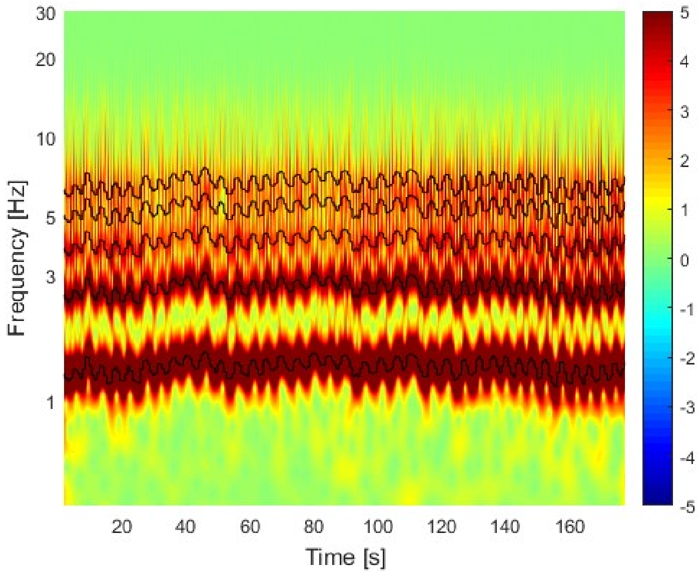

Figure 3.2.3.4 – NIBP in time-frequency domain with CWT, for rest test of subject 225, with black lines for heart rate frequency and super harmonics counted.

For NIBP signal, a reduced time window is counted as done for gyration signal. It has been chosen in order to maintain the signal periodic in the windowed time interval. The reason is that a band pass filter will be applied and leakage effect must be avoid in order to have a good result. The time window selected for NIBP is:

$$49.27\ \mathrm{s} \leq t_w \leq 52.21\ \mathrm{s} \qquad (3.2.3.1)$$

The spectrogram visualised for the reduced time window provides a better insight of the relationship between heart rate frequency, super harmonics and NIBP frequencies.

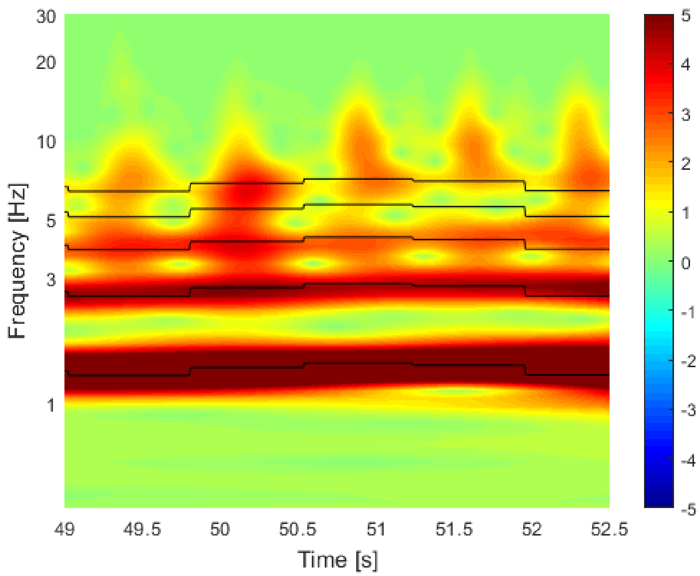

Figure 3.2.3.5 –NIBP in time-frequency domain with CWT, for a reduced time window, with heart rate frequencies and super harmonics (black solid lines), for rest test of subject 225.

It can be deduced that the main heart rate frequency gives a very high contribution to the frequency domain of the NIBP. The super harmonics obtained multiplying it by 2, 3 and 5 represent a significant contribution, too. However, the CWT graph does not show important aspects after 10 Hz.
It is possible to apply a band pass filter to the signal of the reduced time window. In particular, FFT is applied to the reduced signal and a filter passing frequencies form 0 Hz to 22 Hz is applied.

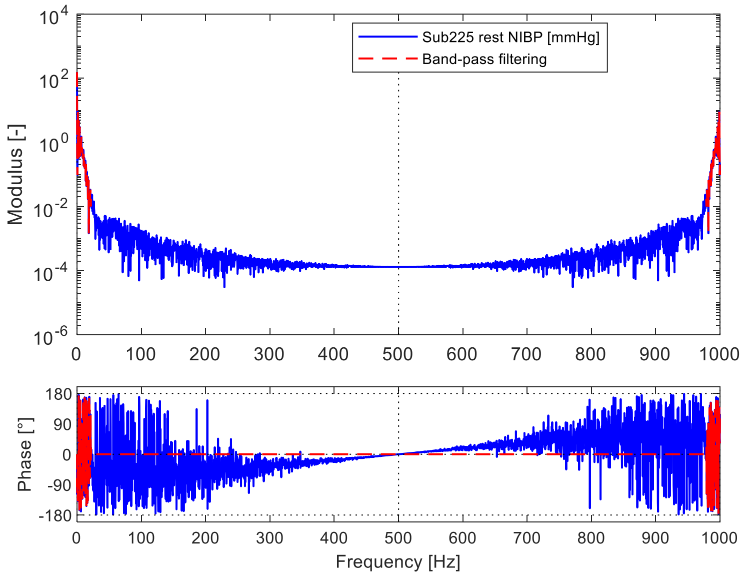

Figure 3.2.3.6 – FFT modulus and phase for NIBP signal in the reduced time window considered (blue solid line) with the band filtered from 0 Hz to 23 Hz (red dashed line).

Then, IFFT is applied to the filtered signal so that a signal in time domain is obtained. It can be seen that passing frequencies from 0 Hz to 22 Hz, the signal obtained from the reduced time interval exactly corresponds to the original signal, without any approximation.

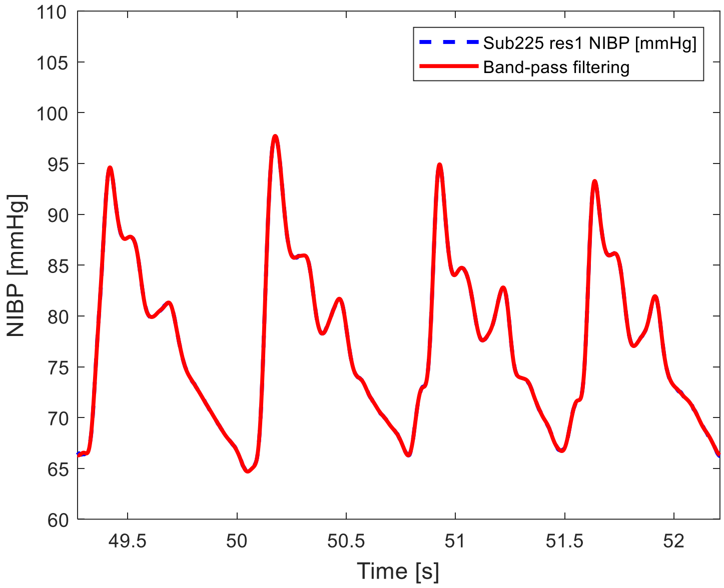

Figure 3.2.3.7 – NIBP for subject 225 at rest test, in time domain, original signal (blue dashed line) and after a band pass filter from 0 to 22 Hz (red solid line), for the reduced time window.

Therefore, the range of frequency for filtering can be reduced. Passing frequencies from 0 Hz to 10 Hz, a quite good representation of the original signal can be obtained. In fact, the CWT spectrogram shows that there is no important information for frequencies higher than 10 Hz.

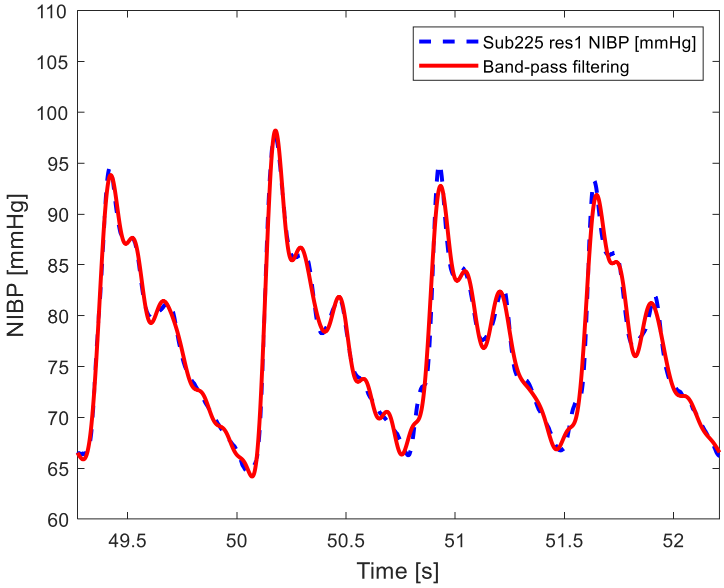

Figure 3.2.3.8 – NIBP for subject 225 at rest test, in time domain, original signal (blue dashed line) and after a band pass filter from 0 to 10 Hz (red solid line), for the reduced time window.

3.3 Time-frequency analysis with variations

Some examples of test and subject variations are provided to see how heart rate frequency and its correlation with detected signals spectrograms vary.

In particular, an example of the intra-subject variation will be given for gyration around X-axis. It means that for the same subject described above, that is subject 225, another test is counted, HLV test.
Then, an example of inter-subject variation is provided for gyration around X-axis. The same test seen before for subject 225, will be analysed for another subject, that is identified with number 19.

3.3.1 Intra-subject variation: HLV test

Gyration around X-axis is considered for HLV test of subject 225. The spectrogram of the signal in time-frequency domain is obtained applying CWT.

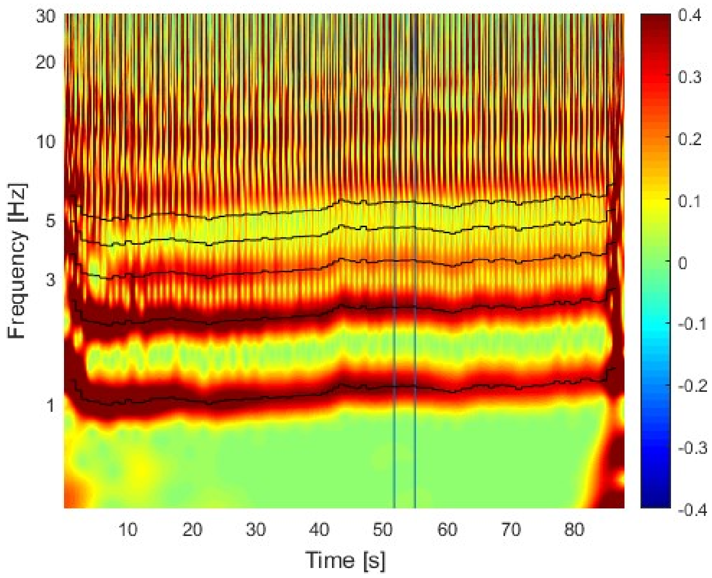

Figure 3.3.1.1 – Gyration g_x in time-frequency domain with CWT, for HLV test of subject 225, with black lines for heart rate frequency and super harmonics counted.

For gyration signal, a reduced time window is selected. It has been chosen in order to maintain the signal periodic in the windowed time interval. The time window selected is the same as for gyration around X-axis defined for rest test:

$$51.89 \text{ s} \leq t_w \leq 55.1 \text{ s} \tag{3.3.1.1}$$

The spectrogram visualised for the reduced time window provides a better insight of the relationship between heart rate frequency, super harmonics and gyration frequencies.

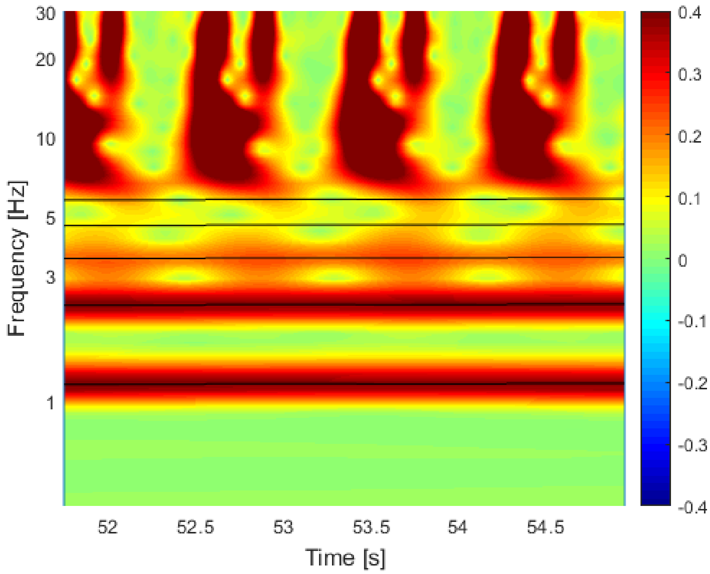

Figure 3.3.1.2 –Gyration g_x in time-frequency domain with CWT, for a reduced time window, with heart rate frequencies and super harmonics (black solid lines), for HLV test of subject 225.

It can be noted that the harmonics most significant for this test are the first one (heart rate frequency), the second one and the third one. The main difference with the rest test is that the harmonics multiplied by 4 is not important in HLV test, while it is in rest test. However, it can be deduced that harmonics around 3 Hz are significant in both rest and HLV test. Meanwhile, as heart rate is a bit lower in HLV test, harmonics around 5 Hz are not as relevant in HLV test as they are in rest test. Then, a high frequency contribution starts from 7 Hz, as well as for rest test gyration spectrogram.

3.3.2 Inter-subject variation: rest test of another subject

Gyration around X-axis is considered for rest test of another subject that is subject 19. The spectrogram of the signal in time-frequency domain is obtained applying CWT.

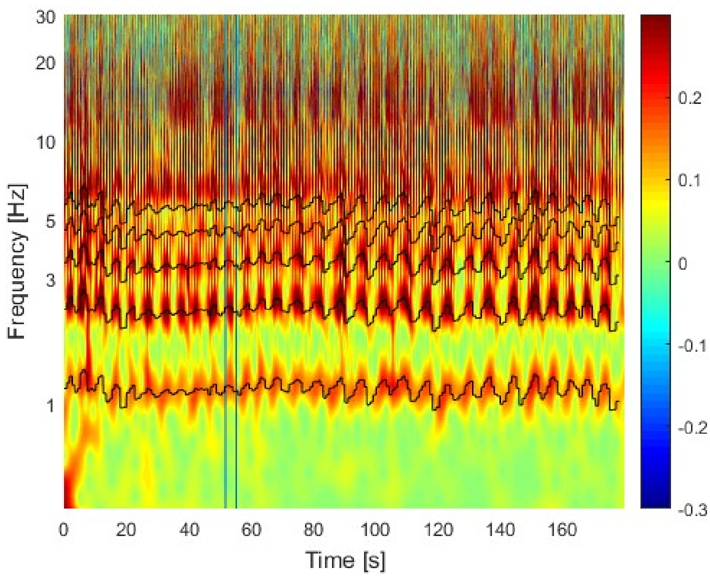

Figure 3.3.2.1 – Gyration g_x in time-frequency domain with CWT, for rest test of subject 19, with black lines for heart rate frequency and super harmonics counted.

For gyration signal, a reduced time window is selected. It has been chosen in order to maintain the signal periodic in the windowed time interval. The time window selected is slightly larger than the window for subject 225:

$$51.78 \text{ s} \leq t_w \leq 55.23 \text{ s} \qquad (3.3.2.1)$$

The spectrogram visualised for the reduced time window provides a better insight of the relationship between heart rate frequency, super harmonics and gyration frequencies.

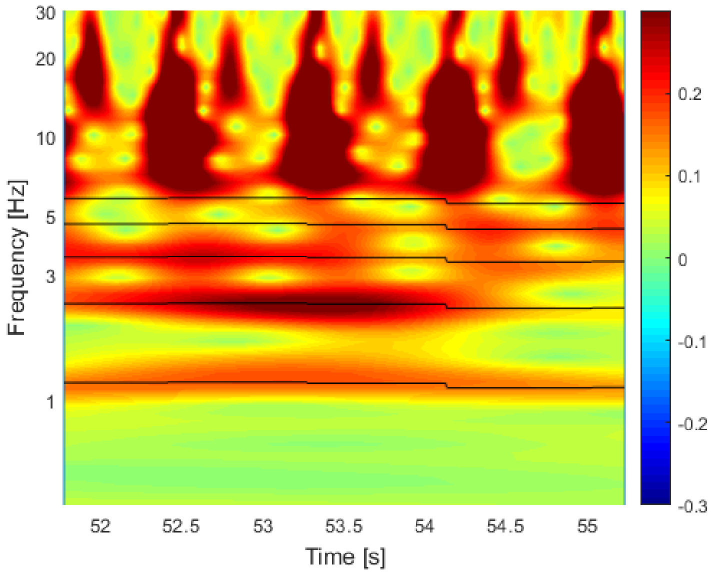

Figure 3.3.2.2 –Gyration g_x in time-frequency domain with CWT, for a reduced time window, with heart rate frequencies and super harmonics (black solid lines), for rest test of subject 19.

It can be noted that almost all the super harmonics are significant for rest test of subject 19. In particular, the super harmonics where heart rate is multiplied by 2 and 3 are the most important for frequency contribution. Then, a high frequency contribution starts from 7 Hz, as well as for subject 225 gyration spectrogram.

4. Lumped parameter model of cardiovascular system

The cardiovascular system (CVS) can be simplified using an equivalent hemodynamic model with the main parameters indicated. A simple hydraulic analogue has been selected from previous detailed studies about it. The objective is to represent a blood vessel with a mechanical system. In order to achieve that, an intermediate conversion form hydraulic to electric model is required.

An equivalent electric model will be obtained, considering the direct correlation between electrical and hydraulic elements. It means that electric current is correlated to blood flow rate "through" vessels, while electric voltage drop is correlated to pressure drop "across" vessels. A conversion from hydraulic to electric units will be applied to define electric and hydraulic capacitance, inductance and resistance numerically.

Then, there are two possible ways to transform an electric model into a mechanical one: Maxwell or Firestone analogy. In this case, Firestone analogy will be chosen because it maintains a very close topology with the equivalent mechanical model. The main reason is that the 1st approach to interpret hydraulic elements, based on Maxwell analogy, would ignore compartments partition of the cardiovascular system. Meanwhile, using Firestone analogy, a 2nd approach is introduced, which gives a more valuable CVS representation. In addition, it will be necessary to add some springs connected to ground in order to ensure a static state for the model. The mechanical model obtained is a mass-spring-damper system with 12 degrees of freedom that includes 4 degrees of freedom for the four chambers of the heart. The dynamic analysis of the 12-DOFs model will be performed in the next chapter.

4.1 Hydraulic model for cardiovascular system

4.1.1 Windkessel concept

The lumped-parameter or zero-dimensional models can be used to obtain simplified representations of the cardiovascular system (CVS) and its main components. This way of modelling can contribute to understand circulatory physiology and hemodynamic interactions among the components. Lumped models can be used in cardiac studies to represent load on the heart or to derive arterial parameters or aortic flow from arterial pressure.

Zero-dimensional modelling started with the Windkessel model of the arterial system. The concept of Windkessel was introduced in the 18th century. In 1735, Hales found that pressure in the arterial system was not constant but changed with heartbeats [22]. He also suggested that the variations in pressure were related to elasticity of the large arteries. Therefore, the large arteries were considered the cause of the Windkessel effect that can be represented with a reservoir, as shown in Figure 4.1.1.1.

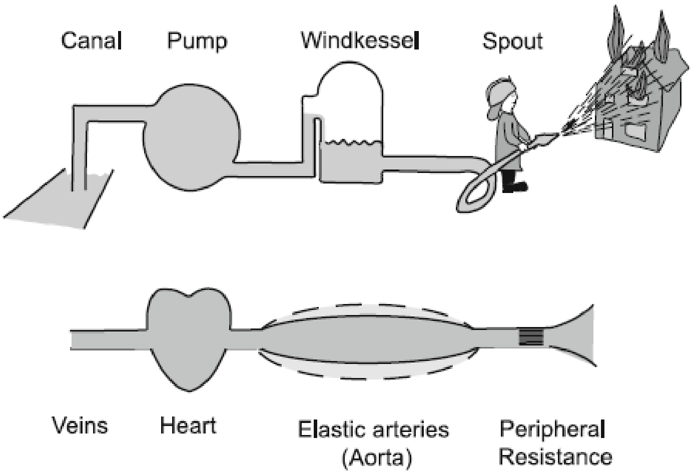

Figure 4.1.1.1 – The concept of Windkessel.

The conventional analogy between hydraulic and electric elements is shown in the following figure. It can be seen that hydraulic resistance corresponds to electric resistance, hydraulic inductance (or inertial term) to electric inductance and hydraulic capacitance (or compliance) to electric capacitance.

Element	Circuit Analogy	Pipe Analogy	Flow Equation
Node	Junction	Junction	Total Flow = 0
Path	Wire	Rigid Pipe	Solve Directly
Resistance	Resistor	Aperture	$F = P/R$
Compliance	Capacitor	Diaphram	$F(t) = C\frac{dP(t)}{dt}$
Inertance	Inductor	Heavy Paddle	$F = \frac{1}{L}\int_{t_0}^{t} P\,dt + F(t_0)$
Switch	Switch	Gate Valve	Solve Directly
Valve	Diode	Check Valve	Solve Directly
Pressure Source	Voltage Source	Pump	Solve Directly
Flow Source	Current Source		$F = F$

Figure 4.1.1.2 – Conventional analogy between electric and hydraulic elements.

A compartment is a part of the system that can be considered as a whole, according to the needed accuracy in the description of circulation [23]. A different number of compartments can be considered to describe the cardiovascular system. It depends on complexity and range of application. The Windkessel models are instances of mono-compartment models because the systemic vasculature is treated as a single block and the internal distribution of pressure and flow rate in the different segments of vessels is not computed.
Multi-compartment models treat the cardiovascular system as a number of segments; each segment is described by its own hydraulic resistance, capacitance and inductance.

4.1.2 Hydraulic model

An example of a lumped-parameter model for cardiovascular system was developed in 1998 [24]. Each compartment was described with a hydraulic resistance which accounts for energy losses in the compartment, a capacitance or compliance to describe the amount of stressed blood volume stored at a given pressure, the hydraulic inductance was assumed to be relevant only for large arteries (like systemic arteries and pulmonary arteries) where blood acceleration is important.
The vascular system is described with eight compartments as shown in Figure 4.2.1. Five compartments define the systemic circulation and three of them describe the arterial peripheral and venous pulmonary circulations:

- Systemic arteries (sa) with capacitance C_{sa}, inductance L_{sa}, resistance R_{sa}
- Splanchnic peripheral circulation (sp) with capacitance C_{sp} and resistance R_{sp}
- Extra splanchnic peripheral circulation (ep) with capacitance C_{ep} and resistance R_{ep}
- Splanchnic venous circulation (sv) with capacitance C_{sv} and resistance R_{sv}
- Extra splanchnic venous circulation (ev) with capacitance C_{ev} and resistance R_{ev}
- Pulmonary arteries (pa) with capacitance C_{pa}, inductance L_{pa}, resistance R_{pa}
- Pulmonary peripheral circulation (pp) with capacitance C_{pp}, resistance R_{pp}
- Pulmonary veins (pv) with capacitance C_{pv}, resistance R_{pv}

Then, the four chambers of the heart are considered:

- Right atrium (ra) with capacitance C_{ra} and resistance R_{ra}
- Right ventricle (rv) with capacitance C_{rv} and resistance R_{rv}
- Left atrium (la) with capacitance C_{la} and resistance R_{la}
- Left ventricle (lv) with capacitance C_{lv} and resistance R_{lv}

The volumetric flow rate is represented with F in the figure. Between each atrium and ventricle (and each ventricle and systemic artery) there is a resistance and a unidirectional valve to represent the cardiac valves. The heart is considered as a pump where the contractility of the left and right atrium is neglected. The contractility is assumed to come from ventricles only. The overall hemodynamic model is shown in the following figure.

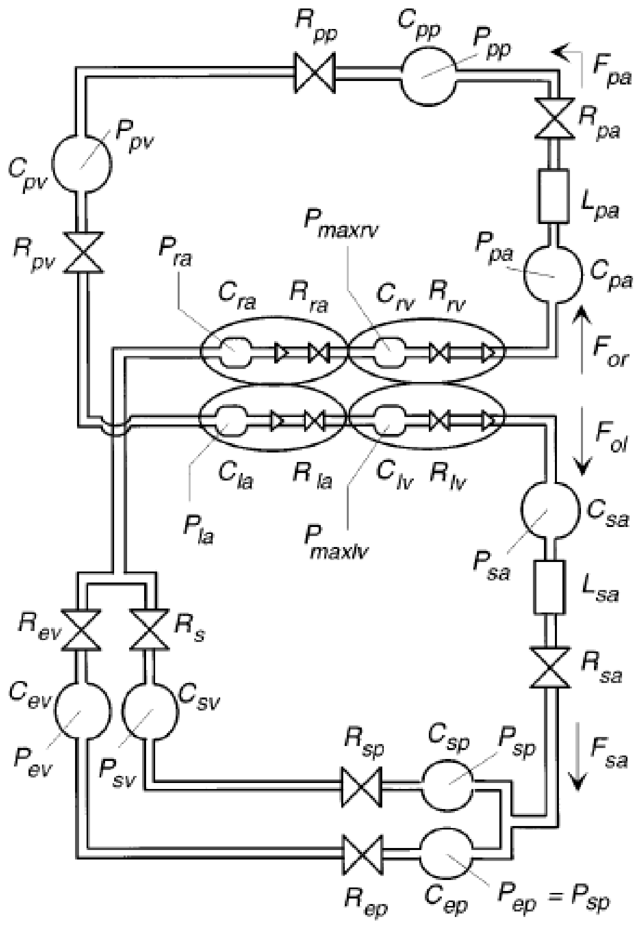

Figure 4.1.2.1 – An example of hemodynamic lumped parameter model for circulatory system.

The splanchnic circulation is composed of gastric, small intestinal, colonic, pancreatic, hepatic, and splenic circulations. There are three main arteries that supply the splanchnic organs but in the model, only one segment is considered for splanchnic arteries and one segment for veins. The extra splanchnic circulation refers to all the other peripheral organs.

Generally, the hydraulic inductance can be represented by an inductor in parallel or in series with the resistor. For example, in the Windkessel model the hydraulic inductance, that is the fourth element, is usually placed in parallel with the arterial resistance. When the inductor in parallel with the resistor, it affects low frequency behaviour of arterial impedance. On the contrary, when it is in series, it affects high frequency behaviour [22]. In this case, of study, low frequencies are more important. In addition, another experimental study [25] demonstrated that L and R in parallel or in series configuration model the input impedance equally in adults. Meanwhile, a larger difference was found with blood vessels of children. Therefore, that confirms the choice of hydraulic inductance in parallel with the resistance, in Figure 4.1.2.2.

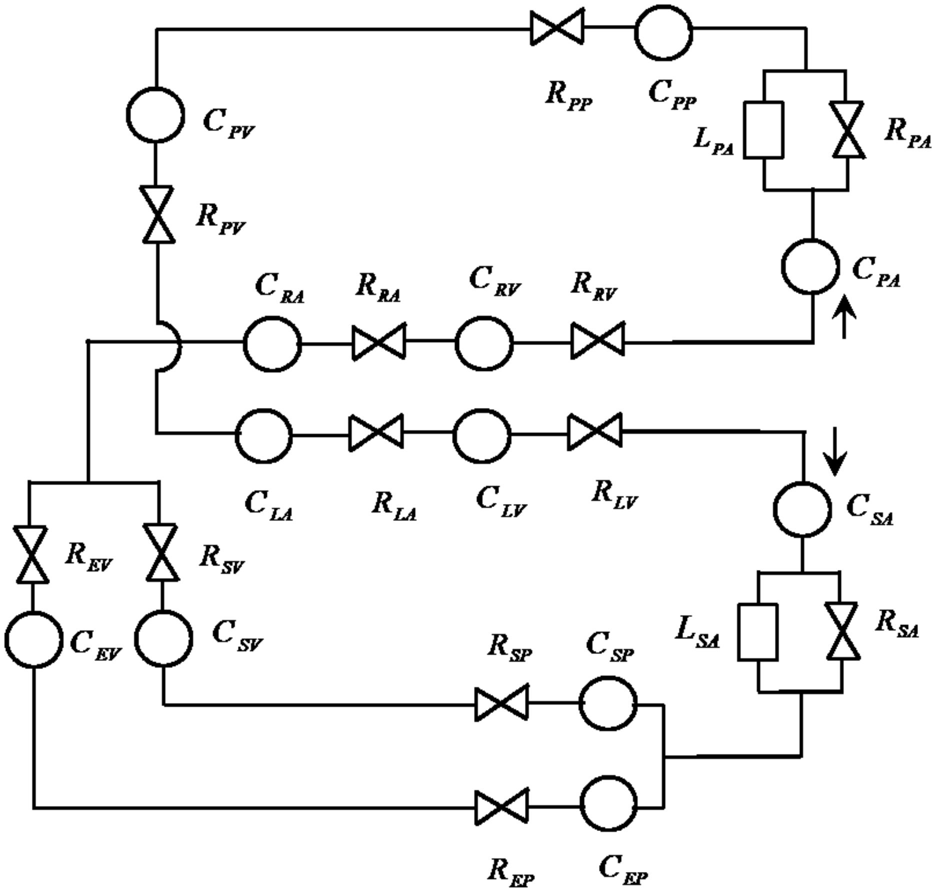

Figure 4.1.2.2 – An example of hemodynamic lumped parameter model for circulatory system with L and R in parallel for arteries.

The values of each parameter of the system have been taken from previous experimental studies and literature. They were all rescaled for a subject with a body weight of 70 kg. The heart rate was assumed to be 72 beats/min (1.2 Hz) with a heart period of 0.833s. Total blood volume is assumed 5300 ml. The values used for the system considered [24, 26] are shown in the following tables. They are reported in medical units as found in literature.

Table 4.1.2.1 – Parameters describing the cardiovascular system.

Hydraulic capacitance [ml/mmHg]		Hydraulic resistance [mmHg·s/ml]		Hydraulic inductance [mmHg·s^2/ml]	
C_{SA}	0.28	R_{SA}	0.06	L_{SA}	$0.22\cdot10^{-3}$
C_{SP}	2.05	R_{SP}	3.307	-	-
C_{SV}	61.11	R_{SV}	0.038	-	-
C_{EP}	1.67	R_{EP}	1.407	-	-
C_{EV}	50.0	R_{EV}	0.016	-	-
C_{PA}	0.76	R_{PA}	0.023	L_{PA}	$0.18\cdot10^{-3}$
C_{PP}	5.80	R_{PP}	0.0894	-	-

C_{PV}	25.37	R_{PV}	0.0056		

Some parameters related to heart chambers and reported in Table 4.1.2.2 will be discussed in this paragraph and in chapter 7 with more details.

Table 4.1.2.2 – Parameters describing the heart.

Left heart parameters		Right heart parameters	
C_{LA} [ml/mmHg]	19.23	C_{RA} [ml/mmHg]	31.25
R_{LA} [mmHg $\cdot$ s/ml]	$2.5\cdot10^{-3}$	R_{RA} [mmHg $\cdot$ s/ml]	$2.5\cdot10^{-3}$
$V_{u,LA}$ [ml]	25	$V_{u,RA}$ [ml]	25
V_{LA} [ml]	150	V_{RA} [ml]	150
$P_{0,LV}$ [mmHg]	1.5	$P_{0,RV}$ [mmHg]	1.5
$k_{E,LV}$ [1/ml]	0.014	$k_{E,RV}$ [1/ml]	0.011
$E_{\max,LV}$ [mmHg/ml]	2.95	$E_{\max,RV}$ [mmHg/ml]	1.75
$k_{R,LV}$ [s/ml]	$3.75\cdot10^{-4}$	$k_{R,RV}$ [s/ml]	$1.4\cdot10^{-3}$
$LV\ stroke\,volume$[ml]	74.1	$RV\ stroke\,volume$[ml]	74.16

For some components of the system, values of capacitance and resistance are not defined explicitly in the tables above. In particular, the values of compliance for left and right ventricles C_{LV} and C_{RV} can be calculated with the reciprocal of the corresponding values $E_{\max,LV}$ and $E_{\max,RV}$:

$$C_{LV} = \frac{1}{E_{\max,LV}} \quad ; \quad C_{RV} = \frac{1}{E_{\max,,RV}} \tag{4.1.2.1}$$

The values for resistances of left and right ventricles R_{LV} and R_{RV} are not provided by literature, hence they have been calculated making some assumptions, and heart excitation functions are used. It is important to note that heart action will be described in details in chapter 7 of this thesis, when pulsating heart will be included in the lumped model, at this moment, only the constitutive functions are used. Resistances for left and right ventricle can be defined as [24]:

$$R_{LV} = k_{R,LV} \cdot p_{\max,LV} \tag{4.1.2.2}$$

$$R_{RV} = k_{R,RV} \cdot p_{\max,RV} \tag{4.1.2.3}$$

where $k_{R,LV}$ and $k_{R,RV}$ are parameters that represent the viscosity of the ventricles, in Table 4.1.2.2; $p_{\max,LV}$ and $p_{\max,RV}$ are isometric pressures of both ventricles. The isometric pressure for left ventricle (LV) is defined with $k_{E,LV}$ and $P_{0,LV}$ that are constant parameters, $E_{\max,LV}$ is the reciprocal of capacitance for left ventricle at maximum contraction, $V_{u,LV}$ is the unstressed volume of left ventricle (that corresponds to the x-axis intercept of the end systolic pressure-volume function) and V_{LV} is the volume of the left ventricle:

$$p_{\max,LV}(t) = \varphi(t) \cdot E_{\max,LV} \cdot (V_{LV} - V_{u,LV}) + [\ 1 - \varphi(t)\ ] \cdot P_{0,LV} \cdot (e^{k_{E,LV} V_{LV}} - 1) \qquad (4.1.2.4)$$

where $\varphi(t)$ is an activation function to represent the contraction of the left and right ventricles. When the activation function is $\varphi(t) = 0$, the ventricle is relaxed (diastole) and the pressure function is exponential. When $\varphi(t) = 1$, the ventricle is contracted (end-systole) and the pressure function is linear. This function can be described with a sinusoidal function that will be discussed in details in chapter 7.
For right ventricle (RV), the equation of isometric pressure is the same as LV but with parameters related to right ventricle instead of left ventricle, so it results:

$$p_{\max,RV}(t) = \varphi(t) \cdot E_{\max,RV} \cdot (V_{RV} - V_{u,RV}) + [\ 1 - \varphi(t)\ ] \cdot P_{0,RV} \cdot (e^{k_{E,RV} V_{RV}} - 1) \qquad (4.1.2.5)$$

The activation function is the same as left ventricle. To evaluate both ventricular resistances, maximum contraction is assumed so that $\varphi(t) = 1$. Consequently, volume V_{LV} corresponds to the end diastolic volume (EDV) of left ventricle. The difference between V_{LV} and $V_{u,LV}$ is assumed to be almost equal to the stroke volume, because the actual end systolic volume (ESV) was not defined in that paper. However, unstressed volume is usually slightly smaller than ESV. Values for reciprocal of capacitance and values for stroke volume comes from Table 4.2.2, where stroke volume is equal to the difference between EDV and ESV. Then, the equation for left ventricle becomes:

$$p_{\max,LV}(t) = \varphi(t) E_{\max,LV} (V_{LV} - V_{u,LV}) \approx E_{\max,LV} (EDV_{LV} - ESV_{LV}) \qquad (4.1.2.6)$$

It is the same for right ventricle, where stroke volume is usually very similar to LV one, in order to ensure a cardiac output balance. Therefore, resistances for LV and RV are calculated with Eq. (4.1.2.2) and Eq. (4.1.2.3). The numerical values obtained for the ventricles with this calculation are shown in this table.

Table 4.1.2.3 – Calculated parameters describing heart ventricles.

Calculated ventricular parameters	
C_{LV} [ml/mmHg]	0.3389
C_{RV} [ml/mmHg]	0.5714
R_{LV} [mmHg·s/ml]	0.08197
R_{RV} [mmHg·s/ml]	0.1817

4.2 Electric model for cardiovascular system

The fundamental concept that connects hydraulic, electric and mechanic systems is the equivalence between powers. For example, the equivalence between hydraulic and electric power must be accomplished:

$$W_{hyd} = \Delta p \cdot Q \,[\mathrm{W}] \Leftrightarrow W_{el} = \Delta v \cdot i \,[\mathrm{W}] \tag{4.2.1}$$

where Δp is pressure drop, Q is flow rate, Δv is voltage drop and i is current. The most common correspondence between them is obtained correlating pressure to voltage and flow rate to current:

$$\Delta p \ [\mathrm{Pa}] \Leftrightarrow \Delta v \ [\mathrm{V}] \tag{4.2.2}$$

$$Q \left[\frac{\mathrm{m}^3}{\mathrm{s}}\right] \Leftrightarrow i \,[\mathrm{A}] \tag{4.2.3}$$

In particular, pressure drop across a hydraulic element corresponds to voltage drop across an electric element, while flow rate through a hydraulic element corresponds to current through an electric element.
Pressure drop and voltage drop are usually written with delta (Δ) operator. When delta (Δ) operator is used across an element, it is assumed to be equal to the difference between the value at the end of the drop arrow and the value at the starting point; it means difference between the highest and the lowest drop value. For resistors, inductors and capacitors the convention of passive users is applied, so the voltage drop is assumed positive in the direction opposite to the direction of the current.

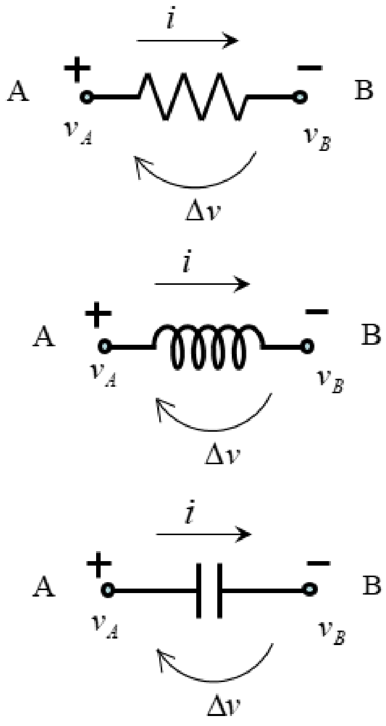

Figure 4.2.1 – Example of current and voltage drop positive direction across a resistor (top), an inductor (centre) and a capacitor (bottom), convention of passive users.

Therefore, it is:

$$\Delta v = v_A - v_B = v_{higher} - v_{lower} > 0 \tag{4.2.4}$$

On the contrary, for the voltage source, the convention is different because it is a voltage generator. Therefore, the voltage drop is positive in the same direction as current, as shown in the following figure.

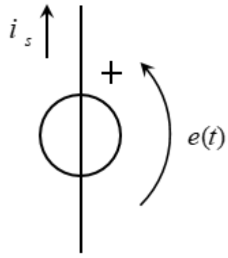

Figure 4.2.2 – Example of current and voltage drop positive direction across a voltage source.

It can be noted that the heart excitation can be described as pressure generated during ventricles contraction. According to the conventional analogy in Eq. (4.2.2), it corresponds to a voltage source in the equivalent electric model.
The International System of Units (SI) is used in this study, meanwhile parameters of hydraulic components are usually measured in hydraulic or medical units (mmHg, ml, s). For this reason, hydraulic units have been converted to SI:

$$133.322\ \text{Pa} = 1\ \text{mmHg} \tag{4.2.5}$$

$$10^{-6}\ \text{m}^3 = 1\ \text{ml} \tag{4.2.6}$$

Applying constitutive laws for each electric element, it can be found that they directly correspond to hydraulic elements.
A hydraulic inductor can be represented as a water wheel connected through a rigid axle to a heavy stone flywheel [27]. As pressure against the paddles of the water wheel is applied over time, the flywheel gradually turns faster. An electric inductor is a coil of wire wrapped around a cylindrical core.

Figure 4.2.3 – Schematic of hydraulic inductor (left) and electric inductor (right).

The hydraulic inductance is the constant of proportionality between pressure drop and flow rate change over time. In the same way, the electric inductance is the constant of proportionality between voltage drop and change of current over time.

$$L_{hyd} = \frac{\Delta p}{dQ/dt} \Leftrightarrow L_{el} = \frac{\Delta v}{di/dt} \tag{4.2.7}$$

In terms of units, the relationship is:

$$L_{hyd}\left[\frac{\text{kg}}{\text{m}^4}\right] \Leftrightarrow L_{el}\,[\text{H}] \tag{4.2.8}$$

A hydraulic resistor is a narrow section of a pipe that causes the pressure to drop in the direction of the flow. When more water is pushed through the narrow section of the pipe, the pressure drop across the resistor increases. An electric resistor causes a voltage drop in a wire.

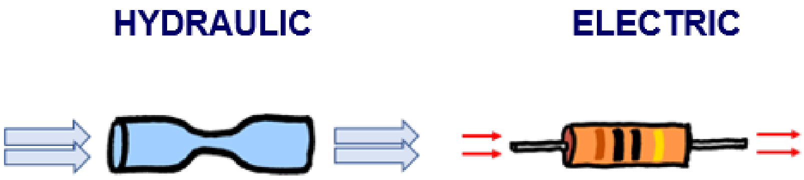

Figure 4.2.4 – Schematic of hydraulic resistor (left) and electric resistor (right).

The hydraulic resistance is the constant of proportionality between pressure drop across the resistor and flow rate through the resistor. Similarly, according to Ohm's law, voltage drop across the resistor is proportional to the current through the resistor with the electric resistance constant of proportionality.

$$R_{hyd} = \frac{\Delta p}{Q} \Leftrightarrow R_{el} = \frac{\Delta v}{i} \tag{4.2.9}$$

In terms of units, the relationship is:

$$R_{hyd}\left[\frac{\text{kg}}{\text{m}^4\,\text{s}}\right] \Leftrightarrow R_{el}\,[\Omega] \tag{4.2.10}$$

A hydraulic capacitor can be represented as a cylinder divided by a flexible rubber sheet. When pressure is applied on one side of the capacitor, the rubber membrane is displaced and the volume stored is proportional to the pressure applied. An electric capacitor is a set of two parallel metal plates separated by an insulator. When a voltage is applied across the capacitor, charge is stored and its amount is proportional to the voltage applied.

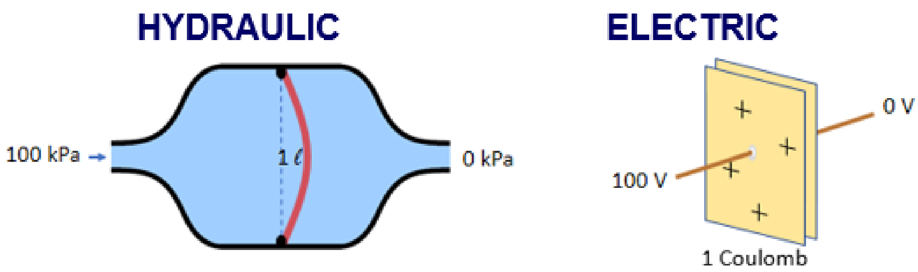

Figure 4.2.5 – Schematic of hydraulic capacitor (left) and electric capacitor (right), with a numerical example.

The hydraulic capacitance is the constant of proportionality between change in volume and change in pressure. It is also called compliance and it describes the ability of a blood vessel wall to expand and contract passively with changes in pressure. Similarly, the electric capacitance is defined as the ratio between charge stored and voltage drop.

$$C_{hyd} = \frac{\Delta Volume}{\Delta p} \Leftrightarrow C_{el} = \frac{\int_0^t i\, dt}{\Delta v} \tag{4.2.11}$$

In terms of units, the relationship is:

$$C_{hyd}\left[\frac{\mathrm{m}^4\,\mathrm{s}^2}{\mathrm{kg}}\right] \Leftrightarrow C_{el}\,[\mathrm{F}] \tag{4.2.12}$$

It means that there is a direct relationship between hydraulic and electric inductance *L,* resistance *R* and capacitance *C*.
It is possible to quantify these units conversions. Some papers define those using numerical values that result in reasonable values for each element [27]. Otherwise, it is possible to assume an absolute correlation of 1:1 between international system units (SI) of hydraulic elements and electric units of electric elements. Therefore, the units' equivalence for pressure-voltage and for flow rate-current is:

$$1\ \mathrm{Pa} = 1\ \frac{\mathrm{kg}}{\mathrm{m\,s}^2} = 1\ \mathrm{V} \tag{4.2.13}$$

$$1\ \frac{\mathrm{m}^3}{\mathrm{s}} = 1\ \mathrm{A} \tag{4.2.14}$$

For inductance, resistance and capacitance it is:

$$1\ \frac{\mathrm{Pa\,s}^2}{\mathrm{m}^3} = 1\ \frac{\mathrm{kg}}{\mathrm{m}^4} = 1\ \mathrm{H} \tag{4.2.15}$$

$$1\ \frac{\mathrm{Pa\ s}}{\mathrm{m}^3} = 1\ \frac{\mathrm{kg}}{\mathrm{m}^4\,\mathrm{s}} = 1\ \Omega \tag{4.2.16}$$

$$1\ \frac{\mathrm{m}^3}{\mathrm{Pa}} = 1\ \frac{\mathrm{m}^4\,\mathrm{s}^2}{\mathrm{kg}} = 1\ \mathrm{F} \tag{4.2.17}$$

It is important to note that the choice of values for units equivalence between hydraulic and electric elements is arbitrary. The numerical value is only a constant that does not affect the dynamics of the element. In fact, hydraulic and electric systems must be dynamically equivalent, so an absolute proportion of 1:1 can be chosen at this point.

An important assumption to make in order to convert the model from hydraulic to electric deals with the physical meaning of the three elements described above: inductance, resistance and capacitance. The final goal is to represent a generic blood vessel compartment with a mechanical mass-damper-spring model (MCK). The electric analogy is used as an intermediate because there are two well known electro-mechanical analogies called Maxwell analogy and Firestone analogy. According to Maxwell analogy, in the electric equivalent circuit the voltage Kirchhoff law (KVL) must be respected. It means that the vessel compartment corresponds to L, R and C electric elements in series. It leads to a differential equation that can be directly related to the mechanical equation of motion of MCK model. Consequently, this analogy considers the inductance as representative of the inertial effects, the resistance of dissipation effects and the reciprocal of capacitance of stiffness properties.
On the other hand, according to Firestone analogy, the current Kirchhoff law (KCL) must be accomplished at the node of the equivalent electric circuit. It means that the vessel is equivalent to a capacitor connected to ground followed by a resistor and an inductor in parallel. It leads to a differential equation that can be directly related to the equation of motion of the MCK model, but in a way that is different from Maxwell analogy. In particular, inertial effects are represented by capacitance, dissipation effects by reciprocal of resistance and stiffness by reciprocal of inductance. The following figure gives a resume of these two possible approaches to pass from hydraulic to electric model and from electric to mechanical one.

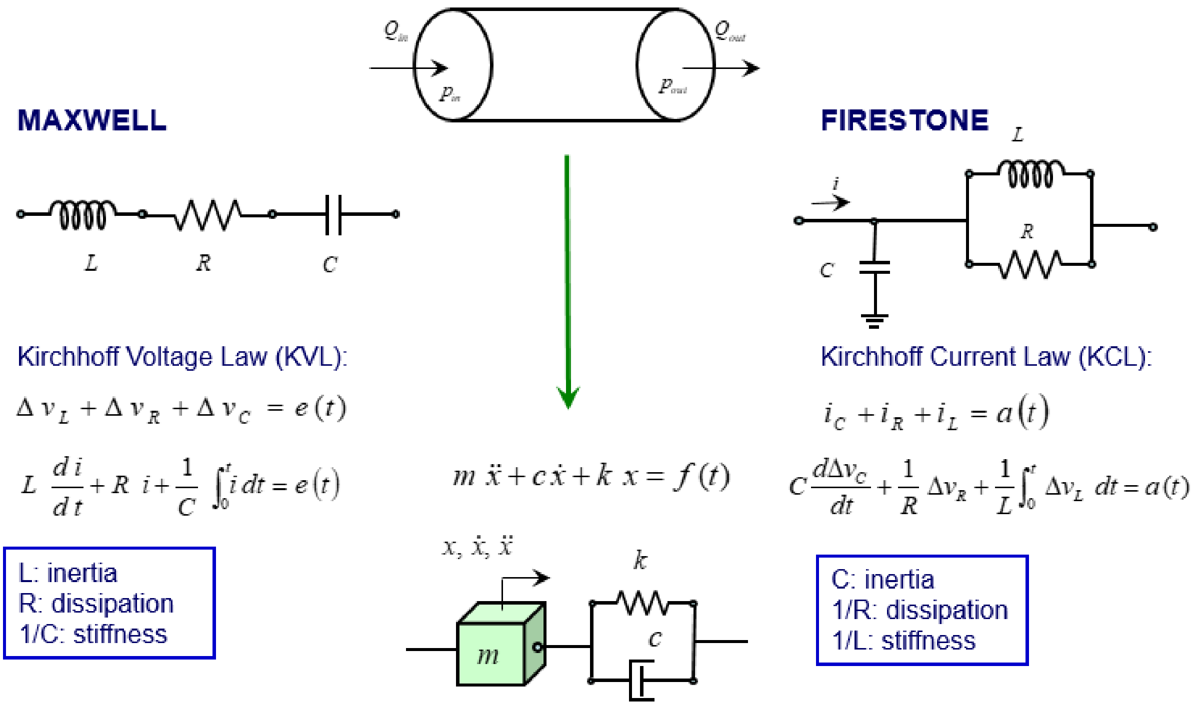

Figure 4.2.6 – Schematic of electro-mechanical analogy for a generic blood vessel using L as inertia (Maxwell analogy, left) and C as inertia (Firestone analogy, right).

4.2.1 Electric analogy: 1st approach

The two possible approaches to convert finally a blood vessel into an equivalent mechanical model, resumed in Figure 4.2.6, refer to a generic blood vessel. In order to find out which is the best approach to apply to the CVS model, the transformations have to be applied to the CVS hydraulic model that is object of this study.

Initially, the 1st approach is assumed, since it is often used in papers related to lumped parameter models of circulatory system. It means that inertial effects are represented by inductance L, while stiffness is represented by reciprocal of capacitance C. Therefore, the equivalent electric circuit is like in the following figure for systemic arteries.

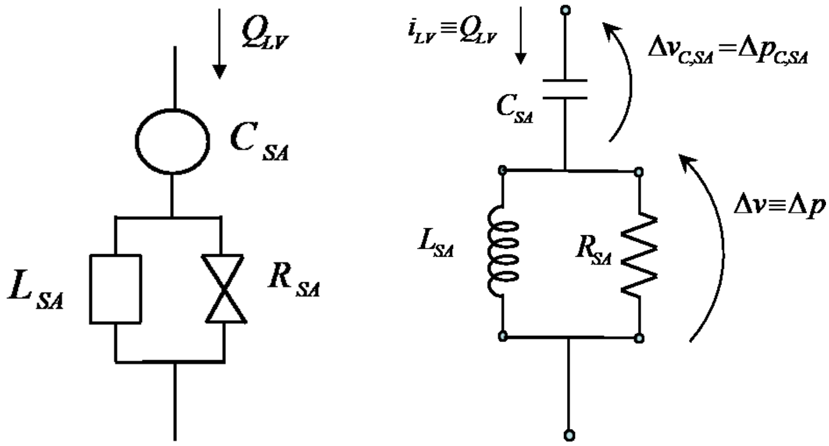

Figure 4.2.1.1 – Systemic arteries hydraulic scheme (left) and equivalent electric circuit with the 1st approach where inductance L represents inertial effects (right).

It can be noted that the capacitor is not connected to ground since it does not have an inertial meaning. Furthermore, the variables across and through elements are defined as the conventional analogy between hydraulic and electric power as in Eq. (4.2.2) and Eq. (4.2.3).
Replacing all the rest of the compartments, the equivalent electric CVS model is like in the following figure. In this study, heart excitation is not included yet. In fact, there are not voltage sources in the electric circuit obtained.

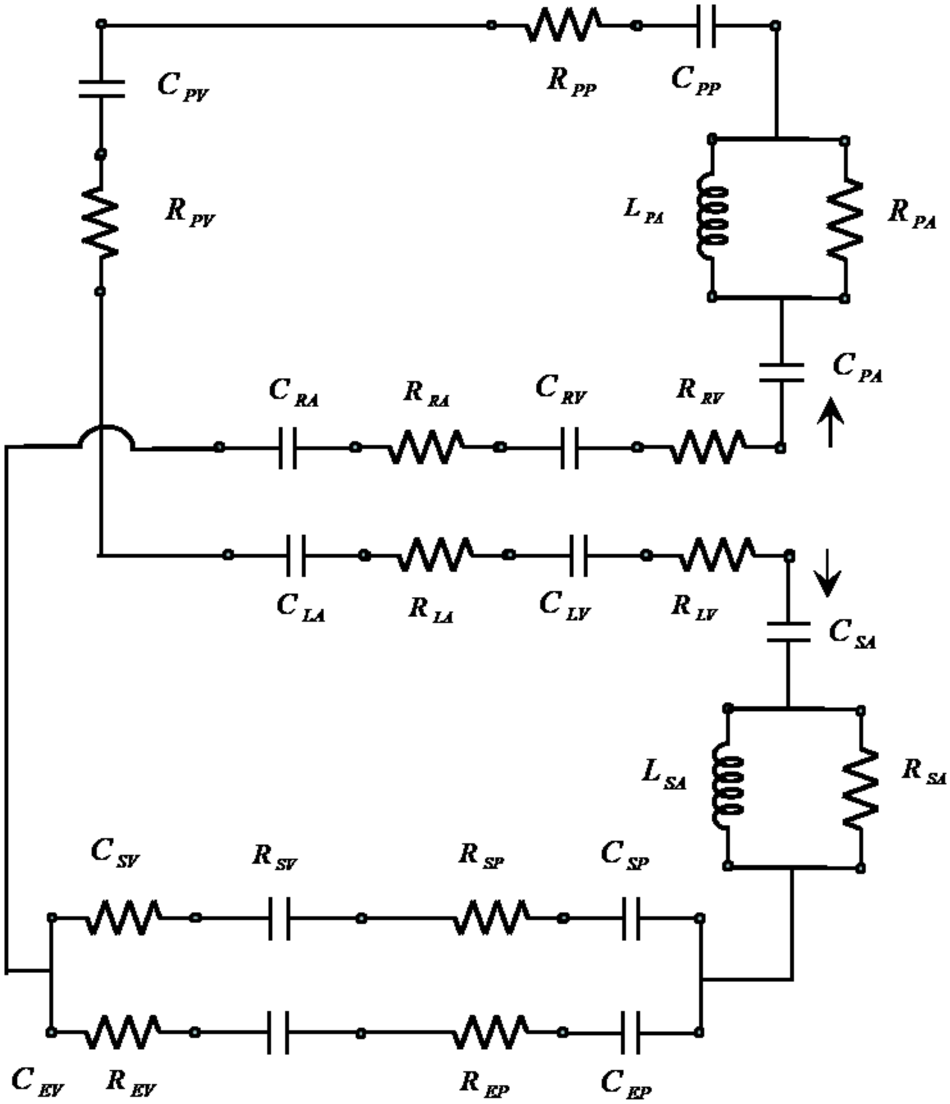

Figure 4.2.1.2 – Proposed electrical equivalent model for circulatory system, with 1st approach (*L* inertia) from hydraulic to electric model.

Using this approach, there are some problems in the electric circuit obtained:

- Resistances and capacitances are in series so they can be reduced to equivalent ones. It means that the compartment partition will be ignored;
- There are only two inductances, so using Maxwell electro-mechanical analogy, the entire system will have only 2 degrees of freedom. Even if *L* and *R* of systemic and pulmonary arteries would be placed in series (that is a valuable alternative), the system will become a 1-DOF mechanical model. Therefore, it would not be possible to analyse the dynamics of each compartment of the circulatory system and a lot of information would be lost.
- To convert this electric model into the mechanical one, it is not possible to use Firestone analogy because capacitors are not connected to ground.

For all these reasons, the 1st approach is not useful to describe the cardiovascular system electrically and mechanically. The 2nd approach is considered.

4.2.2 Electric analogy: 2nd approach

The main difference between the 1st and the 2nd approach is the physical meaning attributed to hydraulic inductance and capacitance. According to the 2nd approach, the inertial effects of the blood vessel are represented by capacitance *C*, while reciprocal of inductance *L* represents stiffness.
The following figure shows this approach applied to systemic arteries compartment.

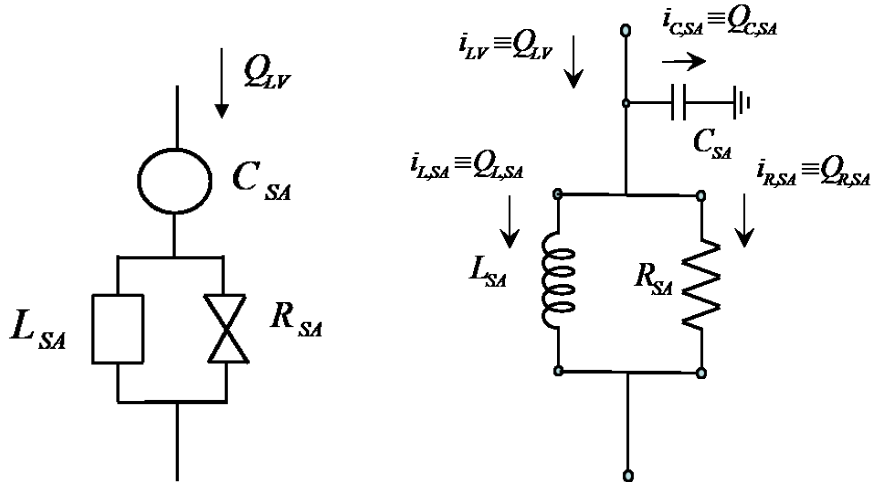

Figure 4.2.2.1 – Systemic arteries hydraulic scheme (left) and equivalent electric circuit with the 2nd approach where capacitance C represents inertial effects (right).

It can be noted that the capacitor is connected to ground since it has the inertial meaning.
Furthermore, the variables across and through elements are defined as in the 1st approach, that is according to the conventional analogy between hydraulic and electric power shown in Eq. (4.2.2) and Eq. (4.2.3).
Replacing all the rest of the compartments with this approach, the equivalent electric circuit obtained is the following. In addition, in this case, heart excitation is not included yet in the study. In fact, there are not voltage sources in the electric circuit obtained.

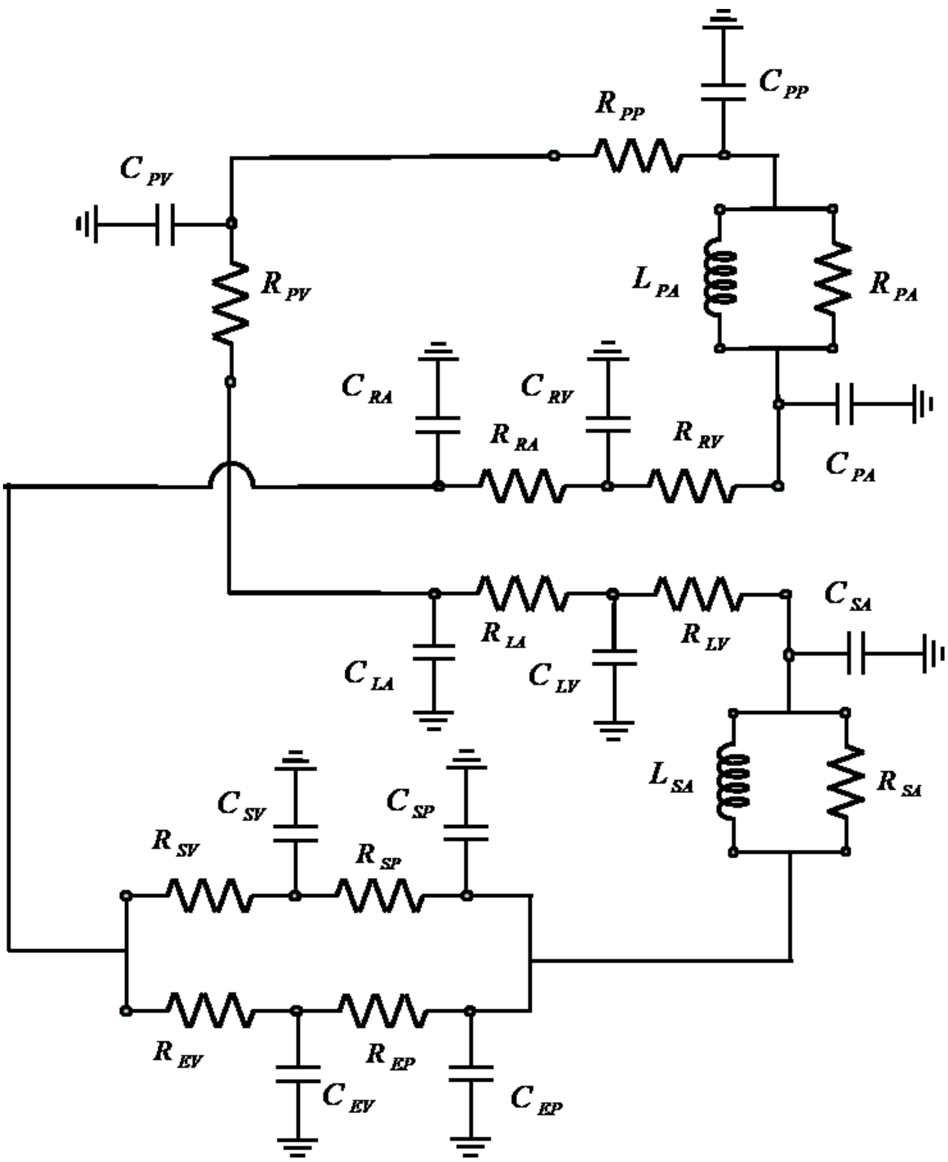

Figure 4.2.2.2 – Proposed electrical equivalent model for circulatory system, with 2nd approach (*C* inertia) from hydraulic to electric model.

It can be noted that each capacitor is connected to ground, so applying Firestone electro-mechanical analogy, each one of them corresponds to a mass. Therefore, it would be possible to analyse the dynamics of each compartment of the cardiovascular system, without ignoring compartment partition like the 1st approach. For this reason, the 2nd approach is preferred for CVS modelling.

4.3 Mechanical model for CVS

In order to obtain the equivalent mechanical model of the cardiovascular system, the equivalence between electric and mechanical power must be accomplished:

$$W_{el} = \Delta v \cdot i \text{ [W]} \Leftrightarrow W_m = f \cdot \dot{x} \text{ [W]} \tag{4.3.1}$$

As shown in Figure 4.2.6, it is possible to choose between two different electro-mechanical techniques for transformation. The conventional method is also called Maxwell analogy; the dual method is called Firestone analogy. More details about the two analogies are given in the Appendix.

4.3.1 Maxwell analogy from electric to mechanical model

Applying the 1st approach in the conversion from hydraulic to electric system, the inertial effects are assumed to be represented by inductance element. It implies to use Maxwell analogy to convert the electric circuit into the equivalent mechanical model.
The main difference between Maxwell and Firestone analogy is the inverted correspondence of the terms to define electrical and mechanical power. In particular, with Maxwell analogy electric voltage drop corresponds to mechanical force and current to velocity, so it results:

$$\Delta v\,[\mathrm{V}] \Leftrightarrow f\,[\mathrm{N}] \tag{4.3.1.1}$$

$$i\,[\mathrm{A}] \Leftrightarrow \dot{x}\left[\frac{\mathrm{m}}{\mathrm{s}}\right] \tag{4.3.1.2}$$

Then, the correlations for the other elements are:

$$L\,[\mathrm{H}] \Leftrightarrow m\,[\mathrm{kg}] \tag{4.3.1.3}$$

$$R\,[\Omega] \Leftrightarrow c\left[\frac{\mathrm{N\,s}}{\mathrm{m}}\right] \equiv c\left[\frac{\mathrm{kg}}{\mathrm{s}}\right] \tag{4.3.1.4}$$

$$\frac{1}{C}\left[\frac{1}{\mathrm{F}}\right] \Leftrightarrow k\left[\frac{\mathrm{N}}{\mathrm{m}}\right] \equiv k\left[\frac{\mathrm{kg}}{\mathrm{s}^2}\right] \tag{4.3.1.5}$$

It can be noted that the electric circuit has only two inductances so there will be only two masses in the mechanical system. As discussed in paragraph 2.1, choosing series configuration for L and R, the system could be reduced to have only one mass, one resistance and one capacitor. In that case, it would become a 1-DOF system. It would imply to ignore compartment partition in CVS, so it would not be useful to describe the dynamics of the entire cardiovascular system. This is the main reason why a 2nd approach is introduced, which involves Firestone analogy from electric to mechanical model.

4.3.2 Firestone analogy from electric to mechanical model

For this case of study, the analogy introduced by Firestone has been preferred. By choosing the 2nd approach, Firestone analogy can be applied to obtain a valuable CVS model.
The main assumption of Firestone analogy is that voltage drop Δv corresponds to velocity $\dot{x}$, therefore current i corresponds to force f in order to have the correspondence in electric and mechanical power:

$$\Delta v\,[\mathrm{V}] \Leftrightarrow \dot{x}\left[\frac{\mathrm{m}}{\mathrm{s}}\right] \tag{4.3.2.1}$$

$$i\,[\mathrm{A}] \Leftrightarrow f\,[\mathrm{N}] \tag{4.3.2.2}$$

The correlations between electric and mechanical components are [28]:

$$C\ [\mathrm{F}] \Leftrightarrow m\ [\mathrm{kg}] \tag{4.3.2.3}$$

$$\frac{1}{R}\left[\frac{1}{\Omega}\right] \Leftrightarrow c\left[\frac{\mathrm{N\,s}}{\mathrm{m}}\right] \equiv c\left[\frac{\mathrm{kg}}{\mathrm{s}}\right] \tag{4.3.2.4}$$

$$\frac{1}{L}\left[\frac{1}{\mathrm{H}}\right] \Leftrightarrow k\left[\frac{\mathrm{N}}{\mathrm{m}}\right] \equiv k\left[\frac{\mathrm{kg}}{\mathrm{s}^2}\right] \tag{4.3.2.5}$$

where m is mass, c is damping coefficient and k is spring stiffness.
Consequently, the constitutive laws for mechanical system can be written starting from Eq. (4.2.11), Eq. (4.2.9) and Eq. (4.2.7) and for each component, it results:

- Mass

$$\dot{x}_{mass} = \frac{1}{m}\int_0^t f_{mass}\,dt \Rightarrow \ddot{x}_{mass} = \frac{1}{m} f_{mass} \Rightarrow f_{mass} = m\,\ddot{x}_{mass} \tag{4.3.2.6}$$

- Damper

$$\dot{x}_{damper} = \frac{1}{c} f_{damper} \Rightarrow f_{damper} = c\,\dot{x}_{damper} \tag{4.3.2.7}$$

- Spring

$$\dot{x}_{spring} = \frac{1}{k}\frac{d\,f_{spring}}{d\,t} \Rightarrow f_{spring} = k\,x_{spring} \tag{4.3.2.8}$$

The equivalence between hydraulic, electric and mechanical systems is resumed in the following table, where state variables and balance equation used in each system are reported. The state variable is defined "across" each element; the variable defined "through" each element is used to obtain the balance equation at the node where $m = 1,..., M$ elements converge.

Table 4.3.2.1 – State variable and balance equation in hydraulic, electric and mechanical analogies.

	Hydraulic	**Electric**	**Mechanical**
State variable (across)	$\Delta p\ [\mathrm{Pa}]$	$\Delta v\ [\mathrm{V}]$	$\dot{x}\left[\frac{\mathrm{m}}{\mathrm{s}}\right]$
Balance equation (through)	$\sum_{m=1}^{M} Q_m = Q_s(t)\ \left[\frac{\mathrm{m}^3}{\mathrm{s}}\right]$	$\sum_{m=1}^{M} i_m = a(t)\ [\mathrm{A}]$	$\sum_{m=1}^{M} f_m = f(t)\ [\mathrm{N}]$

By converting the electric model into the equivalent Firestone mechanical system, the mass-spring-damper model of the cardiovascular system has been derived. Furthermore, some springs connected to ground have been added with respect to the original electric circuit; they are illustrated in red in the following figure. These springs are necessary to ensure a static state of the entire system, in order to be able to study its dynamics. In the scheme, the positive direction of coordinates is reported for each node, too.

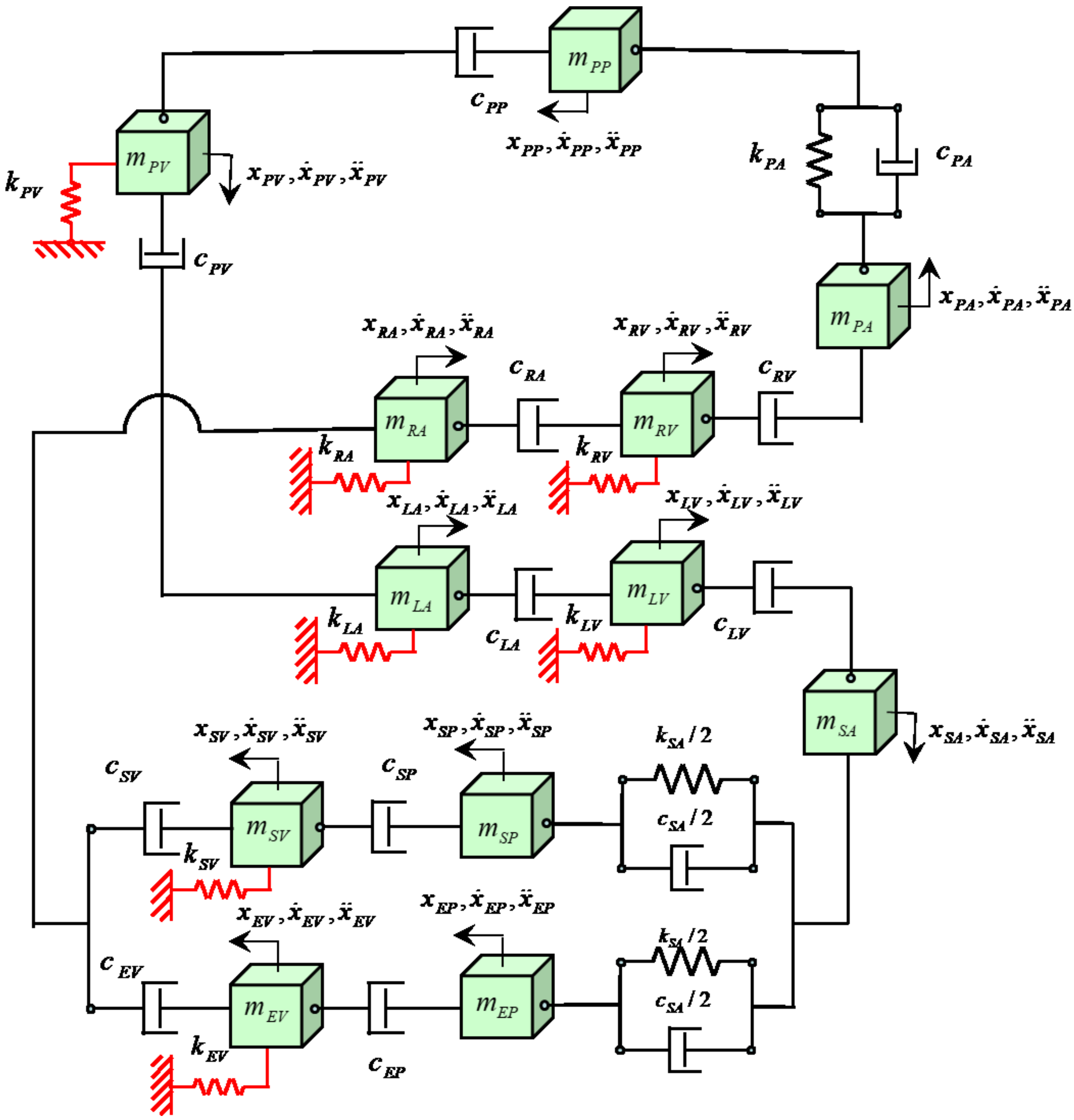

Figure 4.3.2.1 – Proposed mechanical equivalent model for circulatory system, with Firestone analogy (from conventional electric circuit).

In the case of systemic artery and pulmonary artery compartments, spring and damper have been split into two branches, with half constants each. The reason is always related to statics because without that split, there are two masses connected with a rigid link. A spring and damper per each mass ensure a static condition for the system.
It can be noted that, according to Firestone analogy, the electrical elements that are in series remains in series in the mechanical system and it is the same for elements in parallel.
Furthermore, the electric voltage source becomes a velocity imposed to the mass of ventricles. It means that an imposed kinetics for left and right ventricles must be determined, in order to account of the heart action. It will be added to the system in the next step, since heart excitation is not included yet in the equivalent electric and mechanical models.

Overall, the mechanical system derived is composed by 12 degrees of freedom, which correspond to the twelve compartments used to describe the cardiovascular system. Therefore, applying the free body diagram (FBD) to each mass of the mechanical model, twelve equations of motion will be obtained.

5. Dynamics of CVS mechanical model

The final mechanical model of cardiovascular system has been derived applying:

- The 2nd approach from hydraulic to electric model
- Firestone analogy from electric to mechanical model

The corresponding model is shown in Figure 4.3.2.1. In order to describe its dynamics, it is necessary to define matrices for mass, spring and damper. The values for hydraulic elements have been extracted from previous studies on human circulation or similar cases. The values considered are shown in Table 4.1.2.1, Table 4.1.2.2 and Table 4.1.2.3.

5.1 Mass values

According to Firestone analogy, mass is equivalent to electric capacitance (compliance in hydraulics):

$$m \text{ [kg]} \Leftrightarrow C \text{ [F]} \tag{5.1.1}$$

A way to define this relation numerically is to use an equivalence between two ratios. The first one is the ratio between the total mass of the blood in human body and the total compliance in the circulatory system. The second ratio is between the mass of each component j (degree of freedom of the mechanical system obtained) and the corresponding capacitance.

$$m_{tot} : \sum_i C_i = m_j : C_j \tag{5.1.2}$$

The indices i and j goes from 1 to 12, that are the total degrees of freedom of the mechanical system, and correspond to the 12 components called: LA, LV, RA, RV, SA, SP, SV, PA, PP, PV. The total mass of blood is obtained from blood density ρ_{blood} and volume of blood in the entire system V_{tot}:

$$m_{tot} = V_{tot} \ \rho_{blood} \tag{5.1.3}$$

$$V_{tot} = 5300 \text{ ml} = 0.0053 \text{ m}^3 \tag{5.1.4}$$

$$\rho_{blood} = 1060 \text{ kg/m}^3 \tag{5.1.5}$$

The summation of all the compliances can be calculated from values showed in tables for hydraulic model. Therefore, it is possible to calculate mass for each degree of freedom j:

$$m_j = \frac{m_{tot} \, C_j}{\sum_i C_i} \tag{5.1.6}$$

The numerical values that are the same for every degree of freedom are:

$$m_{tot} = 5.618 \text{ kg} \tag{5.1.7}$$

$$\sum_i C_i = 198.4303 \text{ ml/mmHg} = 1.488 \cdot 10^{-6} \ (\text{kg m}^2)/\text{s}^2 = 1.488 \cdot 10^{-6} \ [\text{F}] \tag{5.1.8}$$

It can be noted that the capacitance can be considered in medical units [ml/mmHg] or in SI units [[(kg m^2)/s^2] or in electric units [F]. In any case, the value of the mass obtained is the same because it comes from a proportional ratio as in Eq. (5.1.6).
The following table shows hydraulic capacitance, its corresponding electric capacitance and mass value for each node of the CVS model.

Table 5.1.1 – Mass values from hydraulic and electric capacitance, for each node.

Nodes		Hydraulic	Electric	Mechanic
Number	Name	Capacitance [ml/mmHg]	Capacitance [F] or [(kg m^2)/s^2]	Mass [kg]
1	LA	19.23	$1.442 \cdot 10^{-7}$	0.5444
2	LV	0.3389	$2.542 \cdot 10^{-9}$	0.0096
3	RA	31.25	$2.3439 \cdot 10^{-7}$	0.8848
4	RV	0.5714	$4.2589 \cdot 10^{-9}$	0.0162
5	SA	0.28	$2.1002 \cdot 10^{-9}$	0.0079
6	SP	2.05	$1.5376 \cdot 10^{-8}$	0.0580
7	SV	61.11	$4.5836 \cdot 10^{-7}$	1.7302
8	EP	1.67	$1.2526 \cdot 10^{-8}$	0.0473
9	EV	50	$3.7503 \cdot 10^{-7}$	1.4156
10	PA	0.76	$5.7005 \cdot 10^{-9}$	0.0215
11	PP	5.8	$4.3504 \cdot 10^{-8}$	0.1642
12	PV	25.37	$1.9029 \cdot 10^{-7}$	0.7183

5.2 Spring constant values

The values of the spring constants k_i that describe each spring in the proposed mechanical model have to be defined. According to Firestone analogy, they correspond to the reciprocal of electric inductance L.

$$k\left[\frac{\text{N}}{\text{m}}\right] \equiv k\left[\frac{\text{kg}}{\text{s}^2}\right] \Leftrightarrow \frac{1}{L}\left[\frac{1}{\text{H}}\right] \tag{5.2.1}$$

The electric and the mechanic models must have the same eigenvalues. Therefore, it is possible to use the natural frequency ω_n definition to find numerical values for spring constants [29]. Using Firestone analogy, the correspondence is:

$$\omega_n = \sqrt{\frac{k}{m}} \Leftrightarrow \sqrt{\frac{1}{L\,C}} \tag{5.2.2}$$

In the hydraulic model, the capacitance value is given for each degree of freedom, the inductance value is given only for systemic artery SA and pulmonary artery PA. In the mechanical model, other springs have been added, so other inductance values have to be added. They have been assumed to be equal to the systemic artery inductance because it is the highest value, so it corresponds to a lower spring constant. Therefore, for each degree of freedom *i* the spring constant is derived using natural frequency definition with electric terms and mass values calculated as described in paragraph 5.1. It results:

$$k_i = \omega_{n,i}^{\;2}\, m_i = \left(\frac{1}{L_i\,C_i}\right) m_i \tag{5.2.3}$$

The spring constant values found are shown in the following table, with the corresponding hydraulic and electric inductance values.

Table 5.2.1 – Spring constant values from hydraulic and electric inductance, for each node.

Nodes		Hydraulic	Electric	Mechanic
Number	Name	Inductance [mmHg s^2/ml]	Inductance [H] or [kg/m^4]	Spring constant [N/m]
1	LA	0.00022	$2.9331\cdot10^4$	128.692
2	LV	0.00022	$2.9331\cdot10^4$	128.692
3	RA	0.00022	$2.9331\cdot10^4$	128.692
4	RV	0.00022	$2.9331\cdot10^4$	128.692
5	SA	0.00022	$2.9331\cdot10^4$	128.692
6	SP	-	-	-
7	SV	0.00022	$2.9331\cdot10^4$	128.692
8	EP	-	-	-
9	EV	0.00022	$2.9331\cdot10^4$	128.692
10	PA	0.00018	$2.3998\cdot10^4$	157.290
11	PP	-	-	-
12	PV	0.00022	$2.9331\cdot10^4$	128.692

5.3 Damping coefficients values

According to Firestone analogy, damping coefficient corresponds to the reciprocal of the hydraulic resistance:

$$c\left[\frac{\mathrm{N\,s}}{\mathrm{m}}\right] \equiv c\left[\frac{\mathrm{kg}}{\mathrm{s}}\right] \Leftrightarrow \frac{1}{R}\left[\frac{1}{\Omega}\right] \tag{5.3.1}$$

Damping coefficient can be defined using the damping ratio ζ (zeta) that characterizes the frequency response of a second order differential equation. It is defined as the ratio between the actual damping coefficient and the critical damping, so it is dimensionless:

$$\zeta = \frac{c}{c_{cr}} = \frac{c}{2m\omega_n} \tag{5.3.2}$$

With electric terms, the correspondence is:

$$\xi = \frac{c}{2m\omega_n} \Leftrightarrow \frac{1}{2R}\sqrt{\frac{L}{C}} \tag{5.3.3}$$

Therefore, for each degree of freedom it can be calculated using damping ratio electric definition and mass and spring constant values calculated as described in paragraphs 5.1 and 5.2. It results:

$$c_i = \left(\frac{1}{2\ R_i}\sqrt{\frac{L_i}{C_i}}\right) 2\ \sqrt{k_i\ m_i} \tag{5.3.4}$$

For three degrees of freedom that correspond to pulmonary peripheral circulation (PP), splanchnic peripheral (SP) and extra splanchnic peripheral (EP), the spring constants used are the ones that connect them with the closest node. In particular, k_{PA} is used to define PP natural frequency, $k_{SA}/2$ for SP node and $k_{SA}/2$ for EP node, too. The values calculated for each damper defined in the mechanical system are written in the following table, with the hydraulic and electric resistance values.

Table 5.3.1 – Damping coefficient values from hydraulic and electric resistance, for each node.

Nodes		Hydraulic	Electric	Mechanic
Number	Name	Resistance [mmHg s/ml]	Resistance [Ω] or [kg/(m^4 s)]	Damping coefficient [N s/m]
1	LA	0.0025	$3.333\cdot10^5$	11.3249
2	LV	0.08197	$1.0928\cdot10^7$	0.3454
3	RA	0.0025	$3.333\cdot10^5$	11.3249
4	RV	0.1817	$2.4224\cdot10^7$	0.1558
5	SA	0.06	$7.9993\cdot10^6$	0.4719
6	SP	3.307	$4.4089\cdot10^8$	0.0061
7	SV	0.038	$5.0662\cdot10^6$	0.7451

8	EP	1.407	$1.8758 \cdot 10^8$	0.0142
9	EV	0.016	$2.1332 \cdot 10^6$	1.7695
10	PA	0.023	$3.0664 \cdot 10^6$	1.2310
11	PP	0.0894	$1.1919 \cdot 10^7$	0.3501
12	PV	0.0056	$7.466 \cdot 10^5$	5.0558

5.4 MCK model

The following dynamic matrix problem is considered:

$$\mathbf{M}\ \ddot{\mathbf{x}} + \mathbf{C}\ \dot{\mathbf{x}} + \mathbf{K}\ \mathbf{x} = \mathbf{f}(t) \tag{5.4.1}$$

In this case there are 12 degrees of freedom, therefore **M**, **C** and **K** are mass, stiffness and damping matrices with dimensions 12x12, $\mathbf{x}$ is the vector of displacement (12x1), $\dot{\mathbf{x}}$ is the vector velocity (12x1) and $\ddot{\mathbf{x}}$ is the vector of acceleration (12x1). The vector **f** (t) represents the forces applied on masses but in this case it is initially considered equal to zero because there is no force acting on the system.
Matrix **M** has the twelve masses on the diagonal. The order considered is shown in the following equation.

$$\mathbf{M} = \begin{bmatrix} m_{LA} & 0 & 0 & 0 & 0 & 0 & 0 & 0 & 0 & 0 & 0 & 0 \\ 0 & m_{LV} & 0 & 0 & 0 & 0 & 0 & 0 & 0 & 0 & 0 & 0 \\ 0 & 0 & m_{RA} & 0 & 0 & 0 & 0 & 0 & 0 & 0 & 0 & 0 \\ 0 & 0 & 0 & m_{RV} & 0 & 0 & 0 & 0 & 0 & 0 & 0 & 0 \\ 0 & 0 & 0 & 0 & m_{SA} & 0 & 0 & 0 & 0 & 0 & 0 & 0 \\ 0 & 0 & 0 & 0 & 0 & m_{SP} & 0 & 0 & 0 & 0 & 0 & 0 \\ 0 & 0 & 0 & 0 & 0 & 0 & m_{SV} & 0 & 0 & 0 & 0 & 0 \\ 0 & 0 & 0 & 0 & 0 & 0 & 0 & m_{EP} & 0 & 0 & 0 & 0 \\ 0 & 0 & 0 & 0 & 0 & 0 & 0 & 0 & m_{EV} & 0 & 0 & 0 \\ 0 & 0 & 0 & 0 & 0 & 0 & 0 & 0 & 0 & m_{PA} & 0 & 0 \\ 0 & 0 & 0 & 0 & 0 & 0 & 0 & 0 & 0 & 0 & m_{PP} & 0 \\ 0 & 0 & 0 & 0 & 0 & 0 & 0 & 0 & 0 & 0 & 0 & m_{PV} \end{bmatrix} \tag{5.4.2}$$

Damping coefficients are reported in matrix **C**. It accounts of the dampers shared between two masses.

$$
\mathbf{C} = \begin{bmatrix}
c_{LA}+c_{PV} & -c_{LA} & 0 & 0 & 0 & 0 & 0 & 0 & 0 & 0 & 0 & -c_{PV} \\
-c_{LA} & c_{LA}+c_{LV} & 0 & 0 & -c_{LV} & 0 & 0 & 0 & 0 & 0 & 0 & 0 \\
0 & 0 & c_{RA}+c_{SV}+c_{EV} & -c_{RA} & 0 & 0 & -c_{SV} & 0 & -c_{EV} & 0 & 0 & 0 \\
0 & 0 & -c_{RA} & c_{RA}+c_{RV} & 0 & 0 & 0 & 0 & 0 & -c_{RV} & 0 & 0 \\
0 & -c_{LV} & 0 & 0 & c_{LV}+c_{SA} & -c_{SA}/2 & 0 & -c_{SA}/2 & 0 & 0 & 0 & 0 \\
0 & 0 & 0 & 0 & -c_{SA}/2 & c_{SA}/2+c_{SP} & -c_{SP} & 0 & 0 & 0 & 0 & 0 \\
0 & 0 & -c_{SV} & 0 & 0 & -c_{SP} & c_{SP}+c_{SV} & 0 & 0 & 0 & 0 & 0 \\
0 & 0 & 0 & 0 & -c_{SA}/2 & 0 & 0 & c_{SA}/2+c_{EP} & -c_{EP} & 0 & 0 & 0 \\
0 & 0 & -c_{EV} & 0 & 0 & 0 & 0 & -c_{EP} & c_{EV}+c_{EP} & 0 & 0 & 0 \\
0 & 0 & 0 & -c_{RV} & 0 & 0 & 0 & 0 & 0 & c_{PA}+c_{RV} & -c_{PA} & 0 \\
0 & 0 & 0 & 0 & 0 & 0 & 0 & 0 & 0 & -c_{PA} & c_{PA}+c_{PP} & -c_{PP} \\
-c_{PV} & 0 & 0 & 0 & 0 & 0 & 0 & 0 & 0 & 0 & -c_{PP} & c_{PP}+c_{PV}
\end{bmatrix}
$$
(5.4.3)

In matrix **K,** the spring constants are written.

$$
\mathbf{K} = \begin{bmatrix}
k_{LA} & 0 & 0 & 0 & 0 & 0 & 0 & 0 & 0 & 0 & 0 & 0 \\
0 & k_{LV} & 0 & 0 & 0 & 0 & 0 & 0 & 0 & 0 & 0 & 0 \\
0 & 0 & k_{RA} & 0 & 0 & 0 & 0 & 0 & 0 & 0 & 0 & 0 \\
0 & 0 & 0 & k_{RV} & 0 & 0 & 0 & 0 & 0 & 0 & 0 & 0 \\
0 & 0 & 0 & 0 & k_{SA} & -k_{SA}/2 & 0 & -k_{SA}/2 & 0 & 0 & 0 & 0 \\
0 & 0 & 0 & 0 & -k_{SA}/2 & k_{SA}/2 & 0 & 0 & 0 & 0 & 0 & 0 \\
0 & 0 & 0 & 0 & 0 & 0 & k_{SV} & 0 & 0 & 0 & 0 & 0 \\
0 & 0 & 0 & 0 & -k_{SA}/2 & 0 & 0 & k_{SA}/2 & 0 & 0 & 0 & 0 \\
0 & 0 & 0 & 0 & 0 & 0 & 0 & 0 & k_{EV} & 0 & 0 & 0 \\
0 & 0 & 0 & 0 & 0 & 0 & 0 & 0 & 0 & k_{PA} & -k_{PA} & 0 \\
0 & 0 & 0 & 0 & 0 & 0 & 0 & 0 & 0 & -k_{PA} & k_{PA} & 0 \\
0 & 0 & 0 & 0 & 0 & 0 & 0 & 0 & 0 & 0 & 0 & k_{PV}
\end{bmatrix} \qquad (5.4.4)
$$

5.5 Proportional damping: MK model

It is common to assume proportional damping in order to apply modal analysis of undamped systems to damped systems. The eigenproblem of a *n*-DOF undamped system can be written as:

$$\left(\mathbf{K} - \omega_r^2 \mathbf{M}\right) \mathbf{\Phi}_r = \mathbf{0} \qquad (5.5.1)$$

where $1 \le r \le n$, $\mathbf{\Phi}_r$ is the eigenvector normalised with unitary modal mass and ω_r^2 is the eigenvalue for each degree of freedom of the system.

The matrix $\mathbf{\Phi}$ with all the eigenvectors is called modal matrix. It is orthogonal to mass and stiffness matrices so that $\mathbf{\Phi}^{\mathrm{T}} \mathbf{M} \mathbf{\Phi}$ and $\mathbf{\Phi}^{\mathrm{T}} \mathbf{K} \mathbf{\Phi}$ are diagonal.

Considering proportional damping, the viscous damping matrix **C** is assumed proportional to mass and stiffness matrices with constant coefficients α and β:

$$\mathbf{C} = \alpha \mathbf{M} + \beta \mathbf{K} \qquad (5.5.2)$$

It means that the undamped modal matrix $\mathbf{\Phi}$ can also diagonalise the damping matrix $\mathbf{C}$. In particular, the diagonalised damping matrix becomes:

$$\mathbf{\Phi}^{\mathrm{T}}\mathbf{C}\mathbf{\Phi} = \mathrm{diag}(2\xi_r\,\boldsymbol{\omega}_r) \tag{5.5.3}$$

where the damping ratio is defined as:

$$\xi_r = \frac{\alpha}{2}\frac{1}{\omega_r} + \frac{\beta}{2}\omega_r \tag{5.5.4}$$

Since all the matrices can be diagonalised with this assumption, the equations of motion of the MDOF system can be uncoupled and studied as independent SDOF systems.
Proportional damping is also known as "classical damping" or "Rayleigh damping" model. Caughey and O'Kelly have derived the condition, which the system matrices must satisfy so that viscously damped linear systems possess classical normal modes. In general, linear systems do not satisfy that condition and consequently, they possess complex modes [30].
The CVS mechanical model has many dampers and the damping matrix in Eq. (5.4.3) shows that there is not any proportionality with mass and stiffness matrices, also many damping coefficient values are not on the diagonal. However, it is possible to evaluate the results derived from a proportional damping assumption. In fact, a common approach is to ignore terms off the diagonal of the modal damping matrix $\mathbf{\Phi}^{\mathrm{T}}\mathbf{C}\mathbf{\Phi}$. This method provides approximated results for modal analysis of the system. In order to visualise the model considered, dampers must be taken away from the original CVS model and it can be called MK instead of MCK. It is illustrated in the following figure.

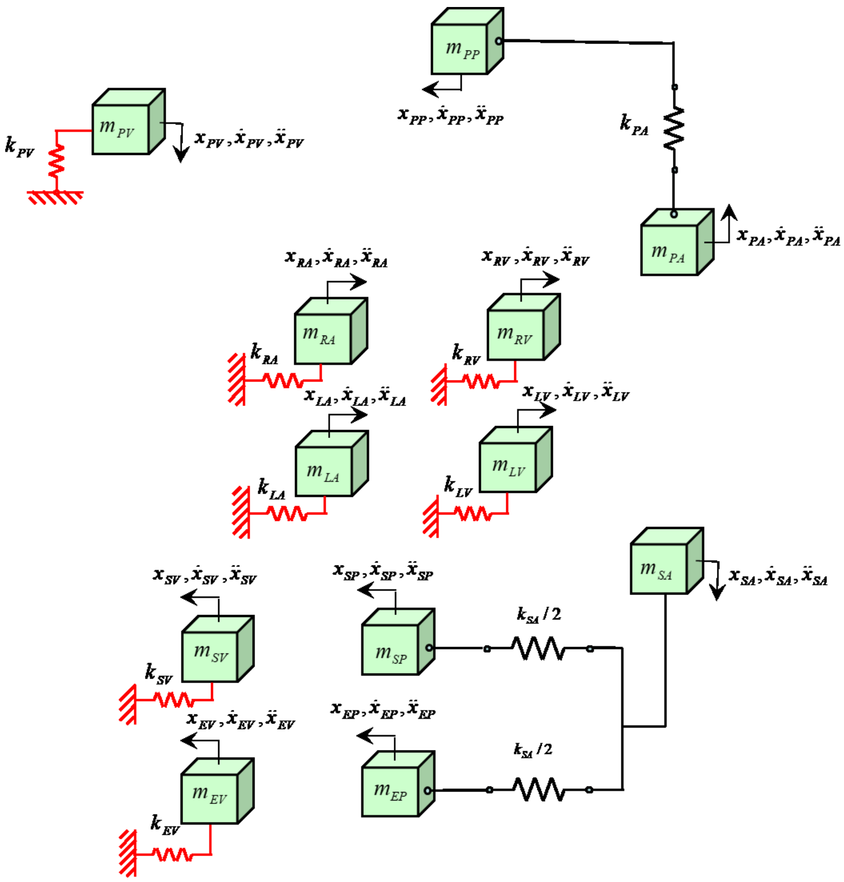

Figure 5.5.1 –Firestone mechanical equivalent model MK without dampers.

It can be noted that deleting all the dampers from mechanical schematic, two subsystems are found to move like rigid bodies. One rigid body motion involves systemic artery, splanchnic and extra splanchnic peripheral circulation compartments (SA, SP, EP); the other one involves pulmonary artery and peripheral pulmonary circulation compartments (PA, PP). In fact, two eigenvalues are equal to zero, as shown in the following paragraph.

5.5.1 MK natural frequencies and damping factor

Eigenvalues can be derived from the CVS undamped or proportionally damped model. Then, natural frequencies ω_n are obtained and converted into [Hz] values.
Assuming proportional damping, damping ratio can be calculated using undamped modal matrix as in Eq. (5.5.3) and ignoring terms off the diagonal of the damping modal matrix.
Results obtained for natural frequencies and damping ratio are shown in the following table.

Table 5.5.1.1 – Natural frequencies obtained solved MK model, assuming proportional damping, and corresponding damping factor for each mode.

Natural frequencies of MK model (C prop.)			
#Mode	ω_n [rad/s]	f [Hz]	ζ [%]
1	$2.9962 \cdot 10^{-9}$	$4.7686 \cdot 10^{-8}$	-
2	$3.3718 \cdot 10^{-9}$	$5.3663 \cdot 10^{-8}$	-
3	8.6245	1.3726	2.52
4	9.5346	1.5175	6.61
5	12.060	1.9195	64.8
6	13.385	2.1303	28.1
7	15.374	2.4469	97.8
8	35.125	5.5904	6.79
9	89.190	14.195	>100
10	90.927	14.471	39.2
11	115.81	18.432	>100
12	132.17	21.036	39.6

It can be noted that CVS model is a 12-DOFs system and 12 natural frequencies and vibrational modes have been derived. In particular, there are:

- two modes of rigid body motion (1st and 2nd modes) where natural frequency is almost zero;
- two overdamped modes (9th and 11th) where damping ratio is greater than 1.

Actually, it is possible to set natural frequencies for overdamped modes equal to zero, like for rigid body modes. The reason is that when overdamping occurs, the system tends to stop oscillating.

5.6 Non proportional damping: MCK model

The CVS system obtained is a multi-degree of freedom (MDOF) system with a damping that cannot be assumed proportional. Therefore, the case of general viscous damping occurs. It has been implemented with a MATLAB script that applies Duncan method method to MCK matrices.
Using the Firestone electric equivalent elements as in Eq. (5.1.1), Eq. (5.2.1) and Eq. (5.3.1), the same method used with MCK model can be applied. The eigenvalues obtained for the mechanical and the electric system are the same and they are shown in the following table. Furthermore, using hydraulic elements in the model matrices, the same eigenvalues as the electric model are obtained. The reason is that the conversion between electric and hydraulic elements (R, L, C) deals only with units.

Table 5.6.1 – Eigenvalues obtained solving MCK model with hydraulic elements, electric equivalent and mechanical equivalent ones with Firestone analogy.

Eigenvalues from MCK model			
#	Hydraulic	Electric	Mechanic Firestone
1	0	0	0
2	0	0	0
3	-0.21275+8.6302j	-0.21275+8.6302j	-0.21203+8.6302j
4	-0.21275-8.6302j	-0.21275-8.6302j	-0.21203-8.6302j
5	-0.58653+9.5845j	-0.58653+9.5845j	-0.58444+9.5847j
6	-0.58653-9.5845j	-0.58653-9.5845j	-0.58444-9.5847j
7	-2.6808+14.758j	-2.6808+14.758j	-2.7100+14.757j
8	-2.6808-14.758j	-2.6808-14.758j	-2.7100-14.757j
9	-4.0189+15.819j	-4.0189+15.819j	-4.0189+15.819j
10	-4.0189-15.819j	-4.0189-15.819j	-4.0189-15.819j
11	-8.6622+17.738j	-8.6621+17.738j	-8.6548+17.726j
12	-8.6622-17.738j	-8.6621-17.738j	-8.6548-17.726j
13	-2.4276+35.039j	-2.4276+35.039j	-2.3839+35.043j
14	-2.4276-35.039j	-2.4276-35.039j	-2.3839-35.043j
15	-35.616+74.107j	-35.616+74.107j	-35.628+83.632j
16	-35.616-74.107j	-35.616-74.107j	-35.628-83.632j
17	-51.609+121.05j	-51.609+121.05j	-51.606+121.05j
18	-51.609-121.05j	-51.609-121.05j	-51.606-121.05j
19	-2.5605	-2.5605	-2.7446
20	-3.3793	-3.3793	-3.3019
21	-5.1823	-5.1823	-5.1839

22	-5.9995	-5.9995	-5.9991
23	-711.47	-711.47	-711.47
24	-1227.2	-1227.2	-1227.2

It can be noted that there are 24 eigenvalues, while the model has 12 degreed of freedom. The reason is connected to the non-classical damping assumed and the method used.
The main dynamic characteristics seen from the values obtained are:

- There are two modes of rigid body motion (1^{st} and 2^{nd} modes);
- The 19^{th}, 20^{th}, 21^{st}, 22^{nd}, 23^{rd} and 24^{th} modes have the imaginary part equal to zero or absolutely negligible, so they can be considered overdamped modes;
- There are 16 complex conjugate eigenvalues, that means underdamped modes.

For this case of study, damping effect is important to analyse the dynamics of the entire system. Therefore, MCK model will be taken into account for more dynamic analysis.

5.6.1 MCK natural frequencies and damping factor

Natural frequencies of a non-proportionally damped MDOF model can be calculated as modulus of complex eigenvalues:

$$|S_r| = |S_{r*}| = \sqrt{\xi_r^2 \omega_r^2 + \omega_r^2 (1-\xi_r^2)} = \sqrt{\xi_r^2 \omega_r^2 + \omega_r^2 - \omega_r^2 \xi_r^2} = \omega_r \tag{5.6.1.1}$$

It applies to underdamped modes. Modes OF rigid body motion and overdamped modes can be assumed to have natural frequency equal to zero. The reason is that there is no significant oscillation of the system.
When eigenvalues are complex, damping ratio for underdamped modes can be calculated as:

$$\xi_r = -\frac{\mathrm{Re}(S_r)}{|S_{r,r*}|} \tag{5.6.1.2}$$

The values of natural frequencies and damping percentage are reported in the following table.

Table 5.6.1.1 – Natural frequencies obtained solved MCK model with Duncan method and corresponding damping factor for each mode.

Natural frequencies of MCK model			
#Mode	ω_n [rad/s]	f [Hz]	ζ [%]
1-2	0	0	-
3-4	8.6328	1.3739	2.46
5-6	9.6025	1.5283	6.09
7-8	15.004	2.3879	18.1
9-10	16.322	2.5977	24.6
11-12	19.726	3.1394	43.9

13-14	35.124	5.5902	6.79
15-16	90.905	14.468	39.2
17-18	131.59	20.944	39.2
19	0	0	>100
20	0	0	>100
21	0	0	>100
22	0	0	>100
23	0	0	>100
24	0	0	>100

It is possible to see a direct correspondence between natural frequencies and damping ratios of MK and MCK models. It is not a good correspondence for some modes because the assumption of proportional damping is too approximate for this model. Therefore, Duncan model results to be more appropriate and accurate in the frequencies and damping ratios obtained.

5.7 Correlation between proportional and non-proportional damping models

It is interesting to look at the correlation between the natural frequencies obtained for the system with proportional damping and for the same system when damping is considered non-proportional. In this paragraph, frequencies will be considered. Then, LUPOS FEM code will be used to represent the CVS model and visualise its mode shapes. In this way, also eigenvectors of MK and MCK models will be compared in detail.

Looking at the frequencies values from Table 5.5.1.1 and Table 5.6.1.1, it can be noted that each eigenvalue of MK model corresponds to two eigenvalues of MCK model. It derives from the method used for complex modal analysis, where the number of eigenvalues is $2n = 24$.

- Each mode of rigid body motion in MK model corresponds to a rigid body mode plus an overdamped mode in MCK model. It is clear that the 1st and 2nd modes of MCK model are rigid body motions, but it is not possible to say which are the relative overdamped modes. It is necessary to look at mod shapes in order to identify them.
- The 3rd mode of MK model seems to correspond to modes 3 and 4 of MCK model, since the frequency values are very close, as well as damping ratio.
- The 4th mode of MK model may correspond to modes 5-6 of MCK model, since the frequency is the same, as well as damping ratio.
- For the same reason as above, mode 8 of MK model may correspond to modes 13-14 of MCK model.
- In MK model, modes 5, 6 and 7 goes from 1.92 Hz to 2.45 Hz with a damping ratio varying from 28 % to 98 %. Otherwise, in MCK model, three couples of modes, that are 7-8, 9-10 and 11-12, goes from 2.39 Hz to 3.14 Hz with a damping ratio much smaller than MK case (form 18 % to 44 %). There may be a correlation between these modes because it is a similar range of frequency.
- Mode 10 of MK model shows the same frequency and damping ratio as underdamped modes 15-16 of MCK model.
- Mode 12 of MK model has a frequency that is very close to the MCK modes 17-18 as well as damping ratio value.

- Overdamped modes 9 and 11 of MK model correspond to four overdamped modes in MCK model. Since frequency is zero for all of them, it is required mode shapes visualisation to determine the actual correlations.

5.8 CVS model variation: reduced spring constants

It is possible to see how the dynamic behaviour of the CVS mechanical model changes applied some variations to the model. The first modification can be reducing spring constant values of springs connected to ground, added to ensure model statics. They were initially assumed to be equal to the lowest spring constant given by literature. In this analysis, they will be assumed to be 100 times smaller than that previous value. It means that only for the springs added arbitrarily, the correspondence between spring constant and electric inductance becomes:

$$k\left[\frac{\mathrm{N}}{\mathrm{m}}\right] \equiv k\left[\frac{\mathrm{kg}}{\mathrm{s}^2}\right] \Leftrightarrow \frac{1}{100 \cdot L}\left[\frac{1}{\mathrm{H}}\right] \tag{5.8.1}$$

The springs involved in this variation refer to left atrium LA, left ventricle LV, right atrium RA, right ventricle RV, splanchnic veins SV, extra splanchnic veins EV and pulmonary veins PV, that means $i = 1,2,3,4,7,9,12$. The values of spring constant for these DOFs in MCK model become:

$$k_i = \omega_{n,i}^{\;2}\, m_i = \left(\frac{1}{100 \cdot L_i\, C_i}\right) m_i \tag{5.8.2}$$

Consequently, also the corresponding damping coefficient values change:

$$c_i = \left(\frac{1}{2\, R_i}\sqrt{\frac{100 \cdot L_i}{C_i}}\right) 2\sqrt{k_i\, m_i} \tag{5.8.3}$$

Solving the same problem for MCK model with non-proportional damping, natural frequencies obtained are shown in the following table, with the corresponding damping ratio.

Table 5.8.1 – Natural frequencies obtained solved MCK model with spring constant values for springs connected to ground reduced 100 times.

Natural frequencies of MCK model with reduced k values		
#Mode	f [Hz]	ζ [%]
1-2	0	-
3-4	0.14752	3.09
5-6	0.1793	16.5
7-8	0.2543	9.19
9-10	5.5866	9.49
11-12	14.436	40.4

13-14	20.944	39.3
15	0	>100
16	0	>100
17	0	>100
18	0	>100
19	0.5175	>100
20	0.7741	>100
21	2.1518	>100
22	4.3791	>100
23	114.96	>100
24	197.01	>100

According to this solution, there are 2 rigid body motion modes, 12 underdamped modes and 10 overdamped modes. The damping percentage is reported only for underdamped modes in the table above. It can be noted that the overall frequency bandwidth of the system is lower than 21 Hz as in the original system. The main aspect of this model is that the system dynamics does not include heart rate frequencies around 1 Hz. Physically, it may mean that with lower spring constant values, there is less stiffness in the system, so the damping effect is dominant. It can be noted that the frequency around 1 Hz corresponds to heart rate recorded experimentally, as shown in CWT graphs. When spring constants are reduced, the CVS model created has natural frequencies quite far from resonance frequencies of actual cardiac activity. Consequently, these new spring constants for the MCK model could work properly, as well as the springs adopted initially.

Since Duncan method was used for MCK model, we expect to find in the corresponding MK model: 2 rigid body motion modes, 6 underdamped modes and 4 overdamped modes. Considering MK model, damping is assumed proportional, so approximated results are expected. To calculate damping ratio, the same calculations done in the previous paragraph have been applied.

Table 5.8.2 – Natural frequencies obtained solved MK model with spring constant values for springs connected to ground reduced 100 times.

Natural frequencies of MK model with reduced k values		
#Mode	f [Hz]	ζ [%]
1	0	-
2	0	-
3	0.1373	26.9
4	0.1517	70.8
5	0.19195	>100
6	0.2130	>100
7	0.2447	>100
8	1.4195	>100
9	1.8432	>100

10	5.5904	9.49
11	14.4715	40.5
12	21.036	39.6

It is not possible to identify exactly the types of modes expected in MK model, for example, it is possible to see only 5 underdamped modes instead of 6 modes expected. More investigation is required to solve this issue. However, it can be noted that the range of frequency is always the same that is under 21 Hz. There is a mode around 1.4 Hz but the corresponding damping factor calculated assuming proportional damping is higher than 1. It may confirm that with less stiffness in the model, damping is significant and it cannot be approximated with proportional damping.

Overall, reducing spring constants, a valid alternative MCK model is obtained to study the dynamics of the system. However, the CVS mechanical model analysed with more attention in this work involves the spring constant values adopted originally rather than reduced values.

5.9 CVS model variation: no rigid body motion

It is possible to avoid modes of rigid body motion adding some springs to the original CVS model. In particular, two springs connected to ground are added for masses related to systemic arteries SA and peripheral pulmonary circulation PP compartments. Spring constants are assumed equal to the other springs connected to ground.

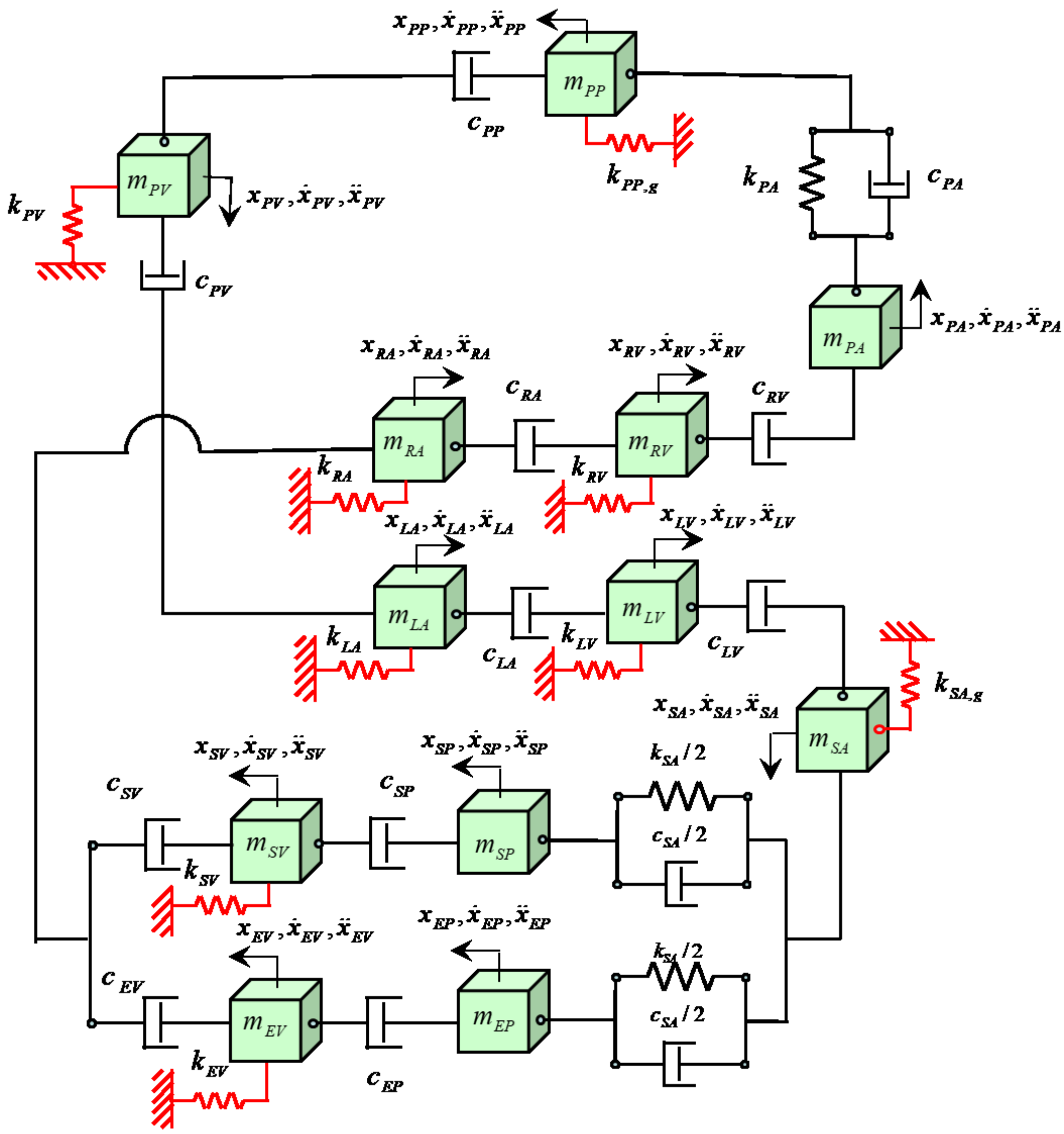

Figure 5.9.1 – Mechanical equivalent model for circulatory system, with Firestone analogy, with two more springs connecting SA and PP to ground.

Applying this variation, it can be noted that there are not rigid body motions if dampers are neglected. Solving complex modal analysis, 20 underdamped modes and 4 overdamped modes are obtained. The natural frequencies are reported in the following table.

Table 5.9.1 – Natural frequencies obtained solved MCK model with more springs to ground, without rigid body motions.

MCK model without rigid body modes		
#Mode	f [Hz]	ζ [%]
1-2	1.374	2.46
3-4	1.528	6.09
5-6	2.393	18.0
7-8	2.598	24.7

9-10	3.149	44.0
11-12	3.879	4.11
13-14	4.601	5.07
15-16	5.619	6.78
17-18	14.57	38.8
19-20	28.98	28.8
21	0	>100
22	0	>100
23	0	>100
24	0	>100

Comparing Table 5.9.1 and Table 5.6.1.1, it is deduced that, in the new model without rigid body motion, there are two natural frequencies that did not appear in the original model: 3.879 Hz and 4.601 Hz. They correspond to four underdamped modes, which had frequency equal to zero in the model with two modes of rigid body motion. The damping percentage is very similar in the two models considered.

It is possible to apply another variation to the CVS model without rigid body motions, which is the reduction of spring constants. In this case, spring constants are divided by 10, then the related inductances are calculated, as well as damping coefficients, as described in the paragraph above.

$$k\left[\frac{\mathrm{N}}{\mathrm{m}}\right] \equiv k\left[\frac{\mathrm{kg}}{\mathrm{s}^2}\right] \Leftrightarrow \frac{1}{10\cdot L}\left[\frac{1}{\mathrm{H}}\right] \qquad (5.9.1)$$

Solving complex modal analysis, which means considering non-proportional damping, 6 overdamped modes and 18 underdamped modes are calculated.

Table 5.9.2 – Natural frequencies obtained solved MCK model without rigid body motions and springs connected to ground reduced 10 times.

MCK model without rigid body motion, with reduced k values		
#Mode	f [Hz]	ζ [%]
1-2	0.4373	7.95
3-4	0.5122	18.2
5-6	0.8088	35.7
7-8	0.9183	11.8
9-10	1.276	43.4
11-12	1.621	14.8
13-14	5.593	7.44
15-16	14.48	39.5
17-18	21.87	37.8
19	0	>100
20	0	>100

21	0	>100
22	0	>100
23	0	>100
24	0	>100

The CVS model considered is still that one with more springs to avoid rigid body motions.
The complex modal analysis gives natural frequencies from 0.4 Hz to 1 Hz, which were not obtained with the original spring constants values. Another difference with respect to the same model with higher spring constants is that frequencies around 2 Hz, 3 Hz and 4 Hz are not obtained. Therefore, when spring constants are reduced, the system tends to have natural frequencies lower than 1 Hz and higher than 5 Hz. The frequency range between 2 Hz and 4 Hz do not describe the system dynamics. This is almost the same result obtained reducing spring constants by 100 for CVS model with rigid body motions (paragraph 5.8). Generally, the mean value of heart rate for a test time history is around 1.3 Hz. CWT graphs show that heart rate is the fundamental frequency for every test performed. Therefore, when spring constants are reduced, the model created have vibrational frequencies that are more different from the fundamental frequency of the cardiac activity. However, as discussed in paragraph 5.8, in this work, the model with reduced spring constants will not be implemented in LUPOS.
On the contrary, adding two springs to avoid rigid body modes, natural frequencies of the system (Table 5.9.1) result more similar to the frequencies obtained from the original system with rigid body motions (Table 5.6.1.1). Furthermore, this variation of the model will be very useful when analysing the kinematic curves over time for each DOF (chapter 7).

6. CVS model built in LUPOS

It is possible to represent the CVS model in LUPOS, which is a lumped parameters open source FEM code developed in MATLAB [29]. It allows to visualise vibrational mode shapes of the system with the corresponding natural frequency. CVS model is a 12-DOFs system and each DOF is represented by its corresponding mass. Therefore, it would be interesting to see which mass moves at each natural frequency of the system and how modal shapes look like.
In order to give a straightforward representation of the model and an easy-to-understand correspondence between the model and the real cardiovascular system, the elements have been rearranged according to the following figure of reference [31].

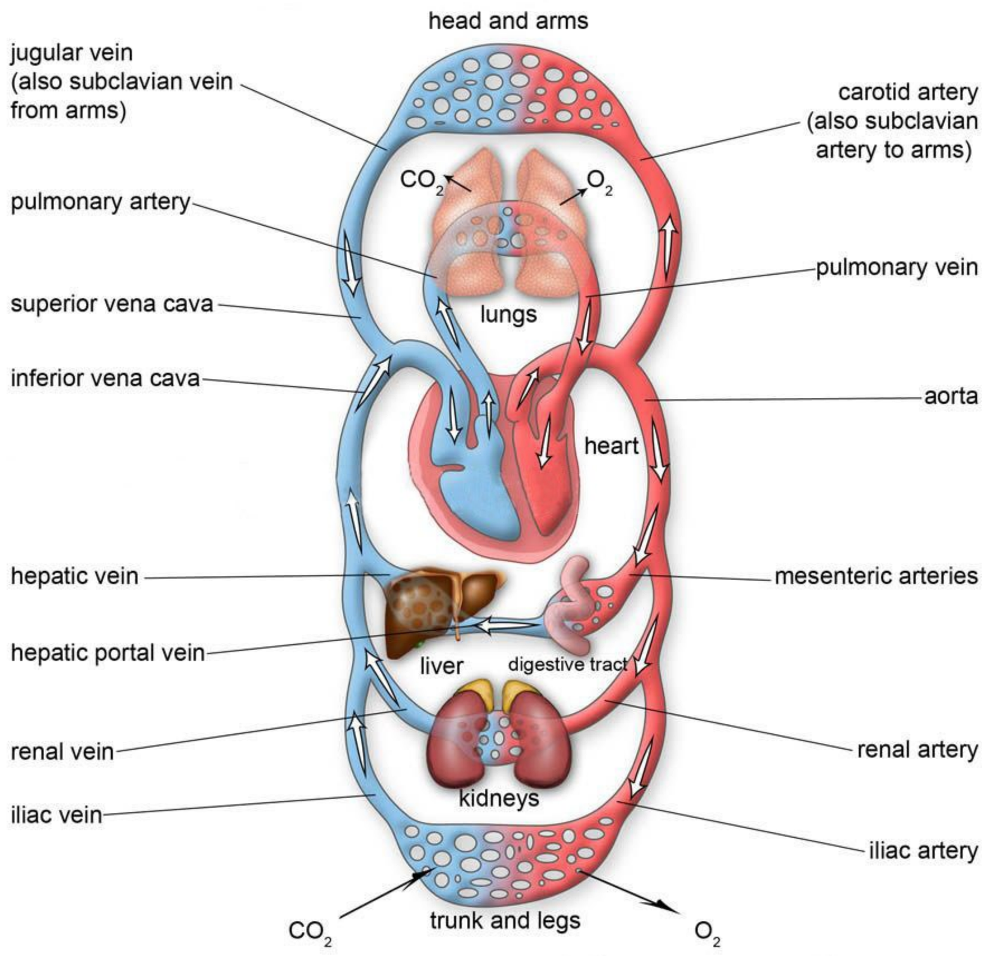

Figure 6.1 – Schematic of cardiovascular system with systemic circulation (red) and pulmonary circulation (blue).

In the schematic in Figure 6.1, left atrium and ventricle of the heart appear on the right side of the figure in red, and they involve oxygenated blood. Meanwhile, right atrium and ventricle of the heart appear on the opposite side of the figure in blue, and they involve deoxygenated blood.

Circulatory blood flow is segregated into two basic divisions: pulmonary circulation and systemic circulation. Pulmonary circulation includes blood flow from right ventricle to the lungs where blood is oxygenated and, then, it returns to left atrium of the heart. Systemic circulation includes blood flow from left ventricle to arteries that collect blood to the human body. In particular, according to the CVS model built, two ways of circulation are considered to split from aorta and main arteries: splanchnic that includes gastrointestinal organs (digestive track organs and liver), and extra splanchnic that includes all the rest of the body. Then, deoxygenated blood returns to right atrium of the heart. The CVS mechanical model built in LUPOS is shown in the following figure. In particular, the four cubes at the centre of the figure represent the four chambers of the heart. The two red cubes represent left atrium (top) and ventricle (bottom); similarly, the two blue cubes represent right atrium (top) and ventricle (bottom). The, the other masses refer to the pulmonary (top of the figure) and systemic (bottom of the figure) circulation indicated in the background schematic.

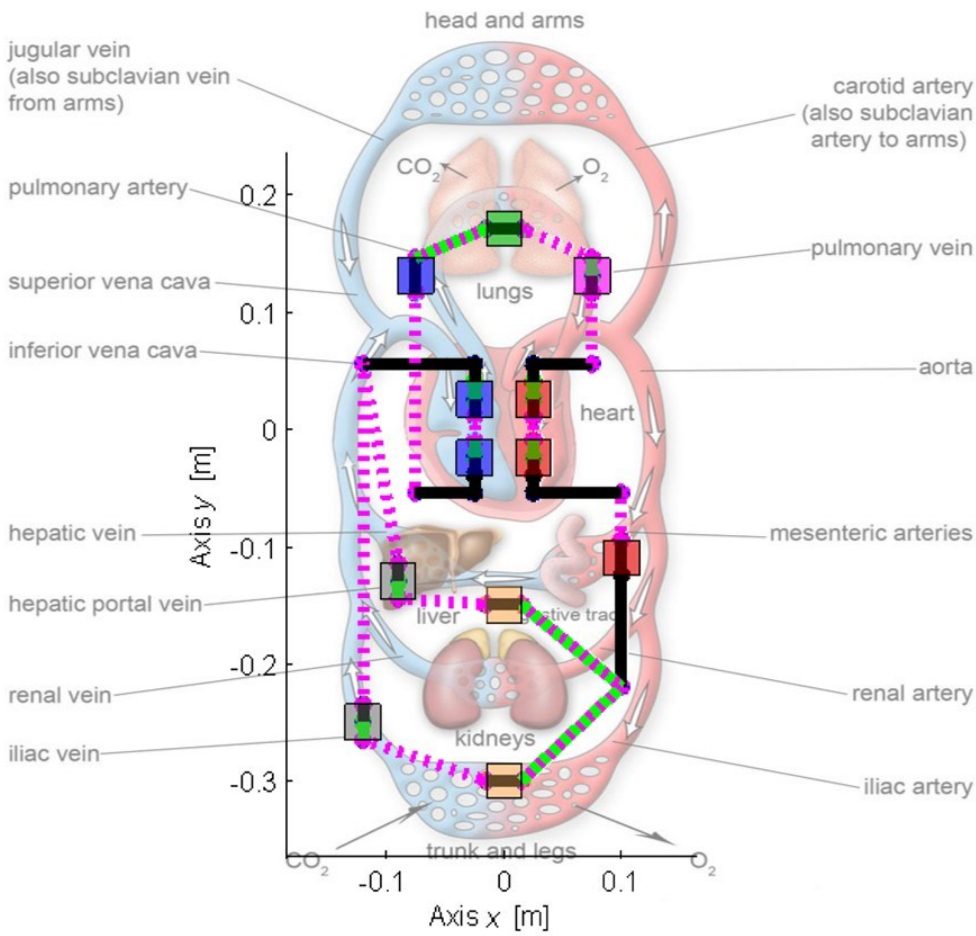

Figure 6.2 – CVS model representation in LUPOS according to the pattern in the background.

To build CVS model in LUPOS, the first thing to define is the geometry that means the position of each node in an absolute reference system. The system of coordinates used is a XY plane with the centre placed at the central point of the heart, X-axis positive from left to right and Y-axis positive from bottom to top. In particular, together with the 12 active “master” nodes, other 12 dual “slave” nodes have been defined. In this way, it is possible to create cubes representing masses in LUPOS using rigid joints and beam elements between each “master” and “slave”

nodes. The density of each beam element is calculated considering its mass value and cube volume.
In this particular case, additional nodes have been created to represent ground, for each spring connected to ground. They have been placed at the same coordinates as each mass centre. Other rigid joints have been added to ensure the geometry desired as in Figure 6.2.
A lumped damping matrix is made to represent dampers between each couple of nodes, as well as a lumped stiffness matrix with spring constants between DOFs couples and between masses and ground.
In Figure 6.2, dampers are represented with magenta dotted lines, springs with green solid lines and rigid joints with black solid lines.
It is important to note that each mass of the model can move only along one direction, which could be X-axis or Y-axis. In fact, boundary conditions are also included in LUPOS to not allow nodes displacement in other directions. Furthermore, an additional MATLAB script was written to reverse eigenvectors sign for some nodes, which have positive displacement in the opposite direction to XY positive axes of the absolute reference system.

6.1 CVS matrices in LUPOS

In LUPOS, the matrices of the dynamic problem are shown graphically. In order to interpret them, the order considered for all the DOFs of the system has to be accounted:

1) LA: left atrium
2) LV: left ventricle
3) RA: right atrium
4) RV: right ventricle
5) SA: systemic arteries
6) SP: splanchnic peripheral circulation
7) SV: splanchnic venous circ.
8) EP: extra-splanchnic peripheral circ.
9) EV: extra-splanchnic venous circ.
10) PA: pulmonary arteries
11) PP: pulmonary peripheral circ.
12) PV: pulmonary veins

In mass, damping and stiffness matrices derived from LUPOS and shown in the following figures, some coloured rectangles are overlapped to identify the contribution of each DOF. In particular, the magenta rectangle include the four chambers of the heart, LA, LV, RA and RV, the green rectangle refers to all the systemic circulation, from SA to EV nodes, then, the blue rectangle refers to pulmonary circulation, which includes PA, PP and PV degrees of freedom.
Mass matrix (12×12) from LUPOS in Figure 6.1.1 is diagonal and it can be seen that the highest contribution involves the circulation in the body that is splanchnic and extra splanchnic. In particular, DOFs number 7 and 9 have the highest mass value. They correspond to the venous circulation that goes from gastrointestinal organs (splanchnic) and all the rest of the body (extra splanchnic) back to heart. It is a reasonable result because blood mass that circulates in human body organs is higher than blood mass in the heart chambers or in the pulmonary circulation. It can be noted that the highest value corresponds to splanchnic circulation (DOF number 7), in fact organs in the digestive track and liver contains the major amount of blood.

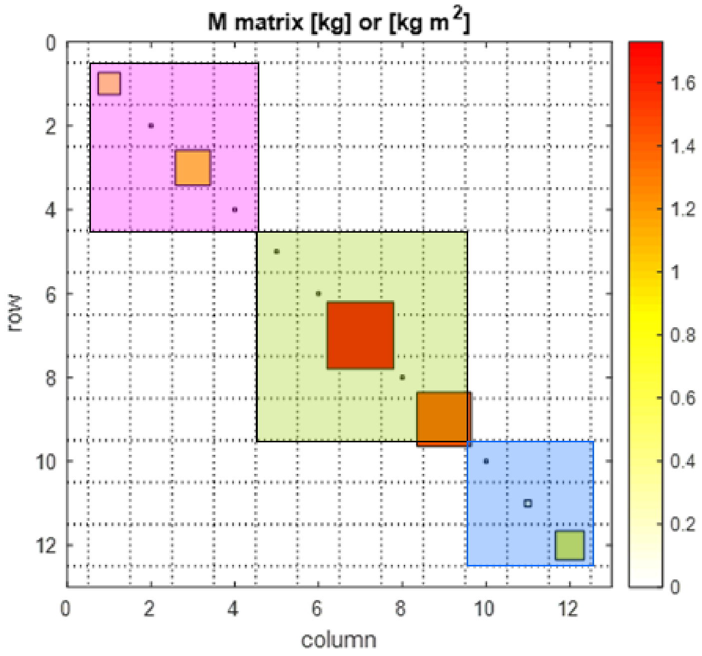

Figure 6.1.1 – Mass matrix of CVS model in LUPOS.

Damping matrix (12×12) from LUPOS in Figure 2.2 shows that the highest damping effect comes from heart chambers, which correspond to DOFs from 1 to 4 in the order considered. It can be deduced that blood circulation in human body is not affected by significant damping. There is a small contribution in pulmonary circulation but it is quite smaller than heart ones.

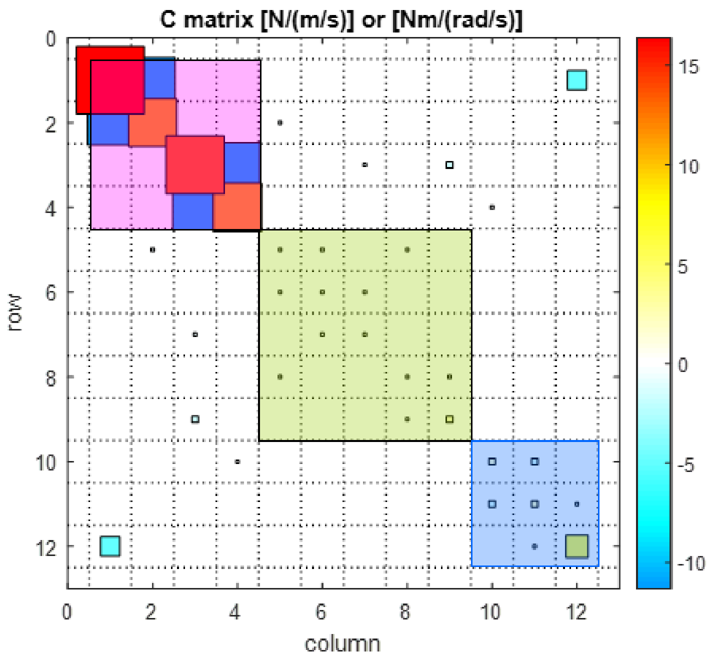

Figure 6.1.2 – Damping matrix of CVS model in LUPOS.

Stiffness matrix (12×12) from LUPOS in Figure 6.1.3 has equal elements on the diagonal, which correspond to the springs connected to ground added for statics reasons. There is an additional spring constant value in human body circulation. However, the highest stiffness effect involve pulmonary circulation, in particular pulmonary arteries and peripheral circulation.

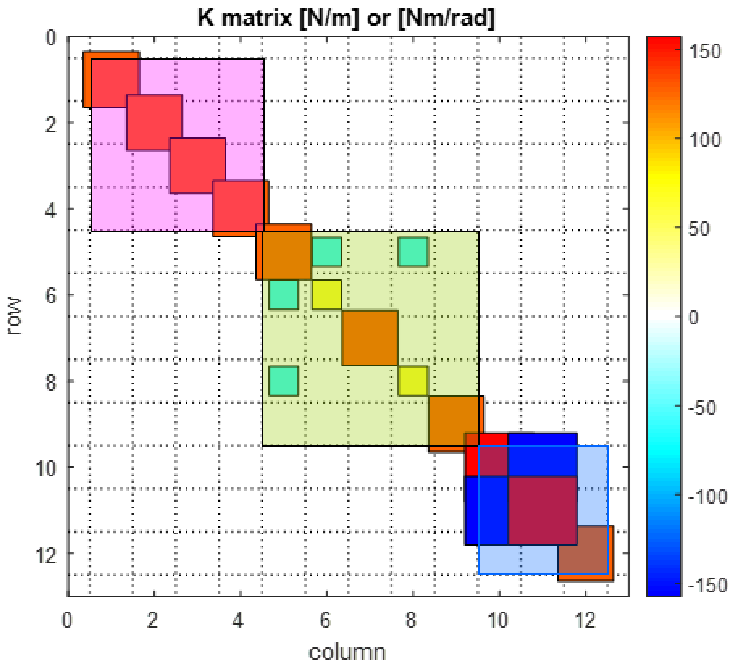

Figure 6.1.3 – Stiffness matrix of CVS model in LUPOS.

6.2 Vibrational modes of CVS model

Vibrational modes of CVS model can be derived considering non-proportional damping or proportional damping assumption. Clearly, the proportional damping assumption will give approximate results that can be considered valuable or not, according to the characteristics of the damping of the system. On the other hand, complex modal analysis will provide more accurate and reliable results. However, a comparison between modes from both cases is useful to better understand model dynamics.

6.2.1 Modes with non-proportional damping

At first, complex modal analysis is performed because it is clear that damping matrix of the CVS model is not proportional. Applying Duncan method, natural frequencies of the system are calculated. Damping ratio is derived to see which modes are underdamped, critically damped or overdamped. The results are reported in the following table, which corresponds to Table 5.6.1.1.

Table 6.2.1.1 – Natural frequencies obtained solved MCK model with Duncan method and corresponding damping factor for each mode.

Natural frequencies of MCK model			
#Mode	ω_n [rad/s]	f [Hz]	ζ [%]
1-2	0	0	-

3-4	8.6328	1.3739	2.46
5-6	9.6025	1.5283	6.09
7-8	15.004	2.3879	18.1
9-10	16.322	2.5977	24.6
11-12	19.726	3.1394	43.9
13-14	35.124	5.5902	6.79
15-16	90.905	14.468	39.2
17-18	131.59	20.944	39.2
19	0	0	>100
20	0	0	>100
21	0	0	>100
22	0	0	>100
23	0	0	>100
24	0	0	>100

From numerical values of natural frequencies and damping percentage, it was deduced that the MCK model has 2 modes of rigid body motion, 6 overdamped modes and 16 underdamped modes. In particular, LUPOS program will calculate a damping ratio equal to 100% for overdamped modes.
The 1st and 2nd modes of the model show two rigid body motions. They can be visualised ignoring dampers and considering only springs. These two rigid motions can be interpreted as two cases when blood vessels act like rigid bodies during circulation.

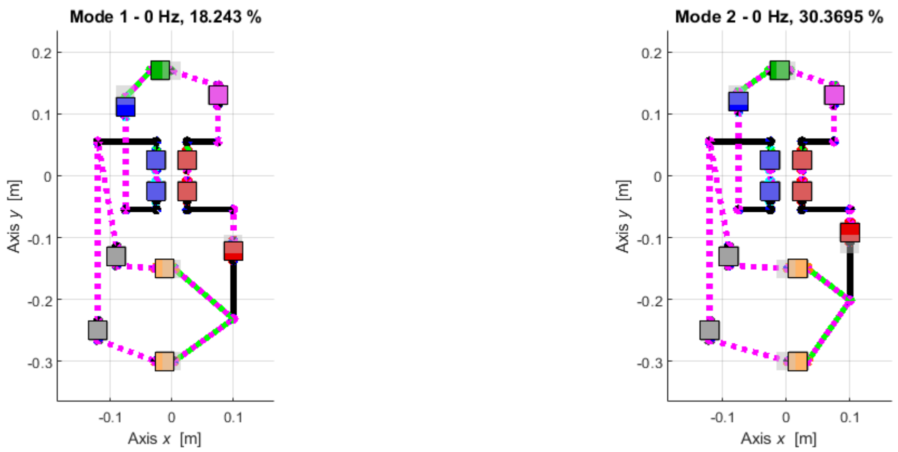

Figure 6.2.1.1 – Mode 1 (left) and mode 2 (right) of CVS model with non-proportional damping: modes of rigid body motion.

It can be noted that mode shapes number 19 and 20 show the two rigid body motions separately. They are overdamped modes so the corresponding frequency is conventionally considered equal to zero. The first rigid body motion involves pulmonary artery PA and pulmonary peripheral circulation PP; the second one involves systemic artery SA, splanchnic and extra splanchnic peripheral circulation SP and PP.

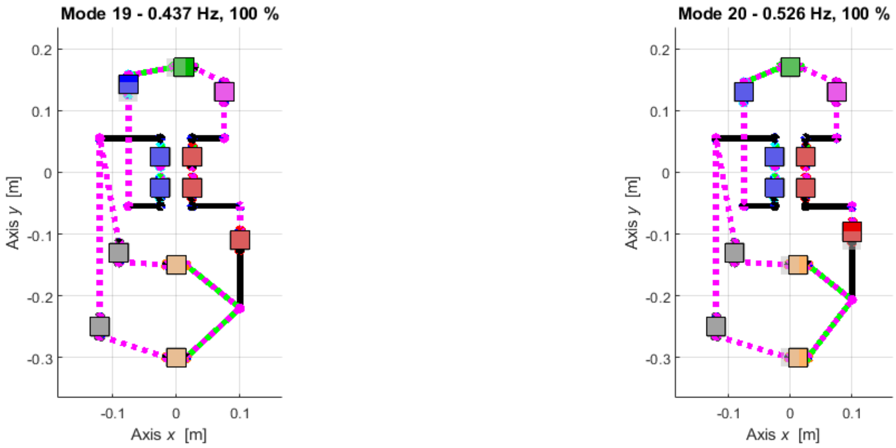

Figure 6.2.1.2 – Overdamped mode 19 (left) and overdamped mode 20 (right) of CVS model with non-proportional damping.

For underdamped modes, eigenvalues are complex conjugate pairs. Therefore, each couple has the same natural frequency and the same mode shape.
At 1.37 Hz (modes 3-4), splanchnic veins SV mass moves. It can be seen as blood pressure mainly changing in veins from abdominal gastrointestinal organs to right atrium.
At 1.53 Hz (modes 5-6), extra splanchnic veins EV mass moves. Similarly, it can be seen as blood pressure mainly changing in venous circulation going from all the rest of the body to right atrium. They are local modes because they involve only one degree of freedom at a time.

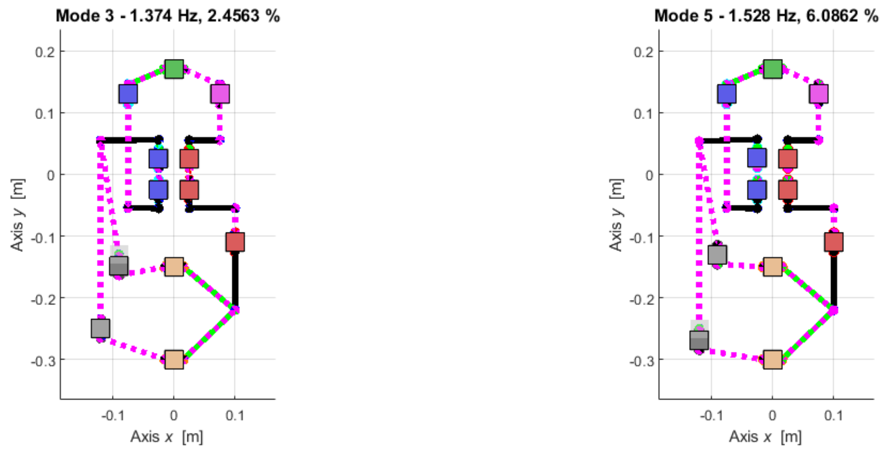

Figure 6.2.1.3 – Underdamped modes 3-4 at 1.37 Hz (left) and underdamped modes 5-6 at 1.53 Hz (right) of CVS model with non-proportional damping.

At 2.39 Hz (modes 7-8), masses in the left side of the heart and pulmonary circulation mostly move.
At 2.59 Hz (modes 9-10), masses in the right side of the heart move.
It can be noted that modes 7-8 and 9-10 are close modes but practically uncoupled. They are global modes since they involve more than one DOF at a time, especially modes 7-8. It may be interesting to investigate more these global modes because it may provide a good correlation with VCG signals detected experimentally.

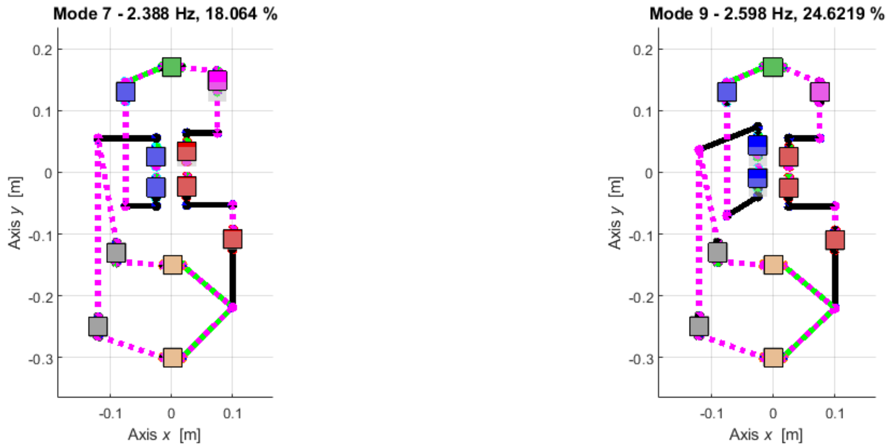

Figure 6.2.1.4 – Underdamped modes 7-8 at 2.39 Hz (left) and underdamped modes 9-10 at 2.59 Hz (right) of CVS model with non-proportional damping.

At 3.14 Hz, masses in the left side of the heart move with some masses in both pulmonary and systemic circulation, almost like at 2.39 Hz (modes 7-8).
At 5.59 Hz, splanchnic and extra splanchnic peripheral circulation SP and EP masses move.
They are global modes, especially modes 11-12 where almost 6 DOFs are involved.

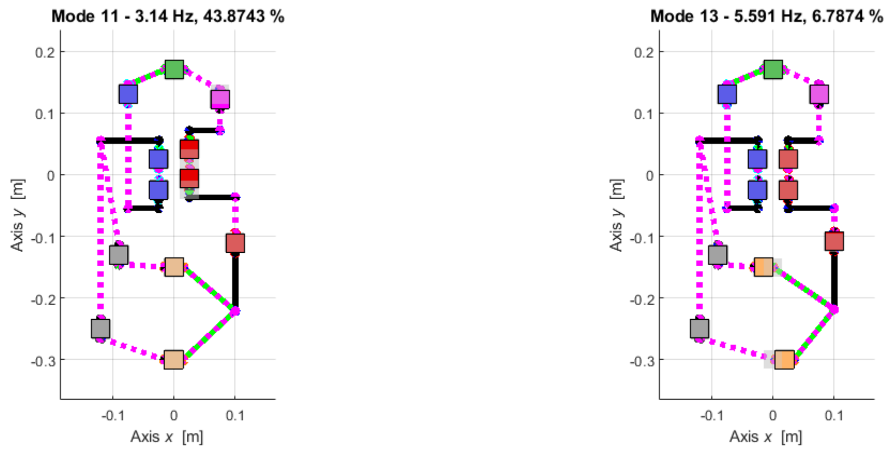

Figure 6.2.1.5 – Underdamped modes 11-12 at 3.14 Hz (left) and underdamped modes 13-14 at 5.59 Hz (right) of CVS model with non-proportional damping.

At 14.47 Hz (modes 15-16), mass corresponding to pulmonary arteries PA moves.
Similarly, at 20.98 Hz (modes 17-18), mass corresponding to systemic arteries SA mass moves.
These two mode shapes can be directly correlated to valve operation. In particular, pulmonary valve opening at 14.47 Hz and aortic valve opening at 20.98 Hz. This result confirms the range of frequency generally attributed to valve opening form experimental studies [1,32], which involve frequencies higher than 12 Hz.

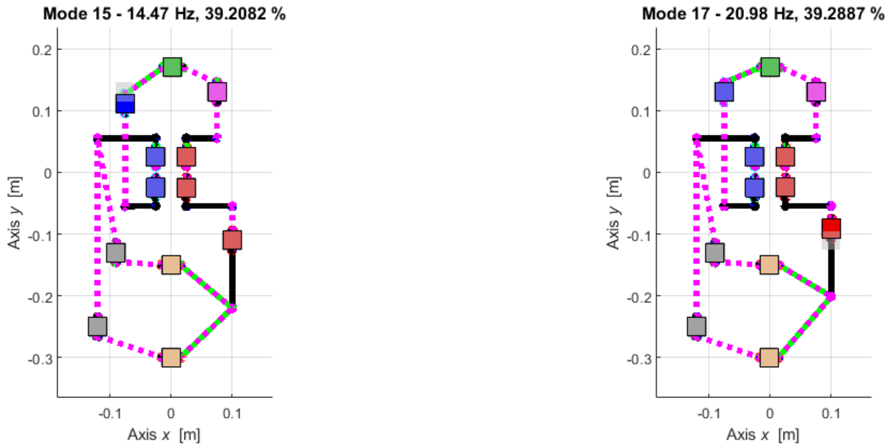

Figure 6.2.1.6 – Underdamped modes 15-16 at 14.47 Hz (left) and underdamped modes 17-18 at 20.98 Hz (right) of CVS model with non-proportional damping.

The first overdamped modes observed are modes 19 and 20, seen before while describing rigid body motions. Then, modes 21, 22, 23 and 24 are other overdamped modes of the system. In particular, mode 21 mostly involves the left side of the heart and systemic circulation. On the contrary, mode 22 mostly involves the right side of the heart and pulmonary circulation. They are global modes because they involve almost 6 DOFs each.

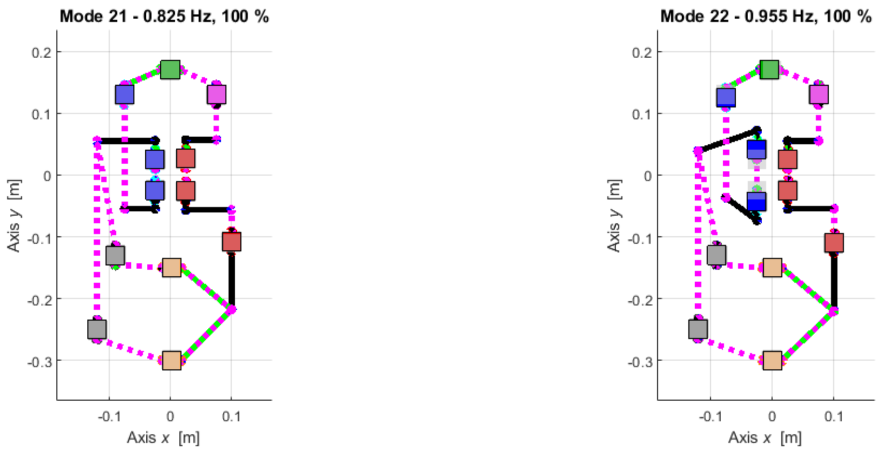

Figure 6.2.1.7 – Overdamped mode 21 (left) and overdamped mode 22 (right) of CVS model with non-proportional damping.

At the following overdamped mode 23, mass corresponding to right ventricle RV moves, so it is a local mode. At mode 24, mass corresponding to left ventricle LV moves; it is a local mode, too. It can be noted that the frequency obtained from LUPOS for these modes are 113 Hz and 195 Hz. They are not actual frequencies of the system vibration. They correspond to imaginary eigenvalues.

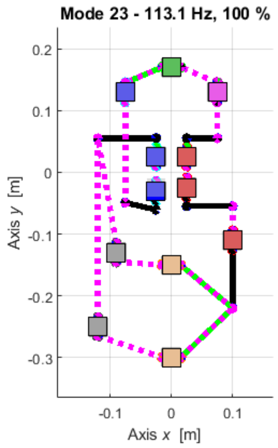

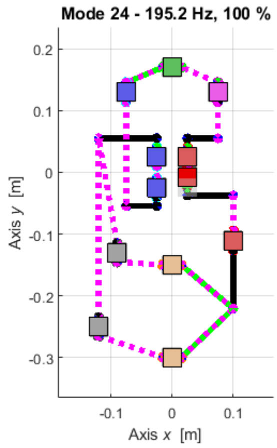

Figure 6.2.1.8 – Overdamped mode 23 (left) and overdamped mode 24 (right) of CVS model with non-proportional damping.

6.2.2 Modes with proportional damping assumption

As discussed in the paragraph above, assuming proportional damping is an approximation for the CVS model. Consequently, it will provide approximated results for underdamped modes. When damping is proportional to mass and stiffness matrices, it becomes a MK model, without dampers. However, the damping modal matrix is not diagonal but terms off the diagonal are ignored and damping ratio is calculated. In this way, values for natural frequencies and corresponding damping percentage values have been calculated. The results are reported in the following table, which corresponds to Table 5.5.1.1 seen before.

Table 6.2.2.1 – Natural frequencies obtained solved MK model, assuming proportional damping, and corresponding damping factor for each mode.

Natural frequencies of MK model (C prop.)			
#Mode	ω_n [rad/s]	f [Hz]	ζ [%]
1	$2.9962 \cdot 10^{-9}$	$4.7686 \cdot 10^{-8}$	-
2	$3.3718 \cdot 10^{-9}$	$5.3663 \cdot 10^{-8}$	-
3	8.6245	1.3726	2.52
4	9.5346	1.5175	6.61
5	12.060	1.9195	64.8
6	13.385	2.1303	28.1
7	15.374	2.4469	97.8
8	35.125	5.5904	6.79
9	89.190	14.195	>100
10	90.927	14.471	39.2
11	115.81	18.432	>100
12	132.17	21.036	39.6

Solving MK problem, 2 modes of rigid body motion, 2 overdamped modes and 8 underdamped modes are obtained. The natural frequency for overdamped mode is reported but it is conventionally assumed equal to zero, as well as for modes of rigid body motion.
The 1st and 2nd modes of MK model are modes of rigid body motion like the 1st and 2nd modes of MCK model. The two subsystems that move as rigid bodies are the same as in the case with non-proportional damping. Consequently, they may be correlated to the overdamped modes 19 and 20 of the MCK model. In fact, each rigid body motion mode of the MK model correspond to a mode of rigid body and an overdamped mode in MCK model.

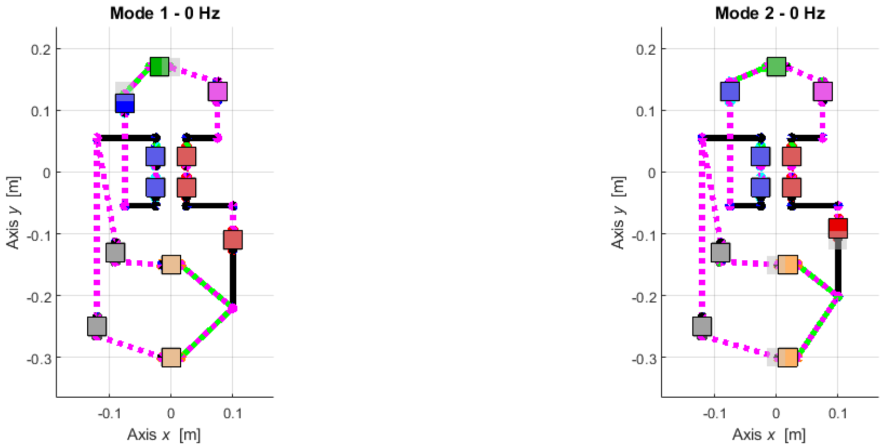

Figure 6.2.2.1 – Mode 1 (left) and mode 2 (right) of CVS model assuming proportional damping: modes of rigid body motion.

At 1.37 Hz (mode 3), splanchnic venous circulation SV mass moves, that means a local mode. In MCK model, it corresponds to modes 3-4 at the same frequency.
At 1.52 Hz (mode 4), extra splanchnic venous circulation EV mass moves, that means another local mode. Similarly, in MCK model, it corresponds to modes 5-6 at the same frequency. It can be noted that each underdamped mode of MK model is correlated to two underdamped modes of the MCK model.

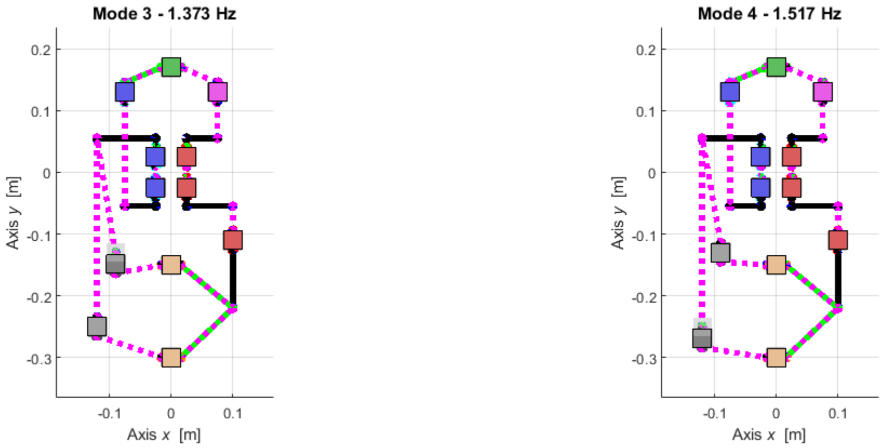

Figure 6.2.2.2 – Underdamped mode 3 at 1.37 Hz (left) and underdamped mode 4 at 1.52 Hz (right) of CVS model assuming proportional damping.

At 1.92 Hz (mode 5), right atrium RA mass moves, it is a local mode. In MCK model, this displacement of RA mass is included in a global mode at 2.59 Hz (modes 9-10).
At 2.13 Hz (mode 6), pulmonary veins PV mass moves, it is a local mode, too. In MCK model, this displacement of PV mass is included in a global mode at 2.39 Hz (modes 7-8).

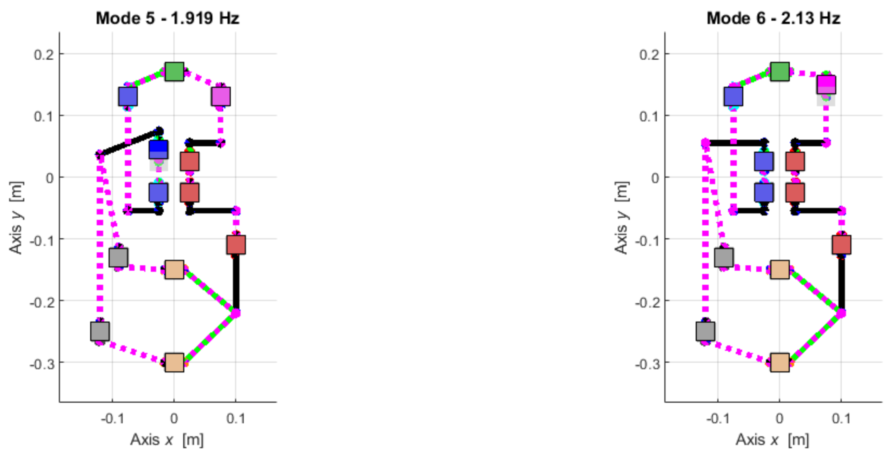

Figure 6.2.2.3 – Underdamped mode 5 at 1.92 Hz (left) and underdamped mode 6 at 2.13 Hz (right) of CVS model assuming proportional damping.

At 2.45 Hz (mode 7), left atrium LA mass moves, it is a local mode In MCK model, LA displacement is included in a global mode at 3.14 Hz (modes 11-12).
At 5.59 Hz (mode 8), splanchnic and extra splanchnic peripheral SP and EP masses move. In MCK model, it corresponds to modes 13-14 at the same frequency.

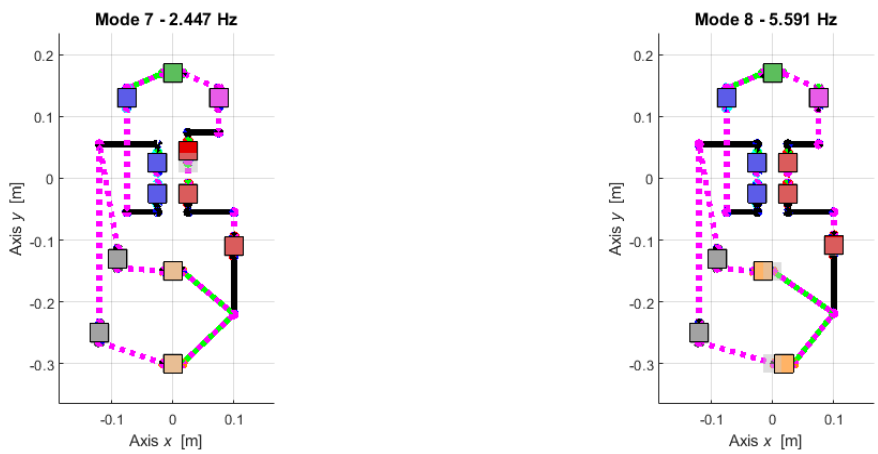

Figure 6.2.2.4 – Underdamped mode 7 at 2.45 Hz (left) and underdamped mode 8 at 5.59 Hz (right) of CVS model assuming proportional damping.

At 14.48 Hz (mode 10), pulmonary arteries PA mass moves. In MCK model, PA displacement corresponds to underdamped modes 15-16 at the same frequency, so it can be interpreted as the pulmonary valve opening.
At 21.07 Hz (mode 12), systemic arteries SA mass moves. In MCK model, it corresponds to underdamped modes 17-18 at 20.98 Hz, which can be seen as the aortic valve opening. As discussed for MCK model, this model confirms that valve operation occurs at frequencies higher than 12 Hz.

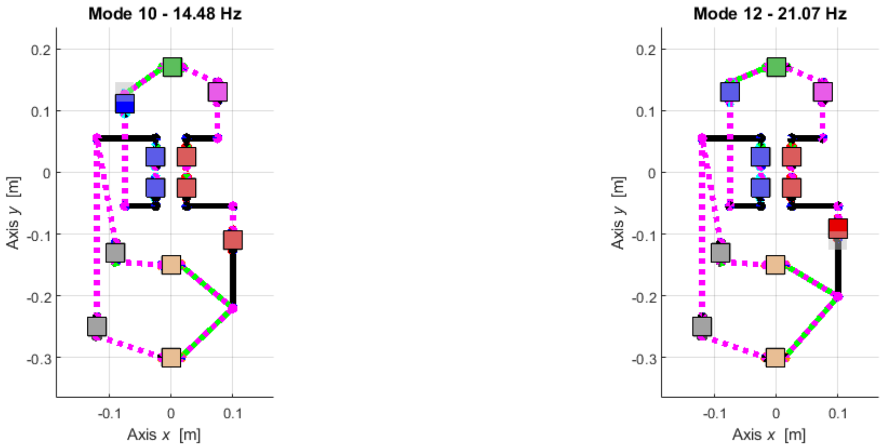

Figure 6.2.2.5 – Underdamped mode 10 at 14.48 Hz (left) and underdamped mode 12 at 21.07 Hz (right) of CVS model assuming proportional damping.

Assuming proportional damping, two overdamped modes can be identified. At 14.19 Hz (mode 9), right ventricle RV mass moves, so it is an overdamped local mode. In MCK model, it corresponds to overdamped local mode 23 at 113 Hz. Furthermore, RV displacement is also included in the global overdamped mode 22 of MCK model.

At 18.43 Hz (mode 11), left ventricle LV mass moves, overdamped local mode. In MCK model, it corresponds to overdamped local mode 24 at 145 Hz. Also, LV displacement is included in the global overdamped mode 21 of MCK model. In fact, each overdamped mode of MK model should be correlated to two overdamped modes in the related MCK model.

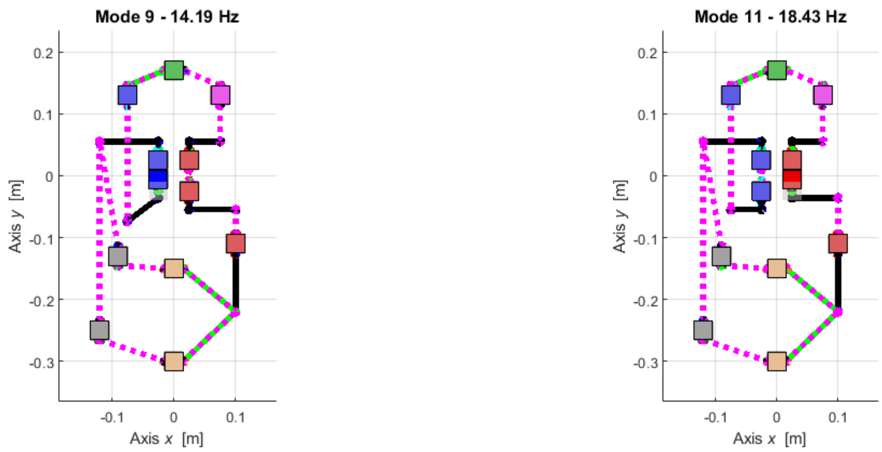

Figure 6.2.2.6 – Overdamped mode 9 (left) and overdamped mode 11 (right) of CVS model assuming proportional damping.

6.3 Variations applied to CVS model: springs in parallel

In order to investigate more the mechanical model created for circulatory system, some variations can be applied. In particular, the springs that have been added for model statics can be placed in parallel with the relative compartment, instead of been connected to ground.

This variation in springs configuration implies a different stiffness matrix for the model because there are more springs shared between some couples of DOFs. Mass and damping matrices do not change.

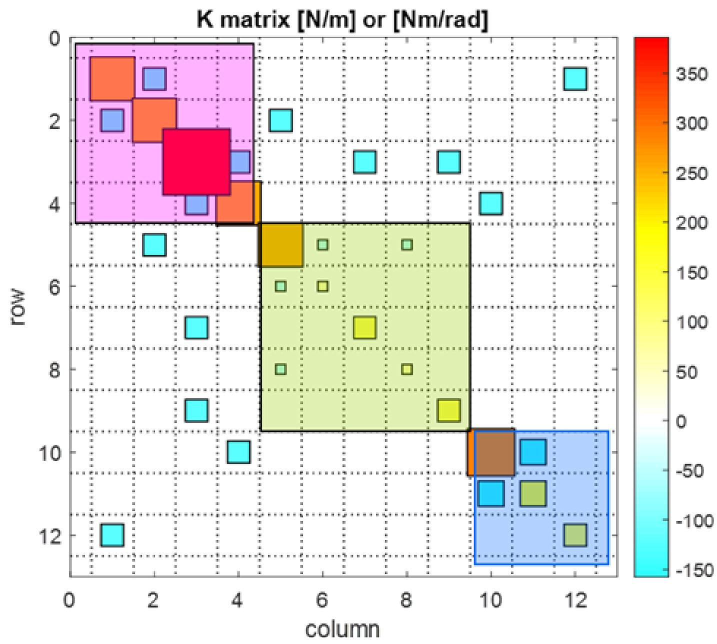

Figure 6.3.1 – Stiffness matrix of CVS model in LUPOS with all the springs connected in parallel.

The stiffness matrix in Figure 6.3.1 shows that more off-diagonal terms appear with respect to the previous stiffness matrix in Figure 6.1.3. Moreover, stiffness contribution from heart chambers increases and from the rest of the body it decreases. A significant spring constant value still occur for systemic and pulmonary arteries (DOFs numbers 5 and 10).

6.3.1 Modes with non-proportional damping

Solving the eigenproblem for the CVS model with this new stiffness matrix, eigenvalues and corresponding eigenvectors change. In particular, considering non-proportional damping and applying the Duncan method for complex analysis, 24 modes are calculated.

Table 6.3.1.1 – Natural frequencies obtained solved MCK model with spring variation and corresponding damping factor for each mode.

Natural frequencies of MCK model			
#Mode	ω_n [rad/s]	f [Hz]	ζ [%]
1	0	0	86.8
2	0	0	99.9
3	0	0	34.9
4-5	9.079	1.445	4.35
6-7	15.79	2.511	15.3

8-9	18.66	2.97	33.16
10-11	23.44	3.731	15.6
12-13	26.19	4.168	20.5
14-15	35.29	5.617	6.97
16-17	118.4	18.85	31.7
18-19	181.6	28.9	30.5
20	0	0	>100
20	0	0	>100
21	0	0	>100
22	0	0	>100
23	0	0	>100
24	0	0	>100

The results show that the 1st, 2nd and 3rd modes are rigid body motions because the frequency is equal to zero and the damping ratio is not greater than 100%. However, it can be noted that mode 2 has a damping ratio very close to 100%. In addition, solving the corresponding MK model with proportional damping assumption, only two modes of rigid body motion are found. In fact, looking at the CVS model ignoring the dampers, only two subsystems move as rigid bodies. Therefore, it will be deduced that this mode with 99.9% damping probably is overdamped instead of rigid body motion. Finally, this modified system with all springs in parallel has: 2 modes of rigid body motion (mode 1 and 3), 16 underdamped modes and 6 overdamped modes.
It is interesting to look at the vibrational mode shapes to see what changed with respect to springs connected to ground.
In this model, there are two large groups involved in the rigid body motion. One is composed by the right side of the heart with pulmonary arteries, pulmonary peripheral circulation and splanchnic and extra splanchnic veins. The other one is composed by the left side of the heart, pulmonary veins, systemic arteries, splanchnic and extra splanchnic peripheral circulation. It is possible to see them ignoring dampers. Modes 1 and 3 correspond to them, as well as two other overdamped modes. In fact, due to the method applied for complex modal analysis, each rigid body motion of MK model is represented by a rigid body motion and an overdamped mode in the MCK model.

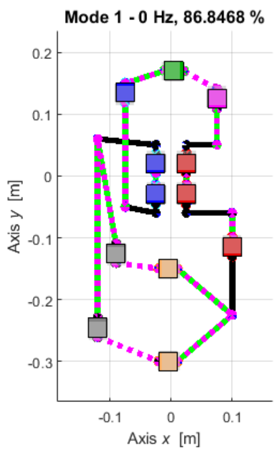

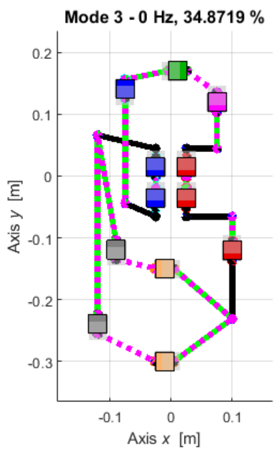

Figure 6.3.1.1 – Mode 1 (left) and mode 3 (right) of CVS model with non-proportional damping: modes of rigid body motion.

It can be noted that the two overdamped modes most correlated to these rigid motions are mode 2 and mode 20. They both occur at 0 Hz and their damping ratio can be considered higher than 100%.

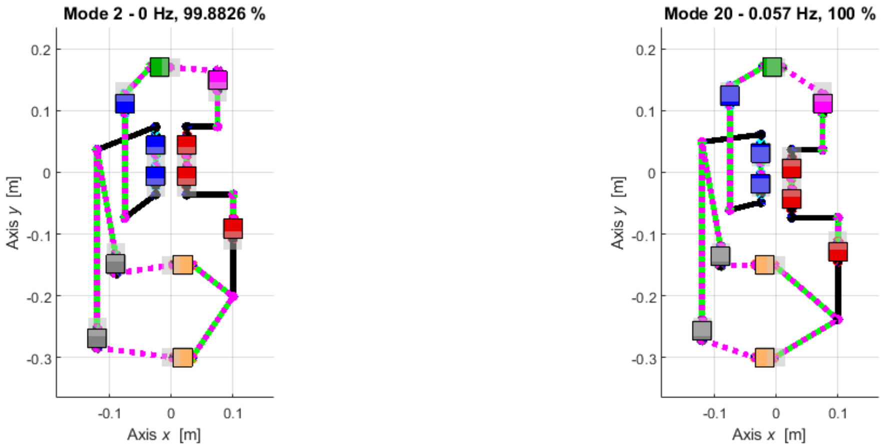

Figure 6.3.1.2 – Overdamped mode 2 (left) and overdamped mode 20 (right) of CVS model with non-proportional damping.

The first underdamped modes are the 4th and 5th at 1.445 Hz. They are the only modes with a frequency lower than 2 Hz. At 1.445 Hz, both splanchnic and extra splanchnic veins masses move together.
In the following modes 6-7, at 2.511 Hz, the highest displacement is performed by pulmonary arteries and pulmonary peripheral circulation, also right atrium and ventricle move.

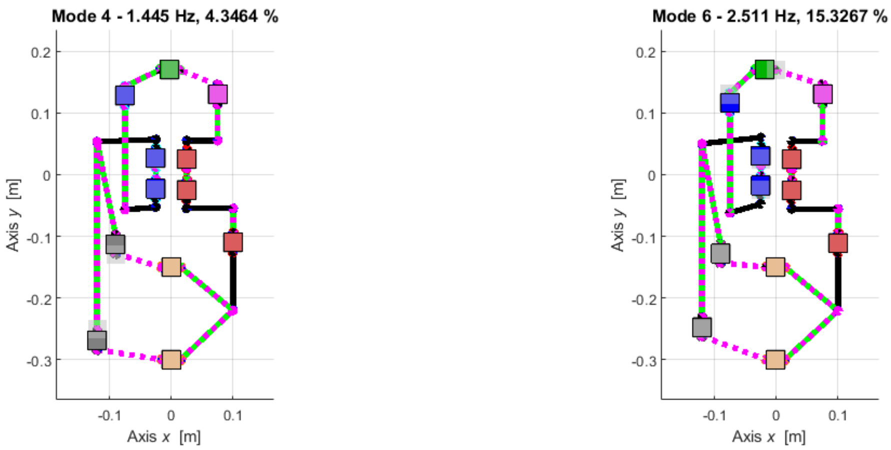

Figure 6.3.1.3 – Underdamped modes 4-5 at 1.445 Hz (left) and underdamped modes 6-7 at 2.511 Hz (right) of CVS model with non-proportional damping.

At 2.974 Hz (modes 8-9), all the masses on the left side of the heart move, it is a global mode.
At 3.731 Hz (modes 10-11), the right part of the heart moves, in particular the same masses as modes 6-7. It can be noted that there is an alternation of modes that involve left or right part of the heart and CVS.

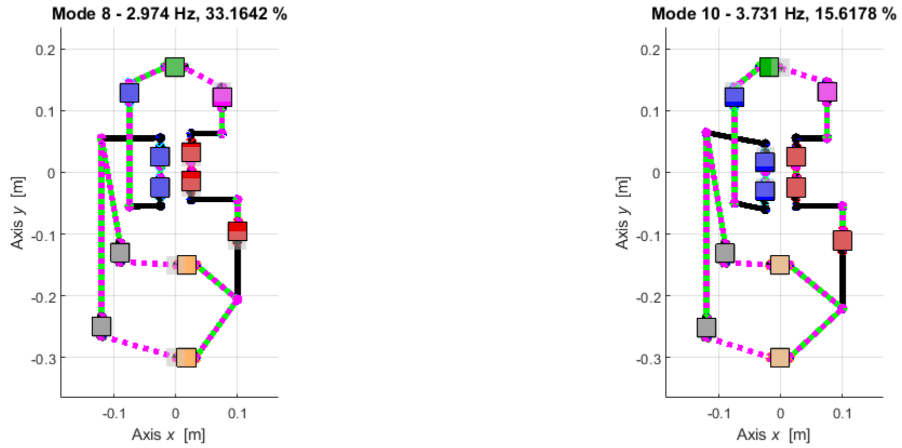

Figure 6.3.1.4 – Underdamped modes 8-9 at 2.974 Hz (left) and underdamped modes 10-11 at 3.731 Hz (right) of CVS model with non-proportional damping.

In fact, the following frequency 4.168 Hz (modes 12-13) involves the same masses as modes 8-9, that are on the left part of the system.
At 5.167 Hz (modes 14-15), something changes in the modes. The mases that move are splanchnic and extra splanchnic peripheral ones. They both move but not synchronously.

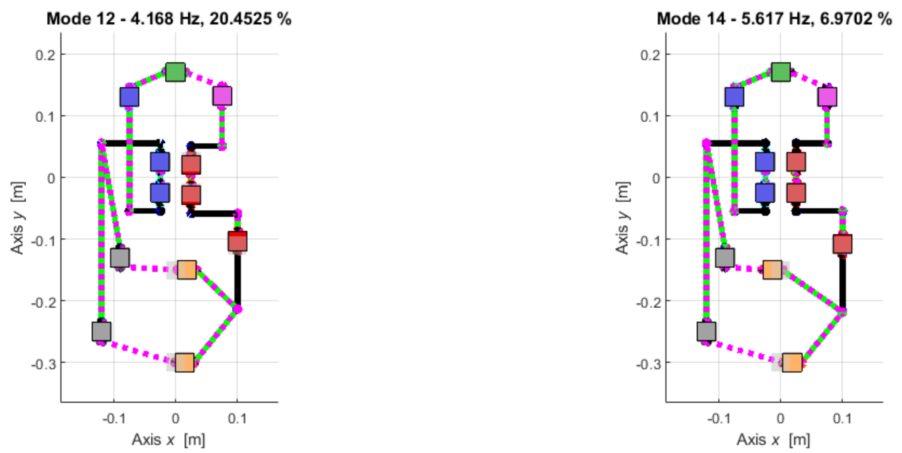

Figure 6.3.1.5 – Underdamped modes 12-13 at 4.168 Hz (left) and underdamped modes 14-15 at 5.617 Hz (right) of CVS model with non-proportional damping.

The following pairs of underdamped modes are significant for the hemodynamic interpretation of the CVS model. At 18.85 Hz (modes 16-17), the pulmonary arteries mass moves, it means that the opening of pulmonary artery is associated to a frequency around 18 Hz. This result respect exactly a past experimental study [32], which demonstrated that valves opening affects frequencies higher than 18 Hz. In the MCK model with spring connected to ground, that threshold frequency results to be around 14 Hz. With this model, the aortic valve opening occurs at 28.9 Hz (modes 18-19).

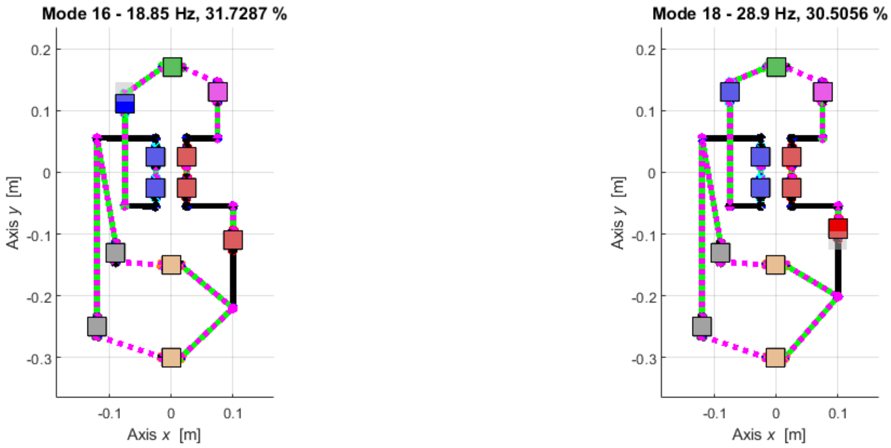

Figure 6.3.1.6 – Underdamped modes 16-17 at 18.85 Hz (left) and underdamped modes 18-19 at 28.9 Hz (right) of CVS model with non-proportional damping.

As discussed above, overdamped modes 2 and 20 are probably correlated to the two modes of rigid body motion. In the overdamped mode 21, masses corresponding to left ventricle, systemic arteries and splanchnic and extra splanchnic peripheral circulation move. In the following mode 22, masses on the opposite side of the heart move, which are right ventricle, pulmonary arteries and pulmonary peripheral circulation masses.

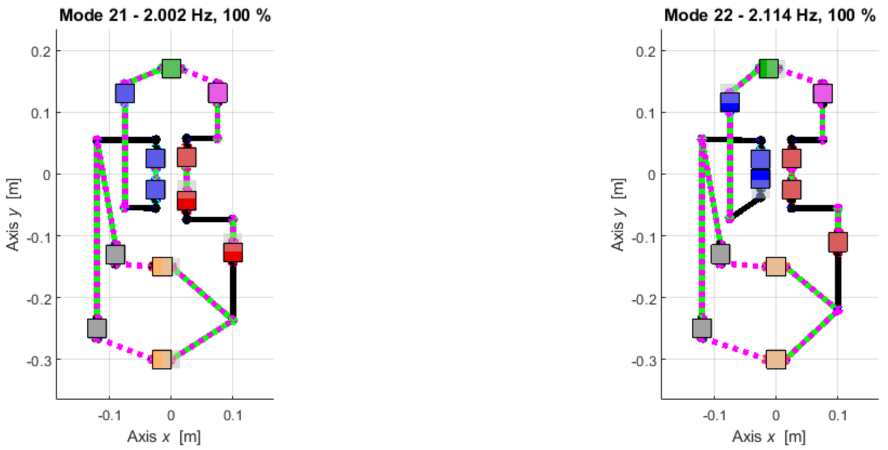

Figure 6.3.1.7 – Overdamped mode 21 (left) and overdamped mode 22 (right) of CVS model with non-proportional damping.

In the following mode 23, left ventricle mass moves. Similarly, in the 24th mode, right ventricle mass moves.

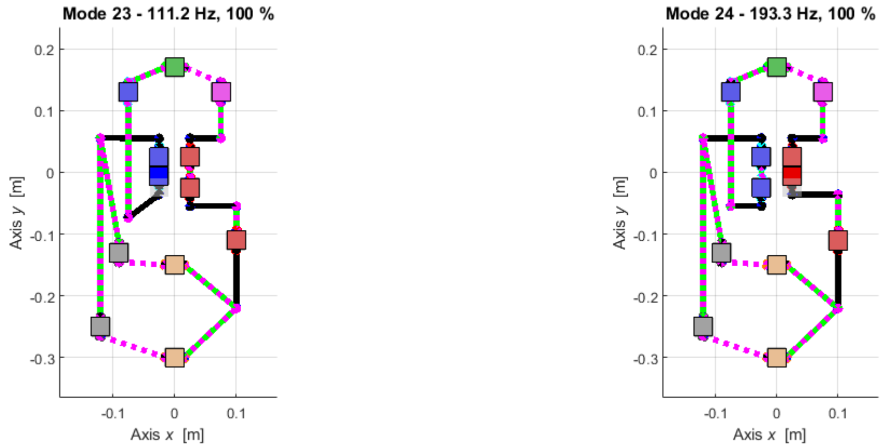

Figure 6.3.1.8 – Overdamped mode 23 (left) and overdamped mode 24 (right) of CVS model with non-proportional damping.

It can be noted that these overdamped modes 21, 22, 23 and 24 almost correspond to the same overdamped modes in the MCK model with springs connected to ground.

6.3.2 Comparison between modes of original and modified model

The vibrational modes and frequencies of the original CVS model are compared with the results of the modified model, where springs are connected in parallel instead of been connected to ground. The main similarities are that:

- In both cases, CVS model has 2 modes of rigid body motion, 16 underdamped modes and 6 overdamped modes.
- As frequency value increases, modes that involve masses on one side of the heart and system are often followed by modes of masses on the opposite side.

In addition, some differences can be deduced:

- The modes of rigid body motion involve all the DOFs of the system when there are not springs connected to ground.
- When springs are in parallel, the entire range of frequency of the system is a bit higher. In fact it goes from 0 up to 29 Hz, instead of 21 Hz. It is due to the different configuration that affects stiffness of the model.
- The valve operation results to occur at 18.9 Hz and 28.9 Hz instead of 14.5 Hz and 20.9 Hz.
- When springs are in parallel, almost every mode of the system is global. Meanwhile, with springs connected to ground, more local modes are observed.

Overall, the CVS model with all springs in parallel has the same frequency range of vibrations as the model defined originally. However, in this work, this new spring configuration will not be applied in details to CVS mechanical model.

7. Pulsating heart model in CVS

There are different ways to model heart excitation in cardiovascular system. In this study, the simplest method is used to describe the pulsating heart with reasonable effectiveness. Many complex phenomena affecting heart excitation will be ignored at this first level of study. For example, the carotid baroreflex interaction with heart investigated by Ursino [24] is not considered in this report. However, some of the assumptions he made [24] have been preserved. The models for the right and left side of the heart are the same, with different numerical values of characteristic parameters. The contractile activity of the atrium is neglected, in fact it is described with a constant hydraulic capacitance, resistance and inductance. Meanwhile, the contractility of the ventricle is taken into account. In order to do that, ventricular pressure-volume loop is used, as well as time-varying ventricular resistance.

7.1 Ventricular pressure as imposed kinematics

7.1.1 Ventricular pressure-volume loop

The ventricular pressure is correlated to ventricular volume with a characteristic loop. With every heart beat, a full loop is described. Left ventricle LV is considered first. The LV pressure-volume loop is derived starting from left ventricular pressure (LVP) and LV volume variation over time [33]. During a single heart period, the cycle can be divided into four basic phases as shown in Figure 7.1.1.1: ventricular filling that corresponds to end diastole (phase a in Figure 7.1.1.1), isovolumetric contraction that is systole (phase b in the figure above), ventricular ejection that still occurs during systole (phase c in the figure) and isovolumetric relaxation of the left ventricle that means diastole.

- When the mitral valve opens, left ventricle is filled, left ventricle volume increases with a small increase in ventricular pressure. This filling phase corresponds to end diastole, in fact it ends when left ventricle reaches its end-diastolic volume EDV, which is the point 1 in the figure above, when muscle contraction starts. It is called phase a in Figure 7.1.1.1.
- As the ventricle begins to contract isovolumetrically (phase b in the figure), the mitral valve closes and the LVP increases, but the LV volume remains the same, resulting in a vertical line form point 1 to point 2 in the figure. During isovolumetric contraction, all valves are closed and systole starts.
- At point 2, the LVP exceeds aortic pressure so the aortic valve opens. The ejection phase starts when LV volume decreases while LV pressure slightly increases up to a peak systolic pressure, called end-systolic pressure. The ejection phase ends when aortic pressure exceeds LVP, so aortic valve closes at point 3 in the figure.
- Then, the ventricle relaxes isovolumetrically while LVP decreases. During relaxation, LV volume is equal to end systolic volume ESV and all valves are closed. When LVP falls below left atrial pressure, mitral valve opens at point 4 in the figure. Then, LV begins filling phase and the loop restarts with the following heart cycle or heartbeat.

Left atrial pressure and aortic pressure curves with respect to left ventricular pressure will be described in the following paragraph. At this point, the focus is on the left ventricular pressure.

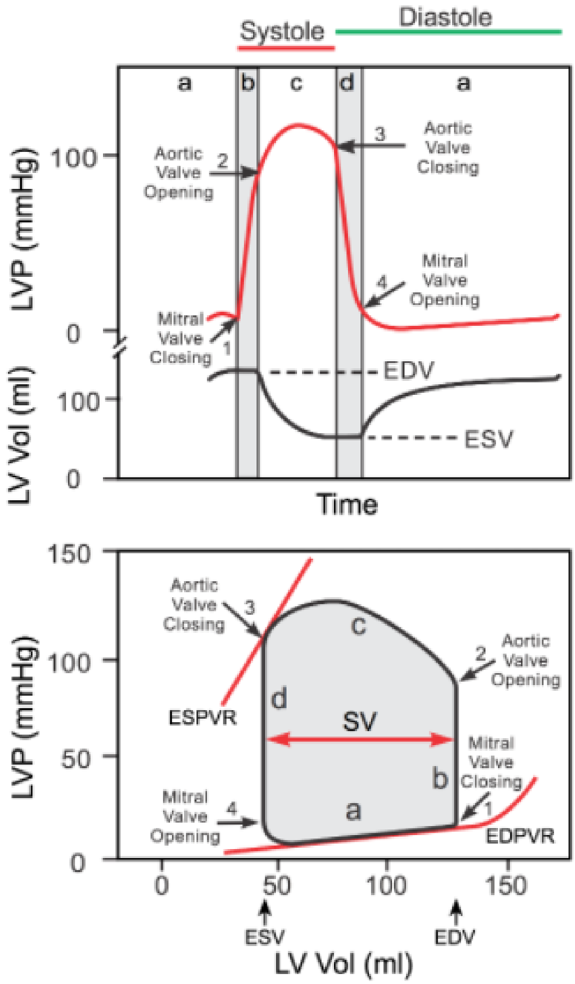

Figure 7.1.1.1 –Left ventricular pressure LVP vs time (above) and left ventricular pressure LVP vs left ventricular volume LV Vol for a heart period.

The difference between EDV and ESV is called stroke volume (SV in the figure above).
When ventricular filling is changed, another loop starts from a different end-diastolic volume and pressure. It has been demonstrated that the left top corners of the different loops, which mean end-systolic pressure points, always occur on a straight line called end-systolic pressure-volume relation ESPVR line. The slope of this line is called end-systolic "elastance" E_{es} and it depends only on the systolic muscle properties. Its value is equal to the reciprocal of capacitance value. In fact, the slope of ESPVR is a measure of cardiac contractility. An increased contractility implies an increased slope of the ESPVR but the intercept volume at zero pressure remains unchanged. The volume at zero pressure is called unstressed volume V_u or V_d in Figure 7.1.1.2, and it is the volume of blood that does not exert any force on the ventricle wall.
Similarly, the end-diastolic pressure of each loop has been found to occur always on an exponential curve called end-diastolic pressure-volume relation EDPVR. The slope of this curve at end diastolic volume is called E_d. The following figure shows these curves [34].

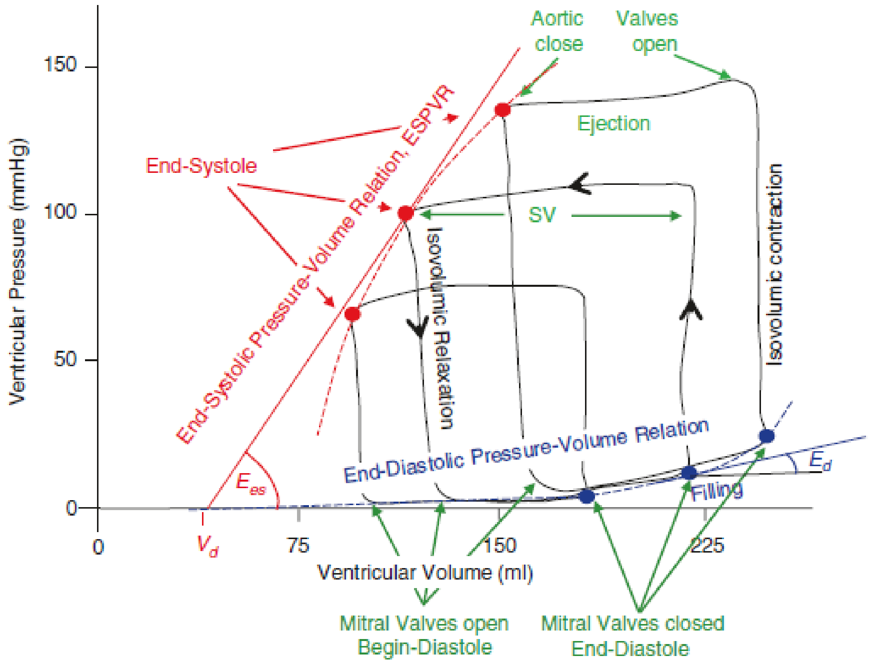

Figure 7.1.1.2 –Ventricular pressure vs volume graph for cardiac cycle with ESPVR and EDPVR curves delimiting all the loops.

The ESPVR line can be described with its maximum slope value $E_{\max,LV}$ that is reciprocal of capacitance at maximum contraction and the corresponding maximum LV volume that is the EDV. In particular, the unstressed volume of the LV is assumed to be almost equal to the ESV because the exact value was not provided by the paper considered [24].
In the same time, the EDPVR curve is described with an exponential function calculated at the EDV point. An activation function is introduced in order to represent LV pressure variation over time. The overall function describing LVP over cardiac cycle is:

$$p_{\max,LV}(t) = \varphi(t) \cdot E_{\max,LV} \cdot (V_{LV} - V_{u,LV}) + [\,1 - \varphi(t)\,] \cdot P_{0,LV} \cdot (e^{k_{E,LV} V_{LV}} - 1) \qquad (7.1.1.1)$$

where $k_{E,LV}$ and $P_{0,LV}$ are constant parameters, $E_{\max,LV}$ is the reciprocal of ventricular capacitance at maximum contraction, $V_{u,LV}$ is the unstressed volume of left ventricle and $\varphi(t)$ is the active function. With the assumptions made, it becomes:

$$p_{\max,LV}(t) = \varphi(t) \cdot E_{\max,LV} \cdot (EDV_{LV} - ESV_{LV}) + [\,1 - \varphi(t)\,] \cdot P_{0,LV} \cdot (e^{k_{E,LV} \cdot EDV_{LV}} - 1) \, (7.1.1.2)$$

The activation function is defined so that when $\varphi(t) = 0$ the ventricle is relaxed (diastole) and the pressure function is exponential. When $\varphi(t) = 1$, the ventricle is contracted (end-systole) and the pressure function is linear. Therefore, it can be described with a sinusoidal function where T is heart period, T_{sys} is the duration of the systole and u is a dimensionless variable that describes the fraction of cardiac cycle and goes from 0 (beginning of systole) to 1.

$$\varphi(t)=\begin{cases}\sin^2\left[\dfrac{\pi\cdot T}{T_{sys}}\cdot u\right] & 0\ \le\ u\ \le\ \dfrac{T_{sys}}{T}\\[2ex] 0 & \dfrac{T_{sys}}{T}\ \le\ u\ \le\ 1\end{cases} \tag{7.1.1.3}$$

In particular, in this study the dimensionless variable u is simplified with respect to the definition given by reference paper [24] and it is assumed to be: $u = t/T$.

It can be noted that the ventricle pressure $p_{\max,LV}(t)$ calculated in Eq. (7.1.1.2) corresponds to the maximum ventricular pressure of the sinusoidal function considered; it is also called isometric or "isovolumic" pressure. It can be seen as the LVP could be approximated by a square sinus waveform, like shown in the following figure.

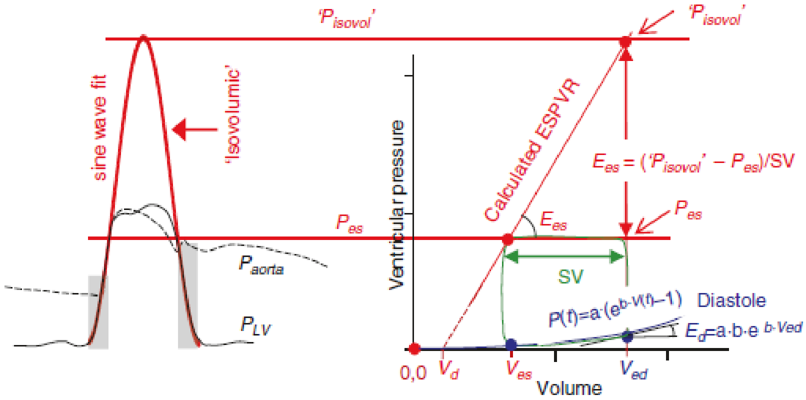

Figure 7.1.1.3 – Ventricular pressure over time graph (left) and over volume graph (right) with the method to obtain trends for functions during diastole and systole.

Since there are viscous effects in left ventricle, the actual LVP is smaller than a sinusoidal wave. In particular, it is possible to account that viscous dissipation with a time-varying ventricular resistance. In fact, it can be defined proportional to the isometric pressure with a constant $k_{R,LV}$, so that it increases during contraction:

$$R_{LV}=k_{R,LV}\cdot p_{\max,LV} \tag{7.1.1.4}$$

Therefore, the instantaneous LVP can be obtained as the difference between the isometric pressure and the product of LV resistance and flow rate out of the ventricle:

$$p_{LV}=p_{\max,LV}-R_{LV}\cdot Q_{out,LV} \tag{7.1.1.5}$$

The cardiac output from the left ventricle $Q_{out,LV}$ is generated when the isometric pressure in the LV is higher than aortic pressure.

$$Q_{out,LV}=\begin{cases}0 & p_{\max,LV}\le p_{SA}\\[1ex] \dfrac{p_{\max,LV}-p_{SA}}{R_{LV}} & p_{\max,LV}>p_{SA}\end{cases} \tag{7.1.1.6}$$

In this case, the aortic pressure is calculated as the pressure of the systemic arteries compartment of the CVS model created. The systemic arterial pressure p_{SA} is derived using the electric conversion performed for the CVS. In particular, the Firestone analogy has been used. It means that the Kirchhoff current law KCL must be accomplished at each node:

$$i_C + i_R + i_L = 0 \tag{7.1.1.7}$$

According to constitutive laws, it results:

$$C\frac{d\Delta v_C}{dt} + \frac{1}{R}\Delta v_R + \frac{1}{L}\int_0^T \Delta v_L \, dt = 0 \tag{7.1.1.8}$$

where $\Delta v_C, \Delta v_R, \Delta v_L$ are the voltage drops across capacitor, resistor and inductor respectively and T is heart period.
In order to obtain the same equation for systemic arteries (SA) compartment, the electric analogous is used, like Figure 4.2.2.1, but now SA compartment is considered individually as in Figure 7.1.1.4.

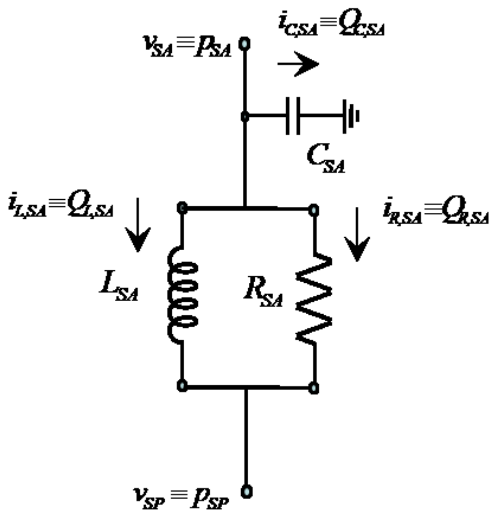

Figure 7.1.1.4 – Systemic arteries compartment electric analogous, obtained with the 2nd approach where capacitance C represents inertial effects.

For the systemic arteries compartment, considering the correspondence between voltage drops and pressure drops, the equation is:

$$C_{SA}\frac{d\,p_{SA}}{dt} + \frac{1}{R_{SA}}(p_{SA} - p_{SP}) + \frac{1}{L_{SA}}\int_0^T (p_{SA} - p_{SP})\,dt = 0 \tag{7.1.1.9}$$

The pressure drop across the SA resistance and inductance can be expressed with the difference between SA pressure and SP pressure, as well as between SA and EP pressure. The reason is that in the original hydraulic model used, SP and EP compartments are connected each other and with SA. Therefore, it can be deduced $p_{SP} = p_{EP}$. Another way to describe SA compartment if the original hydraulic schematic is considered is:

$$C_{SA}\frac{d\,p_{SA}}{dt}+\frac{1}{R_{SA}}(p_{SA}-p_{EP})+\frac{1}{L_{SA}}\int_0^T(p_{SA}-p_{EP})\,dt=0 \qquad (7.1.1.10)$$

In particular, the mechanical spring and damper of systemic arteries compartment are assumed to be split into two equal ramifications. In this way, a spring and a damper with half constant values are connected to splanchnic peripheral circulation SP and the other half part is connected to extra splanchnic peripheral circulation EP. Therefore, systemic arteries spring constant and damping coefficient are divided by two for each branch. In order to integrate this ramification in the hydraulic and electric equivalent systems, this is the correspondence between mechanical values and electric or hydraulic ones:

$$\frac{k_{SA}}{2}\Leftrightarrow\frac{1}{2\cdot L_{SA}};\quad \frac{c_{SA}}{2}\Leftrightarrow\frac{1}{2\cdot R_{SA}} \qquad (7.1.1.11)$$

Applying this ramification and deriving all the terms of the equation to avoid integrals, the equation that describes systemic arteries compartment is:

$$C_{SA}\frac{d\,p_{SA}}{dt}+\frac{1}{2\cdot R_{SA}}(p_{SA}-p_{SP})+\frac{1}{2\cdot R_{SA}}(p_{SA}-p_{EP})+\frac{1}{2\cdot L_{SA}}\int_0^T(p_{SA}-p_{SP})\,dt+\frac{1}{2\cdot L_{SA}}\int_0^T(p_{SA}-p_{EP})\,dt=0$$
(7.1.1.12)

It can be noted that the voltage drop (or pressure drop) across the systemic arteries resistance and inductance involves the splanchnic peripheral pressure and the extra splanchnic peripheral pressure. Since the pressure drop across the two halved SA resistance and inductance is the same, it can be confirmed $p_{SP}=p_{EP}$.

To obtain a reasonable pressure function for left ventricle p_{LV}, the curve for p_{SA} has been derived using Eq. (7.1.1.9) or Eq. (7.1.1.10) neglecting p_{SP} or p_{EP}. In addition, a second derivation has been applied, so the differential equation used to obtain the arterial pressure curve is:

$$C_{SA}\frac{d^2\,p_{SA}}{dt^2}+\frac{1}{R_{SA}}\frac{dp_{SA}}{dt}+\frac{1}{L_{SA}}p_{SA}=0 \qquad (7.1.1.13)$$

Implementing these equations in MATLAB, the resulting p_{LV} curve imposed to left ventricle is shown in the following figure in black.

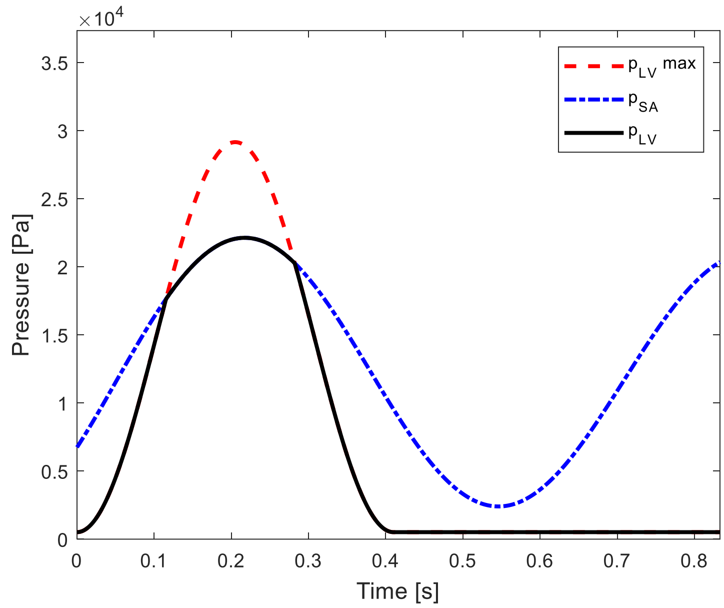

Figure 7.1.1.5 – Left ventricular pressure (black solid line) with isometric pressure (red dashed line) and assumed systemic arteries pressure (blue dash-dot line), for a cardiac cycle.

Then, using flow rate definition in Eq. (7.1.16), cardiac output from left ventricle is derived.

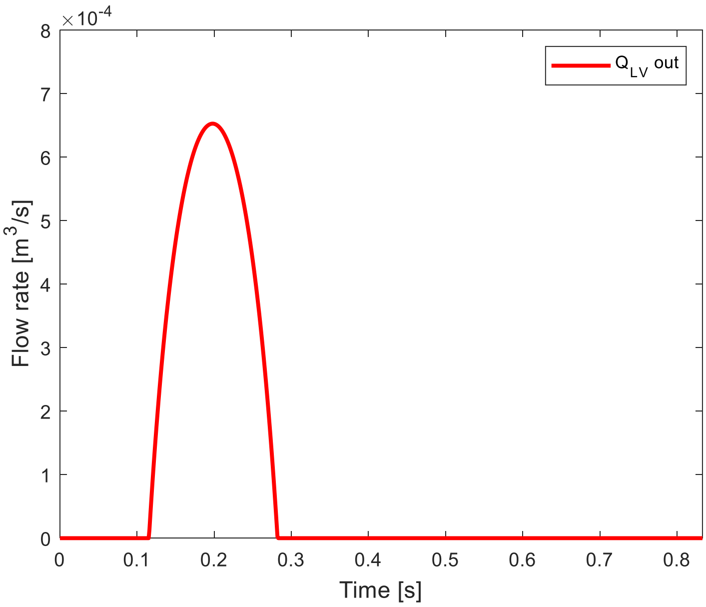

Figure 7.1.1.6 – Cardiac output from left ventricle in a single cardiac cycle.

The integral of the cardiac output, which is the area under the curve in the figure above, corresponds to the volume of blood ejected from left ventricle each cardiac cycle. It is the stroke volume of left ventricle and according to the numerical values used, it has been calculated:

$$\int_0^T Q_{out,LV}\, dt = 7.597 \cdot 10^{-5} \ \text{m}^3 \tag{7.1.1.14}$$

It is an acceptable value because the stroke volume initially assumed for pressure derivation was about 74 ml. Furthermore, the normal range for left ventricular stroke volume is between 70 ml and 110 ml [35, 36].
For right ventricle, the functions that describe its pressure are the same as left ventricle ones. The values of the parameters used change because they refer to right ventricle RV instead of left ventricle LV. Their values have been given in tables from papers. The activation function is the same one defined for left ventricle. The isometric right ventricular pressure is:

$$p_{\max,RV}(t) = \varphi(t) \cdot E_{\max,RV} \cdot (EDV_{RV} - ESV_{RV}) + [\ 1 - \varphi(t)\ ] \cdot P_{0,RV} \cdot (e^{k_{E,RV} \cdot EDV_{RV}} - 1) \quad (7.1.1.15)$$

And the instantaneous right ventricular pressure is obtained subtracting the viscous losses term:

$$p_{RV} = p_{\max,RV} - R_{RV} \cdot Q_{out,RV} \quad (7.1.1.16)$$

Right ventricular resistance is defined by isometric pressure with a constant of proportionality:

$$R_{RV} = k_{R,RV} \cdot p_{\max,RV} \quad (7.1.1.17)$$

The cardiac output form right ventricle is defined as the cardiac output from left ventricle, but the pressure of reference is pulmonary arteries pressure instead of systemic arteries pressure:

$$Q_{out,RV} = \begin{cases} 0 & p_{\max,RV} \le p_{PA} \\ \dfrac{p_{\max,RV} - p_{PA}}{R_{RV}} & p_{\max,RV} > p_{PA} \end{cases} \quad (7.1.1.18)$$

Therefore, it can be deduced that right ventricular pressure depends on pulmonary artery pressure.
The pulmonary arteries pressure can be described with a differential equation considering that PA compartment includes a mass and a spring and damper in parallel mechanically. The schematic is similar to the SA compartment (Figure 7.1.1.4) but with different pressure and flow rate values. Applying Firestone, the equation derived is:

$$C_{PA} \frac{d\,p_{PA}}{dt} + \frac{1}{R_{PA}}(p_{PA} - p_{PP}) + \frac{1}{L_{PA}} \int_0^T (p_{PA} - p_{PP})\,dt = 0 \quad (7.1.1.19)$$

It depends on peripheral pulmonary circulation pressure PP. To obtain a valid right ventricular pressure function, the curve adopted for p_{PA} is derived considering only pulmonary arteries compartment, neglecting p_{PP}. Therefore, applying another derivation with respect to time it is:

$$C_{PA} \frac{d^2\,p_{PA}}{dt^2} + \frac{1}{R_{PA}} \frac{dp_{PA}}{dt} + \frac{1}{L_{PA}} p_{PA} = 0 \quad (7.1.1.20)$$

The resulting right ventricular pressure curve is showed in the following figure, obtained in MATLAB.

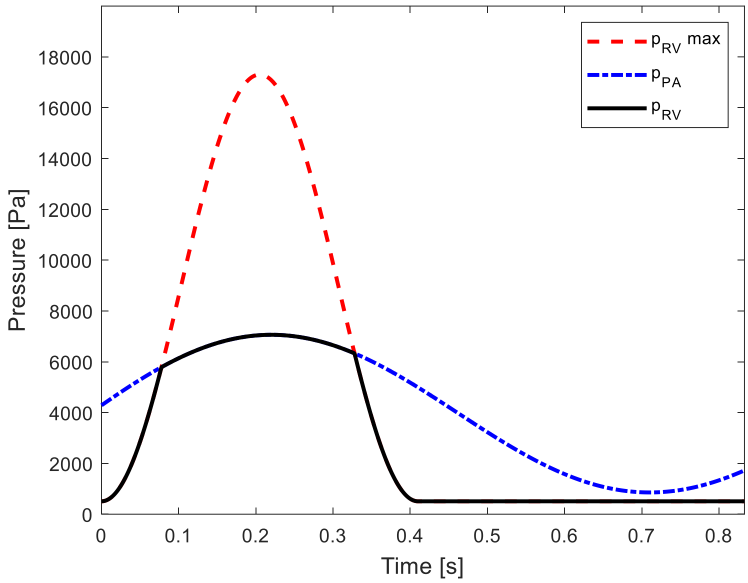

Figure 7.1.1.7 – Right ventricular pressure (black solid line) with isometric pressure (red dashed line) and assumed pulmonary arteries pressure (blue dash-dot line), for a heart cycle.

Then, using flow rate definition in Eq. (7.1.1.18), cardiac output from left ventricle is derived.

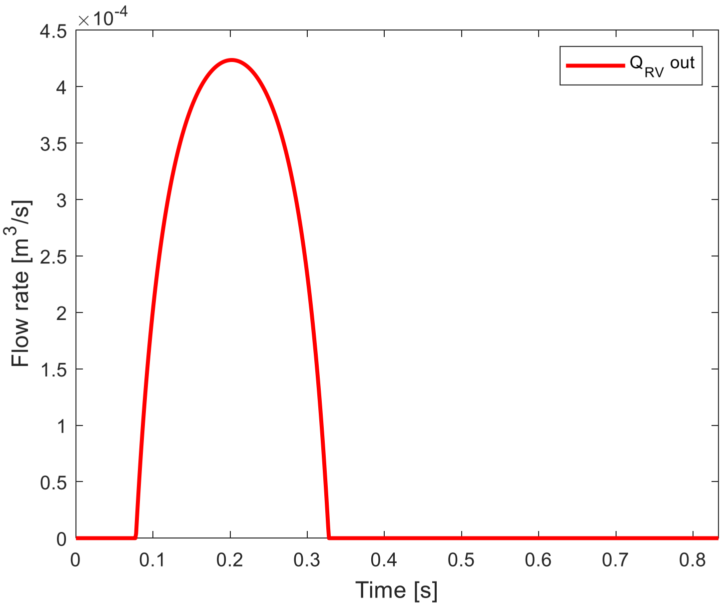

Figure 7.1.1.8 – Cardiac output from right ventricle in a single cardiac cycle.

The integral of the cardiac output, which is the area under the curve in the figure above, corresponds to the volume of blood ejected from left ventricle each cardiac cycle. It is the stroke volume of left ventricle and according to the numerical values used, it has been calculated:

$$\int_0^T Q_{out,LV}\, dt = 7.925 \cdot 10^{-5}\ \text{m}^3 \tag{7.1.1.21}$$

It is an acceptable value because the stroke volume initially assumed for pressure derivation was about 74.1 ml. Furthermore, the normal range for right ventricular stroke volume is similar to the left ventricle one. The reason is that stroke volume from the two ventricles should be almost the same because a big difference between them could cause disease in blood circulation [37].

7.1.2 Integral and derivative of ventricular pressure

The approach used to convert the hydraulic model into the equivalent electric implies to make a correspondence between electric voltage drop and hydraulic pressure drop. According to Firestone analogy, electric voltage drop corresponds to mechanical velocity difference. In Table 4.3.2.1 there is a resume of the state variable and balance equation analogy for hydraulic, electric and mechanical systems. These analogies implies the equivalence of blood pressure drop and velocity of masses in the MCK model. In the CVS model, the ventricular pressure function over time is imposed. For left ventricle, the black curve obtained in Figure 7.1.1.5 is used as imposed velocity on LV mass. In order to find the corresponding displacement, integration is applied. Similarly, the pressure function is derived with respect to time to obtain the corresponding acceleration.
The following graphs show the kinematics imposed to left ventricle for one heart period.

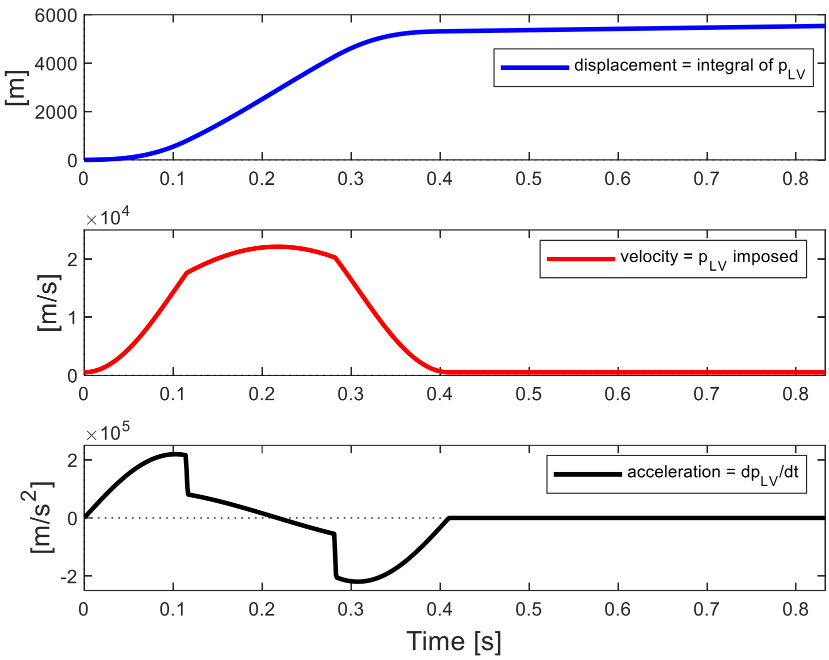

Figure 7.1.2.1 – Imposed kinematics on left ventricle: displacement or integral of p_{LV} (top), velocity or p_{LV} (centre), acceleration or derivative of p_{LV} (bottom).

For the right ventricle, the pressure function derived is the black curve in Figure 7.1.1.7. Applying integration and derivation, the imposed kinematics is obtained for right ventricle, too. It is clear that pressure in right ventricle is almost three times smaller than pressure in left ventricle. It makes also pressure integral and derivative in RV to be almost three times smaller than LV.

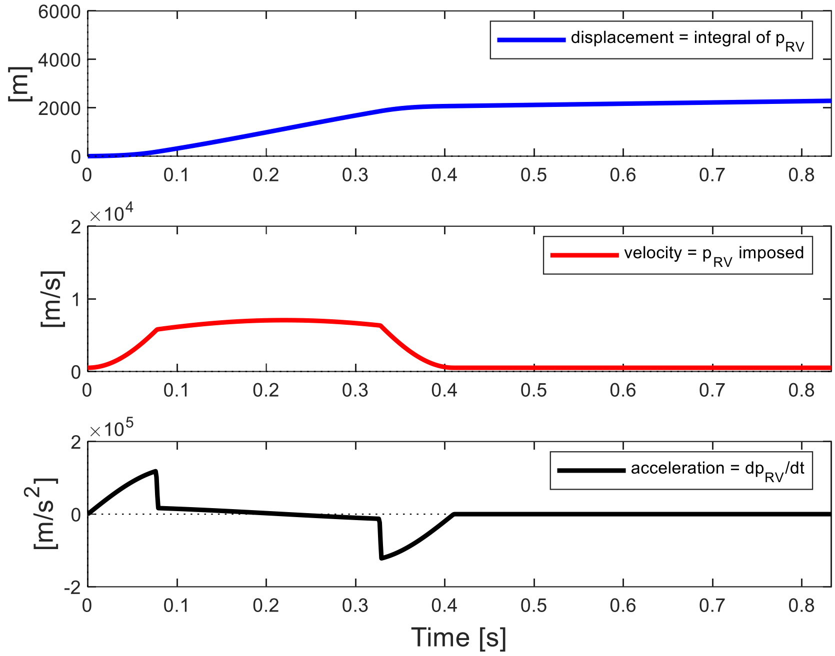

Figure 7.1.2.2 – Imposed kinematics on right ventricle: displacement or integral of p_{RV} (top), velocity or p_{RV} (centre), acceleration or derivative of p_{RV} (bottom).

At t = 0 s, imposed velocities are different from zero for both left and right ventricles. It is due to the functions used to define pressures. In the following figures, it can be noted that velocity positive value at t = 0 s is very similar for LV and RV. Initial displacement is equal to zero for both ventricles, while acceleration reaches a positive value that in LV is almost twice the RV value.

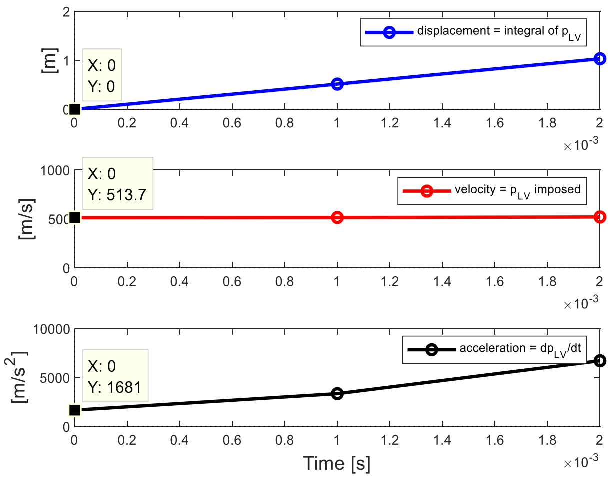

Figure 7.1.2.3 – Detail of imposed kinematics on left ventricle at t = 0 s: displacement or integral of p_{LV} (top), velocity or p_{LV} (centre), acceleration or derivative of p_{LV} (bottom).

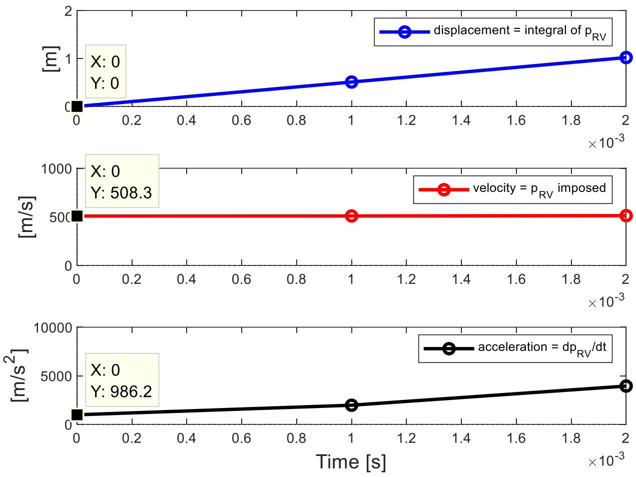

Figure 7.1.2.4 – Detail of imposed kinematics on right ventricle at t = 0 s: displacement or integral of p_{RV} (top), velocity or p_{RV} (centre), acceleration or derivative of p_{RV} (bottom).

7.2 Dynamic problem with imposed kinematics

In the CVS model created, pressure of left ventricle and right ventricle is imposed; it corresponds to an imposed velocity on masses LV and RV of the model. Consequently, the entire kinematics of those two DOFs is imposed, since from the already defined velocity, the corresponding imposed displacement and acceleration can be obtained. It generates a significant change in the dynamic matrix problem describing the model. Originally, it is:

$$\mathbf{M}\ \ddot{\mathbf{x}} + \mathbf{C}\ \dot{\mathbf{x}} + \mathbf{K}\ \mathbf{x} = \mathbf{f}(t) \tag{7.2.1}$$

where mass, damping and stiffness matrices are $n \times n$ matrices; acceleration, velocity, displacement and zero vectors are $n \times 1$, with $n = 12$ which includes all the degrees of freedom of the system. The external forces vector $\mathbf{f}(t)$ is equal to zero in our CV model because there are no external forces applied. At this point, kinematics is imposed to DOFs number 2 and 4, which correspond respectively to left ventricle and right ventricle, according to the order chosen. Therefore $x_{LV}, \dot{x}_{LV}, \ddot{x}_{LV}$ and $x_{RV}, \dot{x}_{RV}, \ddot{x}_{RV}$ are known and the unknown variables of the system are only 10 instead of 12. Only 10 equations are necessary to solve the system. The two equations related to DOFs called LV and RV can be neglected. It implies **M**, **C** and **K** matrices to lose the 2nd and 4th rows and columns. They become $(n-i) \times (n-i)$ matrices, where i = 2 is the number of DOFs with imposed kinematics. The resulting 10×10 matrices are called $\mathbf{M}_{IKs}$, $\mathbf{C}_{IKs}$, $\mathbf{K}_{IKs}$ and they are defined:

$$
\mathbf{M}_{IKs} = \begin{bmatrix}
m_{LA} & 0 & 0 & 0 & 0 & 0 & 0 & 0 & 0 & 0 \\
0 & m_{RA} & 0 & 0 & 0 & 0 & 0 & 0 & 0 & 0 \\
0 & 0 & m_{SA} & 0 & 0 & 0 & 0 & 0 & 0 & 0 \\
0 & 0 & 0 & m_{SP} & 0 & 0 & 0 & 0 & 0 & 0 \\
0 & 0 & 0 & 0 & m_{SV} & 0 & 0 & 0 & 0 & 0 \\
0 & 0 & 0 & 0 & 0 & m_{EP} & 0 & 0 & 0 & 0 \\
0 & 0 & 0 & 0 & 0 & 0 & m_{EV} & 0 & 0 & 0 \\
0 & 0 & 0 & 0 & 0 & 0 & 0 & m_{PA} & 0 & 0 \\
0 & 0 & 0 & 0 & 0 & 0 & 0 & 0 & m_{PP} & 0 \\
0 & 0 & 0 & 0 & 0 & 0 & 0 & 0 & 0 & m_{PV}
\end{bmatrix} \tag{7.2.2}
$$

$$
\mathbf{C}_{IKs} = \begin{bmatrix}
c_{LA}+c_{PV} & 0 & 0 & 0 & 0 & 0 & 0 & 0 & 0 & -c_{PV} \\
0 & c_{RA}+c_{SV}+c_{EV} & 0 & 0 & -c_{SV} & 0 & -c_{EV} & 0 & 0 & 0 \\
0 & 0 & c_{LV}+c_{SA} & -c_{SA}/2 & 0 & -c_{SA}/2 & 0 & 0 & 0 & 0 \\
0 & 0 & -c_{SA}/2 & c_{SA}/2+c_{SP} & -c_{SP} & 0 & 0 & 0 & 0 & 0 \\
0 & -c_{SV} & 0 & -c_{SP} & c_{SP}+c_{SV} & 0 & 0 & 0 & 0 & 0 \\
0 & 0 & -c_{SA}/2 & 0 & 0 & c_{SA}/2+c_{EP} & -c_{EP} & 0 & 0 & 0 \\
0 & -c_{EV} & 0 & 0 & 0 & -c_{EP} & c_{EV}+c_{EP} & 0 & 0 & 0 \\
0 & 0 & 0 & 0 & 0 & 0 & 0 & c_{PA}+c_{RV} & -c_{PA} & 0 \\
0 & 0 & 0 & 0 & 0 & 0 & 0 & -c_{PA} & c_{PA}+c_{PP} & -c_{PP} \\
-c_{PV} & 0 & 0 & 0 & 0 & 0 & 0 & 0 & -c_{PP} & c_{PP}+c_{PV}
\end{bmatrix} \tag{7.2.3}
$$

$$
\mathbf{K}_{IKs} = \begin{bmatrix}
k_{LA} & 0 & 0 & 0 & 0 & 0 & 0 & 0 & 0 & 0 \\
0 & k_{RA} & 0 & 0 & 0 & 0 & 0 & 0 & 0 & 0 \\
0 & 0 & k_{SA} & -k_{SA}/2 & 0 & -k_{SA}/2 & 0 & 0 & 0 & 0 \\
0 & 0 & -k_{SA}/2 & k_{SA}/2 & 0 & 0 & 0 & 0 & 0 & 0 \\
0 & 0 & 0 & 0 & k_{SV} & 0 & 0 & 0 & 0 & 0 \\
0 & 0 & -k_{SA}/2 & 0 & 0 & k_{SA}/2 & 0 & 0 & 0 & 0 \\
0 & 0 & 0 & 0 & 0 & 0 & k_{EV} & 0 & 0 & 0 \\
0 & 0 & 0 & 0 & 0 & 0 & 0 & k_{PA} & -k_{PA} & 0 \\
0 & 0 & 0 & 0 & 0 & 0 & 0 & -k_{PA} & k_{PA} & 0 \\
0 & 0 & 0 & 0 & 0 & 0 & 0 & 0 & 0 & k_{PP}
\end{bmatrix} \tag{7.2.4}
$$

These matrices are obtained in LUPOS [29] multiplying by a transformation matrix $\mathbf{T}_{IKS}$ with size $n \times (n-i)$. It is a sparse matrix used to convert matrices from $n \times n$ to $(n-i) \times (n-i)$ dimension.

$$
\mathbf{T}_{IKs}^{T}\,\mathbf{M}\,\mathbf{T}_{IKs} = \mathbf{M}_{IKs} \tag{7.2.5}
$$

$$
\mathbf{T}_{IKs}^{T}\,\mathbf{C}\,\mathbf{T}_{IKs} = \mathbf{C}_{IKs} \tag{7.2.6}
$$

$$
\mathbf{T}_{IKs}^{T}\,\mathbf{K}\,\mathbf{T}_{IKs} = \mathbf{K}_{IKs} \tag{7.2.7}
$$

They come from the definition of displacement, velocity and acceleration as $(n-i) \times 1$ vectors:

$$\mathbf{x} = \mathbf{T}_{IKs}\,\mathbf{x}_{IKs} \tag{7.2.8}$$

$$\dot{\mathbf{x}} = \mathbf{T}_{IKs}\,\dot{\mathbf{x}}_{IKs} \tag{7.2.9}$$

$$\ddot{\mathbf{x}} = \mathbf{T}_{IKs}\,\ddot{\mathbf{x}}_{IKs} \tag{7.2.10}$$

Similarly, the eventual external force vector is transformed:

$$\mathbf{f}_{IKs} = \mathbf{T}_{IKS}^{T}\,\mathbf{f} \tag{7.2.11}$$

Even if the equations related to LV and RV masses are not included, there are still some terms in the damping matrix that multiplies imposed velocities $\dot{x}_{LV}$ and $\dot{x}_{RV}$. They can be identified in the original damping matrix $\mathbf{C}$ (12×12), they are the damping coefficients in the 2nd and 4th columns that are not on the diagonal. Therefore, the imposed kinematics becomes like a force for the reduced system 10×10 and the damping term on the right of the equation is a matrix with dimensions $(n-i)\times i = 10\times2$:

$$\mathbf{T}_{IKs}^{T}\,\mathbf{C}\,\boldsymbol{\delta} = \begin{bmatrix} -c_{LA} & 0 \\ 0 & -c_{RA} \\ -c_{LV} & 0 \\ 0 & 0 \\ 0 & 0 \\ 0 & 0 \\ 0 & 0 \\ 0 & -c_{RV} \\ 0 & 0 \\ 0 & 0 \end{bmatrix} \tag{7.2.12}$$

It can be defined with the matrix product $\mathbf{T}_{IKs}^{T}\,\mathbf{C}\,\boldsymbol{\delta}$, where $\boldsymbol{\delta}$ is a sparse matrix $(n\times i)$ used to correlate the imposed variables to the corresponding places in the matrix before. It is the damping term that multiplies velocity vector. It could be derived for mass and stiffness terms in the same way. In fact, the time-dependent dynamic problem is:

$$\mathbf{M}_{IKs}\,\ddot{\mathbf{x}}_{IKs} + \mathbf{C}_{IKs}\,\dot{\mathbf{x}}_{IKs} + \mathbf{K}\,\mathbf{x}_{IKs} = \mathbf{f}_{IKs} - \mathbf{T}_{IKs}^{T}\,\mathbf{M}\boldsymbol{\delta}\,\ddot{\mathbf{x}}_{in} - \mathbf{T}_{IKs}^{T}\,\mathbf{C}\boldsymbol{\delta}\,\dot{\mathbf{x}}_{in} - \mathbf{T}_{IKs}^{T}\,\mathbf{K}\boldsymbol{\delta}\,\mathbf{x}_{in} \tag{7.2.13}$$

where imposed displacement, velocity and acceleration vectors $\mathbf{x}_{in}, \dot{\mathbf{x}}_{in}, \ddot{\mathbf{x}}_{in}$ have dimension $i\times t$ that means they considers the evolution of the kinematics over time. It can be noted that the force effect from imposed kinematics is subtracted to eventual external forces. In the case of CVS model, there are no external forces, so that term is equal to zero. Besides, the mass and stiffness terms related to imposed kinematics (on the right of the equation above) are equal to zero. There is only the damping term. The reason is that dampers related to LV and RV compartments are connected in parallel with SA and PA masses, as well as with LA and RA masses respectively, these connections generate the terms seen in Eq. (7.2.12). On the contrary, springs of LV and RV compartments are connected to ground and mass matrix is diagonal, therefore, they do not appear as force.

In order to solve the problem, a model was built in Simulink to obtain displacement, velocity and acceleration over time for the 10 DOFs of the system. In Simulink model, a transient was used to make the simulation over time. However, it slightly affect only the first heartbeat.

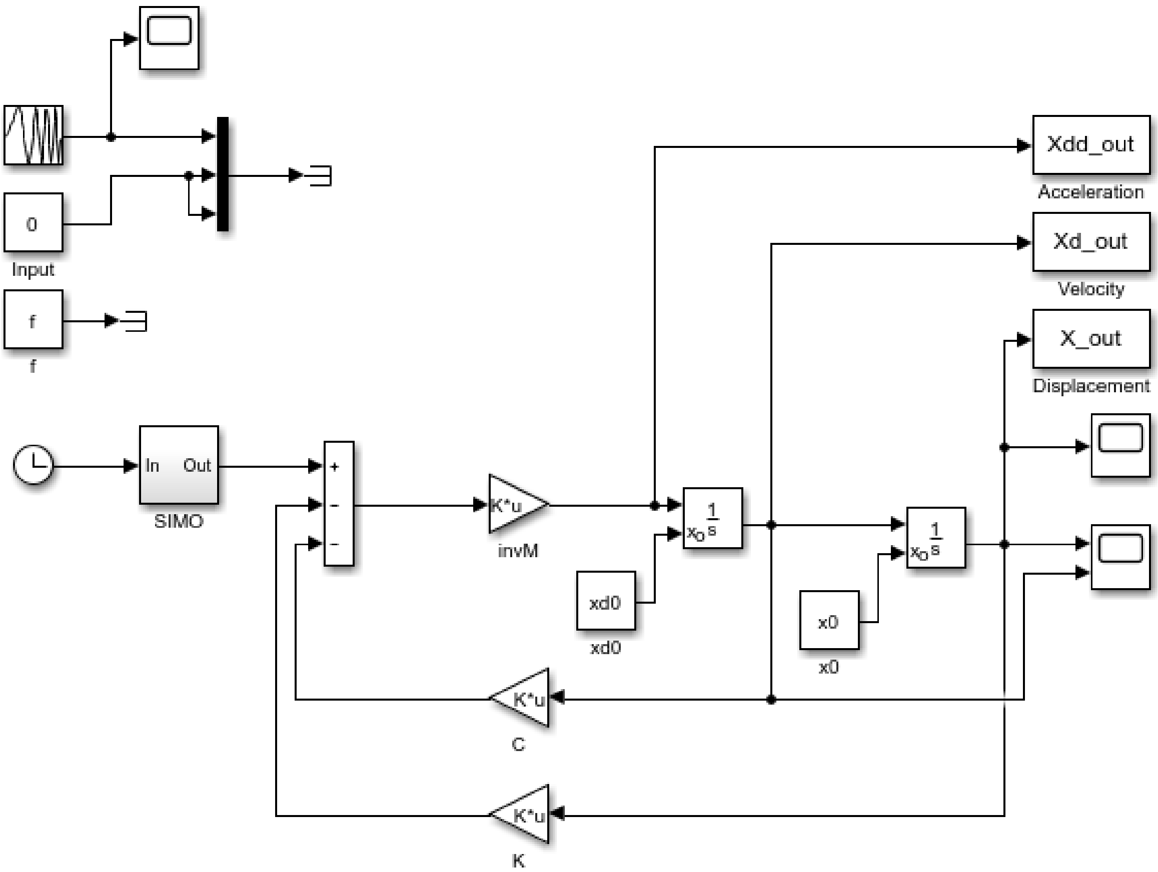

Figure 7.2.1 – Model created in Simulink to solve the 2nd order systems of equation for 10 DOFs (excluding the DOFs with imposed kinematics).

Then, a MATLAB script has been created to collect information from Simulink and LUPOS to extend histories of displacement, velocity and acceleration over time to all the 12 DOFs of the CVS model. The main MATLAB scripts used to solve the problem with imposed kinematics are reported in Appendix.
For all the DOFs of the system, the history of displacement, velocity and acceleration is obtained over time, when velocity or hydraulic blood pressure is imposed for ventricles DOFs. The following graphs have been obtained repeating the heart period considered, which is 0.833 s. It means that a single heart rate of 1.2 Hz or 72 beats/min excites the system.
Initially, the original CVS mechanical model is considered, where two modes of rigid body motion exist. Due to those rigid body motions, the displacement curve over time in Figure 7.2.2 there are two curves that tend to rise continuously every heartbeat. In Figure 7.2.3, a zoom on those curves is reported. It demonstrates that they are correlated to the rigid body motion because the DOFs performing that unusual behaviour are SA, EP and SP, as well as PA and PP. They correspond to the two subsystems involved in rigid body modes, according to the CVS mechanical model created. In particular, the curve related to the rigid body motion of SA, SP and EP nodes increases faster and with a higher amplitude than the other one related to PA and PP. It

is reasonable because pressure in systemic circulation is found to be higher than pressure in the pulmonary circulation.

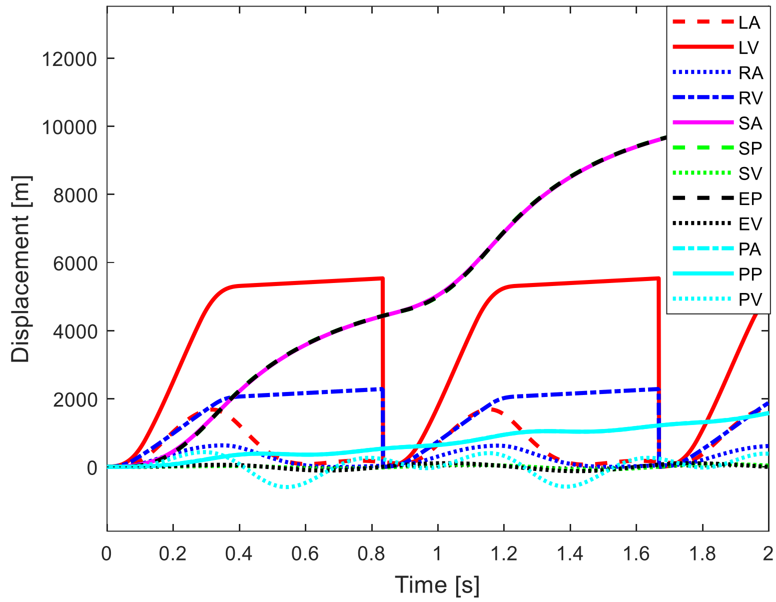

Figure 7.2.2 – Displacement of each DOF of CVS model for two cardiac cycles.

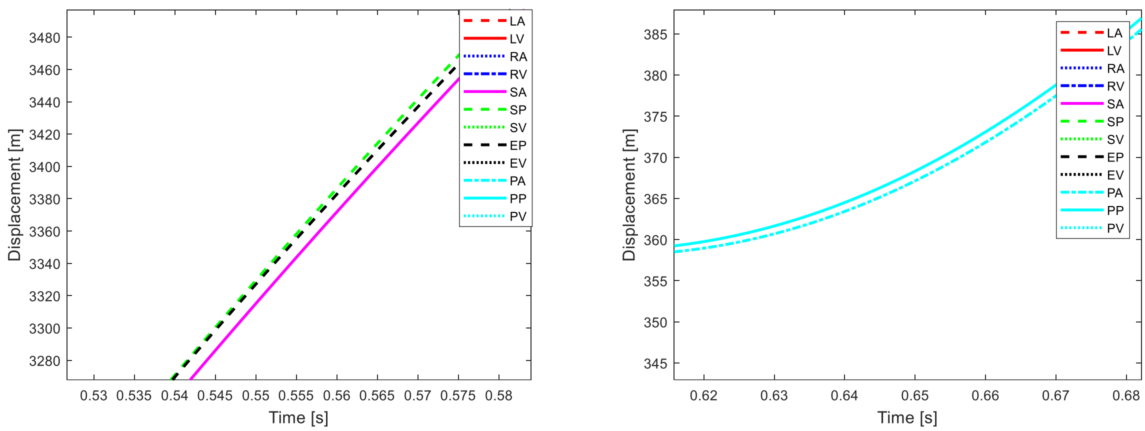

Figure 7.2.3 – Zoom on displacement over time of SA, SP and EP group of rigid body motion (left), as well as PA and PP group (right).

This result shows that displacement of some DOFs would tend to rise every heartbeat causing a drift. Therefore, the CVS model with more springs connected to ground is considered, so that there is no rigid body motion. Using this model with only underdamped and overdamped modes, the displacement graph over time is found to be reliable for all DOFs.

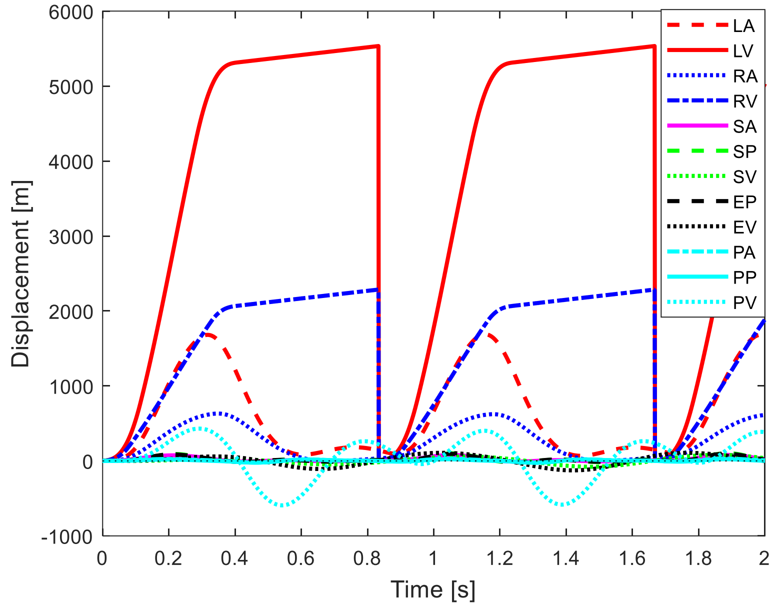

Figure 7.2.4 – Displacement of each DOF of CVS model for two cardiac cycles, without rigid body motion.

The initial displacement is equal to zero for all DOFs.

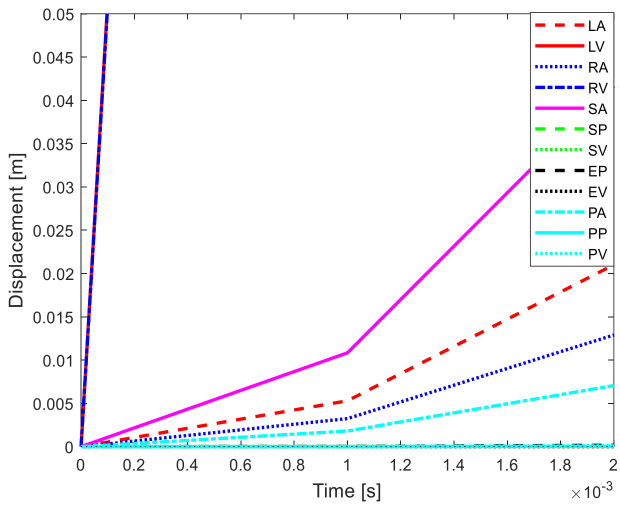

Figure 7.2.5 – Detail of displacement of each DOF of CVS model without rigid body motion, around zero seconds.

The corresponding velocity waveforms are reported in Figure 7.2.6 for the same heartbeats. These curves correspond to pressure over time for every node.

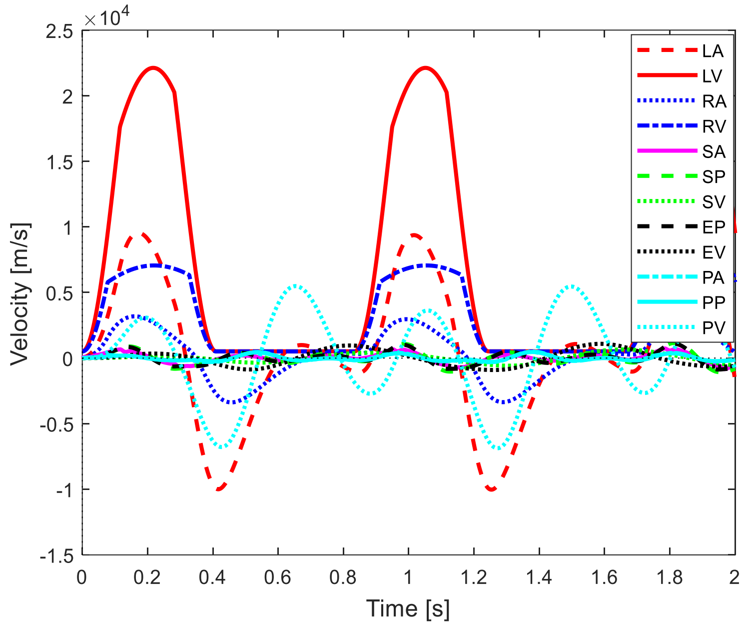

Figure 7.2.6 – Velocity of each DOF of CVS model for two cardiac cycles, without rigid body motion.

It can be noted that initial velocity is different from zero only for LV and RV, in particular they reach similar values at zero seconds, as seen in Figure 7.1.2.1 and Figure 7.1.2.2. The other DOFs has initial velocity equal to zero.

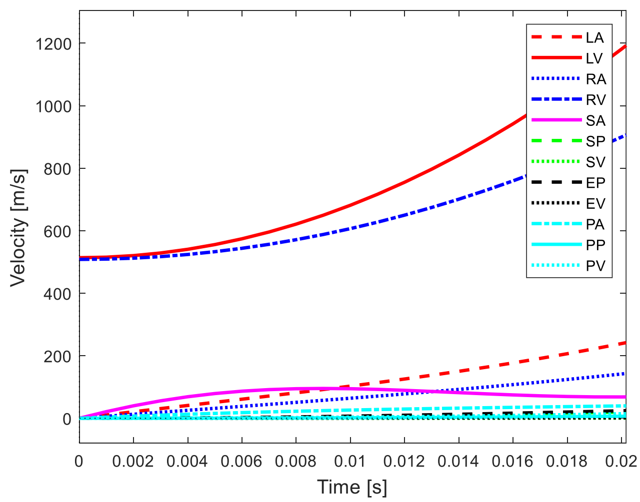

Figure 7.2.7 – Detail of velocity of each DOF of CVS model around zero seconds.

Form the velocity derivation, acceleration curves are obtained.

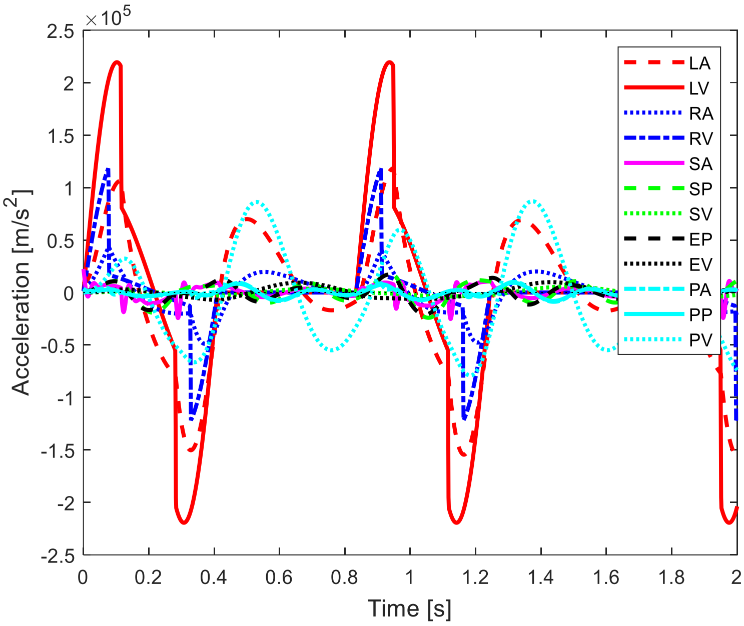

Figure 7.2.8 – Acceleration of each DOF of CVS model for two cardiac cycles, without rigid body motion.

The initial acceleration is different from zero for LA, LV, RA, RV and PA, while it is equal to zero for the other nodes. It depends on the trend of the velocity waveforms around zero seconds.

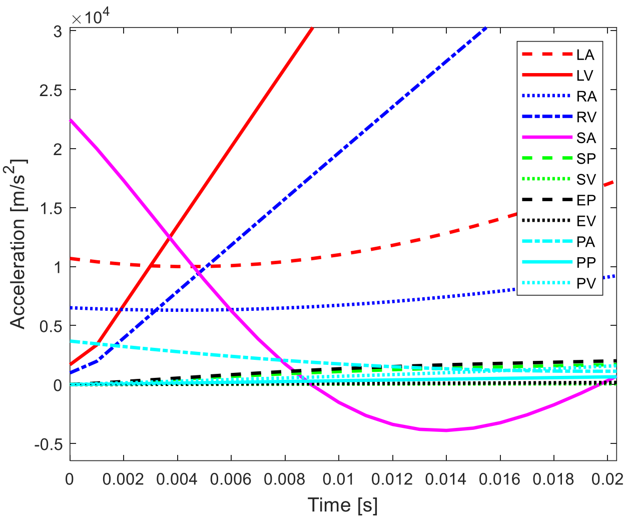

Figure 7.2.9 – Detail of acceleration of each DOF of CVS model around zero seconds.

7.3 Hemodynamic interpretation of the results: pressure

The first graph to be analysed in details is the pressure over time, which corresponds to velocity of each mass of the CVS model.

7.3.1 Blood pressure in heart chambers

Initially, the heart chambers are considered with a zoom for only two repetitions of the heart period.

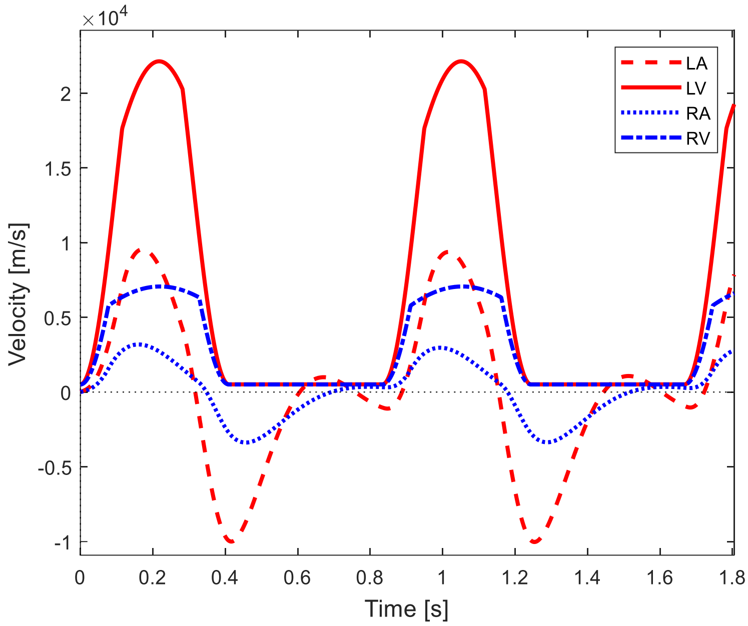

Figure 7.3.1.1 – Velocity (or pressure) of right and left atria and ventricles, for two cardiac cycles.

The left and right ventricular pressures are imposed, in fact they corresponds to the normal waveforms measured with catheterization. The left and atrial pressures are derived from the model. A way to compare ventricular and atrial pressure involves the electrocardiogram.
The ECG signal records the strength and timing of the electrical activity in the heart [38]. It shows each phase of the electrical signal as it travels through the heart. It begins in the right and left atria causing their contraction and it is recorded as point P in the ECG graph (Figure 7.3.1.2). Then, the electric signal passes form the atria to the ventricles with a time delay, allowing the ventricles to fill with blood. This phase corresponds to the PR segment. Then, the signal causes the ventricles to contract and to pump blood to the lungs and to the body. It is recorded as the QRS waves on the ECG, usually called QRS complex. The following T wave corresponds to the recovering of ventricles, which recover their normal electrical state, muscles relax and stop contracting, allowing ventricular filling with blood from the atria. The ST interval represents the beginning of the ventricular relaxation, while the QT interval represents both the contraction and following recovery of the ventricles. The QT segment lengthens at a slower heart rate and shortens at a faster heart rate.

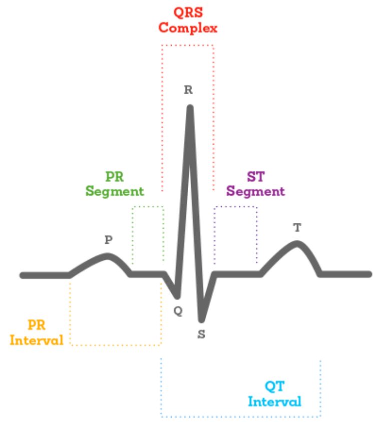

Figure 7.3.1.2 – Schematic of a ECG signal with characteristic points.

The correspondence between left ventricular pressure waveform and ECG signal is showed in the following figure [39]. According to several ventricular catheterization to measure blood pressure, the R-peak of ECG corresponds with the ascending part of the ventricular pressure waveform, which is the beginning of systolic phase. It is important to note that T-wave of ECG occurs almost at the ventricular pressure peak, with a small delay. However, T-wave still occurs during systole and it ends when diastole starts and ventricular pressure starts to decreases.

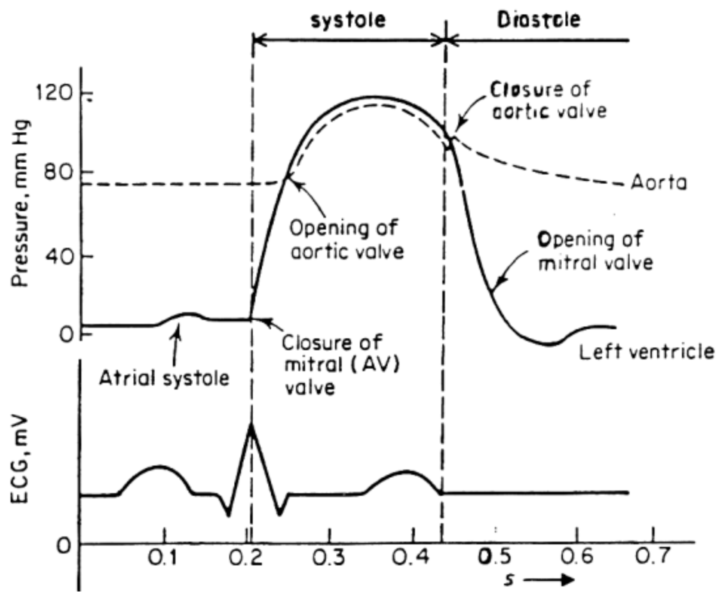

Figure 7.3.1.3 – Left ventricular pressure, ECG and hemodynamic events during cardiac cycle.

In the same time, it is interesting to see which is the relationship between ECG and left atrial pressure waveform. Some experimental recordings [40] show that left atrial pressure has a positive deflection called a-wave, which corresponds to P-wave of ECG. Hemodynamically, it occurs when atria contract. The following positive deflection is the c-wave that corresponds to QRS complex and ventricular contraction. However, it is very small and it is not visible every time. After a descending trend (descendent x-wave), the left atrial pressure waveform has another increase in pressure called v-wave. It corresponds to T-wave of ECG that is passive atrial refilling, followed by ventricular filling from left atrium (descendent y-wave).

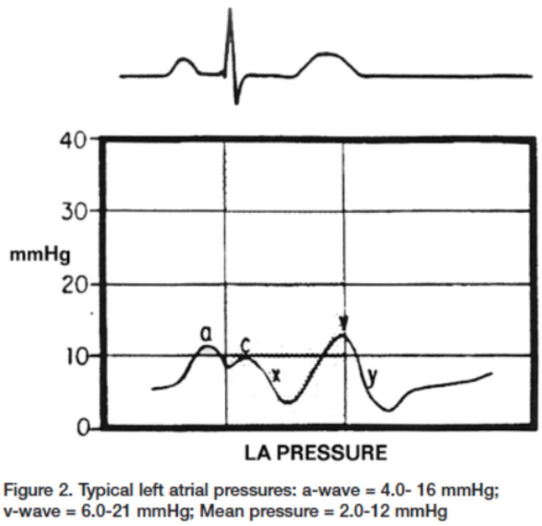

Figure 7.3.1.4 – ECG (top) and left atrial pressure (bottom) during cardiac cycle.

Thanks to the relationship with ECG shown in Figure 7.3.1.3 and Figure 7.3.1.4, it is possible to correlate left ventricular and atrial pressure for a typical patient without cardiovascular diseases. In particular, it demonstrates that left atrial a-wave occurs at end-diastole and v-wave occurs at end-systole.

The LV and LA velocity waveforms obtained for the model almost respect this relationship. It can be noted that LA waveform has a first peak during systole, which may correspond to actual v-wave, and a second slight peak at end-diastole, right before LV pressure rise, which may correspond to a-wave. It demonstrates that a-wave intensity is lower than v-wave for LA. The main incoherence is that the results obtained do not show a delay between LA and LV pressure peaks, which usually occurs in real recordings. Another issue deal with pressure range. In the velocity graphs obtained, the Y-axis should represent the pressure values in Pascal. The LA pressure range is commonly lower than 20 mmHg that means about 2700 Pa.

For the right ventricle and atrium, a similar relationship is found because both ventricular and atrial waveforms of the right side of the heart have almost the same trends as the left side. The main difference is that the range of pressure in the right side of the heart is considerably lower than the left side. The right ventricular pressure has the same waveform as the left ventricle but the maximum (RV systolic pressure) is usually lower than 30 mmHg or 4000 Pa. The RV and LV pressure curve are almost synchronous because the ventricles almost contract simultaneously [41].

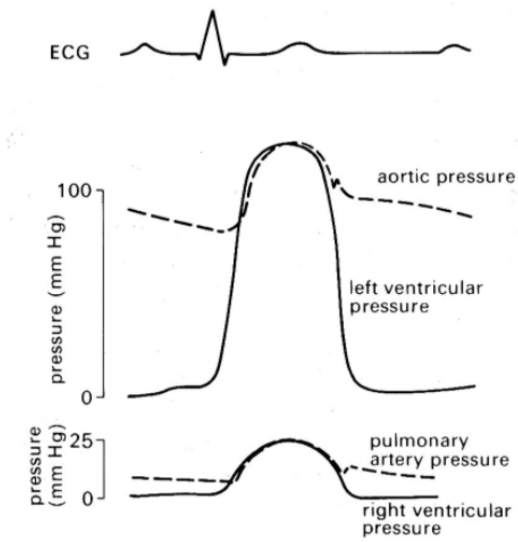

Figure 7.3.1.5 – ECG (top), left ventricular pressure (centre) and right ventricular pressure (bottom) during cardiac cycle.

The right atrium pressure curve recorded experimentally is very similar to the left atrial one. In particular, the a-wave corresponds to P-wave in ECG and v-wave corresponds to T-wave in ECG [40]. The main difference is that RA waveform occurs in a narrower range of pressure. In fact, the normal RA pressure is lower than 10 mmHg or 1300 Pa.

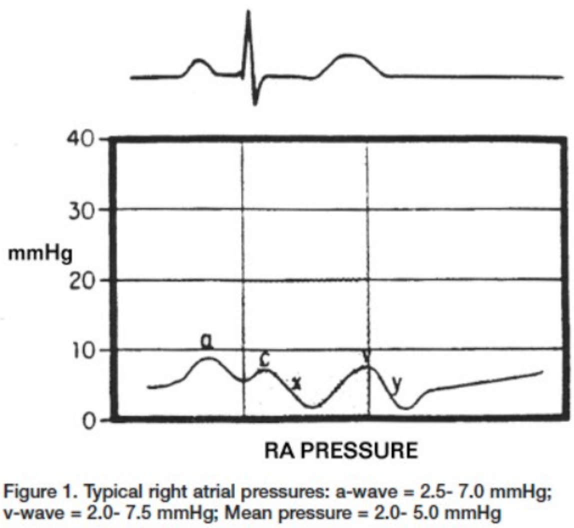

Figure 7.3.1.6 – ECG (top) and right atrial pressure (bottom) during cardiac cycle.

In the velocity graph obtained for LV, RV, LA, RA masses of CVS model (Figure 7.3.1.1), it is demonstrated that LA and RA velocity (or pressure) curves are almost synchronous as well as LV and RV waveforms. Furthermore, the peak values reached by LA curve are almost the double of the peak values reached by RA curve. That confirms the experimental signals seen above and it is due to the lower hydraulic capacitance found in left atrium.

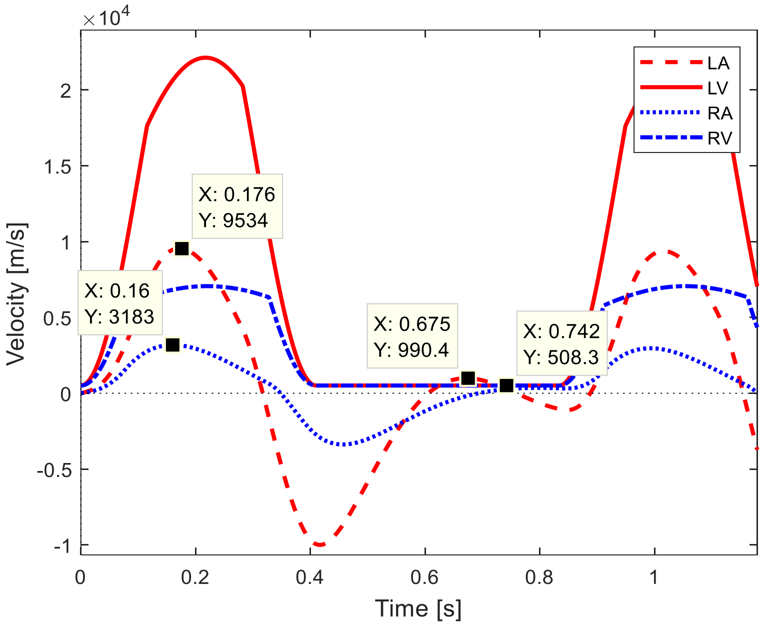

Figure 7.3.1.7 – Velocity (or pressure) of right and left atria and ventricles with a-peaks and v-peaks, for one cardiac cycle.

Since Y-axis corresponds to pressure in Pascal, the numerical a-waves and v-waves values are higher than experimental ranges. It is an aspect of the model that needs to be investigated and fixed properly, so that pressure waveforms become more representative of real invasive detection.

7.3.2 Blood pressure in arteries

It is interesting to look at pressure waveforms for systemic and pulmonary arteries. In order to do that, the left and right ventricles will be counted because they are directly connected. Pressure curves obtained for the CVS model when rigid body motion is not included are shown in Figure 7.3.2.1.

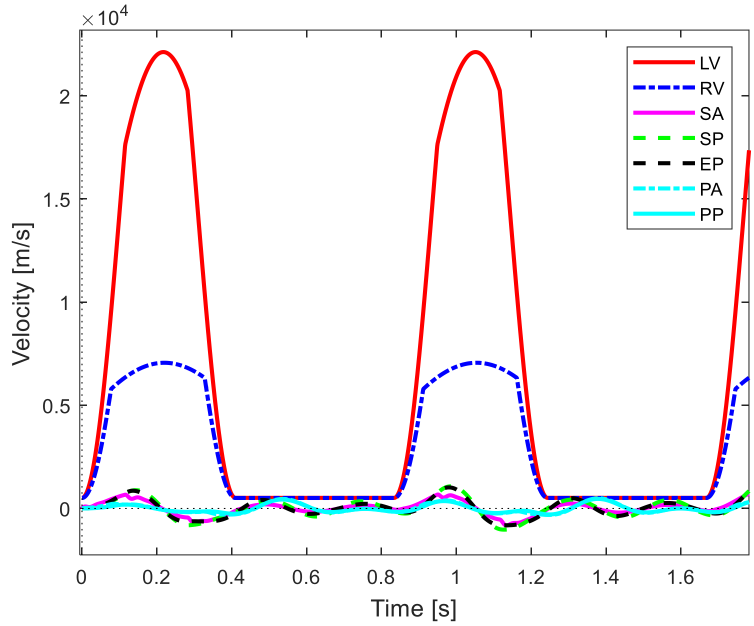

Figure 7.3.2.1 – Velocity (or pressure) of systemic and pulmonary arteries compartment and left and right ventricles, for two cardiac cycles, without rigid body motion.

It can be noted that systemic arteries (SA) pressure has the same shape and amplitude as peripheral circulation in human body (SP and EP). A detailed view demonstrates that SA pressure (or velocity) curve is synchronous with SP and EP curves; moreover, they have the same amplitude.

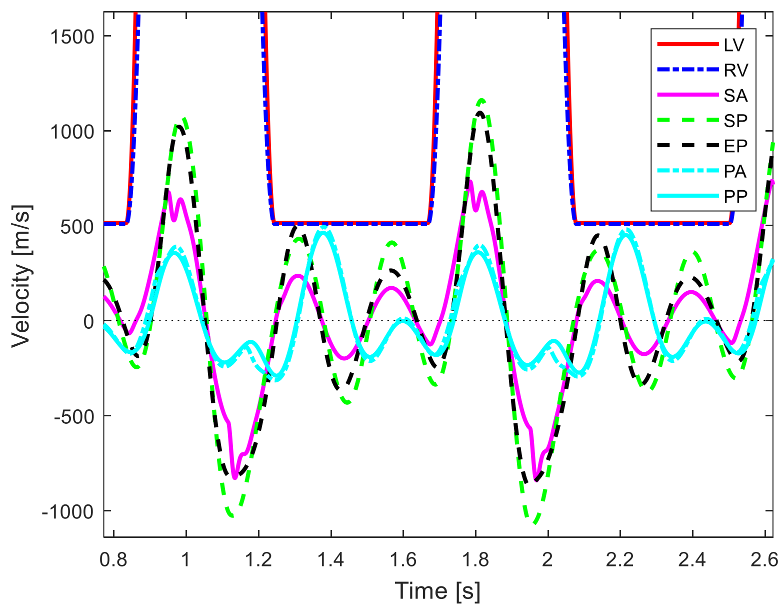

Figure 7.3.2.2 – Detailed view of velocity (or pressure) of right and left ventricles, systemic and pulmonary arteries for two cardiac cycles.

In Figure 7.3.2.2, pulmonary arteries are included, too. In particular, pulmonary arteries PA pressure almost coincides with pulmonary peripheral circulation PP pressure. The velocity curve

related to pulmonary circulation reaches a small peak when SA velocity is minimum at end-systole, then it reaches a higher peak with a delay with respect to SA. This relationship means that systemic and pulmonary circulation reach almost the same velocity (or pressure) only during systole. It means that during ventricular contraction, pressure in systemic and pulmonary arteries rises in the same way; then, when ventricular relaxation begins, pulmonary pressure (PA, PP) shows a delay with respect to systemic one (SA, SP, EP). An important deduction from Figure 7.3.2.2 is that SA compartment in our CVS model does not correspond to aorta. Instead, SA compartment refers to systemic arteries when they are closer to human splanchnic and extra splanchnic organs, called SP and EP compartments.
According to invasive measurements, aortic pressure should have the shape shown in Figure 7.3.2.3. It reports some examples of left ventricular and aortic pressures measured by catheterization for patients with different levels of aortic stenosis [42]. The aortic stenosis causes the aortic valve to not open fully, so the aortic valve narrows and the left ventricle has to work more to pump blood out. The left ventricular pressure becomes much higher than aortic pressure. The pressure gradient across the aortic valve is normally a few mmHg but it becomes very high with stenosis, also greater than 100 mmHg [43].

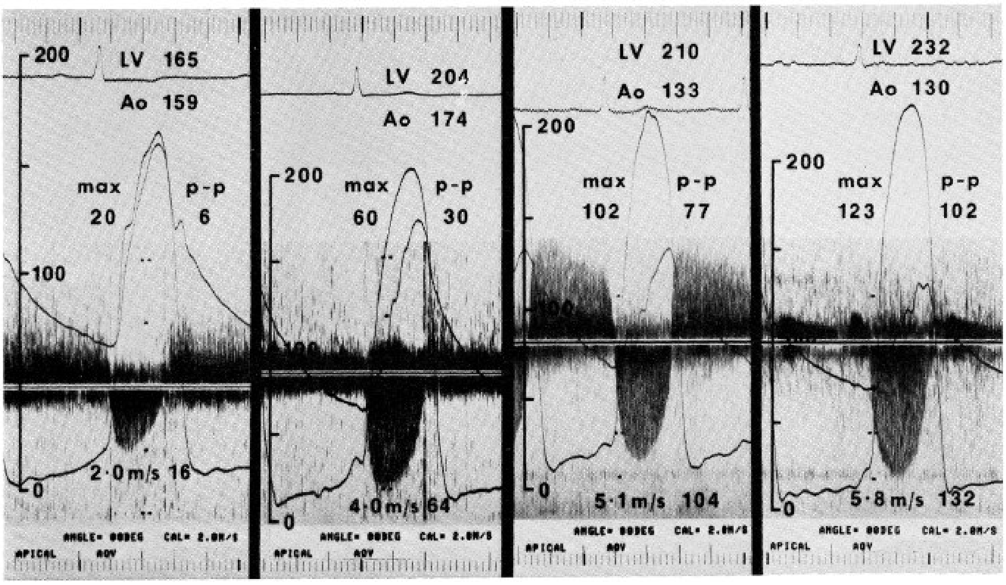

Figure 7.3.2.3 – Left ventricular pressure and the aortic pressure measured by the dual catheter for normal case (left) to sever aortic stenosis case (right); there is also the ejection velocity measured by Doppler echocardiogram (black shadows).

The SA pressure obtained in the CVS model without rigid body motion (Figure 7.3.2.2) is completely different from actual aortic pressure.
On the contrary, when rigid body motions are counted for CVS model, which implies two springs less, the pressure waveform of SA compartment results more similar to aortic pressure. It is shown in Figure 7.3.2.4, where SA pressure curve starts from 0 Pa at 0 s but from the second cardiac cycle, it reaches an offset pressure different from zero all the time. However, SA pressure results to be too much lower than ventricular pressure peak. In particular, in this model, the pressure gradient that is the difference between LV pressure peak and SA pressure peak is about 10000 Pa or 75 mmHg. It would correspond to a high aortic stenosis. More investigation could be applied to the model in order to reproduce a normal relationship between LV and SA pressure curves, which means a gradient about 10 mmHg or 1300 Pa. Figure 7.3.2.4 shows that

the SA pressure peak occurs during late systole. It is coherent with the normal pressure invasive measurements.

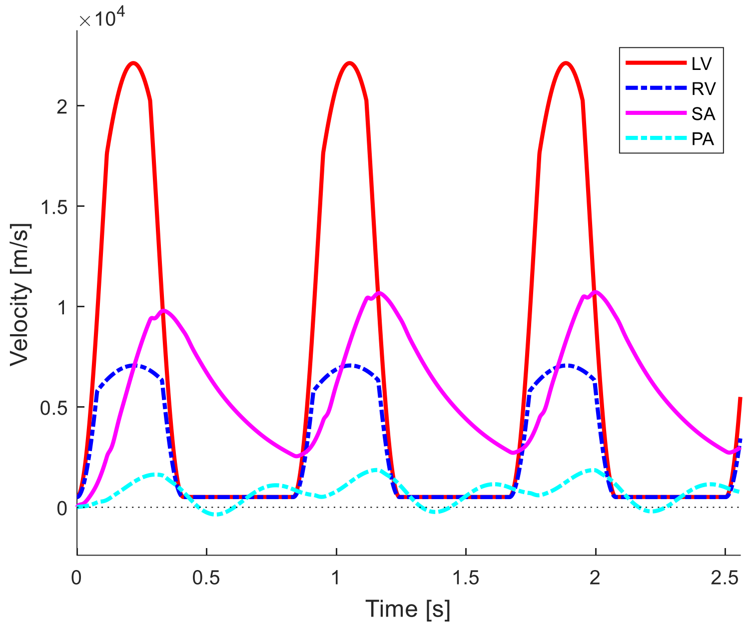

Figure 7.3.2.4 – Velocity (or pressure) of systemic and pulmonary arteries compartment and ventricles, for three cardiac cycles, when CVS model includes modes of rigid body motion.

For pulmonary arteries, some experimental measurements are normally done at two levels: pulmonary artery pressure and pulmonary capillary wedge pressure (PCWP). Pulmonary artery pressure waveform is normally synchronous with right ventricular pressure waveform. It differs for the range of values because the PA waveform has a diastolic pressure a bit higher than diastolic pressure of RA. The pulmonary artery pressure normally recorded is shown in the following figure [44].

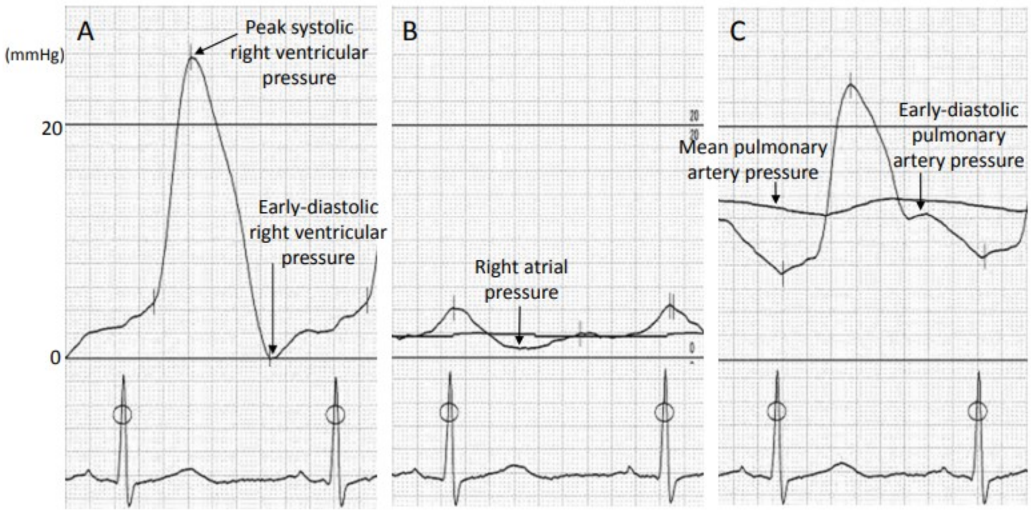

Figure 7.3.2.5 – Measurements of right ventricular pressure (left), right atrial pressure (centre) and pulmonary arterial pressure (right).

Using heart catheterization from right ventricle to pulmonary capillaries, the waveform of pressure detected changes as in the following figure [44].

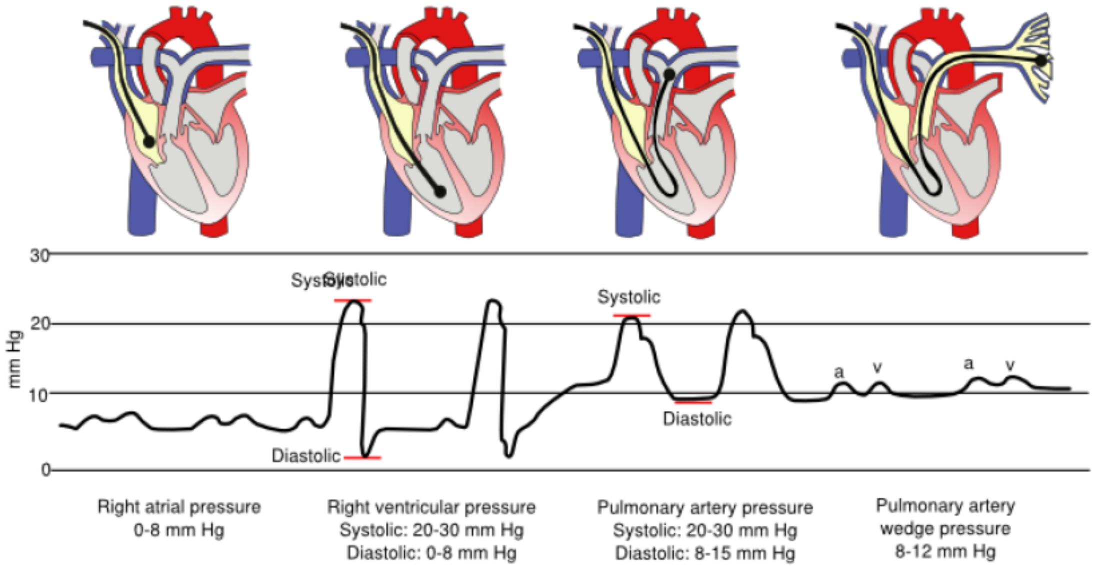

Figure 7.3.2.6 – Pressure measured with right heart catheterization from right atrium (left), to right ventricle, to pulmonary artery, to pulmonary capillaries (right).

For pulmonary capillaries, pressure waveform recorded is very similar to LA pressure waveform, as shown in Figure 7.3.2.7. The only difference is that PCWP curve is slightly shifted to the right with respect to LA pressure waveform.

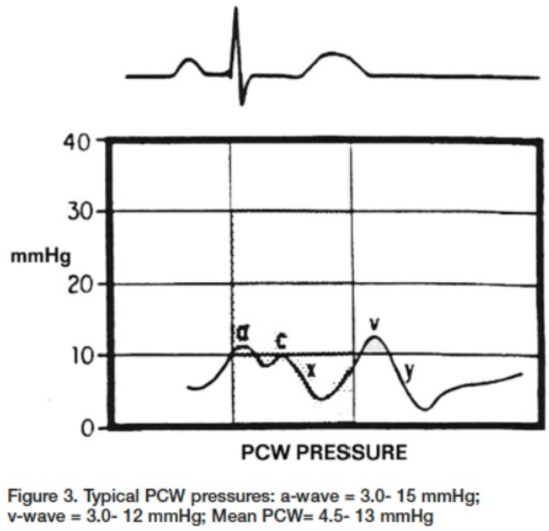

Figure 7.3.2.7 – ECG (top) and pulmonary capillary wedge pressure PCWP (bottom) recorded during cardiac cycle.

In the CVS model created, PA and PP pressure waveforms almost coincide. It can be noted in Figure 7.3.2.4 that their shape is quite different from the normal pulmonary arterial pressure because it performs many intermediate peaks. The shape of PA, PP, SA, SP and EP pressure waveforms obtained from CVS model is very similar to the PCWP shape described before. In particular, Figure 7.3.2.8 shows that PA, PP, SA, SP and EP pressures seem to reach a-wave peak when systole starts and v-wave peak when diastole starts. It can demonstrate that their peaks occur shifted to the right with respect to LA or RA curve, as demonstrated experimentally [40].

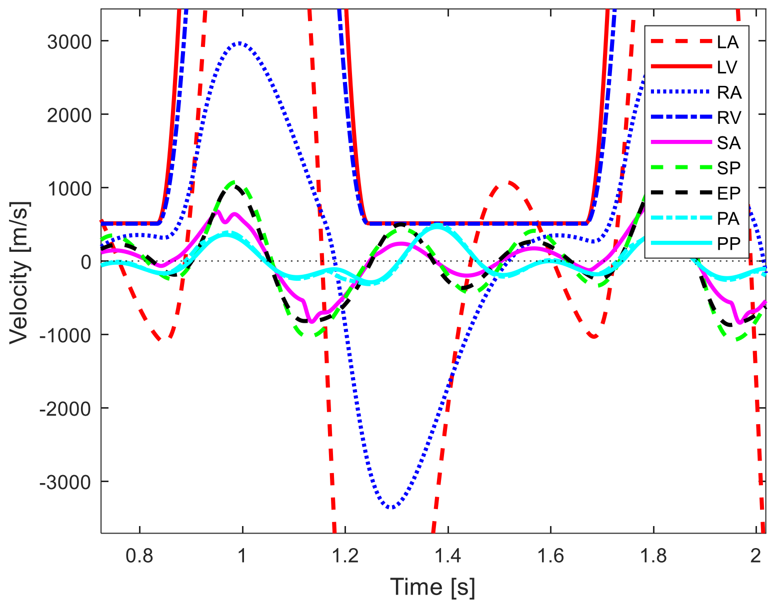

Figure 7.3.2.8 – Velocity (or pressure) waveforms for ventricles, atria, systemic arteries, pulmonary arteries and peripheral circulation, without rigid body motion.

The waveforms obtained for PA and PP almost coincide, in fact some zoom on them show that there are some parts of the curves that do not overlap exactly, but the trend of both waveforms is the same.

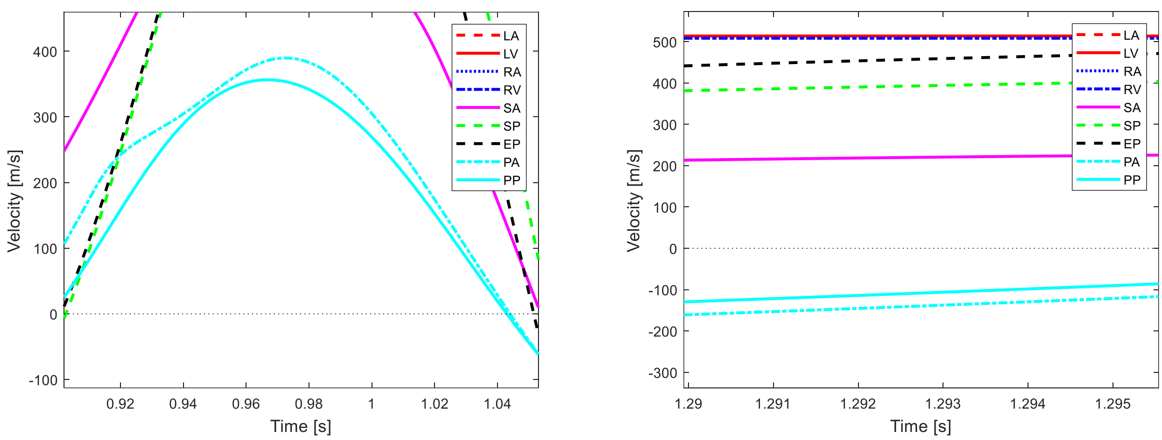

Figure 7.3.2.9 – Detail of PA and PP pressure (or velocity) waveform.

If modes of rigid body motion are considered for CVS model, the pulmonary arteries pressure waveforms differ from the case without rigid body motion, but they still respect the general PCWP waveform (Figure 7.3.2.10).

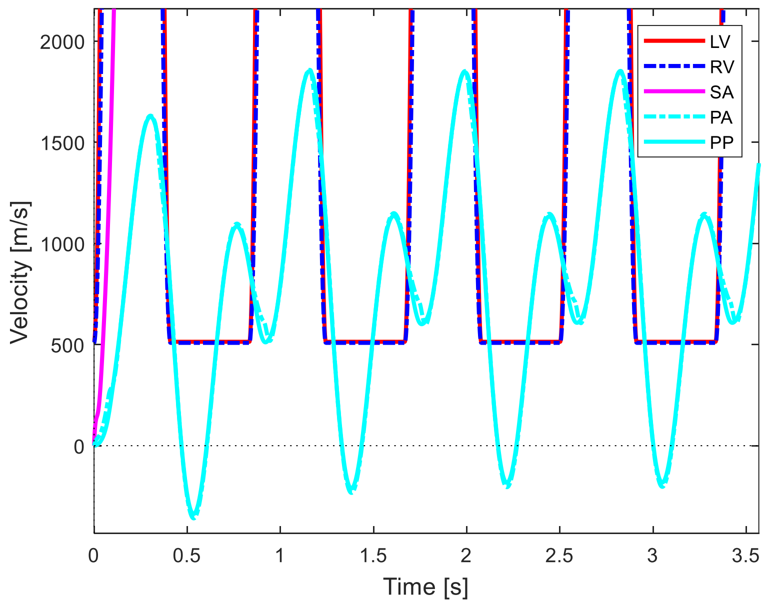

Figure 7.3.2.10 – Detail of velocity (or pressure) waveforms for pulmonary arteries, when CVS model includes rigid body motion.

7.3.3 Blood pressure in veins

Adding the pulmonary veins pressure to the graph, it can be noted that PV pressure waveform is almost synchronous with left atrial pressure waveform. The reason is that pulmonary veins return to left atrium, so they are close to it, consequently, pressure in PV compartment is very similar to pressure in RA compartment.

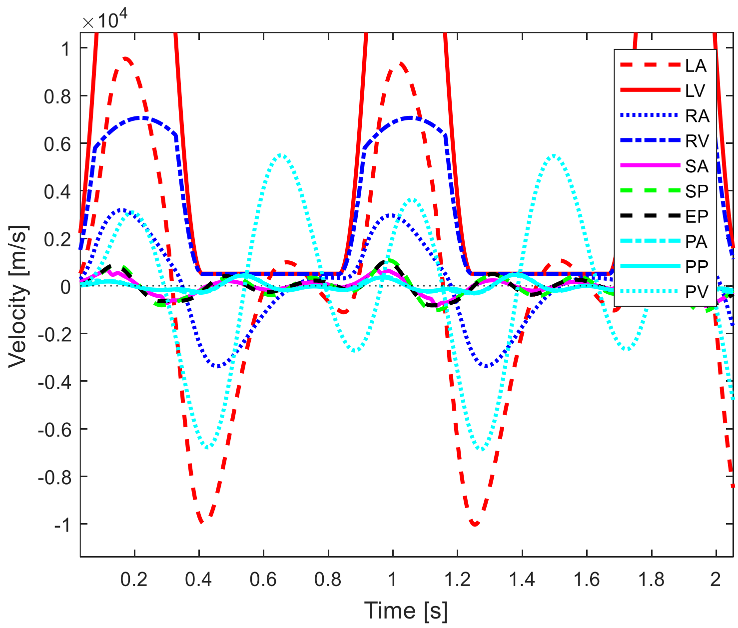

Figure 7.3.3.1 – Velocity (or pressure) waveforms for ventricles, atria, arteries, peripheral circulation and pulmonary veins.

For systemic venous circulation, waveforms are different from pulmonary circulation. For splanchnic and extra splanchnic venous circulation, the results from the model show their relationship with right atrium. The reason is that veins from SV and EV compartments return to right atrium, so their pressure will be similar in some way. Looking at splanchnic and extra splanchnic venous circulation in details (Figure 7.3.3.2 and Figure 7.3.3.3), some reasonable deductions can be done. First, pressure in both SV and EV compartment has the same shape over time because they both refers to veins from the body to the right atrium. However, there is a small delay and difference in amplitude between SV and EV waveforms for the first three cardiac cycles. In particular, EV pressure is higher in amplitude than SV pressure and EV peak slightly anticipates the SV one. The reason might be correlated to the position of the organs in human body. In fact, the SV veins come from digestive organs, which are closer to the heart than all the rest of human body. Then, after this transient of about one cardiac period, SV and EV curves become almost synchronous and with the same amplitude (Figure 7.3.3.3).

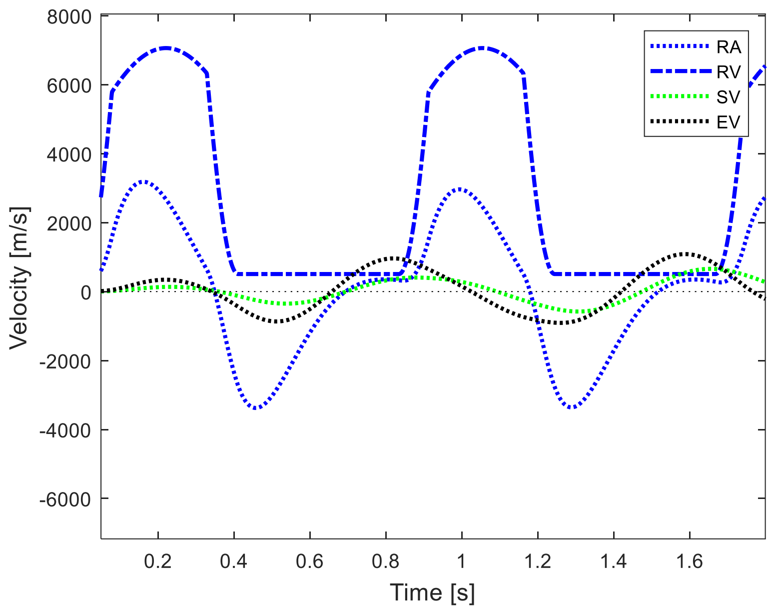

Figure 7.3.3.2 – Velocity (or pressure) waveforms for right atrium and ventricle, splanchnic and extra splanchnic veins, for two cardiac cycles, with an initial transient.

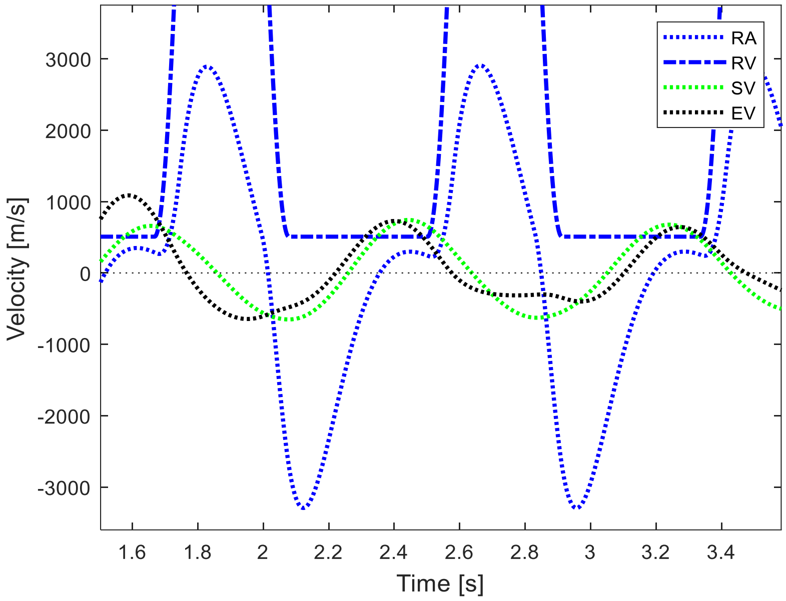

Figure 7.3.3.3 – Velocity (or pressure) waveforms for right atrium and ventricle, splanchnic and extra splanchnic veins, after the initial transient.

A type of venous circulation that is commonly measured is the central venous pressure CVP. It is the blood pressure measured in the vena cava, which is the vena to collect deoxygenated blood from the body to the right atrium. The following figure shows a typical detected CVP waveform [45].

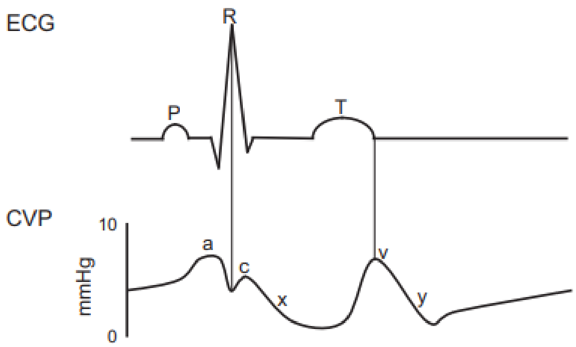

Figure 7.3.3.4 – ECG (top) and central venous pressure CVP measured at vena cava (bottom).

It can be noted that detected central venous pressure exactly corresponds to detected right atrium pressure, in shape and pressure range. This occurs because vena cava is very close and directly connected to right atrium.
Meanwhile, the SV and EV circulation of the proposed CVS model include the veins from all the human body. The pressure waveforms of SV and EV compartments have one positive peak per cardiac cycle. It occurs when a-wave of RA waveform occurs, just before the v-wave of RA curve. Physically, it means that pressure in the veins from human body reaches its maximum first and then RA begins its passive filling phase (v-wave or RA pressure curve).

7.3.4 Pressure as velocity in LUPOS model

It is possible to use LUPOS FEM code to visualise the time response of the system with imposed kinematics. In particular, pressure at each node can be visualised as displacements of the masses in LUPOS. Besides, the sign of the eigenvectors with positive axis direction opposite to absolute axis reference has been corrected. The following figure shows a screenshot from the pressure or velocity over time, for the original CVS model, where rigid body motion was allowed (Figure 7.3.4.1 on the left) and for the CVS model with more springs added, so that rigid body motion does not exist (Figure 7.3.4.1 on the right). Time animation of the entire system has been performed in LUPOS for about five heart periods and the screenshots in Figure 7.3.4.1 show their characteristic behaviour in the two cases indicated.

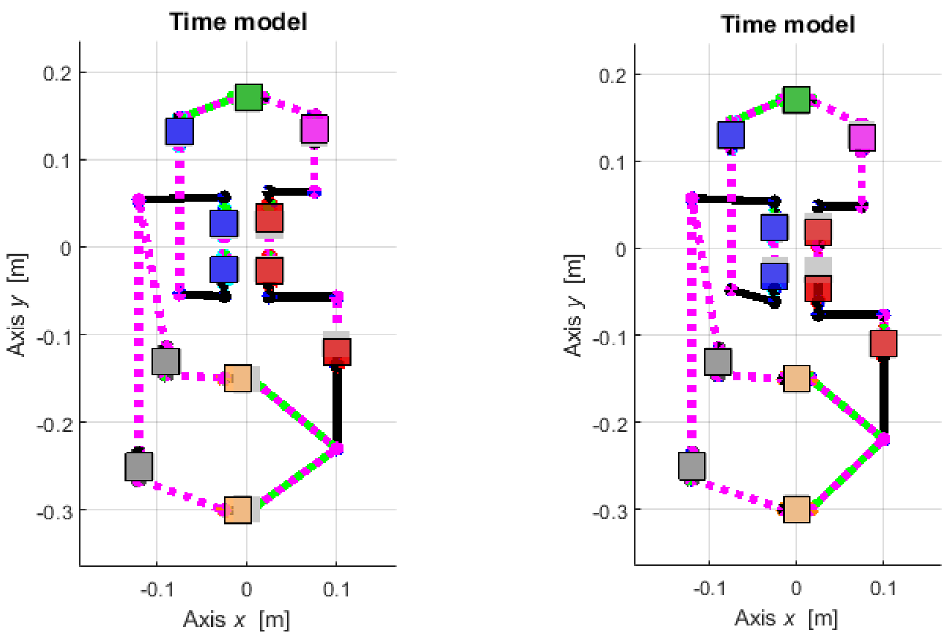

Figure 7.3.4.1 – Screenshots of pressure (or velocity) over time, for CVS model with rigid body motion (left) and for CVS model without rigid body motion (right).

It can be noted that when rigid body motion occurs, masses corresponding to SA, SP and EP have a significant velocity. In fact, that corresponds to a high amplitude of pressure waveform. On the contrary, when rigid body motion is not allowed, only heart chambers have a significant velocity. The other masses (like SA, SP, EP) have a very slow velocity, so that their displacement in LUPOS is quite negligible. That corresponds to a low amplitude of pressure waveform in the time response of the system.
Overall, LUPOS can be very useful to analyse displacement, velocity and acceleration of each mass of the system. In the same time, it allows to see how pressure integral, pressure itself and pressure derivative vary for each compartment, at a time. This way of time response representation of the entire model will be investigated more in the next steps.

7.4 Hemodynamic interpretation of the results: pressure derivative

Another important waveform to analyse is the acceleration response of the 12-DOFs system, which corresponds to derivative of pressure. Hemodynamically, the derivative of pressure of left ventricle is the most used. Many experimental studies have been performed to prove that LV derivative of pressure with respect to time provides information about myocardial contractility. Therefore, the derivative of pressure of left ventricle will be considered first. Figure 7.4.1. shows a recording of LV pressure and derivative calculation, obtained from experiments in a dog with tachycardia-induced cardiomyopathy [46].

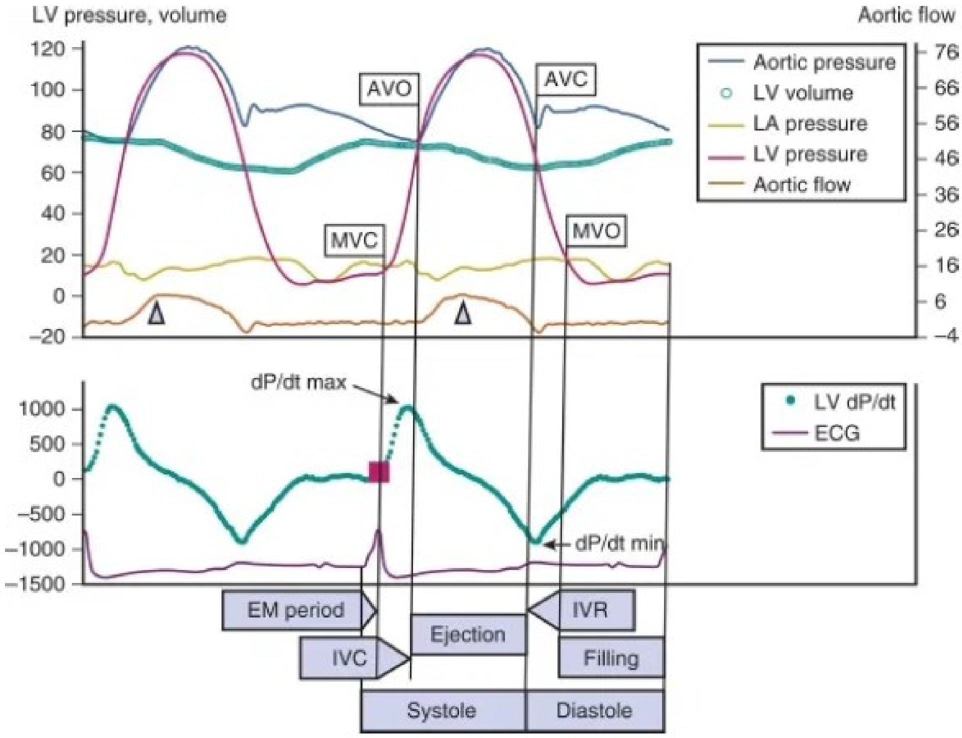

Figure 7.4.1 – LV pressure (top) and LV dp/dt (bottom) from experiments in a dog.

In general, LV pressure derivative can be used to define end-diastolic pressure of the pressure-volume loop of left ventricle. It is assumed to occur when the derivative of pressure over time reaches 10% of its maximum. It is indicated with a magenta point in Figure 7.4.1. An important aspect of dp/dt curve is that blood ejection from left ventricle starts when LV dp/dt curve reaches its positive peak (maximum), and it ends when the curve reaches its negative peak (minimum). As ejection ends, diastolic phase begins.

Using our CVS model, the derivative of LV pressure waveform has the same shape and amplitude as experimental results. It can be seen in Figure 7.4.2, together with the derivative of pressure for the other heart chambers. It can be noted that the right ventricle has the same shape of dp/dt over time but its amplitude is almost half the left ventricular one.

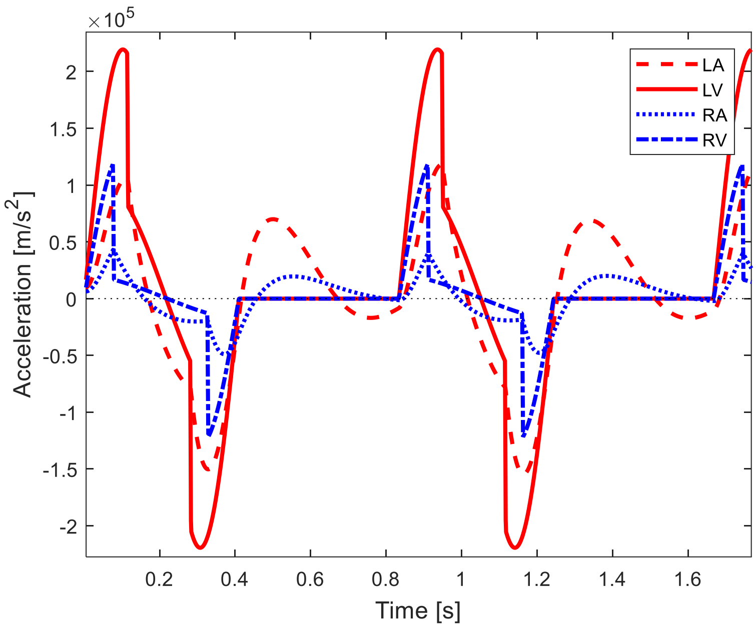

Figure 7.4.2 – Derivative of pressure for LA, LV, RA, RV, from time response of CVS model, without modes of rigid body motion.

The most significant point of the waveform is the maximum because it is usually correlated to ventricular contractility. Many recent studies demonstrate a correlation between the maximum peak of LV pressure derivative and the maximum of arterial pressure derivative. In particular, an experimental study performed in patients with advanced heart failure shows a linear regression [47]. The arterial pressure considered is the peripheral arterial pressure, which is usually femoral or radial, measured by a catheter. Defining with $(dp_{LV}/dt)_{\max}$ the maximum of LV pressure derivative and with $(dp_{art}/dt)_{\max}$ the maximum of arterial pressure derivative, the linear regression found is:

$$\left(\frac{dp_{LV}}{dt}\right)_{\max} = 1.25 \cdot \left(\frac{dp_{art}}{dt}\right)_{\max} \tag{7.4.1}$$

It has been proposed in order to estimate contractility using peripheral arterial pressure, which can be measured with techniques that are not totally invasive, since it is a peripheral pressure, not central. However, arterial pressure detected varies with different cardiac factors and conditions. In particular, variations of stroke volume and cardiac output have been performed in the experiments. The best monitoring of LV dp/dt using arterial measurements occurs in patients with lower cardiac output and lower stroke volume. For example, in the subgroup of patients with lower cardiac output, the linear regression is shown in the following figure.

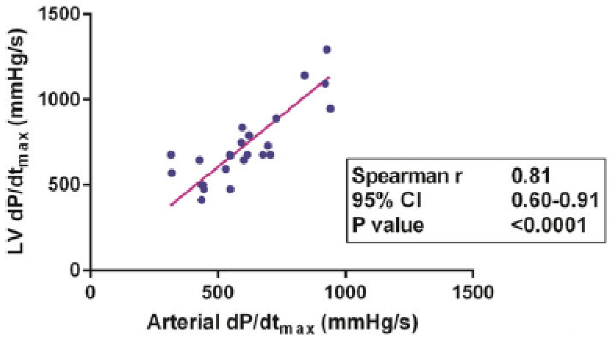

Figure 7.4.3 – Arterial and left ventricular $(dp/dt)_{max}$ in patients with lower cardiac output (CO < 6 l/min), from an experimental study.

The pressure derivative of LV and systemic arteries can be compared in the waveforms over time obtained from CVS model. In Figure 7.4.4, it can be noted that the maximum value of LV dp/dt results to be about three times the maximum value of SA pressure derivative. It does not respect the constant of proportionality seen in Eq. (7.4.1). The reason may be correlated to the fact that SA compartment does not represent the same peripheral pressure measured experimentally in the paper discussed above.

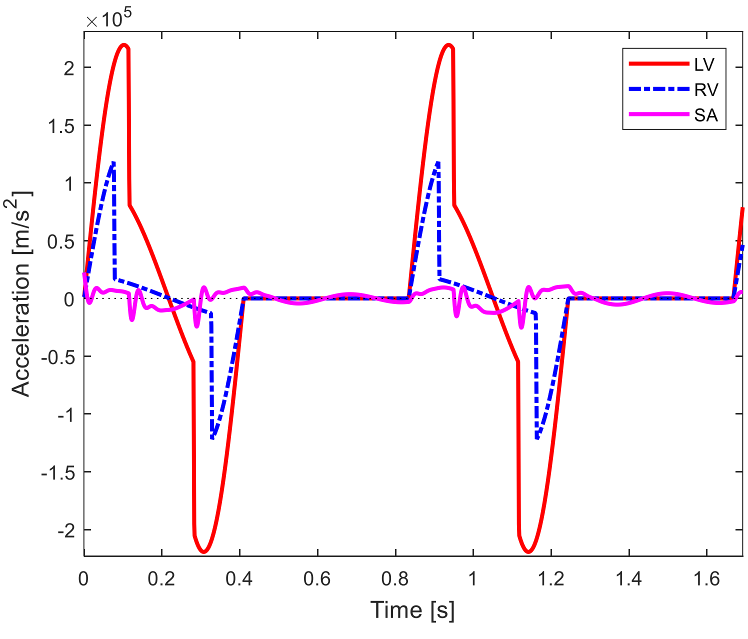

Figure 7.4.2 – Derivative of pressure for ventricles and systemic arteries compartment SA, from time response of CVS model, without modes of rigid body motion.

The waveforms obtained and reported in Figure 7.4.2 must be investigated more in order to improve the CVS model. The objective would be to obtain time response of the system in displacement, velocity and acceleration that is directly correlated to experimental hemodynamic results for pressure integration, pressure itself and pressure derivation over time.

7.5 Ventricular pressure with time-varying heart rate

The ventricular pressure functions were generated considering only a heart period of 0.833 s that means a single heart rate of 1.2 Hz or 72 beats/min (or bpm); also, the time responses analysed above derived from the repetition of the same heart rate over time. In order to generate time responses that are more representative of real heartbeats, a time-varying heart rate is assumed. For example, beat rate is assumed varying from 60 bpm to 120 bpm with intermediate steps of 1 bpm. A sampling frequency of 2000 Hz for the entire pressure waveform is chosen. The pressure function is built with this time-varying heart rate, then the corresponding integral and derivative are calculated. Figure 7.5.1 shows the results for left ventricular function and Figure 7.5.2 for right ventricular function. At first glance, it can be noted that right ventricular pressure is almost three times smaller than left ventricular one. Consequently, integral and derivative waveforms reflect the same relationship.

For the range of beat rate variation considered, time history lasts about 42 s. The pressure waveform over time show that when beat rate increases, heart period decreases, so the LV systolic pressure curve narrows. Consequently, when beat rate increases, the peaks of pressure derivative curve become closer and their amplitude increases. It is due to the narrowing of the pseudo-sinusoidal pressure curve. However, the waveform corresponding to the integral of pressure continues to decrease as beat rate increases because the area under the pressure segment for each cardiac cycle gradually narrows. These trends are encountered in both left and right ventricular waveforms over time, which correspond to velocity, acceleration and displacement respectively.

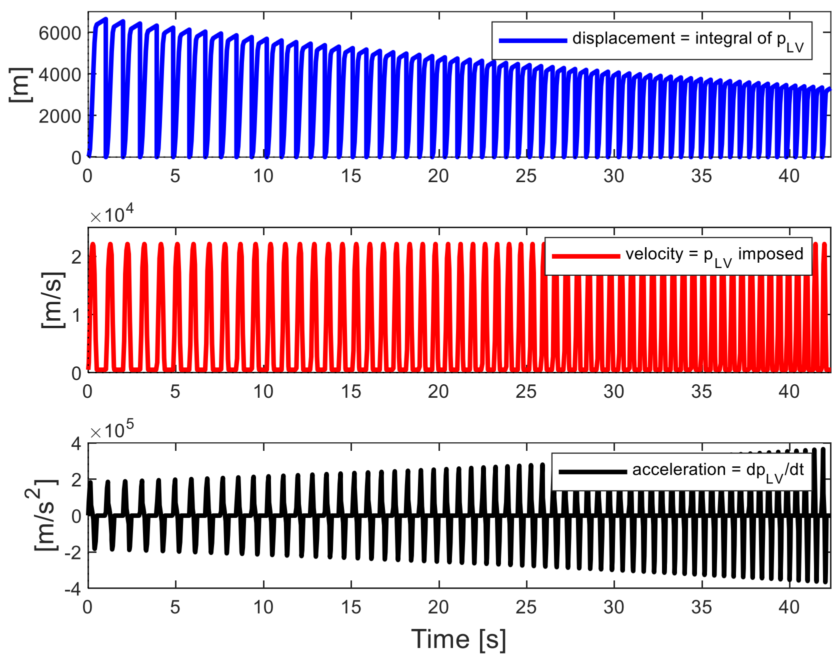

Figure 7.5.1 – Imposed kinematics on left ventricle when heart rate varies from 60 bpm to 120 bpm, with intermediate steps of 1 bpm and a sampling frequency of 2000Hz: displacement (top), velocity (centre), acceleration (bottom).

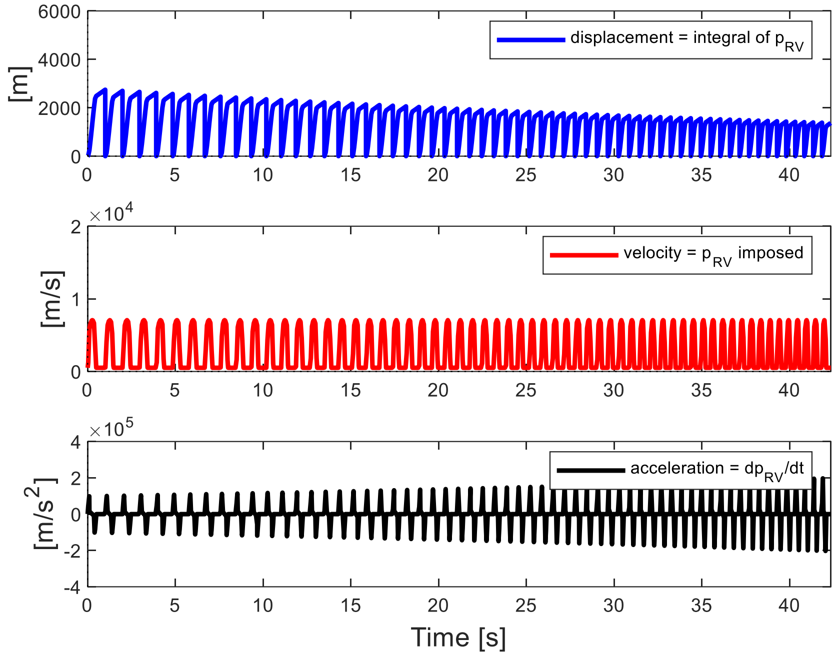

Figure 1.5.2 – Imposed kinematics on right ventricle when heart rate varies from 60 bpm to 120 bpm, with intermediate steps of 1 bpm and a sampling frequency of 2000Hz: displacement (top), velocity (centre), acceleration (bottom).

In the following figures, the same ventricular functions are reported with a zoom on heart rate from 75 bpm to 80 bpm, with intermediate steps of 1 bpm. According to the definition of ventricular function for this CVS model, each cardiac cycle starts with systole, which corresponds to the pseudo-sinusoidal curve.

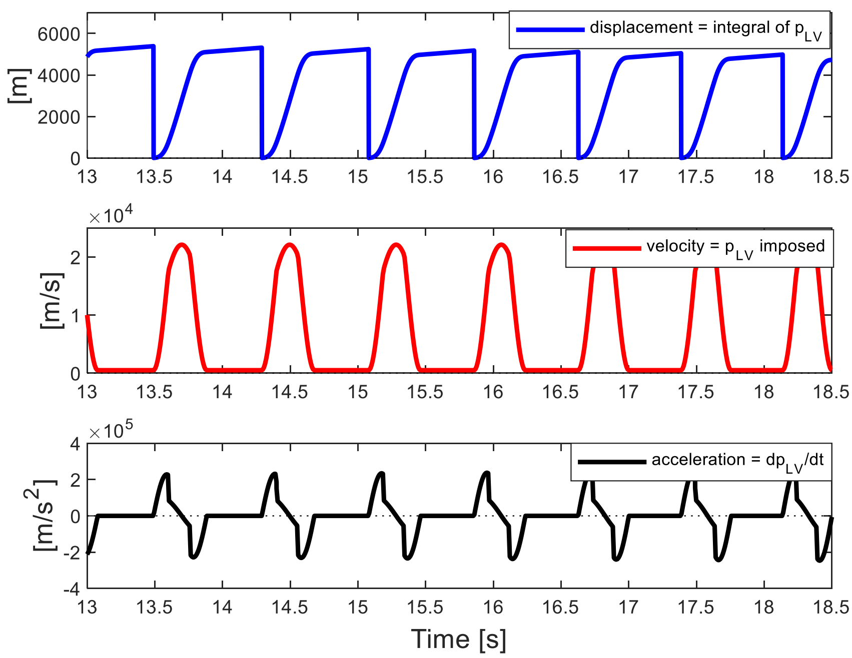

Figure 7.5.3 – Detail of imposed kinematics on left ventricle when heart rate from 75 bpm to 80 bpm, with intermediate steps of 1 bpm and a sampling frequency of 2000Hz.

The same detail of ventricular functions is given for right ventricle.

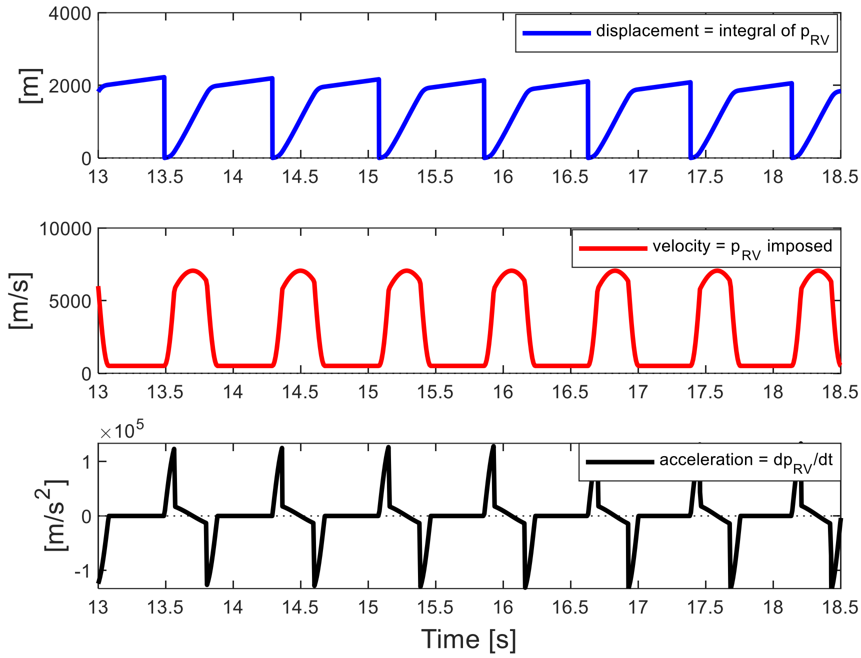

Figure 7.5.4 – Detail of imposed kinematics on right ventricle when heart rate varies from 75 bpm to 80 bpm, with intermediate steps of 1 bpm and a sampling frequency of 2000Hz.

It is possible to see the pressure function in frequency domain with FFT. Then, a band-pass filter can be applied to find out which frequency bandwidth mainly characterise the ventricular pressure defined using time-varying heart rate. Figure 7.5.5 shows FFT modulus and phase for left ventricular pressure with beat rate from 60 bpm to 120 bpm. A band-pass filter to pass frequencies form 0 to 20 Hz is applied.

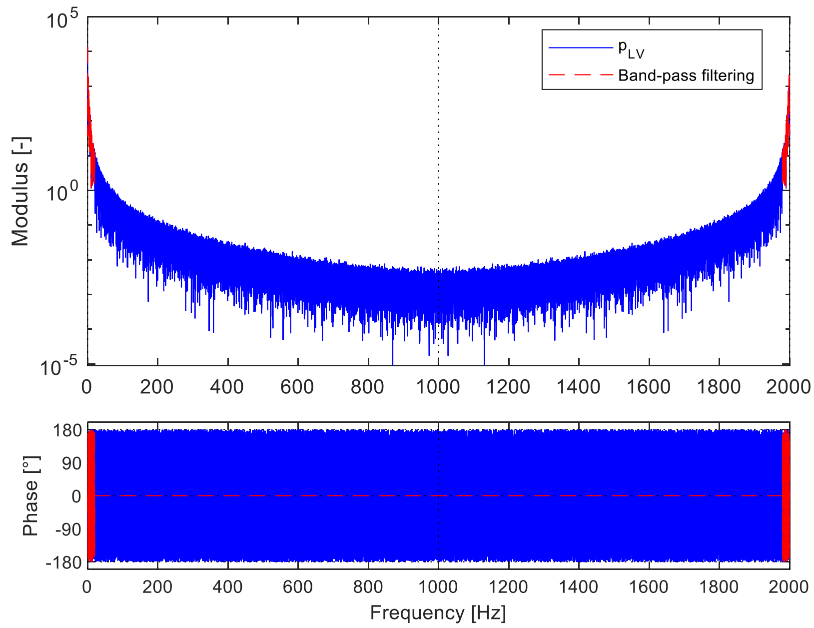

Figure 7.5.5 – FFT modulus and phase of left ventricular pressure with HR varying gradually from 60 bpm to 120 bpm, with a band-pass filter form 0 to 20 Hz.

Thus, IFFT is applied to the signal filtered and it is compared with the original signal in time domain. For left ventricular pressure, the frequency bandwidth from 0 to 20 Hz results to be representative of the entire pressure signal defined.

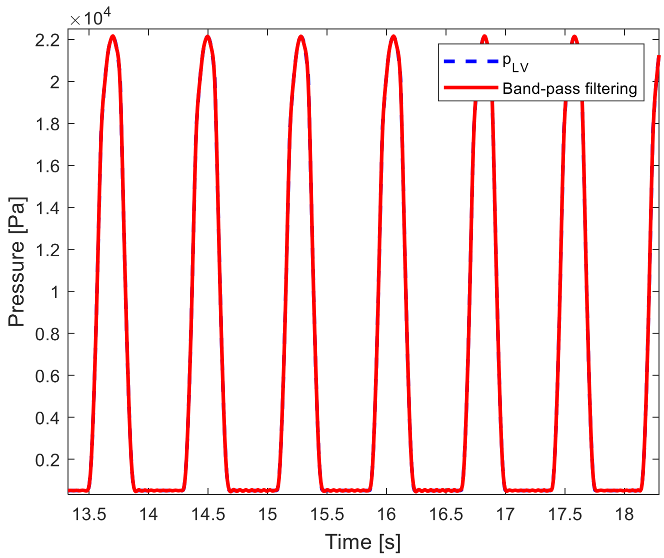

Figure 7.5.6 – Left ventricular pressure over time (blue dashed line) and IFFT of signal filtered from 0 to 20 Hz (red solid line), when heart rate varies from 75 bpm to 80 bpm.

Looking at some details of the IFFT graph, it can be noted that the filtered signal almost coincides with the original signal.

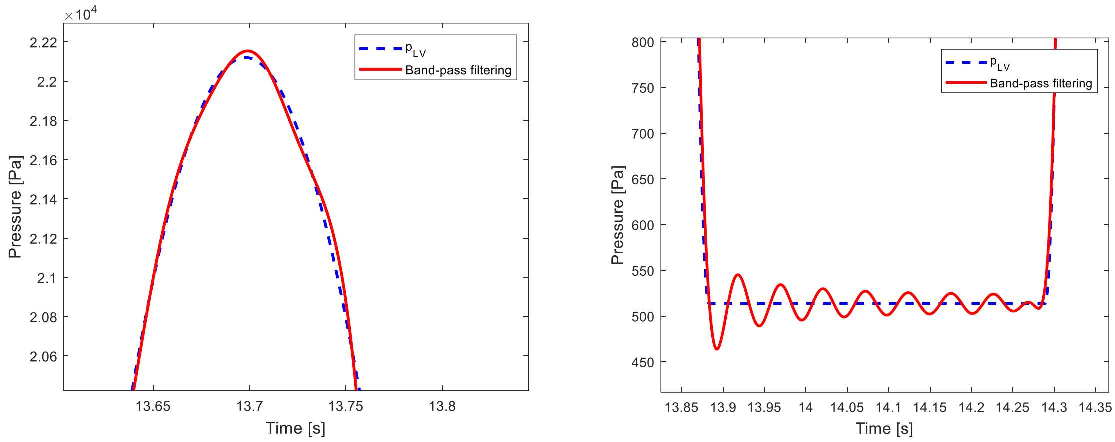

Figure 7.5.7 – Detail of left ventricular pressure over time (blue dashed line) and IFFT of signal filtered from 0 to 20 Hz (red solid line).

For right ventricular pressure, the FFT and the same band-pass filter are applied. As well as left ventricular pressure, the frequency bandwidth from 0 to 20 Hz results to represent properly the right ventricular pressure with HR varying from 60 bpm to 120 bpm. In fact, comparing original signal and IFFT after filtering, the curves almost coincides.

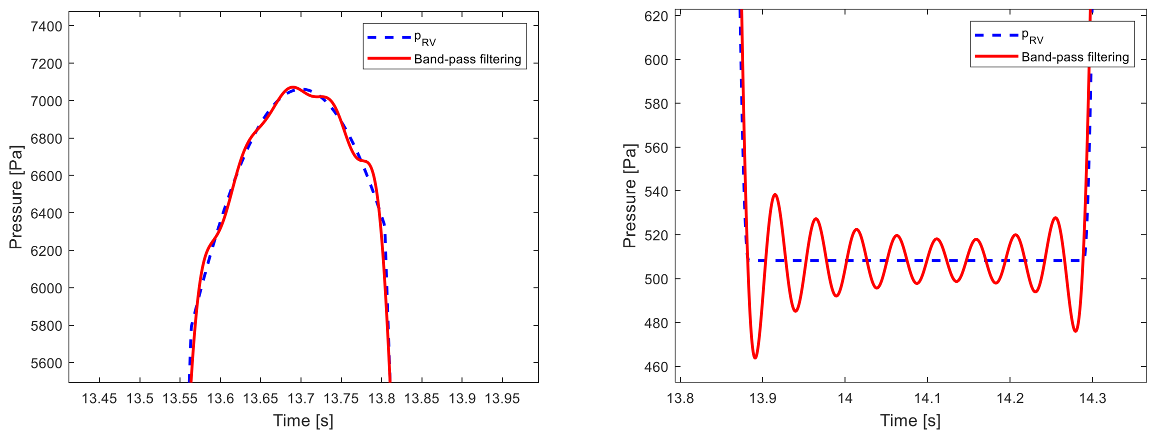

Figure 7.5.8 – Detail of right ventricular pressure over time (blue dashed line) and IFFT of signal filtered from 0 to 20 Hz (red solid line).

The results obtained with FFT and IFFT can be visualised in time-frequency domain. Continuous Wavelet Transforms can be applied to left and right ventricular pressure signals defined. The spectrograms obtained demonstrate that the dominant frequency range for each ventricular pressure is lower than 20 Hz (Figure 7.5.9 and Figure 7.5.10). In the following spectrograms, the time interval does not include 2 s at the beginning and 2 s at the end of the entire history. In this way, the transient behaviour of the CWT is neglected.
It can be noted that frequency increases linearly over time for both ventricles. Obviously, it depends on the assumption of the beat rate rising 1 bpm per time.

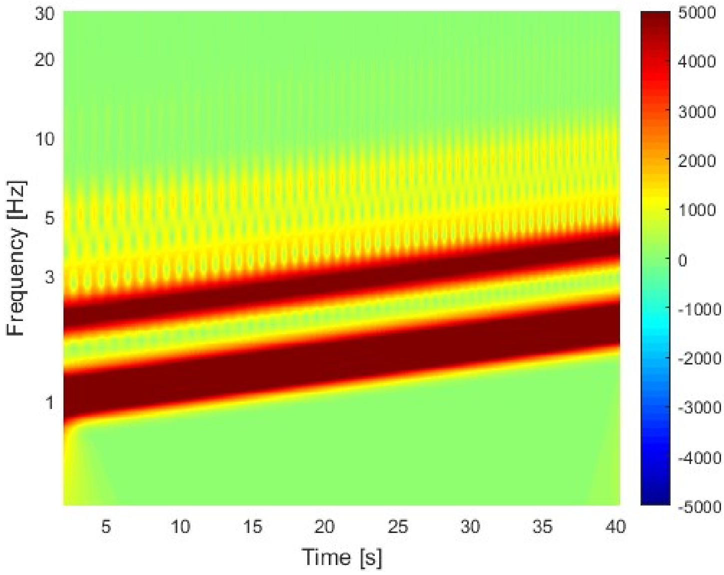

Figure 7.5.9 – CWT graph of left ventricular pressure with HR from 60 bpm to 120 bpm and sampling frequency of 2000 Hz.

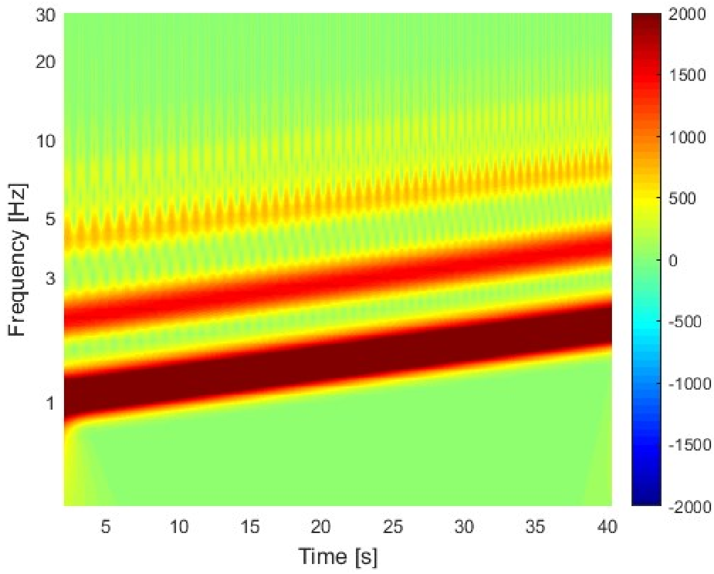

Figure 7.5.10 – CWT graph of right ventricular pressure with HR from 60 bpm to 120 bpm and sampling frequency of 2000 Hz.

In the pressure spectrograms for both ventricles, the main frequency starts from 1 Hz up to around 2 Hz. It depends on the imposed beat rate. Then, other significant super harmonics occur with the same linear ascending trend. In particular, the last harmonic starts from 5 Hz up to around 10 Hz. Moreover, the frequency intensity for left ventricle is higher than right ventricle. Clearly, it is due to the higher pressure values of left ventricle with respect to right ventricle.

7.6 Time response of CVS model with time-varying HR

Applying the time-varying heart rate defined above, the time responses of the CVS model slightly change and they look more similar to the real hemodynamic behaviour of circulatory system. The CVS model used for this time-simulation is the MCK model without rigid body motions. The displacement of each DOF is similar to the previous one (Figure 7.2.4). The difference is that in this case, heart period gradually reduces, while in the previous time response it was constant. Moreover, when HR increases, the amplitude of the displacements decreases. As seen before, it is due to the narrowing of pressure waveform.

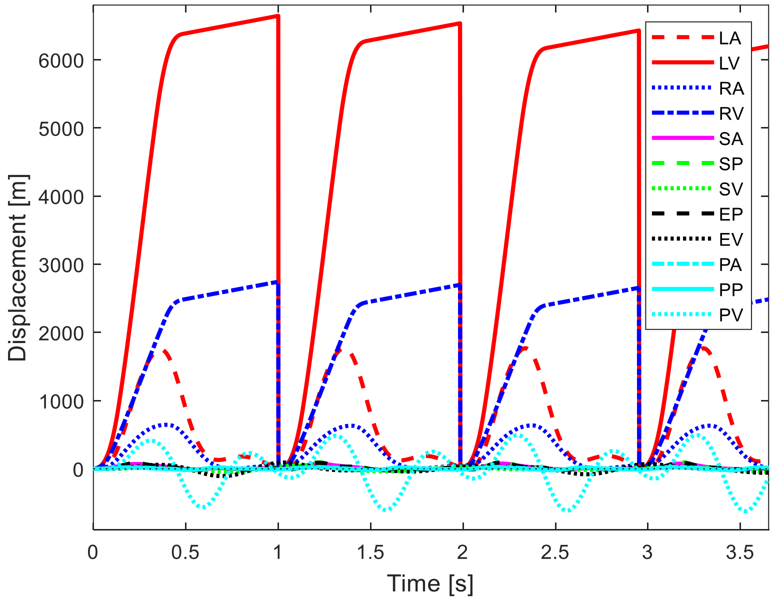

Figure 7.6.1 – Displacement or integral of pressure for all 12 DOFs, with heart rate varying from 60 bpm to 62 bpm.

The pressure waveforms obtained with time-varying HR have the same trends as the previous case with constant HR. The difference is that heart period gradually decreases, so the pressure pseudo-sinusoidal curves narrow beat by beat.

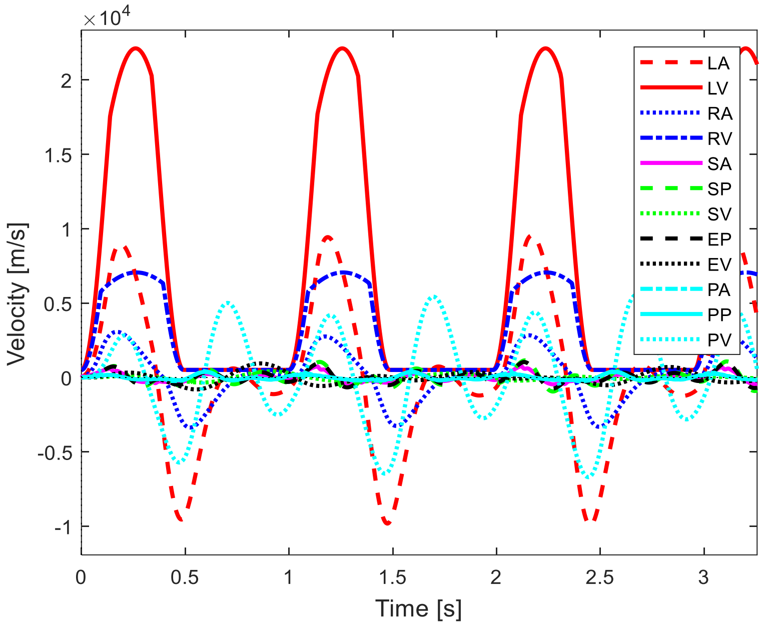

Figure 7.6.2 – Velocity or pressure for all 12 DOFs, with heart rate varying from 60 bpm to 62 bpm.

The derivative of pressure or acceleration waveforms result to have the two opposite peaks closer to each other, when heart rate increases. In addition, the amplitude of the waveforms gradually increases, in fact peaks values rises over time.

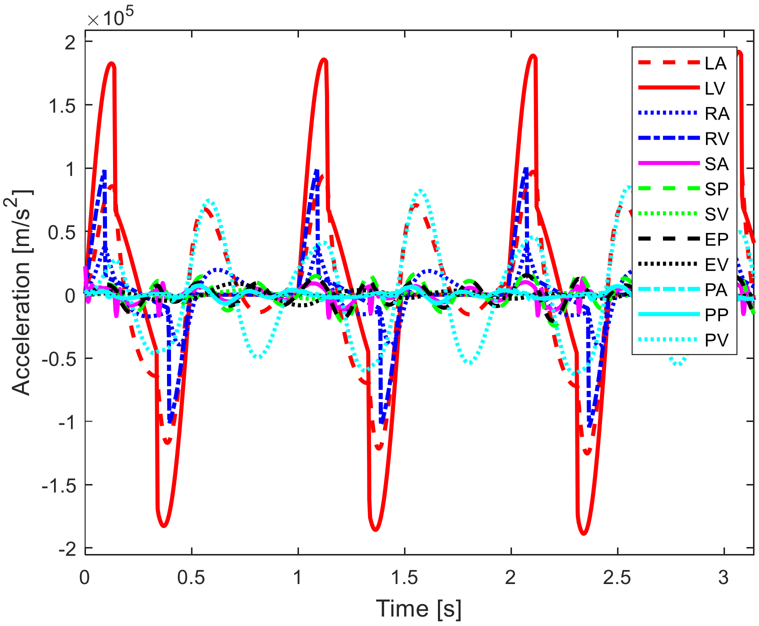

Figure 7.6.3 – Acceleration or pressure derivative for all 12 DOFs, with heart rate varying from 60 bpm to 62 bpm.

Overall, the pressure waveforms obtained with beat rate progression have the same trends and shapes of the case reported in paragraph 7.3 with only one heart period. As seen in the graphs of ventricular functions and time responses of all DOFs, the duration of pressure curves and the

amplitude of pressure derivative curves change progressively. However, the comparisons between velocity, acceleration and real recordings made for constant HR remain valid for time-varying HR.
It is possible to visualise the internal dynamics of the CVS model in time-frequency domain. In particular, CWT graphs are obtained for each DOF of the system. Initially, pressure curves over time are investigated for each compartment, which correspond to the velocity of each DOF. The CWT graphs in Figure 7.5.9 and Figure 7.5.10 represent the pressure (or velocity) of the two ventricles, which descend from the imposed kinematics on LV and RV masses. Then, time response of the two atria is obtained from the simulation. For left atrium, pressure or velocity shows a high frequency content in the fundamental, which starts from 1 Hz and then increases linearly with HR. In particular, the frequency contribution is higher for heart rates after 80 bpm. Moreover, there is a significant contribution of the second harmonic that starts from 2 Hz.

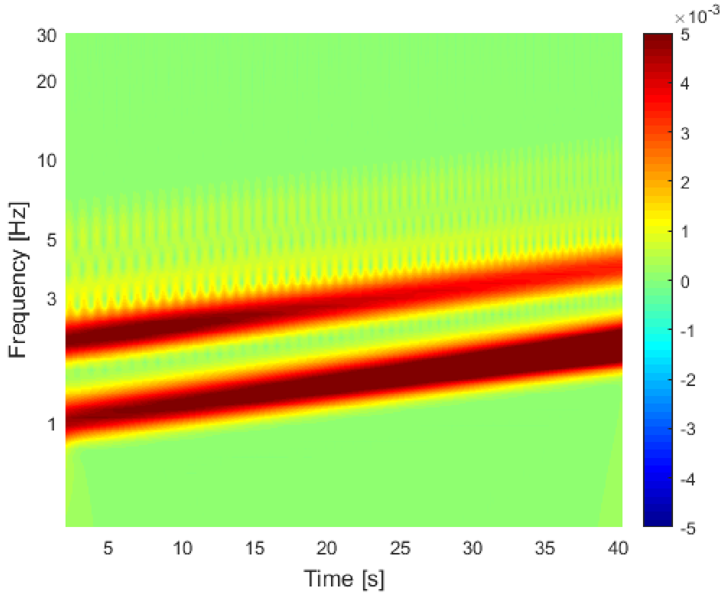

Figure 7.6.4 – CWT graph of LA compartment pressure (or velocity) when HR varies from 60 bpm to 120 bpm with a sampling frequency of 2000 Hz.

For right atrium pressure or velocity, time-frequency graph shows that there is a high frequency content in the fundamental that starts from 1 Hz and it remains significant for all beat rates. Meanwhile, the frequency content of the other harmonic from 2 Hz to 4 Hz is slightly lower than left atrium case.

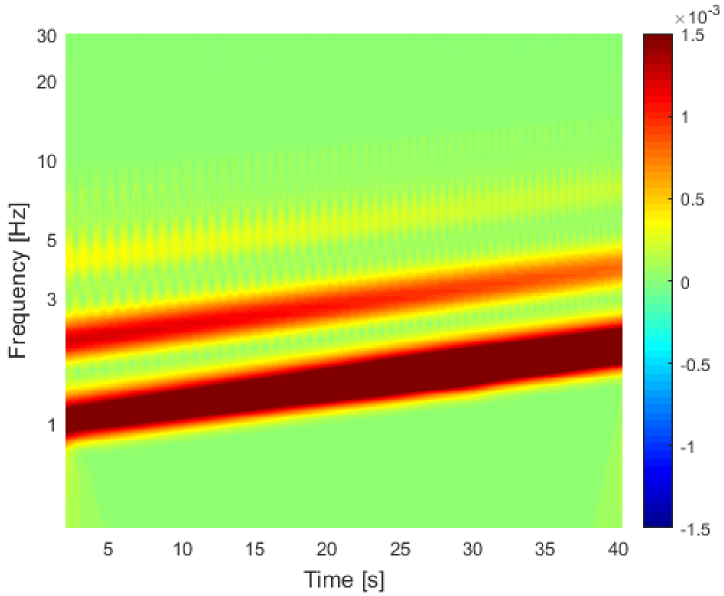

Figure 7.6.5 – CWT graph of RA compartment pressure (or velocity) when HR varies from 60 bpm to 120 bpm with a sampling frequency of 2000 Hz.

Figure 7.6.6 represents the time-frequency graph for pressure (or velocity) of systemic arteries compartment (SA). It shows that the fundamental frequency starting from 1 Hz characterises SA dynamics at every beat rate. The first super harmonic becomes very significant for heart rates higher than 80 bpm, which correspond to the time instant around 20 s. For beat rates between 75 bpm and 80 bpm, which is almost between 13 s and 20 s, another super harmonic occurs between 3 Hz and 5 Hz.

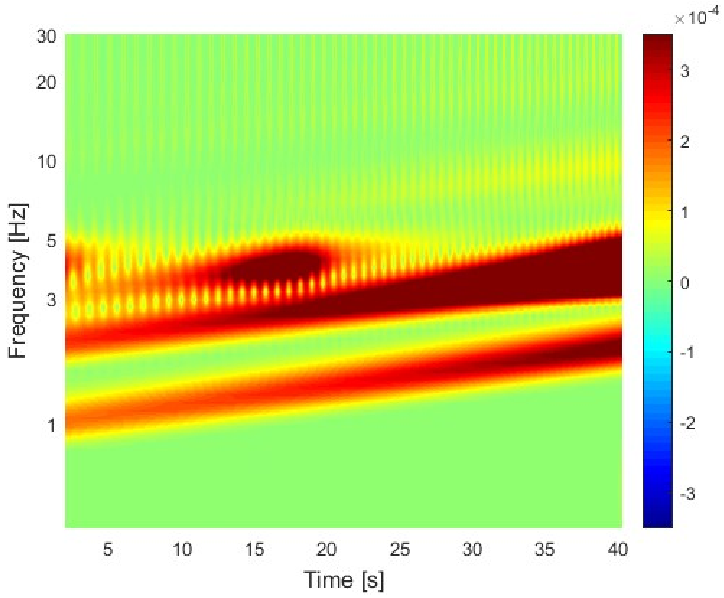

Figure 7.6.6 – CWT graph of SA compartment pressure (or velocity) when HR varies from 60 bpm to 120 bpm with a sampling frequency of 2000 Hz.

The systemic arteries compartment is followed by the splanchnic peripheral circulation compartment (SP) and the extra-splanchnic peripheral circulation compartment (EP). In the CVS model, the same spring and damper connect SP and EP masses to SA mass. Therefore, their behaviour in time-frequency domain results to be the same, in fact the CWT graphs in Figure 7.6.6 and Figure 7.6.7 are almost the same.

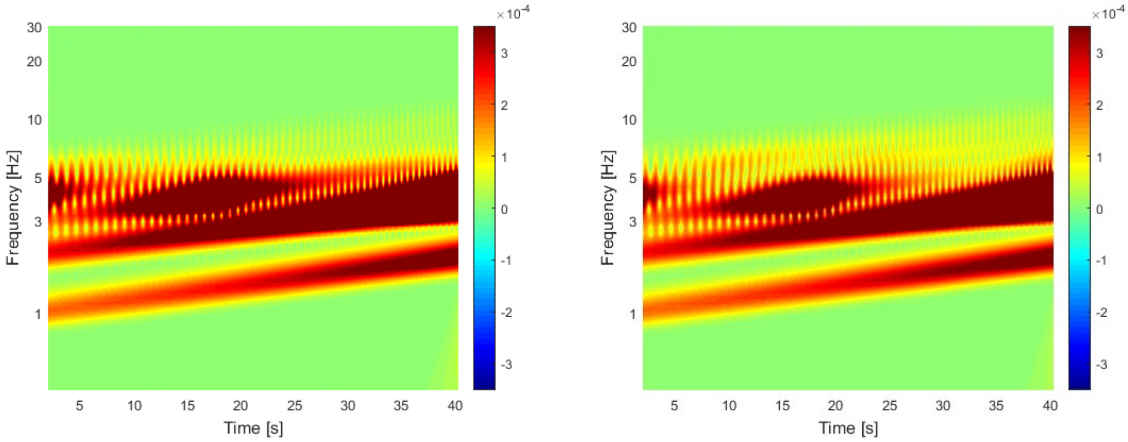

Figure 7.6.7 – CWT graph of pressure (or velocity) of SP (left) and EP (right) compartments when HR varies from 60 bpm to 120 bpm with a sampling frequency of 2000 Hz.

Both SP and EP compartments are connected to venous compartments, which are called SV and EV respectively. The splanchnic venous circulation compartment (SV) pressure or velocity shows a high contribution of the fundamental frequency. It starts from 1 Hz at 60 bpm, then its frequency content increases significantly between 70 bpm and 90 bpm. There is another contribution of the first super harmonics starting from 2 Hz up to 5 Hz, but it is quite lower than the main harmonic.
For the extra-splanchnic venous circulation (EV) compartment, pressure or velocity shows a high contribution of the fundamental frequency for almost all the beat rates. Moreover, a slight contributon of the first super harmonic occurs. In both SV and EV velocity time-frequency graphs, it can be noted that the main frequency includes a bandwidth between 1 Hz and 2 Hz.

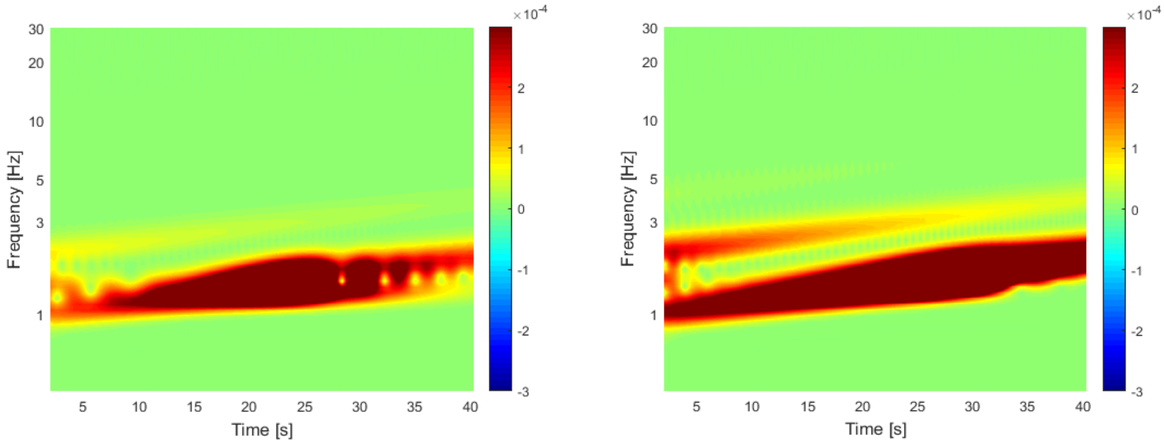

Figure 7.6.8 – CWT graph of pressure (or velocity) of SV (left) and EV (right) compartments when HR varies from 60 bpm to 120 bpm with a sampling frequency of 2000 Hz.

Looking at the pulmonary circulation, the first compartment encountered according to blood flow direction is the pulmonary arteries compartment (PA). Pressure or velocity of PA element is characterised by the main frequency starting from 2 Hz at 60 bpm up to 5 Hz at 120 bpm. The

contribution of the harmonic starting from 1 Hz is lower than the other compartments. However, it increases its content around 2 Hz for beat rates about 100 bpm. Moreover, some super harmonics around 5 Hz occurs between 60 bpm and 70 bpm, as well as between 80 bpm and 90 bpm.
The pressure or velocity of the peripheral pulmonary circualtion compartment (PP) shows the same dynamics as PP compartment. In fact, the frequencies over time are the same.

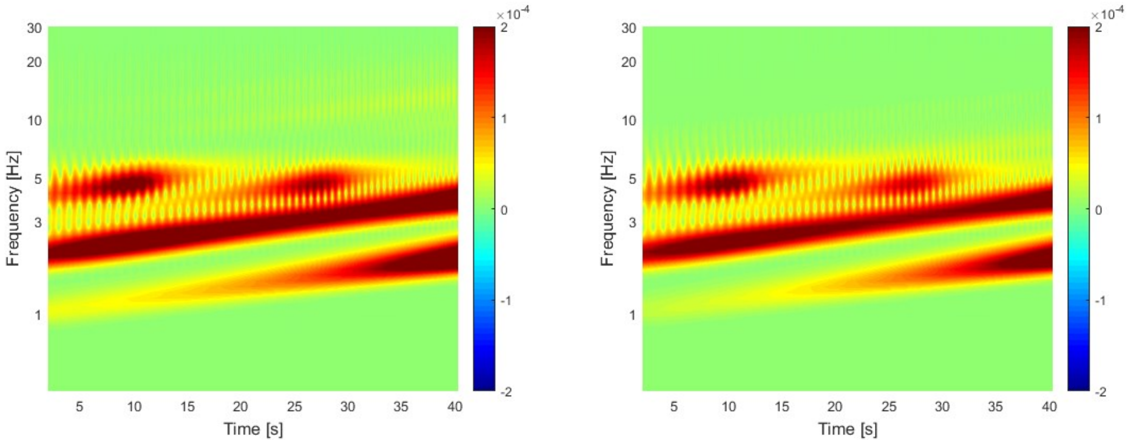

Figure 7.6.9 – CWT graph of pressure (or velocity) of PA (left) and PP (right) compartments when HR varies from 60 bpm to 120 bpm with a sampling frequency of 2000 Hz.

For the venous pulmonary circulation compartment (PV), pressure or velocity in time-frequency domain has two main harmonics: one starts from 1 Hz and the other one from 2 Hz at 60 bpm. It can be noted that lower beat rates have higher frequency content between 2 Hz and 3 Hz. Meanwhile, beat rates higher than 80 bpm show higher contribution of frequencies between 1 Hz and 2 Hz.

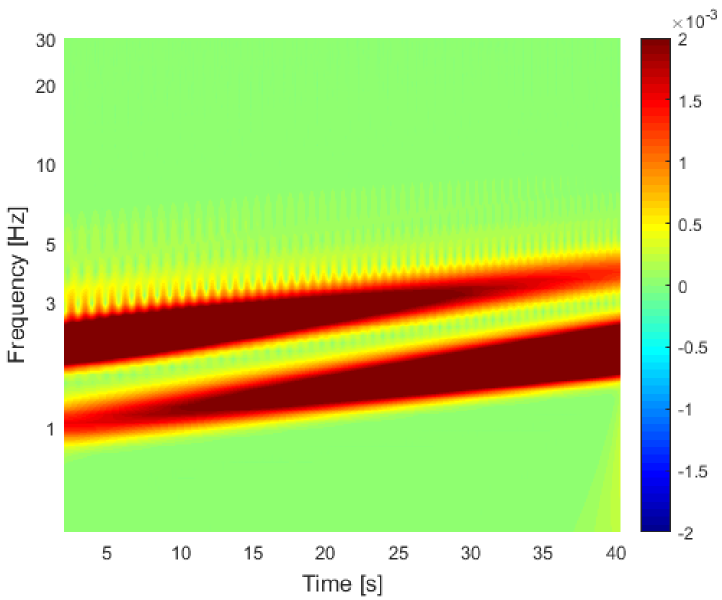

Figure 7.6.10 – CWT graph of pressure (or velocity) of PV compartment when HR varies from 60 bpm to 120 bpm with a sampling frequency of 2000 Hz.

It is interesting to analyse in time-frequency domain also the derivative of pressure or acceleration for each DOF of the system. There are many similarities in the CWT spectrograms and some differences can be identified.
Looking at the CWT graphs of acceleration of left and right ventricles DOFs, it can be noted that the contribution of higher frequencies is visible. In velocity (or pressure) spectrograms (Figure 7.5.9 and Figure 7.5.10), the frequency content is lower than 10 Hz. Instead, in acceleration (or pressure derivative) spectrograms, super harmonics between 10 Hz and 30 Hz are visualised.

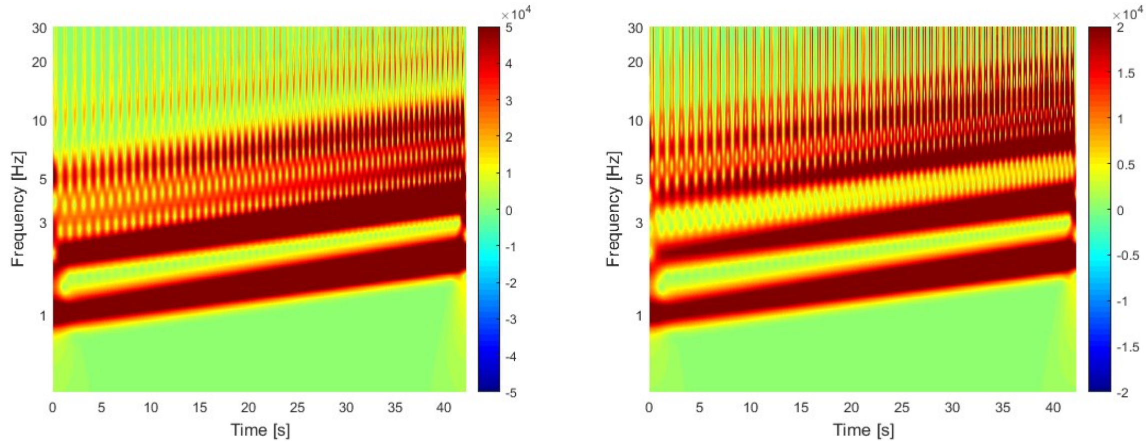

Figure 7.6.11 – CWT graph of LV (left) and RV (right) compartments pressure derivative (or acceleration) when HR varies from 60 bpm to 120 bpm with a sampling frequency of 2000 Hz.

For left atrium acceleration, the main frequencies are the fundamental from 1 Hz to 2 Hz (at 120 bpm), and the super harmonic from 2 Hz to 3 Hz. Then, there are other important contributions from super harmonics from 3 Hz to 4 Hz, and from 5 Hz to 6 Hz. In the right atrium acceleration spectrograms, the fundamental and the first super harmonics appear, too. Then, an important super harmonic starts from 4 Hz (at 60 pm) and another one starts from 9 Hz up to 10 Hz at 120 bpm.

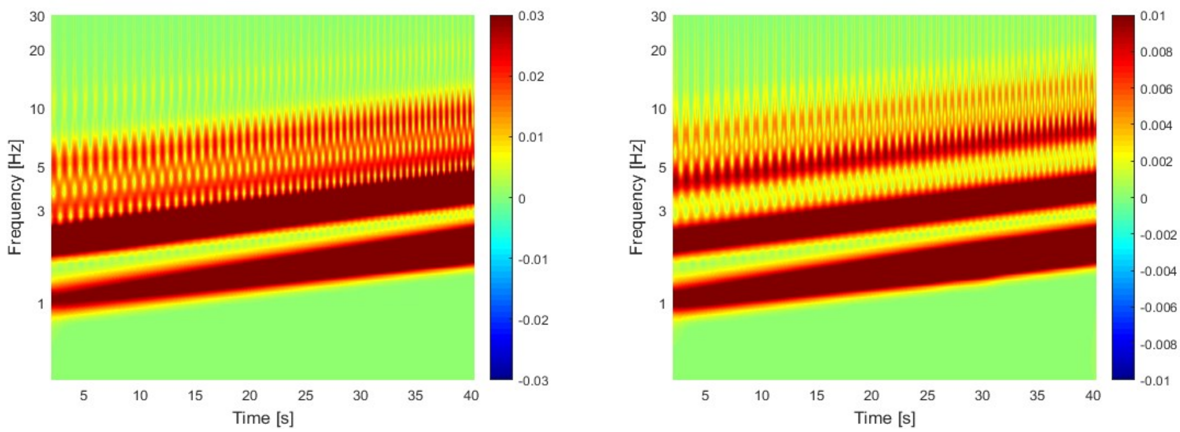

Figure 7.6.12 – CWT graph of LA (left) and RA (right) compartments pressure derivative (or acceleration) when HR varies from 60 bpm to 120 bpm with a sampling frequency of 2000 Hz.

The acceleration of SA mass in time-frequency domain shows the same frequencies as SA velocity (Figure 7.6.6). The main difference is that the spectrogram of SA acceleration (or derivative of pressure) shows a significant frequency contribution around 10 Hz for beat rates after 80 bpm, as well as between 10 Hz and 30 Hz.

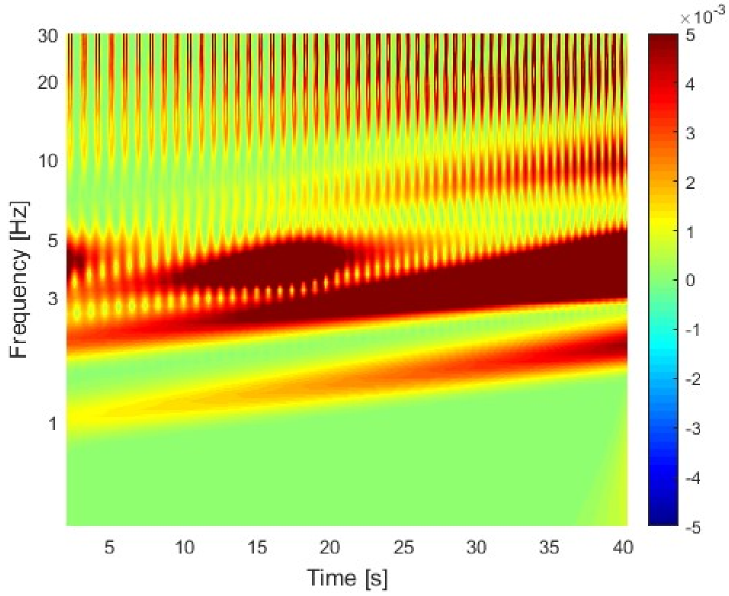

Figure 7.6.13 – CWT graph of SA compartment pressure derivative (or acceleration) when HR varies from 60 bpm to 120 bpm with a sampling frequency of 2000 Hz.

For the compartments connected to SA node, which are called SP and EP, acceleration has a CWT graph similar to SA acceleration CWT graph (Figure 7.6.13). The main difference is that in the splanchnic and extra-splanchnic peripheral compartments all the vibrational frequencies are lower than 10 Hz for every heartbeat.

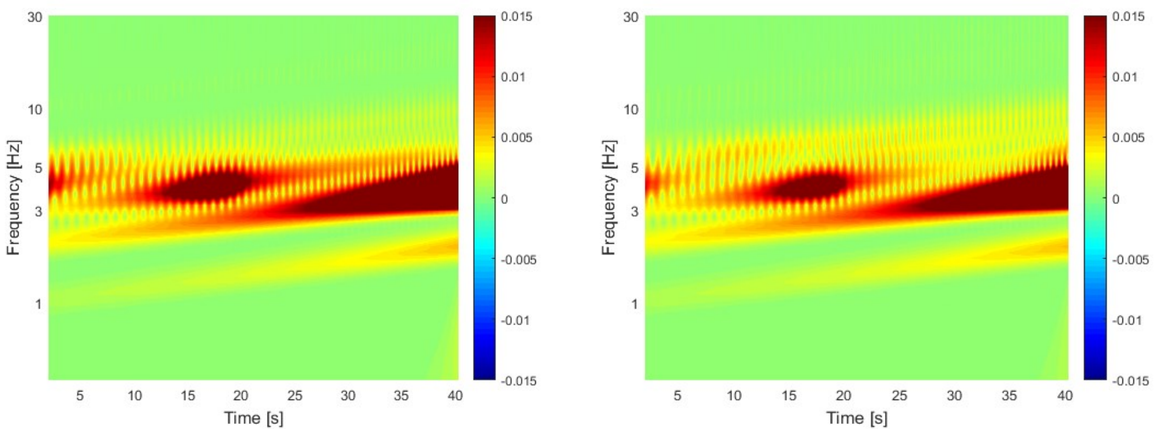

Figure 7.6.14 – CWT graph of SP (left) and EP (right) compartments pressure derivative (or acceleration) when HR varies from 60 bpm to 120 bpm with a sampling frequency of 2000 Hz.

CWT graphs of the acceleration of venous compartments SV and EV are almost the same as the graphs for velocity of the same compartments (Figure 7.6.8).

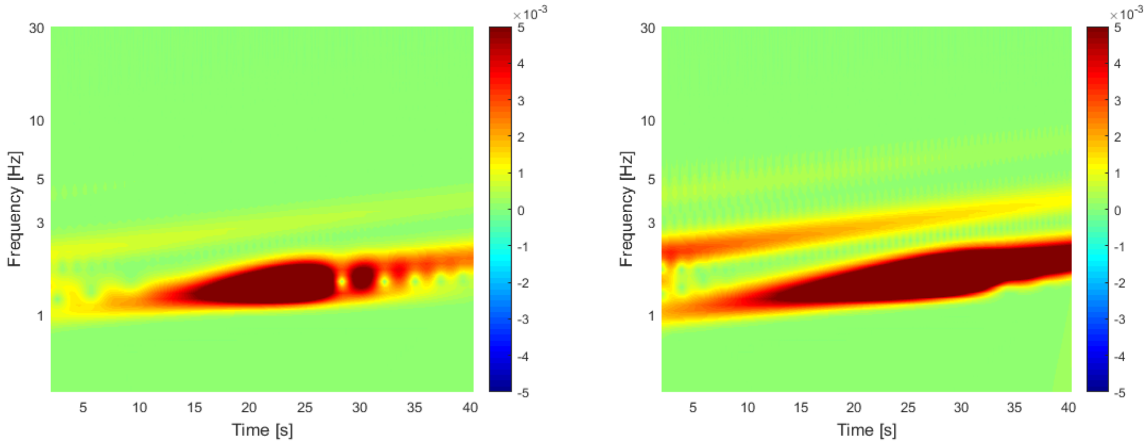

Figure 7.6.15 – CWT graph of SV (left) and EV (right) compartments pressure derivative (or acceleration) when HR varies from 60 bpm to 120 bpm with a sampling frequency of 2000 Hz.

For pulmonary circulation, the acceleration of PA and PP masses has a significant frequency content from2 Hz at 60 bpm to 3 Hz at 120 bpm. Moreover, there is a high contribution around 5 Hz for 65-70 bpm and 85-90 bpm. For PA compartment, there is another contribution between 10 Hz and 20 Hz for beat rates after 85 bpm.

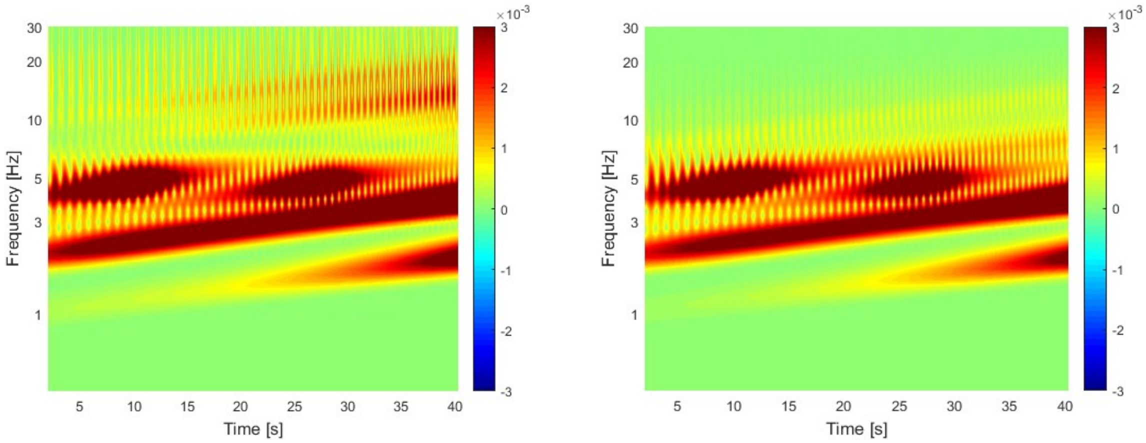

Figure 7.6.16 – CWT graph of PA (left) and PP (right) compartments pressure derivative (or acceleration) when HR varies from 60 bpm to 120 bpm with a sampling frequency of 2000 Hz.

The frequencies of PV dynamics are the same for velocity and acceleration. In fact, the main frequencies identified in the spectrogram for PV velocity or pressure are the same for PV acceleration or derivative of pressure. Overall, frequencies for PV compartment are lower than 10 Hz.

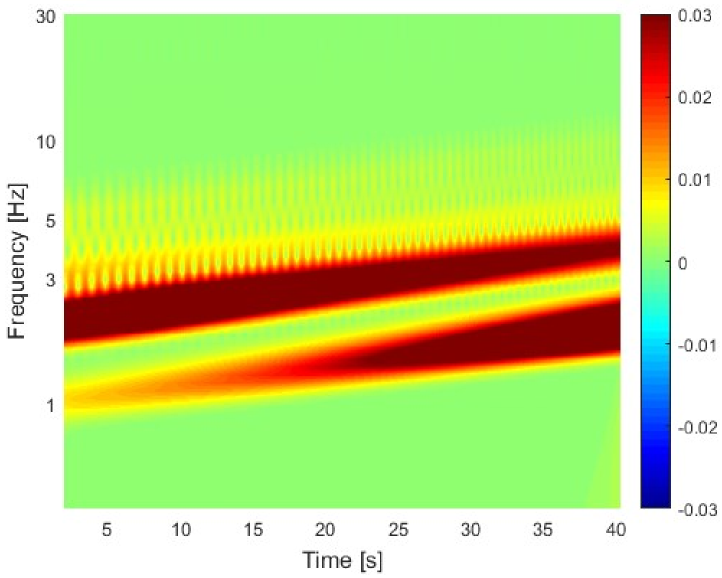

Figure 7.6.17 – CWT graph of PV compartment pressure derivative (or acceleration) when HR varies from 60 bpm to 120 bpm with a sampling frequency of 2000 Hz.

Therefore, the HR range selected for the model simulation provides results that can be directly correlated to different real beat rates.

7.7 Comparison between model responses and experimental measurements

The signals recorded during NiPAMS experiments have been analysed in time-frequency domain, as discussed in chapter 3. Simultaneously, the internal dynamics of each compartment of CVS model can be visualised in time-frequency domain, too. Consequently, it is interesting to compare the spectrograms of experimental data with spectrograms of some related DOFs of the model. It is useful to check the robustness of the model created, which is a significant goal.

The experimental data detected are basically two types: VCG and NIBP. The heart rate of every test has been detected, too. It slightly varies over time but it can be considered mostly between 70 bpm and 85 bpm.

The NIBP signal is blood pressure recorded by a finger cuff. The CWT graph for a generic subject, like subject 225, at rest is reported in Figure 3.2.3.5 for a reduced time window. The finger can be represented by the extra-splanchnic peripheral circulation compartment of the CVS model. Thus, the CWT graph of EP velocity (or pressure) is considered for comparison, focusing on the heart rate between 70 bpm and 85 bpm (Figure 7.7.1).

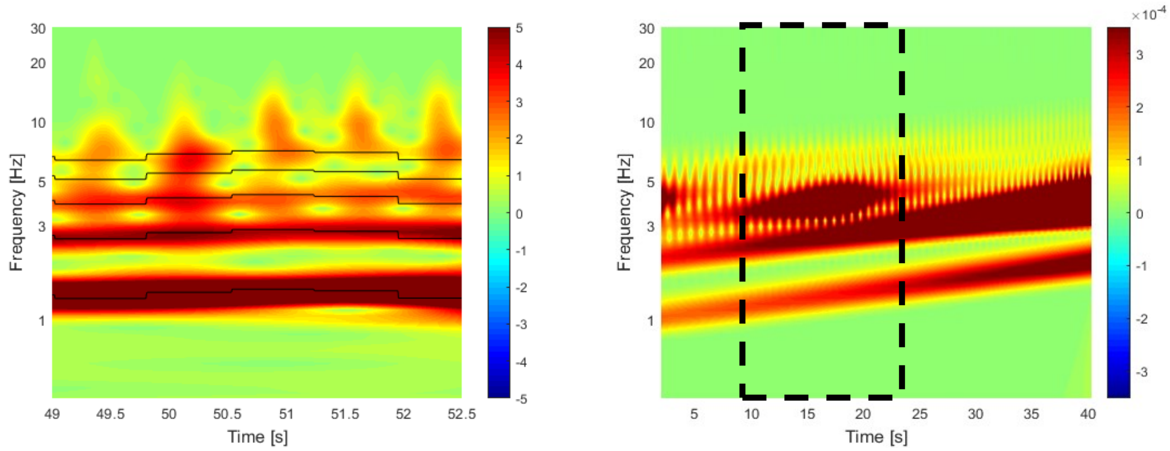

Figure 7.7.1 – CWT graphs of NIBP, subject 225 at rest (left) and velocity (or pressure) of EP compartment of the model (right), for 70-85bpm (black dashed rectangle on the right).

This comparison shows a clear correspondence between NIBP measurements and EP dynamics in time-frequency domain. For the HR range 70-85 bpm that characterises rest tests, there is a fundamental frequency around 1.3 Hz and a significant super harmonic around 3 Hz. In addition, a significant frequency content occurs around 5 Hz. A slight contribution goes from 5 Hz to 10 Hz, too. In the EP spectrogram, it does not appear with the same intensity for heart rates different from 70-85 bpm range.

Other experimental measurements that can be used for comparison are the VCG signals. They were detected by the IMU sensor placed at the xiphoid process of the sternum. It is possible to consider more than one DOF of the CVS model for comparison. The compartments of CVS model that are close to sternum are: left ventricle (LV), right ventricle (RV), systemic arteries (SA) and pulmonary arteries (PA). The test considered is always at rest, hence the HR varies between 70 bpm and 85 bpm, as seen above. In particular, gyration around X-axis, for subject 225 at rest, is considered. Moreover, it is possible to analyse the spectrograms for the accelerations detected, too. In that case, the results would be the same because the CWT graph of acceleration (e.g. Figure 3.2.2.4) has almost the same frequency content as gyration ones.

The CWT graphs used for comparison have been already discussed in chapter 3 and paragraph 7.6; however, they are reported here again for clarity.

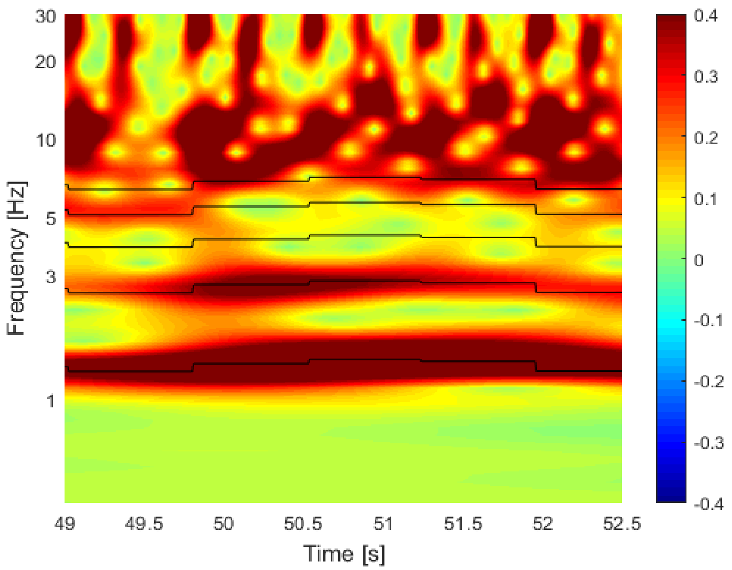

Figure 7.7.2 – CWT graphs of gyration around X-axis, subject 225 at rest.

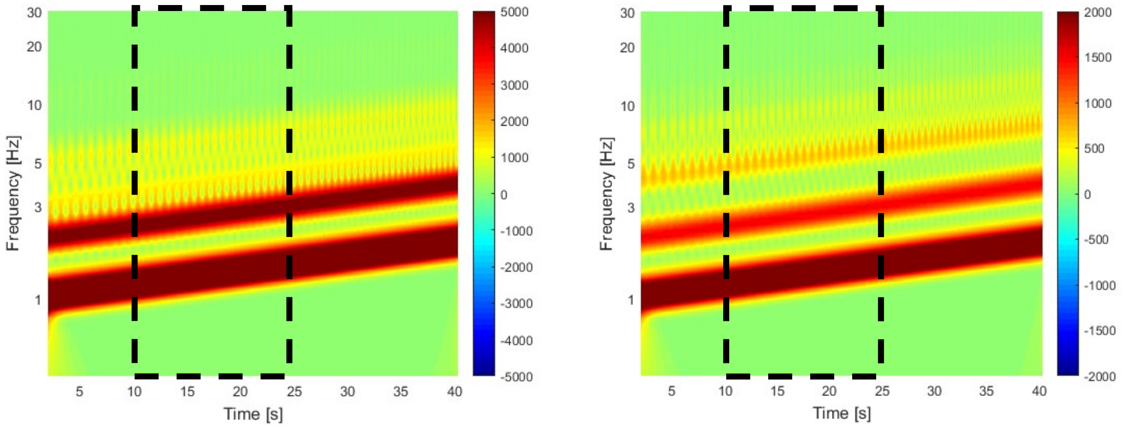

Figure 7.7.3 – CWT graphs of velocity (or pressure) of LV (left) and RV (right) compartments of the model, for 70-85bpm (black dashed rectangle).

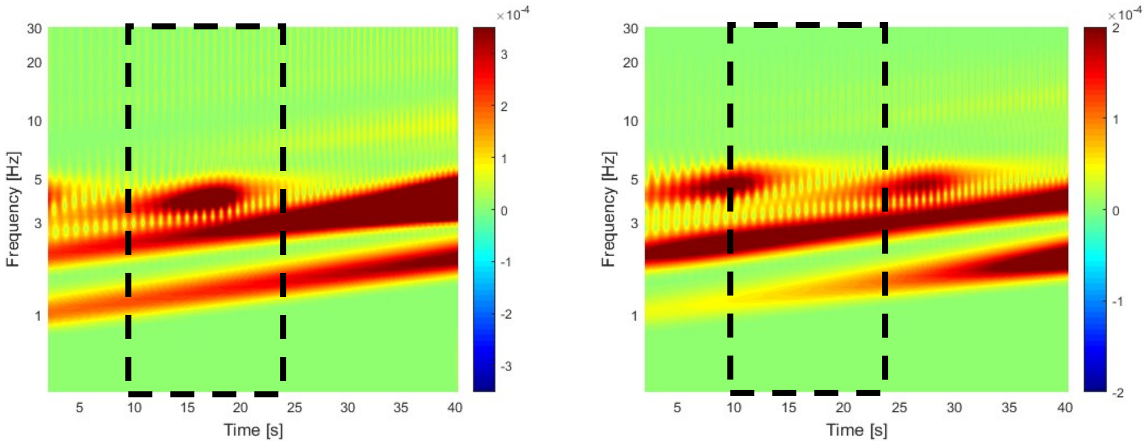

Figure 7.7.4 – CWT graphs of velocity (or pressure) of SA (left) and PA (right) compartments of the model, for 70-85bpm (black dashed rectangle).

The CWT graphs of LV and RV velocity (or pressure) show a fundamental frequency around 1.3 Hz and a super harmonic around 3 Hz. Then, other super harmonics occur between 5 Hz and 10 Hz. The SA velocity spectrogram is very similar to EP, in fact, a significant contribution appear around 5 Hz for 70-85 bpm, but frequencies above 5 Hz are not visible. The PA velocity spectrogram shows a contribution around 5 Hz, even if it reaches its maximum just before and after the 70-85 bpm range. Also for PA velocity spectrogram, frequencies above 5 Hz are not visible.

A significant aspect of the internal dynamics of the CVS model can be deduced looking at SA and PP CWT graphs. It is that the frequency content around 5 Hz occurs only once in SA graph, while in PA it occurs twice with a delay with respect to SA one.

The VCG spectrograms usually show a frequency content also between 5 Hz and 30 Hz, as in Figure 7.7.2. In order to visualise higher frequencies, the spectrograms of acceleration for the same DOFs are considered.

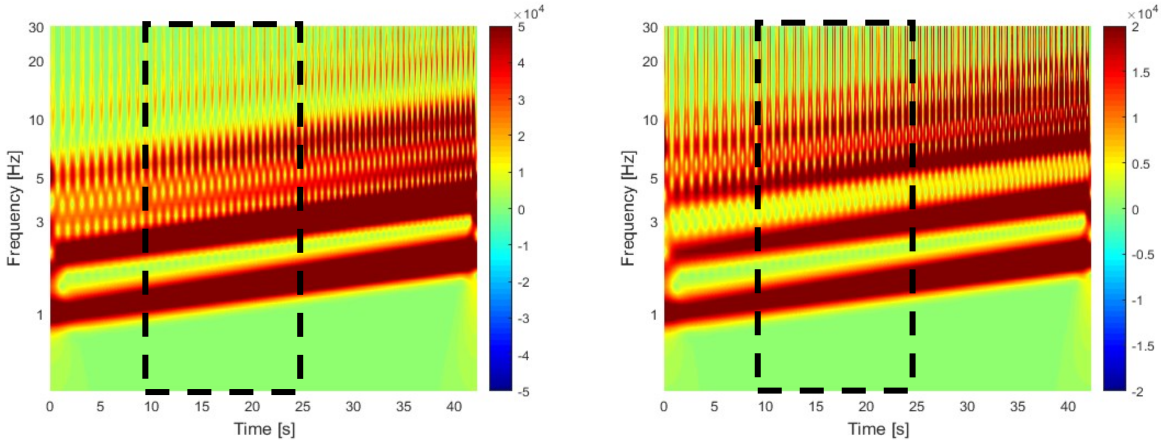

Figure 7.7.5 – CWT graphs of acceleration (or pressure derivative) of LV (left) and RV (right) compartments of the model, for 70-85bpm (black dashed rectangle).

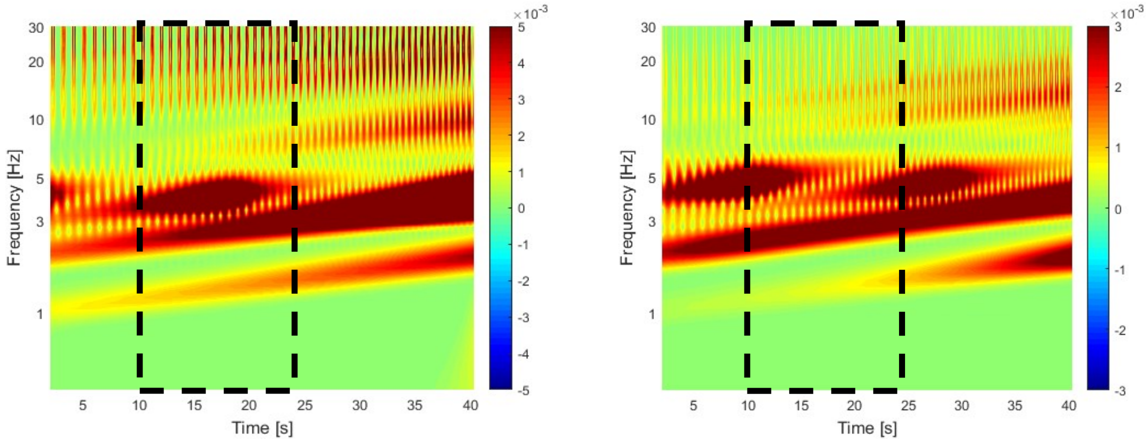

Figure 7.7.6 – CWT graphs of acceleration (or pressure derivative) of SA (left) and PA (right) compartments of the model, for 70-85bpm (black dashed rectangle).

Using accelerations, it is easier to visualise contributions of higher frequencies. Figure 7.7.5 and Figure 7.7.6 show that LV, RV, SA and PA has a significant frequency content around 7 Hz and especially from 12 Hz to 20 Hz. Therefore, a good correspondence can be determined between VCG signals and a combination of LV, RV, SA and PA compartments, in time-frequency domain.

Conclusions

A lumped parameter model of cardiovascular system can be useful to estimate blood pressure at different compartments of human body. Therefore, it could represent a valuable tool to correlate blood pressure prediction with VCG signals detected in NiPAMS experiments. This work demonstrates that this correlation exists in time-frequency domain. Consequently, it confirms the validity of the analogies used to transform the original hydraulic model from literature into an equivalent electric model and, finally, into an equivalent mechanical model.

In fact, the dynamic analysis of the mechanical model initially built for cardiovascular system shows two modes of rigid body motion, six overdamped modes and sixteen underdamped modes. It is important to note that the frequency range of CVS vibrations goes from 0 Hz to 21 Hz. It respects the frequency range highlighted in time-frequency analysis of CWT graphs for VCG signals. In particular, the heart rate frequency results to be the fundamental in experiments and natural frequencies close to it appear in CVS model, too. Similarly, some super harmonics can be identified in VCG spectrograms and in CVS mechanical modes. In particular, heart rate frequency is usually around 1 Hz; the most significant super harmonics are around 3 Hz and 5 Hz for all gyration and acceleration signals analysed in this thesis. Furthermore, a band-pass filtering for VCG signals confirmed that the frequency bandwidth form 0 Hz to 23 Hz provides a reliable representation of the entire signal detection.

The CVS model shows some significant global modes at 2.39 Hz (modes 7-8), 2.59 Hz (modes 9-10) and 3.14 Hz (modes 11-12), where many DOFs move at a time. These modes and their natural frequencies will be counted to improve the hemodynamic interpretation of the model dynamics. An important aspect of the model is that it demonstrates that aortic and pulmonary valves operation occurs at 14.47 Hz (modes 15-16) and 20.98 Hz (modes 17-18), that are frequencies higher than 12 Hz, as expected and predicted by previous experimental studies.

When some springs are added to the model, the modes of rigid body motion do not exist anymore and the system has four overdamped modes and twenty underdamped modes. In addition, the range of frequency slightly extends to 29 Hz, which still corresponds to the bandwidth from VCG time-frequency analysis. The valve operation occurs at higher frequencies that are 18.9 Hz for pulmonary valve and 28.9 Hz for aortic valve. The rest of the modes are mainly global modes. Finally, it can be deduced that it is possible to add more springs to ground to avoid rigid body motions, without significant changes in the natural frequencies of the MCK model.

The other variations applied to the model in previous chapters, like reducing spring constants or changing springs from ground to parallel configuration, give valid alternatives for CVS model. Although, in this work, they have been implemented just for comparison with the model built originally.

In order to have a time response of the model, heart excitation is added. According to the analogies implemented to build the final model, ventricular pressure functions defined over time corresponds to imposed kinematics on LV and RV masses. Displacement, velocity and acceleration over time are obtained for each DOF of the system with imposed kinematics effect. However, the most important response is velocity or pressure. Pressure waveforms predicted by the model are compared with the pressure waveforms detected with invasive measurements. It is possible to find a robust correspondence for DOFs corresponding to heart ventricles and atria. For the other compartments, the correspondence between predicted velocity and measured pressure waveforms is not so clear; more investigation is required to figure it out. Acceleration curves have been seen in detail only for ventricles because pressure derivative of left ventricle usually gives information about contractility. A good correspondence is found but it would be interesting to look at acceleration curves of the other compartments, too. Similarly, displacement

curves could be deepen for all DOFs. Another important conclusion deals with time responses of the model in time-frequency domain. In particular, applying time-varying heart rate, the spectrograms of velocity (or pressure) for each DOF are derived. Comparing the EP velocity spectrogram with NIBP one, a good correspondence of the main frequencies appears. Meanwhile, comparing LV, RV, SA and PA velocity spectrograms with VCG ones, a correspondence is visible only for frequencies lower than 5 Hz. Moreover, considering the acceleration spectrograms for the same DOFs, it is easier to visualise a correlation with VCG CWT graphs also for higher frequencies between 7 Hz and 30 Hz. In this initial study, the heart rate range considered goes from 70 bpm to 85 bpm because rest test are used. It would be interesting to compare model responses and experimental data in time-frequency domain for different heart rate ranges, in order to account the various tests performed experimentally.
Overall, the results of the simulation demonstrate the strength of the model, since they show how internal dynamics of each DOF is affected by the heart excitation imposed. More in-depth comparisons between model responses and experimental results can be made in time and frequency domain. A significant next investigation would be the correlation between model responses and central blood pressure. If necessary, more DOFs could be added to represent other specific circulatory compartments. These proposals for future developments could improve the CVS model and effectively verify its robustness.

Appendix

Mechanic-electric analogy

It is possible to convert a mechanical system into an electric system and vice versa using analogy. There are two existing analogies between mechanical and electric systems. The conventional analogy was proposed by J. C. Maxwell in the 19th century. Then, in 1933 F. A. Firestone proposed a new analogy in order to overcome some limitations of the old ones [28].
The electric constitutive laws that define the characteristic elements of an electric circuit are:

- Inductance L [H]

$$\Delta v_L = L \frac{d\,i}{d\,t} \tag{1.1}$$

- Resistance R [Ω]

$$\Delta v_R = R\,i \tag{1.2}$$

- Capacitance C [F]

$$\Delta v_C = \frac{1}{C}\int_0^t i\,dt \tag{1.3}$$

where $\Delta v_L, \Delta v_R, \Delta v_C$ are the voltage drops [V] across the inductor, the resistor and the capacitor respectively and $i\,(t)$ is the current [A]. Other characteristic elements are:

- Voltage generator (electromotive force) $e\,(t)$ [V]
- Current generator $a\,(t)$ [A]

The fundamental analogy concept is the energy conservation, hence there is a correspondence between the mechanic and electric power:

$$\text{Mechanic power} \Leftrightarrow \text{Electric power} \tag{1.4}$$

$$W_m = f \cdot \dot{x} \text{ [W]} \quad \Leftrightarrow \quad W_{el} = \Delta v \cdot i \text{ [W]} \tag{1.5}$$

where f is a force [N] and $\dot{x}$ is a velocity [m/s]. The two analogies associate the terms of Eq. (1.5) in different ways.
Another significant difference is that each analogy adopts one of the Kirchhoff's laws in order to correlate the mechanical system to the electric system.
Using FBD (Free Body Diagrams), the dynamics of a mass-spring-damper mechanical system can be described with the following equation:

$$m\,\ddot{x} + c\,\dot{x} + k\,x = f(t) \tag{1.6}$$

where m is the mass, c is the damping coefficient [and k is the spring stiffness.
The analogies considered describe this mechanical system with two different equivalent electric circuits.

1.1 The conventional analogy

According to the conventional analogy, current corresponds to velocity; consequently, from the power correspondence in Eq. (1.5), voltage is regarded as analogous to force:

$$i \Leftrightarrow \dot{x} \tag{1.1.1}$$

$$\Delta v \Leftrightarrow f \tag{1.1.2}$$

The conventional analogy considers the Kirchhoff's second law or voltage law (KVL), which states that the algebraic sum of all voltages around a closed path (or loop) is zero [48]. With M voltages in the loop, KVL equation is:

$$\sum_{m=1}^{M} \Delta v_m = 0 \tag{1.1.4}$$

Replacing the definition of the voltage drops described in Eq. (1.1), Eq. (1.2) and Eq. (1.3), it results:

$$L \frac{d\,i}{d\,t} + R\; i + \frac{1}{C} \int_0^t i\, dt = e(t) \tag{1.1.5}$$

Then, the definition of charge q [C] can be used to replace the integral and its derivatives; a differential equation is obtained

$$L \frac{d^2 q}{d\,t^2} + R \frac{d\,q}{d\,t} + \frac{1}{C}\, q = e(t) \tag{1.1.6}$$

Looking at Eq. (1.6) and Eq. (1.1.6), the correspondences of electric elements with mechanical elements can be noted. A mass m, which always has one terminal on the earth, is represented by an inductance L. A damping coefficient c is correlated to a resistance R. A spring is represented by a condenser, in particular the spring's constant k is associated with the reciprocal of the capacitance C.

$$L \Leftrightarrow m \tag{1.1.7}$$

$$R \Leftrightarrow c \tag{1.1.8}$$

$$\frac{1}{C} \Leftrightarrow k \tag{1.1.9}$$

The steady solution of Eq. (1.1.6) with $e(t) = E e^{j\omega t}$ and the electric impedance Z is:

$$i = \frac{E}{R + \mathrm{j}\left(\omega L - \dfrac{1}{\omega C}\right)} = \frac{E}{Z} \tag{1.1.10}$$

The steady state solution of Eq. (1.6) with a forced vibration $f(t) = fe^{j\omega t}$ is calculated as:

$$\dot{x} = \frac{f}{c + \mathrm{j}\left(\omega m - \frac{k}{\omega}\right)} = \frac{f}{z} \tag{1.1.11}$$

with the mechanical impedance z. According to the mechanic-electric analogy, the mechanical impedance must corresponds to the electric impedance in order to fit with the other correlations. When elements are connected in series, the electric impedance Z is the summation of impedances: Meanwhile, it is found that the mechanical impedance z in series is the reciprocal of the sum of the reciprocal of each impedance.

$$Z = Z_1 + Z_2 + Z_3 + \ldots \Leftrightarrow z = \frac{1}{\frac{1}{z_1} + \frac{1}{z_2} + \frac{1}{z_3} + \cdots} \tag{1.1.12}$$

It is the contrary for the configuration in parallel:

$$Z = \frac{1}{\frac{1}{Z_1} + \frac{1}{Z_2} + \frac{1}{Z_3} + \cdots} \Leftrightarrow z = z_1 + z_2 + z_3 + \ldots \tag{1.1.13}$$

It means that with the conventional analogy, when the mechanical elements are connected in parallel, the analogous electric elements must be connected in series. It is shown in Figure 1.1.1, where c is the spring's compliance that is the reciprocal of spring's stiffness k, $\bar{r}$ is the damping coefficient c and E is the electromotive force.

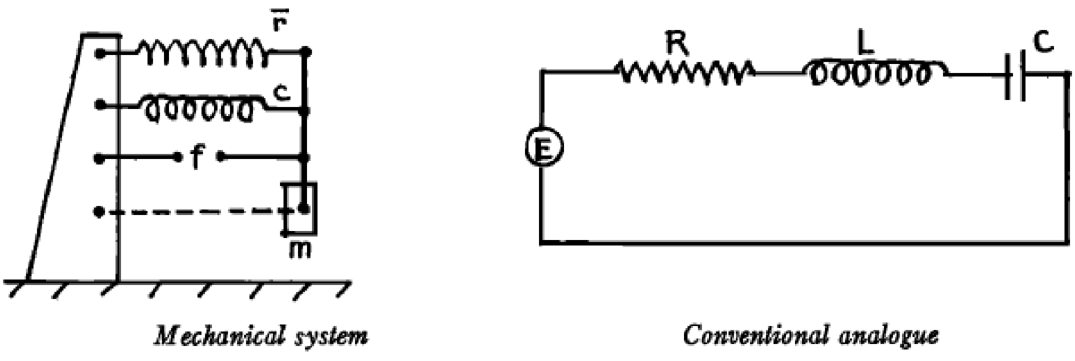

Figure 1.1.1 – Example of a mechanical system with elements in parallel (left) and the equivalent electric system with elements in series (right), using the conventional analogy.

1.2 Firestone analogy

According to Firestone analogy, voltage corresponds to velocity, hence from power correspondence in Eq. (1.5), current is regarded as analogous to force:

$$\Delta v \Leftrightarrow \dot{x} \tag{1.2.1}$$

$$i \Leftrightarrow f \tag{1.2.2}$$

In contrast with the traditional analogy, Firestone considers the Kirchhoff's first law or current law (KCL). It states that the algebraic sum of currents entering a node is zero, or that the sum of the current entering a node is equal to the sum of the currents leaving the node. With N branches connected to the node, KCL equation is:

$$\sum_{n=1}^{N} i_n = 0 \tag{1.2.3}$$

By considering the current through the condenser, the resistance and the inductor, it results:

$$i_C + i_R + i_L = a(t) \tag{1.2.4}$$

Since for Firestone analogy current corresponds to force as Eq. (1.2.1), it can be noted the correlation between Eq. (1.2.4) and the mechanical system Eq. (1.6).
For the other electric elements correspondences, a mass m, which always has one terminal on the earth, is represented by a capacitance C. A damping coefficient c is correlated to the reciprocal of a resistance R. A spring is represented by an inductor, in particular the spring's constant k is associated with the reciprocal of the inductance L.

$$C \Leftrightarrow m \tag{1.2.5}$$

$$\frac{1}{R} \Leftrightarrow c \tag{1.2.6}$$

$$\frac{1}{L} \Leftrightarrow k \tag{1.2.7}$$

The new analogy introduces a new term, bar impedance $\bar{z}$, which is defined as *velocity across/force through*, that is the reciprocal of the mechanical impedance z from previous analogy. In this way, the similarity of these two equations can be seen:

$$\dot{x} = f \cdot \bar{z} \Leftrightarrow E = i \cdot Z \tag{1.2.8}$$

It leads to define mechanical impedance as electric impedance. The objective is to calculate bar impedances for mechanical elements in series like electric impedances in series:

$$Z = Z_1 + Z_2 + Z_3 + \dots \Leftrightarrow \bar{z} = z_{{}_1} + \bar{z}_2 + \bar{z}_3 + \dots \tag{1.2.9}$$

For elements in parallel, the correspondence is with the reciprocal of the sum of the reciprocals:

$$Z = \frac{1}{\frac{1}{Z_1} + \frac{1}{Z_2} + \frac{1}{Z_3} + \dots} \Leftrightarrow \bar{z} = \frac{1}{\frac{1}{\bar{z}_1} + \frac{1}{\bar{z}_2} + \frac{1}{\bar{z}_3} + \cdots} \tag{1.2.10}$$

Consequently, with Firestone analogy, a series mechanical circuit corresponds to an equivalent series electric circuit, as shown in Figure 1.2.1.

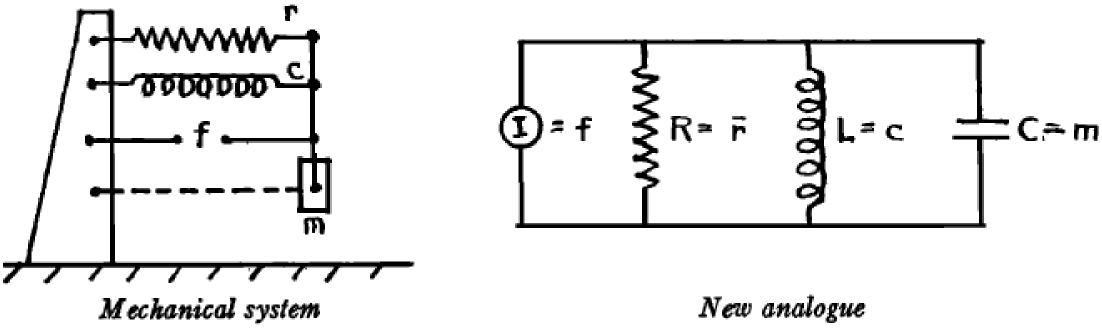

Figure 1.2.1 – Example of a mechanical system with elements in parallel (left) and the equivalent electric system with elements in parallel (right), using Firestone analogy.

1.3 Comparison between conventional and Firestone analogy

The analogy proposed by Firestone solves some of the main limitations of the previous analogy.

- In the conventional analogy, there was a correspondence between an electromotive force “across” and a mechanical force “through”. In Firestone analogy, it exists between current “through” and force “through” an element. It means that there is a better correlation between the analogous quantities used.
- In the conventional analogy, mechanical elements connected in parallel refer to electric elements in series and vice versa. This correspondence exists also when combining mechanical and electric impedances. In the new analogy, there is a direct correlation between mechanical and electric elements in series or in parallel. In addition, mechanical impedances in series (or parallel) are combined like electric impedances in series (or parallel).
- The conventional analogy respects the Kirchhoff’s second law or voltage law (KVL) but there is not a mechanical analogous for the Kirchhoff’s first law or current law (KCL). The reason is that it correlates voltage with force and current with velocity, but velocities in mechanical system do not respect KCL. Firestone analogy respects both Kirchhoff’s laws in mechanical systems because it correlates voltage with velocity and current with force.

The conventional mechanic-electric analogy is incomplete in certain particulars, which make it difficult to apply in practice, especially with complicated mechanical systems.
Firestone analogy is more complete and allows obtaining an equivalent electric circuit in a more intuitive manner.

Reference

[1] Lortie M., Plant D., D'Mello Y., Skoric J., Hakim S., Clairmonte N., Aboulezz E., "Non-invasive physiological activity monitoring system (NiPAMS)", Project Report, McGill University, 2019.
Lortie,Plant,DMello_NiPAMS Report_2019.pdf

[2] D'Mello Y., Skoric J., Hakim S., Aboulezz E., Clairmonte N., Lortie M., Plant D.V., "Identification of the vibrations corresponding with heart sounds using vibrational cardiography", *Accepted to the 42nd Annual International Conference of the IEE Engineering in Medicine and Biology Society (EMBC),* 2020.
DMello,Skoric,Hakim_Identification of the vibrations corresponding with heart sounds vibrational cardiography_2020.pdf

[3] Zanetti J.M., Tavakolian K., "Seismocardiography: past, present and future", *Proc. 35th Annual International Conference of the IEEE EMBS*, Osaka, Japan, 2013, pp. 7004-7007.
Zanetti,Tavakolian_Seismocardiography past, present and future_2013.pdf

[4] Tadi M. J., Lehtonen E., Saraste A., Tuominen J., Koskinen J., Teras M., Airaksinen J., Pankaala M., Koivisto T., "Gyrocardiography: a new non-invasive monitoring method for the assessment of cardiac mechanics and the estimation of hemodynamic variables", *Scientific Reports,* 7(6823), 2017.
Tadi,Lehtonen,Saraste_Gyrocardiography a new non-invasive monitoring method for the assessment of cardiac mechanics and the estimation of hemodynamic variables_2017.pdf

[5] http://www.wikipedia.org available in 2020-09-22.
Wikipedia_Cardiac cycle_2020.pdf

[6] McEniery C.M., Cockcroft J.R., Roman M.J., Franklin S.S., Wilkinson I.B., "Central blood pressure: current evidence and clinical importance", *European Heart Journal*, 35, 2014, pp. 1719-1725.
McEniery,Cockcroft,Roman_Central blood pressure current evidence and clinical importance_2014.pdf

[7] http://www.slideplayer.com available in 2020-10-19.
Slideplayer_Anterior muscles origin on pelvis or vertebral column_2020.pdf

[8] Shirwany N.A., Zou M., "Arterial stiffness: a brief review", *Acta Pharmacologica Sinica*, 31, 2010, pp. 1267-1276.
Shirwany,Zou_Arterial stiffness a brief review_2010.pdf

[9] Wilkinson I.B., Mohammad N.H., Tyrrell S., Hall I.R., Webb D.J., Paul V.E., Levy T., Cockcroft J.R., "Heart rate dependency of pulse pressure amplification and arterial stiffness", *American Journal of Hypertension,* 15, 2002, pp. 24-30.
Wilkinson,Mohammad,Tyrrell_Heart rate dependency of pulse pressure amplification and arterial stiffness_2002.pdf

[10] http://www.heart.org available in 2020-10-19.
Heart_All about heart rate(pulse)_2020.pdf

[11] D'Mello Y., Skoric J., Xu S., Roche P.J.R., Lortie M., Gagnon S., Plant D.V., "Real-time cardiac beat detection and heart rate monitoring from combined seismocardiography and gyrocardiography", *IEEE Sensors Journal,* 19(16), 2019, p. 3472.
DMello,Skoric,Roche_Real-time cardiac beat detection and heart rate monitoring from combined seismocardiography and gyrocardiography _IEEESensJ2019.pdf

[12] Dehkordi P., Khosrov-Khavar F., Di Rienzo M., Iman O.T., Schmidt S.E., Blaber A.P., Sorensen K., Strujik J.J., Zakeri V., Lombardi P., Shandhi M.M.H., Borairi M., Zanetti J.M., Tavakolian K., "Comparison of different methods for estimating cardiac timings: a

comprehensive multimodal echocardiography investigation”, *Frontiers in Physiology,* 10(1057), 2019.
Dehkordi,Khosrov-Khavar,Di Rienzo_Comparison of different methods for estimating cardiac timings a comprehensive multimodal echocardiography investigation_2019.pdf

[13] Peter L., Kracik J., Cerny M., Noury N., Polzer S., “Mathematical model based on the shape of pulse waves measured at a single spot for the non-invasive prediction of blood pressure”, *Processes*, 8(442), 2002.
Peter,Kracik,Cerny,Noury,Polzer_Mathematical model based on the shape of pulse waves measured at a single spot for the non-invasive prediction of blood pressure_2002.pdf

[14] Chemla D., Aptecar E., Hébert J.L., Coirault C., Loisance D., Lecarpentier Y., Nitenberg A., “Short-term variability of pulse pressure and systolic and diastolic time in heart transplant recipients”, *American Physiological Society*, 279, 2000, pp. H122-H129.
Chemla,Aptecar,Hebert_Short-term variability of pulse pressure and systolic and diastolic time in heart transplant recipients_2000.pdf

[15] Bruss Z. S., Raja A., “Physiology, Stroke Volume”, *StatPearls*, 2020.
Bruss,Raja_Physiology, stroke volume_2020.pdf

[16] Paisal M.S.A., Taib I., Ismail A.E., Arifin A.M.T., Darlis N., “An analysis of blood pressure waveform using Windkessel model for normotensive and hypertensive conditions in carotid artery”, *Journal of Advanced Research in Fluid Mechanics and Thermal Sciences,* 57(1), 2019, pp. 69-85.
Paisal,Taib,Ismail,Arifin,Darlis_An analysis of blood pressure waveform using Windkessel model for normotensive and hypertensive conditions in carotid artery_2019.pdf

[17] https://doctorlib.info available in 2020-11-03
Doctorlib_Cardiac dynamics_2020.pdf

[18] Waite L., Fine J., *Applied biofluid mechanics*, McGraw-Hill, United State of America, 2007.

[19] Vennin S., Li Y., Willemet M., Fok H., Gu H., Charlton P., Alastruey J., Chowienczyk P., “Identifying hemodynamic determinants of pulse pressure: a combined numerical and physiological approach”, *Hypertension,* 70, 2017, pp. 1176-1182.
Vennin,Willemet,Fok,Gu,Charlton,Alastruey,Chowienczyk_Identifying hemodynamic determinants of pulse pressure a combined numerical and physiological approach_2017.pdf

[20] Pauca A.L., O’Rourke M.F., Kon N.D., “Prospective evaluation of a method for estimating ascending aortic pressure from the radial artery pressure waveform”, *Hypertension*, 38, 2001, pp. 932-937.
Pauca,ORourke,Kon_Prospective evaluation of a method for estimating ascending aortic pressure from the radial artery pressure waveform_2001.pdf

[21] https://wikipedia.org available in 2021-02-05.
Wikipedia_Continuous noninvasive arterial pressure_2021.pdf

[22] Westerhof N., Lankhaar J.W., Westerhof B.E., “The arterial Windkessel”, *Medical and Biological Engineering*, 2008.
Westerhof,Lankhaar,Westerhof_The arterial Windkessel_2008.pdf

[23] Formaggia L., Veneziani A., *Reduced and multiscale models for the human cardiovascular system*, 7th VKI Lecture Series, Biological fluid dynamics, Von Karman Institute, Belgium, 2003.
Formaggia,Veneziani_Reduced and multiscale models for the human cardiovascular system_2003.pdf

[24] Ursino M., “Interaction between carotid baroregulation and the pulsating heart: a mathematical model”, *American Journal of Physiology*, 275, 1998, pp. H1733-H1747.
Ursino_ Interaction between carotid baroregulation and the pulsating heart: a mathematical model_1998.pdf

[25] Burattini R., Di Salvia P.O., "Development of systemic arterial mechanical properties from infancy to adulthood interpreted by four-element Windkessel", *Journal of applied physiology*, 103, 2007, pp. 66-79.
`Burattini,Di Salvia_Development of systemic arterial mechanical properties from infancy to adulthood interpreted by four-element windkessel_2007.pdf`

[26] Ursino M., Antonucci M., Belardinelli E. "Role of active changes in venous capacity by the carotid baroreflex: analysis with a mathematical model", *American Journal of Physiology*, 267, 1994, pp. H2531-H2546.
`Ursino,Antonucci,Belardinelli_Role of active changes in venous capacity by the carotid baroreflex analysis with a mathematical model_1994.pdf`

[27] https://ataridogdaze.com available in 2020-12-22.
`Ataridogdaze_Electric circuit and the hydraulic analogy_2020.pdf`

[28] Firestone F.A., "A new analogy between mechanical and electrical systems", *Journal of the Acoustical Society of America*, 3, 1933, pp. 249-267.
`Firestone_A new analogy between mechanical and electrical systems_1933.pdf`

[29] Bonisoli E., *LUPOS - LUmped Parameters Open Source FEM code*, release 2020-09-16, Politecnico di Torino, 2020.
`LUPOS_Tutorial_2020-09-16.pdf`

[30] Adhikari S., "Damping modelling using generalized proportional damping", *Journal of Sound and Vibration*, 293, 2006, pp. 156-170.
`Adhikari_Damping modelling using generalized proportional damping_2006.pdf`

[31] http://www.medicalook.com available in 2021-01-25.
`Medicalook_Routes of circulation_2021.pdf`

[32] Castiglioni P., Faini A., Parati G., Rienzo M.D., "Wearable seismocardiography", *Annual international Conference of the IEEE Engineering in Medicine and Biology Society*, Lyon, France, 2007, pp. 3954-3957.
`Castiglini,Faini,Parati,Rienzo_Wereable seismocardiography_2007.pdf`

[33] https://cvphysiology.com available in 2021-02-05.
`CVphysiology_Ventricular pressure-volume relationship_2021.pdf`

[34] Westerhof N., Stergiopulos N., Noble M.I.M., Westerhof B.E., *Snapshot of hemodynamics*, Springer, Switzerland, 2019.

[35] Hudsmith L.E., Petersen S.E.P., Francis J.M., Robson M.D., Neubauer S., "Normal human left and right ventricular and left atrial dimensions using steady state free precession magnetic resonance imaging", *Journal of Cardiovascular Magnetic Resonance*, 7, 2005, pp. 775-782.
`Hudsmith,Peterson,Francis_Normal human left and right ventricular and left atrial dimensions using steady state free precession magnetic resonance imaging_2005.pdf`

[36] https://edwards.com available in 2021-02-12.
`Edwards_Normal hemodynamic parameters_2021.pdf`

[37] Mandapaka S., Hamilton C.A., Morgan T.M., Hundley G., "Simultaneous measurement of left and right ventricular volumes and ejection fraction during dobutamine stress cardiovascular magnetic resonance", *Journal of computed assisted tomography*, 35(5), 2011, pp. 614-617.
`Mandapaka,Hamilton,Morgan,Hundley_Simultaneous measurement of left and right ventricular volumes and ejection fraction during dobutamine stress cardiovascular magnetic resonance_2011.pdf`

[38] https://alivecor.com available in 2021-02-14.
`Alivecor_What is an ECG_2021.pdf`

[39] Townsend N., *Medical electronics*, Michaelmas term course, University of Liverpool, 2001.
`Townsend_Medical electronics_2001.pdf`

[40] Foucha B.K., “The ABCs of A to V: right atrial/left atrial (PCW) pressures”, *Cath Lab Digest*, 17(5), 2009.
`Foucha_The ABCs of A to V right atrial left atrial (PCW) pressures_2009.pdf`

[41] Parker K.H., *Mechanics of circulation: chapter 11*, Department of bioengineering course, Imperial College London, 2013.
`Parker_Mechanics of circulation chapter 11_2013.pdf`

[42] Currie P.J., Seward J.B., Reeder G.S., Vlietstra R.E., Bresnahan D.R., Bresnahan J.F., Smith H.C., Hagler D.J., Tajik A.J., “Continuous-wave Doppler echocardiographic assessment of severity of calcific aortic stenosis: a simultaneous Doppler-catheter correlative study in 100 adult patients”, *Circulation*, 71(6), 1985, pp. 1162-1169.
`Curie,Seward,Reeder_Continuous-wave Doppler echocardiographic assessment of severity of calcific aortic atenosis a simultaneous Doppler-catheter correlative study in 100 adult patients_CircJ1985.pdf`

[43] https://cvphysiology.com available in 2021-02-14.
`CVphysiology_Valvular stenosis_2021.pdf`

[44] https://pcipedia.org available in 2021-02-14.
`PCIpedia_Right heart catheterization_2021.pdf`

[45] Tansey E.A., Montgomery L.E.A., Quinn J.G., Roe S.M., Johnson C.D., “Understanding basic vein physiology and venous blood pressure though simple physical assessments”, *Advances in Physiology Education*, 43, 2019, pp. 423-429.
`Tansey,Montgomery,Quinn,Roe,Johnson_Understanding basic vein physiology and venous blood pressure though simple physical assessments_2019.pdf`

[46] https://thoracickey.com available in 2021-02-13.
`Thoracickey_Left ventricular systolic function_2021.pdf`

[47] Ostadal P., Vondrakova D., Kruger A., Janotka M., Naar J., “Continual measurement of arterial dP/dtmax enables minimally invasive monitoring of left ventricular contractility in patients with acute heart failure”, *Critical Care*, 23(364), 2019.
`Ostadal,Vondrakova,Kruger,Janotka,Naar_Continual measurement of arterial dPdtmax enables minimally invasive monitoring of left ventricular contractility in patients with acute heart failure_2019.pdf`

[48] Alexander C.K., Sadiku M.N.O., *Fundamentals of electric circuits, fifth edition*, McGraw-Hill, New York, 2013.

Acknowledgments

This entire course of study gave me the opportunity to enrich my knowledge and to acquire new skills, in an engineering field that attracts me ever more. It has been a period of continuing personal formation, from the interaction with professors and classmates during lessons, to my study experiences abroad, to my activity of thesis.
I would like to thank Prof. Bonisoli and Eng. Lisitano for trust and attention towards me starting from the beginning of my activity of thesis. Our discussions have been always stimulating and interesting. Prof. Bonisoli, thank you very much for the valuable time you dedicated to the project and to several meetings.
I would like to thank Prof. Amabili for this great opportunity to interact with McGill University. It has been a very enriching experience for me. I really appreciate your support and moments of confrontation. I would like to thank Prof. Plant and Eng. Lortie for letting me participate in the NiPAMS project. I really appreciate your dedication to the project. Thank you very much for your time and attention during our meetings and discussions. It has been a great pleasure to collaborate with your prestigious university and company.
I would like to thank all the members of the team I worked with during this period: Yannick, Galib, James, Angus, Nathan, Ezz. I really enjoyed working with you, sharing our ideas and feedback along the way. I have learned a lot from this collaboration and I hope I was able to provide a positive contribution to your interesting project.
I am grateful to have met kind and passionate people that I will never forget.
Moreover, I enjoyed staying for some months in Montreal, which is an important place for me.
Special thanks to my sister, my mother, my father, my grandmother Maria and to all my big family with a big heart.